Bioconjugation of Peptides on Cube-octameric Silsesquioxanes

TECHNISCHE UNIVERSITÄT DARMSTADT

Vom Fachbereich Chemie
der Technischen Universität Darmstadt

zur Erlangung des akademischen Grades eines

Doktor-Ingenieurs (Dr.-Ing.)

genehmigte
kumulative Dissertation

vorgelegt von

Dipl.-Ing. Sebastian Fabritz
aus Worms

Referent:	Prof. Dr. Harald Kolmar
Korreferenten:	Prof. Dr. Markus Biesalski
	Prof. Dr. Alessandro Dondoni (University of Ferrara, Italy)

Tag der Einreichung:	22. Oktober 2012
Tag der mündlichen Prüfung:	04. Dezember 2012

Darmstadt 2013

Die vorliegende Arbeit wurde unter der Leitung von Herrn Prof. Dr. Harald Kolmar am Clemens Schöpf-Institut für Organische Chemie und Biochemie der Technischen Universität Darmstadt seit November 2008 angefertigt.

Everything that can be counted does not necessarily count; everything that counts cannot necessarily be counted.

Einstein

Danksagung

Prof. Dr. Harald Kolmar: Vielen Dank, dass Sie mir die Möglichkeit gegeben haben Teil der wissenschaftlichen Gemeinschaft zu werden. Ich weiß Ihre immer offene Tür und Ihren Rat sehr zu schätzen. Danke für die guten letzten Jahre.

Dr. Olga Avrutina: Du warst mir Mentorin und Beschützerin. Das werde ich dir nie vergessen. Ich danke dir für deine konstante und umfangreiche Unterstützung.

Maria und **Robert**: Vielen Dank für euren Rat und Unterstützung in jeder Lebenslage. Ihr seid Teil von dem was mir am wichtigsten ist – Familie.

Sebastian und **Doreen**: Durch eure Unterstützung konnte ich das Projekt „Nanopartikel“ zu einem erfolgreichen Abschluss bringen. Danke, dass ihr dazu beigetragen habt. Wir sind ein gutes Team. Ich schätze eure gute Laune und den damit einhergehenden angenehmen Humor.

Janine, **Tim**, **Franzi** und **Alexander** – Meine Clique, mein Rudel, mein Freundeskreis. Vielen Dank für die guten gemeinsamen Stunden. Ich wünsche mir, dass es in der Zukunft noch mehr werden.

Barbara Diestelmann: Vielen Dank für deine Unterstützung in meinem Kampf mit der Bürokratie. Ich habe es besonders geschätzt mich mit dir über unser gemeinsames Hobby auszutauschen.

Martin und **Michael**: Ich danke euch stellvertretend für das Chemiker-Team. Ihr wart im Alltag immer hilfreich zur Stelle!

Prof. Dr. Sigfried Neumann: Die Gespräche mit Ihnen haben mich in der kritischen Phase zwischen Promotion und neuem Job in meiner Entscheidungsfindung sehr gestärkt. Vielen Dank.

Die gesamte **Arbeitsgruppe Kolmar** war mir ein Zuhause mit allem was dazu gehört.
Danke euch allen!

Vieles ist alleine nicht möglich! Deshalb gilt mein besonderer Dank auch meinen **Kooperationspartnern** und **Koautoren**.

Die Ergebnisse der vorliegenden Arbeit wurden an folgenden Stellen vorgestellt, veröffentlicht oder zur Veröffentlichung eingereicht:

[1] Sebastian Fabritz, Dirk Heyl, Viktor Bagutski, Martin Empting, Eckhard Rikowski, Holm Frauendorf, Ildiko Balog, Wolf-Dieter Fessner, Jörg. J. Schneider, Olga Avrutina and Harald Kolmar, *Towards click bioconjugations on cube-octameric silsesquioxane scaffolds*, *Org. Biomol. Chem.*, 2010, **8**, 2212-2218.

[2] Sebastian Fabritz,‡ Sebastian Hörner,‡ Martin Empting, Doreen Könning, Michael Reinwarth, Christian Dietz, Bernhard Glotzbach, Holm Frauendorf, Harald Kolmar and Olga Avrutina, *From Pico to Nano: Biofunctionalization of Cube-octameric Silsesquioxanes by Peptides and Miniproteins*, *Org. Biomol. Chem.*, 2012, **10**, 6287-6293.

[3] Sebastian Hörner,‡ Sebastian Fabritz,‡ Henry D. Herce, Olga Avrutina, Christian Dietz, Robert W. Stark, M. Cristina Cardoso and Harald Kolmar, *Cube-octameric silsesquioxane-mediated cargo peptide delivery into living cancer cells*, *Org. Biomol. Chem.*, 2013, **11**, 2258-2265.

[4] Sebastian Fabritz,‡* Sebastian Hörner,‡ Olga Avrutina and Harald Kolmar, *Bioconjugation on Cube-Octameric Silsesquioxanes*, *Org. Biomol. Chem.*, 2013, **11**, 2224-2236.

[5] Sebastian Fabritz,‡ Franziska Maaß,‡ Olga Avrutina, Tim Heiseler, Björn Steinmann and Harald Kolmar, *A sensitive method for rapid detection of alkyl halides and dehalogenase activity using a multistep enzyme assay*, *AMB Express*, 2012, **2**:51.

Koautorenschaften:
[6] Olga Avrutina, Martin Empting, Sebastian Fabritz, Matin Daneschdar, Holm Frauendorf, Ulf Diederichsen and Harald Kolmar, *Application of copper(I) catalyzed azide–alkyne [3+2] cycloaddition to the synthesis of template-assembled multivalent peptide conjugates, Org. Biomol. Chem.*, 2009, **7**, 4177-4185.

[7] Martin Empting, Olga Avrutina, Reinhard Meusinger, Sebastian Fabritz, Michael Reinwarth, Markus Biesalski, Stephan Voigt, Gerd Buntkowsky, Harald Kolmar, *"Triazole Bridge": Disulfide-Bond Replacement by Ruthenium-Catalyzed Formation of 1,5-Disubstituted 1,2,3-Triazoles*, *Angew. Chem. Int. Ed.*, 2011, **50**, 5207–5211.

[8] Michael Reinwarth, Bernhard Glotzbach, Michael Tomaszowski, Martin Empting, Sebastian Fabritz, Olga Avrutina, Harald Kolmar, *Oxidative folding of peptides with cystine-knot architecture: kinetic studies and optimization of folding conditions*, *ChemBioChem*, 2013, **14**, 137-146.

Posterbeiträge:
Sebastian Fabritz, Martin Empting, Dirk Heyl, Holm Frauendorf, Olga Avrutina, Wolf-Dieter Fessner, Jörg J. Schneider and Harald Kolmar, *Utility of Copper(I)-Catalyzed Azide-Alkyne [3+2] Cycloaddition towards the Synthesis of Organic-Inorganic Covalent Hybrides*, 9th German Peptide Symposium, 2009.

Sebastian Fabritz, Olga Avrutina, Martin Empting, Michael Reinwarth, Sebastian Hörner and Harald Kolmar, *Bioconjugation on polyhedral silsesquioxanes*, 10th German Peptide Symposium, 2011.

Sebastian Hörner, Sebastian Fabritz, Olga Avrutina, Henry D. Herce, Christian Dietz, Robert W. Stark, M. Cristina Cardoso and Harald Kolmar, *Cube-octameric Silsesquioxanes: Nanoscaffolds for Tumor Imaging and Drug Delivery*, EMBO Conference Series: Chemical Biology, 2012.

Inhaltsverzeichnis

Abkürzungsverzeichnis

AFM	atomic force microscopy
BODIPY	boron-dipyrromethene
CD	cyclodextrin
COSS	cube-octameric silsesquioxane
CuAAC	copper-catalyzed azide-alkyne cycloaddition
DCM	dichloromethane
DIC	*N,N'*-diisopropylcarbodiimide
DIEA	*N*,*N*-diisopropylethylamine
DMEM	Dulbecco's modified Eagle medium
DMF	dimethylformamide
DMSO	dimethyl sulfoxide
DNA	deoxyribonucleic acid
DOTA	1,4,7,10-tetraazacyclododecane-1,4,7,10-tetraacetic acid
ECM	extracellular matrix
ESI	electrospray ionization
FCS	fetal calf serum
FITC	fluorescein isothiocyanate
FRET	Förster Resonance Energy Transfer
FTICR	Fourier transform ion cyclotron resonance
Gd	gadolinium
HBTU	2-(1H-benzotriazole-1-yl)-1,1,3,3-tetramethyluronium hexafluorophosphate
HR	high resolution
ICM	intracellular matrix
IR	infrared
LC	liquid chromatography
MeCN	acetonitrile
MRI	magnetic resonance imaging
MS	mass spectrometry
MTBE	methyl tertiary butyl ether
MTT	(3-(4,5-dimethylthiazol-2-yl)-2,5-diphenyltetrazolium bromide
NMR	nuclear magnetic resonance
PAMAM	polyamidoamine
PCNA	Proliferating Cell Nuclear Antigen
PBLG	poly-γ-benzyl-L-glutamate
PEG	polyethylene glycol
PEI	polyethlyenimine
POSS	polyhedral oligomeric silsesquioxane
PyBop	(benzotriazol-1-yl-oxytripyrrolidinophosphonium hexafluorophosphate)
RFP	red fluorescent protein
RP-HPLC	reversed-phase high-performance liquid chromatography
SNP	silica nanoparticle
SPAAC	strain promoted azide-alkyne cycloaddtion
TAT	trans-activator of transcription
TBAI	tetrabutylammonium iodide
TEC	photoinduced free-radical thiol-ene coupling
TES	triethylsilane
TFA	trifluoroacetic acid
TG	thermogravimetry
TMGA	*N*,*N*-tetramethylguanidinium azide
XTT	(2,3-bis-(2-methoxy-4-nitro-5-sulfophenyl)-2H-tetrazolium-5-carboxanilide)

1. Forschungsfeld, Intention der Arbeit und wissenschaftlicher Erkenntnisgewinn

Die biomedizinische Forschung hat in den letzten Jahrzehnten erhebliche Fortschritte gemacht und zu neuen Erkenntnissen über verschiedene komplexe Krankheitsbilder wie Krebs oder AIDS beigetragen. Das detailgenaue Wissen über Zellkommunikation und -interaktion hat zur Entwicklung von individualisierten Behandlungsansätzen geführt. Patientenspezifische Vakzinierungen gegen Tumore, aber auch die Möglichkeit auf Krebszellen überexprimierte Rezeptoren gezielt anzusprechen sind Beispiele für neue therapeutische Ansätze.

In diesem Zusammenhang sind funktionalisierte Nanopartikel in den Fokus des wissenschaftlichen Interesses gelangt, da mit ihnen biologische Liganden z.B. für die funktionelle Beeinflussung von Rezeptoren auf Zelloberflächen, von Proteinen der extrazellulären Matrix oder von Enzymen in Blut oder Lymphe in vielfacher Kopie auf einem stabilen und inerten Grundgerüst bereit gestellt werden können. Auf Nanopartikeln basierende molekulare Plattformen lassen sich unter anderem den folgenden Kategorien zuordnen (siehe Übersichtsartikel [1]):

- Gold-Nanopartikel
- Seltenerd-Nanopartikel
- Liposomen
- Kohlenstoffnanoröhrchen
- Magnetische Nanopartikel
- Quantum Dots
- Polymerische Partikel
- Silika-Nanopartikel

Die Materialauswahl für molekulare Werkzeuge in der Biomedizin hängt von deren spezifischen Anforderungen ab. Generell wünschenswert für Anwendungen am Menschen sind eine geringe Toxizität, ein kompakter Aufbau, eine steuerbare Halbwertszeit der Kernstruktur, selektiv ansprechbare reaktive Gruppen sowie eine günstige kommerzielle Verfügbarkeit. Vertreter der silikatbasierten Nanopartikel (SNP) erfüllen dieses spezielle Anforderungsbündel in hohem Maße. Kubisch-oktamerische Silsesquioxane (COSS)[2] können als kleinste Vertreter der SNP-Familie aufgefasst werden. Sie zeichnen sich durch ihre besondere Symmetrie aus und werden chemisch durch die allgemeine Formel $(RSiO_{1,5})_8$ beschrieben, wobei R für Wasserstoff oder eine aliphatische organische Gruppe steht.[2] Trotz des nur 0.5-0.7 nm kleinen Kerns[3] stellen diese organisch-anorganischen Hybridnanopartikel acht stöchiometrisch adressierbare Funktionalitäten zur Verfügung (siehe Abbildung 1).

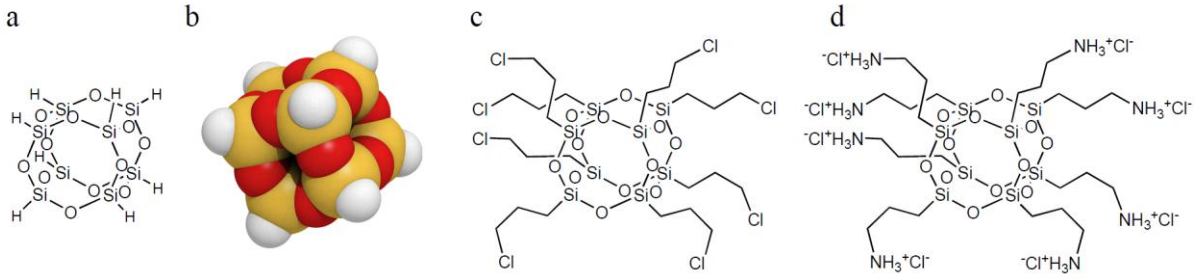

Abbildung 1: COSS Strukturen. a, b: Chemische Struktur eines unfunktionalisierten kubischen Silsesquioxans; gelb: Siliziumatome, rot: Sauerstoffatome, weiß: Wasserstoffatome, c: Oktachloropropyl-COSS, d: Oktaaminopropyl-COSS Hydrochlorid.

Zielsetzung des vorgestellten Promotionsprojektes war die achtfache Konjugation von bioaktiven peptidischen Liganden mit kubisch-oktamerischen Silsesquioxan-Nanopartikeln. Dieses Hauptziel gliedert sich in folgende Teilaufgaben:

- Synthese von COSS mit Funktionalitäten, die für Biokonjugationen geeigneten sind
- Erarbeitung der Grundlagen zur enzymatischen Modifizierung von halogenierten COSS („Dehalogenase Projekt“)
- Physikalische und chemische Charakterisierung der neuen COSS-Grundgerüste
- Etablierung der Kupfer(I)-katalysierten Alkin-Azid [3+2] Zykloaddition als Konjugations Methode für COSS-Grundgerüste
- Entwicklung einer nicht kern-destruktiven Konjugationsmethode
- Nachweis der Methodenanwendbarkeiten mit der Hilfe von kleinen chemischen Liganden („Proof of principle“)
- Konjugation von COSS mit linearen Oligopeptiden
- Konjugation von COSS mit Cystinknoten-Miniproteinen und Sekundärstrukturen ausbildenden Peptiden
- Topologische Studien der erhaltenen Konjugate mit der Hilfe von AFM
- Nachweis der Bioaktivtät der synthetisierten Konjugate
- Erste *in vitro* Experimente mit Peptid-COSS-Derivaten

Der Anwendungsschwerpunkt von COSS-Derivaten in der biomedizinischen Chemie liegt in den Bereichen Arzneimitteltransport,[4, 5] bildgebende Verfahren für die Tumordiagnostik[6] und der Verwendung COSS-basierter Sonden, die z.B. eine Beurteilung von Enzymaktivitäten erlauben.[7, 8] Zum Einschleusen bioaktiver Moleküle in das Zellinnere eignen sich besonders polykationische Partikel. Als prominente Beispiele dafür können der Oktaamino-COSS,[5] aber auch Lysin-[4] bzw. Polyamidoamindendrimere[9] mit Silsesquioxankern genannt werden. Letztere haben besondere Aufmerksamkeit erregt, da sie im Vergleich zu konventionellen Dendrimeren eine erhöhte Frachtkapazität aufweisen.[9] Globuläre, siloxan-basierte Dendrimere finden nicht nur beim Arzneimittetransport Anwendung, sondern auch als MRI Kontrastmittel in bildgebenden Verfahren zur Erkennung von tumorösen Zellen.[10, 11] Verwendung als Sonden finden zum Beispiel fluorierte kubisch-oktamerische Silsesquioxane für ^{19}F-NMR Applikationen,[7, 8] COSS-Ferrocen-Konjugate als Redox-Sensoren[12] oder fluorophormarkierte Derivate.[5, 13]

Es gibt mehrere experimentelle Zugänge zur Synthese biofunktionalisierter kubisch-oktamerischer Silsesquioxane. So sind amino- und chloropropyl-funktionalisierte COSS durch säurekatalysierte Kondensation von Trimethoxysilylethern oder Trichlorsilanen zugänglich.[14, 15] Trotz der langen Reaktionszeit von bis zu sechs Wochen überzeugt die Synthese durch ihre Einfachheit und ihre absolute Reaktionsausbeute im Multigrammmaßstab. Weitere interessante Funktionalisierungen bieten COSS Nanopartikel mit jeweils acht Azido-,[16-19] Aminooxy-,[3] Carbonyl-,[20] Carboxy-,[21] Epoxy-,[22] Hydroxy-[15] oder Vinylfunktionalitäten.[23] Partikel, die gemischte reaktive Gruppen im Verhälnis 1:7 anbieten, kann man über stöchiometrisch kontrollierte Reaktionen erhalten,[24] prinzipiell aber auch durch eine zweistufige Kondensation.[25] Bei dieser Synthesestrategie wird zuerst eine Käfigstruktur mit einer fehlenden Ecke gebildet. Diese Lücke wird in einem zweiten Kondensationsschritt mit Hilfe eines anders modifizierten Monomers geschloßen.

Wasserlösliche COSS-Derivate wurden aufgrund ihrer besonderen symmetrischen Eigenschaften schon seit 1998 als Grundgerüste zur Oligomerisierung von biologisch relevanten Liganden eingesetzt. Damals wurden bereits Oktaamino-COSS (Abbildung 1 d) *via* Amidbindung mit Zuckerlactonen[15, 26] und einzelnen Aminosäuren[27] dekoriert. Die Funktionalisierung mit Oligosacchariden oder funktionalen Peptiden konnte jedoch noch nicht realisiert werden. Für eine vollständige Absättigung der acht reaktiven Funktionalitäten eines COSS muss jeder Kupplungsschritt an jedem einzelnen der bis zu acht zur Verfügung stehenden Arme mit maximaler Effizienz verlaufen. So sinkt die Gesamtausbeute für eine Oktafunktionalisierung auf unter 6 %, wenn man von einer 70 %igen Ausbeute für einen einzelnen Kupplungsschritt ausgeht. Erst die Entwicklung neuer, mit hoher Effizienz verlaufender bioorthogonaler Konjugationsmethoden hat die direkte Ligation von

Biomolekülen mit COSS ermöglicht. Diese Konjugationsverfahren sollen unter anderem folgenden Ansprüchen genügen („Click"-Reaktionen):[28] Hohe Ausbeuten, breite bzw. einfache Anwendbarkeit, keine oder leicht zu entfernende Nebenprodukte, d.h. eine hohe Atomeffizienz und die schnelle Bildung eines einzelnen Produktes.

Eine Reaktion, die alle diese Anforderungen erfüllt, ist die Kupfer(I)-katalysierte Alkin-Azid [3+2] Zykloaddition (CuAAC).[29] Beide verwendete Funktionalitäten weisen einen hohen Grad an Bioorthogonalität auf und lassen sich deshalb z.B. problemlos in bioaktive Peptide mit variierender Seitenkettenkomposition integrieren. Die Azido-Gruppe ist ein Pseudohalogen und kann deshalb durch nukleophile Substitution von bromierten oder iodierten Vorläufermolekülen eingeführt werden.[16, 17] Dementsprechend ist ein Oktaazido-COSS nach einem Halogenaustausch von Chlor nach Brom gut über den leicht zu synthetisierenden Oktachloro-Nanopartikel (Abbildung 1 c) zugänglich. Die erfolgreiche Darstellung dieses würfelförmigen Oktaazido-Grundgerüsts hat nicht nur die Anbindung von Zuckern erleichtert,[17, 19, 30] sondern auch die Verknüpfung mit seitenkettenentschützten und bioaktiven Peptiden (z.B. okta-RGD-Peptid) ermöglicht.[16]

Bei der CuAAC handelt es sich allerdings um eine basen-katalysierte Reaktion, die beim Arbeiten mit biologischen Komponenten normalerweise im wässrigen System durchgeführt wird. In diesem Milieu ist die Stabilität der SNP auf wenige Stunden beschränkt.[31, 32] Dieser Zeitraum erscheint zwar ausreichend um Experimente mit COSS-Konjugaten auszuführen, jedoch kann ihre Synthese mit zunehmender Größe der Liganden wesentlich mehr Zeit in Anspruch nehmen. Der Einsatz eines wasserfreien Reaktionsystem basierend auf aprotischen Lösungsmitteln (z.B. DMF), erlaubt es diesem Problem auszuweichen. Eine weitere elegante Möglichkeit besteht darin, bei der Alkin-Azid [3+2] Zykloaddition auf den Einsatz von Metallkatalysatoren zu verzichten. Dies ist durch die Verwendung reaktiver zyklischer Alkinderivate möglich.[33] Die inherente Spannung in Zyklooctinverbindungen ermöglicht Reaktionen ohne den für biologische Systeme oft schädlichen Kupferkatalysator und ohne die Verwendung von zusätzlicher Base in neutralem gepuffertem Milieu.[33]

COSS weisen in saurer Umgebung die höchste strukturelle Stabilität auf. Deshalb ist der Schritt hin zu einer säurekatalysierten Konjugationsreaktion naheliegend.[31, 32] Eine unter diesen Bedingungen adressierbare Funktonalität stellt der Aldehyd dar. Er zeichnet sich unter anderem durch seine gute Einführbarkeit in peptidische Liganden aus. Entweder wird eine unnatürliche Aminosäure mit geschützter Aldehydfunktion an einer passenden Stelle in der Aminosäuresequenz eingeführt [34, 35] oder es wird *N*-terminal ein Glyoxylrest durch Periodatoxidation eines endständigen Serinrestes generiert.[36]

Als Reaktionspartner versprechen insbesondere Aminooxyverbindungen ($R\text{-}O\text{-}NH_2$) hohe Reaktionsgeschwindigkeiten. Aufgrund ihrer hohen Reaktivität[37] erscheint es sinnvoll, Bausteine mit geschützter Funktionalität zu nutzen[38-40] und diese erst durch saure Abspaltung bei der eigentlichen Kupplung wieder freizusetzen. Die Verwendung eines Adaptermoleküls (z.B. Boc-Aminooxy-essigsäure), das sowohl eine Carbonsäuregruppe als auch eine Aminooxyfunktionalität besitzt, lässt eine simple Modifizierung von Oktaamino-COSS *via* Amidbindung zu.[3] Für die Reaktion können sowohl kommerziell verfügbare mono-Boc- als auch leicht zugängliche ethoxylidengeschützte Aminooxybausteine verwendet werden. Die so mögliche Oximierung von COSS erlaubt deren effiziente Verknüpfung mit Peptiden mit bis zu 35 Aminosäuren z.B. $[KVSALKE]_5$. Die Anzahl an verknüpfbaren Liganden wird in solchen Fällen nicht mehr allein durch die Reaktionsgeschwindigkeit beschränkt sondern vielmehr durch die sterische bzw. elektrostatische Abstoßung der Liganden untereinander.[3]

Mit dieser Arbeit wurden verschiedene experimentelle Zugänge für die Synthese biofunktionalisierter COSS erschlossen. Ein erstes Beispiel der Beeinflussung eines zentralen zellulären Prozesses (DNA-Replikation in höheren Zellen) zeigt das Anwendungspotential dieser Nanopartikel (Kapitel 3.3). Das Forschungsfeld der biofunktionalisierten COSS wird im nachfolgenden Review-Artikel im Detail ausgeführt. Auf die originalen Arbeiten mit Bezug zu dieser Thematik wurde bereits hingewiesen (unterstrichene Zitate). Eine zusätzliche Arbeit beschreibt eine konzeptionelle Vorarbeit zur Synthese von alkoholischen und aldehydischen Partikeln durch Biotransformation halogenierter COSS durch Haloalkandehalogenasen (Kapitel 3.4).

Weitere auf Seite iv aufgelistet Arbeiten haben keinen direkten Bezug zur Kernthematik der Dissertation und wurden deshalb nicht abgedruckt.

Referenzen

1. W. R. Algar, D. E. Prasuhn, M. H. Stewart, T. L. Jennings, J. B. Blanco-Canosa, P. E. Dawson and I. L. Medintz, *Bioconjugate Chem.*, 2011, **22**, 825-858.
2. D. B. Cordes, P. D. Lickiss and F. Rataboul, *Chem. Rev.*, 2010, **110**, 2081-2173.
3. S. Fabritz, S. Hörner, D. Könning, M. Empting, M. Reinwarth, C. Dietz, B. Glotzbach, H. Frauendorf, H. Kolmar and O. Avrutina, *Org. Biomol. Chem.* , 2012, **10**, 6287-6293.
4. T. L. Kaneshiro, X. Wang and Z. R. Lu, *Mol. Pharm.* , 2007, **4**, 759-768.
5. C. McCusker, J. B. Carroll and V. M. Rotello, *Chem. Commun.*, 2005, 996-998.
6. M. Q. Tan, X. M. Wu, E. K. Jeong, Q. J. Chen, D. L. Parker and Z. R. Lu, *Mol. Pharm.* , 2010, **7**, 936-943.
7. K. Tanaka, N. Kitamura and Y. Chujo, *Bioorgan Med. Chem.*, 2012, **20**, 96-100.
8. K. Tanaka, N. Kitamura, K. Naka and Y. Chujo, *Chem. Commun.*, 2008, 6176-6178.
9. K. Tanaka, K. Inafuku, K. Nakab and Y. Chujo, *Org. Biomol. Chem.*, 2008, **6**, 3899-3901.
10. M. Q. Tan, X. M. Wu, E. K. Jeong, Q. J. Chen and Z. R. Lu, *Biomacromolecules*, 2010, **11**, 754-761.
11. M. Tan, S. M. Burden-Gulley, W. Li, X. Wu, D. Lindner, S. M. Brady-Kalnay, V. Gulani and Z. R. Lu, *Pharm. Res.*, 2012, **29**, 953-960.
12. K. Tanaka, N. Kitamura, Y. Takahashi and Y. Chujo, *Bioorgan. Med. Chem.*, 2009, **17**, 3818-3823.
13. K. Y. Pu, K. Li and B. Liu, *Adv. Mater.*, 2010, **22**, 643-646.
14. U. Dittmar, B. J. Hendan, U. Florke and H. C. Marsmann, *J. Organomet. Chem.*, 1995, **489**, 185-194.
15. F. J. Feher, K. D. Wyndham, D. Soulivong and F. Nguyen, *J. Chem. Soc. Dalton*, 1999, 1491-1497.
16. S. Fabritz, D. Heyl, V. Bagutski, M. Empting, E. Rikowski, H. Frauendorf, I. Balog, W. D. Fessner, J. J. Schneider, O. Avrutina and H. Kolmar, *Org. Biomol. Chem.* , 2010, **8**, 2212-2218.
17. D. Heyl, E. Rikowski, R. C. Hoffmann, J. J. Schneider and W. D. Fessner, *Chem.-Eur. J.* , 2010, **16**, 5544-5548.
18. V. Ervithayasuporn, X. Wang and Y. Kawakami, *Chem. Commun.*, 2009, 5130-5132.
19. B. Trastoy, M. E. Perez-Ojeda, R. Sastre and J. L. Chiara, *Chem.-Eur. J.*, 2010, **16**, 3833-3841.
20. B. W. Manson, J. J. Morrison, P. I. Coupar, P. A. Jaffres and R. E. Morris, *J. Chem. Soc. Dalton*, 2001, 1123-1127.
21. A. Boullanger, G. Gracy, N. Bibent, S. Devautour-Vinot, S. Clement and A. Mehdi, *Eur. J. Inorg. Chem.* , 2012, 143-150.
22. R. M. Laine, J. W. Choi and I. Lee, *Adv. Mater.*, 2001, **13**, 800-803.
23. H. Xu, B. Yang, J. Wang, S. Guang and C. Li, *J. Polym. Sci. Part A: Polym. Chem.*, 2007, **45**, 5308-5317.
24. F. J. Feher, K. D. Wyndham, R. K. Baldwin, D. Soulivong, J. D. Lichtenhan and J. W. Ziller, *Chem. Commun.*, 1999, 1289-1290.
25. J. F. Brown and L. H. Vogt, *J. Am. Chem. Soc.* , 1965, **87**, 4313-4317.
26. F. J. Feher, K. D. Wyndham and D. J. Knauer, *Chem. Commun.*, 1998, 2393-2394.
27. F. J. Feher, K. D. Wyndham, M. A. Scialdone and Y. Hamuro, *Chem. Commun.*, 1998, 1469-1470.
28. H. C. Kolb, M. G. Finn and K. B. Sharpless, *Angew. Chem.-Int. Edit.*, 2001, **40**, 2004-2021.
29. V. V. Rostovtsev, L. G. Green, V. V. Fokin and K. B. Sharpless, *Angew. Chem.-Int. Edit.*, 2002, **41**, 2596-2599.
30. B. Trastoy, D. A. Bonsor, M. E. Pérez-Ojeda, M. L. Jimeno, A. Méndez-Ardoy, J. M. García-Fernández, E. J. Sundberg and J. L. Chiara, *Adv. Funct. Mater.*, 2012, DOI: 10.1002/adfm.201200423
31. J. Henig, E. Toth, J. Engelmann, S. Gottschalk and H. A. Mayer, *Inorg. Chem.* , 2010, **49**, 6124-6138.
32. E. Rikowski and H. C. Marsmann, *Polyhedron*, 1997, **16**, 3357-3361.
33. J. M. Baskin, J. A. Prescher, S. T. Laughlin, N. J. Agard, P. V. Chang, I. A. Miller, A. Lo, J. A. Codelli and C. R. Bertozzi, *P. Natl. Acad. Sci. USA*, 2007, **104**, 16793-16797.
34. T. Groth and M. Meldal, *J. Comb. Chem.*, 2001, **3**, 34-44.
35. J. C. Spetzler and T. Hoeg-Jensen, *J. Pept. Sci.*, 2001, **7**, 537-551.
36. K. F. Geoghegan and J. G. Stroh, *Bioconjugate Chem.*, 1992, **3**, 138-146.
37. A. Dirksen, T. M. Hackeng and P. E. Dawson, *Angew. Chem.-Int. Edit.* , 2006, **45**, 7581-7584.
38. I. P. Decostaire, D. Lelievre, H. Zhang and A. F. Delmas, *Tetrahedron Lett.*, 2006, **47**, 7057-7060.
39. S. Foillard, M. O. Rasmussen, J. Razkin, D. Boturyn and P. Dumy, *J. Org. Chem.*, 2008, **73**, 983-991.
40. V. Dulery, O. Renaudet and P. Dumy, *Tetrahedron Lett.*, 2007, **63**, 11952-11958.

3D Visualisierung: QuteMol, M. Tarini, P. Cignoni, C. Montani, *IEEE T. Vis. Comp. Gr.*, 2006, **12** ,1237-1244.

2. Einleitung

2.1. Bioconjugation on Cube-Octameric Silsesquioxanes

Sebastian Fabritz, Sebastian Hörner, Olga Avrutina and Harald Kolmar

Org. Biomol. Chem., 2013,**11**, 2224-2236
DOI: 10.1039/C2OB26807H
Received 14 Sep 2012, Accepted 23 Oct 2012
First published on the web 24 Oct 2012

Graphical Abstract:

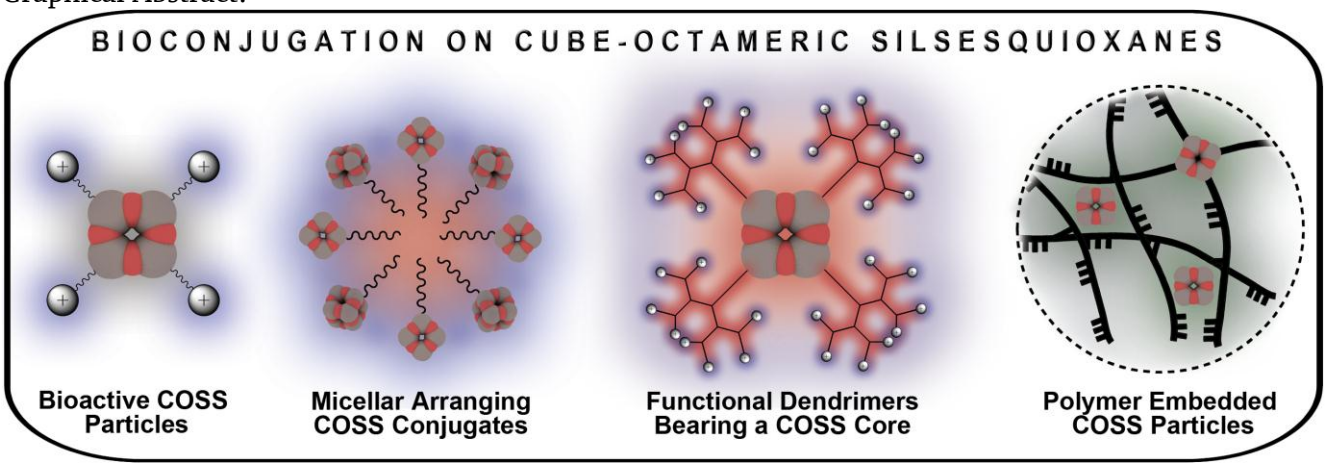

Short Summary:
Cube-octameric silsesquioxane species suitable for bioconjugation and the expanded arsenal of respective conjugation methods are described. Relevant COSS characteristics and the application of COSS derivatives in biological systems are discussed.

Organic & Biomolecular Chemistry

Dynamic Article Links ►

Cite this: DOI: 10.1039/c0xx00000x

www.rsc.org/xxxxxx

PERSPECTIVE

Bioconjugation on Cube-Octameric Silsesquioxanes

Sebastian Fabritz‡*, Sebastian Hörner‡, Olga Avrutina and Harald Kolmar

Received (in XXX, XXX) Xth XXXXXXXXX 20XX, Accepted Xth XXXXXXXXX 20XX

DOI: 10.1039/b000000x

Small, compact, and highly symmetric cube-octameric silsesquioxanes have recently attracted increased attention as scaffolds for tailor-made bioconjugates. The expanded arsenal of effective conjugation methods (CuAAC, TEC, oxime ligation) allow one to decorate these nanoparticles bearing up to eight addressable organic substituents, with a wide range of biorelevant ligands, among them carbohydrates, peptides, miniproteins, reporter molecules, and rare-earth chelates. Low toxicity of COSS-based molecules combined with solubility in aqueous systems and half-life sufficient for *in-vivo* studies make these structures attractive targets for a number of applications, among them drug delivery, tumor diagnostics and therapy.

1 Introduction

Cube-octameric silsesquioxanes (COSS) widely used in fine-tuned polymeric compositions (the topic is reviewed in [1-3]), have recently found biochemical application in their monomeric form. A broad range of COSS-based hybrid systems has been developed, which are used in drug development, delivery, and diagnostics.[4-6] Currently, bio-inspired research taking advantage of these versatile scaffolds is a fast-growing field, and it seems like the era of COSS has just begun.

COSS belong to the group of silica nanoparticles and are highly symmetric hybrid molecules comprising an inorganic core composed of silicon and oxygen. Every silicon atom is linked to an organic residue allowing for further modifications. The molecular composition of silsesquioxanes, first reported in 1874,[7] is given by the empirical formula $(RSiO_{1,5})_{2n}$ where n is an integer and R substitutes hydrogen or aliphatic organic groups.[8, 9] Silsesquioxanes bearing pendant functional groups have been first synthesized in the 1990th by hydrolytic condensation of organosilicon monomers $RSiX_3$ (Fig. 1, R = organic residue; X = halogen or alkoxide).[10, 11] Today, fine-tuned experimental procedures employing tetra-*n*-butylammonium fluoride[12] or di-*n*-butyltin dilaurate[13] as a catalyst allow for multigram production of COSS within several days.

Polyhedral silsesquioxanes are classified depending on either the number of silicon atoms within their core (T_6, T_8, T_{10}, T_{12},... T_n; T stands for a silicon atom bearing three oxygens also connected to silicon) or according to their geometry (octahedral, decahedral, etc.). Interestingly, the cubic cage architecture is favoured in organo-silsesquioxanes due to steric effects,[12] while silsesquioxanes bearing small organic residues form polyhedrals with n = 10, 12, 14, and 16.[8, 9]

To date, two approaches are generally applied to the synthesis of functional COSS derivatives. Functional moieties can be introduced upon corner capping of incompletely condensed COSS cores[14] (see section 3.1) or, alternatively, an intact T_8 cage can be modified towards COSS derivatives with tailor-made reactive moieties. Improvements of synthetic strategies allowing for the manipulation of pendant organic groups (see section 2 and 3), as well as recent commercial availability of a wide range of silsesquioxane monomers have contributed to the rapid development of COSS chemistry within the last decades.

Clemens-Schöpf Institute of Organic Chemistry and Biochemistry, Technische Universität Darmstadt, Petersenstr. 22, 64287 Darmstadt, Germany. Email: SFabritz@Biochemie-TUD.de

‡ These authors contributed equally to this work.

Sebastian Fabritz

Sebastian Fabritz, born 1982, studied Chemistry in Darmstadt and spent an academic year at the University of Bristol, UK. He received the Dr. Anton Keller Foundation award for exceptional achievements in the diploma chemist main exams. He is currently at the final stage of his PhD thesis dealing with biofunctionalization of COSS under supervison of Prof. Harald Kolmar.

Sebastian Hörner

Sebastian Hörner, born 1982, studied chemistry at the Technische Universität Darmstadt and spent an academic year at the University of Alcalá de Henares (Spain). Actually he is working on his PhD thesis focused on bioconjugations on nanoparticle scaffolds, under supervision of Prof. Harald Kolmar.

2 Functionalization of COSS scaffolds

Several different approaches for the functionalization of the inorganic COSS core have been reported to date (reviewed in [15]). Although the main efforts in this field are aimed at the derivatization of fully condensed COSS particles, chemical modifications of their monomeric precursors are known as well.[16] To date, the condensation of commercially available halo- or aminopropyl-substituted alkoxysilanes is the most popular method as it provides diverse COSS particles allowing for the variation of their pendant functional residues. Indeed, taking the octachloropropyl COSS as a starting compound, a number of functional groups can be introduced by nucleophilic substitution, among them azides,[17-19] nitriles,[20] thiocyanates,[11] as well as bromides[18] and iodides.[11] These groups allow for further modifications towards e.g. carboxylic acids[20] or alcohols.[21]

Another versatile COSS particle is the 3-aminopropyl-substituted one. Besides direct conversion into azides,[22, 23] carboxylates,[21] and alkenes,[21] various functionalities could be introduced onto this framework by amide coupling using respective derivatives of carboxylic acids.[21, 24] Finally, octaphenyl silsesquioxanes allow for the incorporation of aminophenyl, azidophenyl,[25] carboxyphenyl,[26] and maleimidophenyl[27] groups by aromatic nitration with subsequent hydrogenation followed by further modifications. COSS modifications resulting in addressable functional groups are listed in Table 1.

Interestingly, several enzymes have been recently identified which are able to catalyze siloxane bond formation.[28-30] Enzyme-mediated modifications of COSS ligands have been reported by Ihara *et al.*[28-31] Hence, transformations employing enzymatic catalysis can be considered as interesting alternatives to chemical methods that merit further exploration.

Starting from hydrido-silsesquioxanes as the simplest COSS derivatives, epoxides[32] and nitriles[11] can be installed in the siloxane framework upon hydrosilation using alkene-bearing building blocks. In the same manner olefinic residues carrying epoxide[32, 33] groups can be incorporated into spherosilicates, COSS-like particles bearing additional eight silicon atoms (Fig. 2, Q8 particles). The introduced epoxide moieties allow for a subsequent transformation into hydroxy, azide, or nitrophenyl functionalities by oxirane ring-opening reaction.[33] *Vice versa*, silicon-bearing benzaldehyde building blocks can be attached to olefinic COSS derivatives.[34]

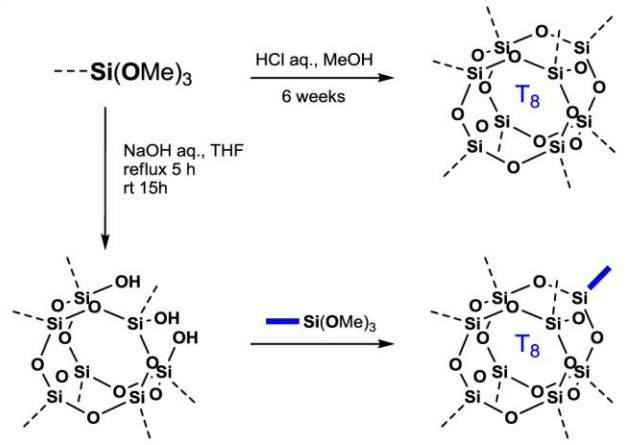

Fig. 1 Organosilicon monomers SiX_3 (exemplary depicted as methoxy derivative) can be condensed to form a cube-like cage structure. The formation of a desired condensation product is solvent- and time dependent and can be therefore controlled.[11, 14] Incompletely condensed COSS allow for the introduction of a heterogeneous residue at one corner of the cage. Dotted and fat blue bonds depict organic ligands.

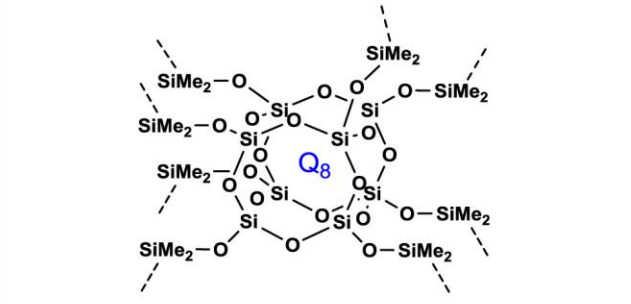

Fig. 2 Schematic depiction of a Q_8 silica partile. Q indicates that each core silicon atom features four oxygen interactions. Dotted bonds depict organic ligands.

3 Bioorthogonal functionalized COSS scaffolds

3.1 Homofunctional COSS scaffolds

COSS scaffolds that allow for bioconjugations are listed in Table 1. For biochemical applications, azidopropyl-functionalized COSS are widely used (see section 7) as they are bioorthogonally addressable either *via* the copper-catalyzed azide-alkyne cycloaddition (CuAAC)[35] or by the strain-promoted cycloaddition (SPAAC)[36] employing cyclooctyne derivatives. Alternatively, the

Olga Avrutina

Olga Avrutina,, born 1970, studied chemistry in Belarusian State University (Minsk). In 2006, she completed her doctorate under supervision of Prof. Ulf Diederichsen at Georg-August-Universität Göttingen. She is currently working in the research group of Prof. Harald Kolmar. Her interests focus on design and synthesis of bioactive multivalent peptides and proteins.

Harald Kolmar

Harald Kolmar, born 1961, is full professor at the Technische Universität Darmstadt, where he heads since 2005 the Department of Applied Biochemistry. His current scientific interests mainly focus on protein engineering and design, nanobiotechnology, chemical biology and development of tailor-made peptides for applications in diagnostics and therapy.

oxime ligation turned out to be an particularly powerful method for the oligomerization of aldehyde-bearing ligands on a COSS scaffold.[24] Aminooxy moieties can be grafted onto octaaminopropyl COSS by amide coupling using a respective carboxylic acid derivative.[24] Oximation provides the selectivity required for biochemical applications, addressing bioorthogonal aldehyde or ketone groups[37] which can be easily incorporated into peptides and proteins by mild sodium periodate oxidation of *N*-terminal serine residues.[38] *Vice versa*, aldehyde-bearing silsesquioxanes[34] can be considered as potential candidates for the conjugation with aminooxy-decorated biomolecules. Another substituted silsesquioxane is the octavinyl COSS as it can be addressed *via* thiol-ene[39] or cross-coupling reactions.[40]

Apart from the discussed amine, azide, and vinyl substituents which have already demonstrated their utility for COSS-based ligations with biomolecules, a number of other functional moieties were applied for bioconjugations. Thus, introduction of epoxides allows for the reaction with amine- or hydroxyl-bearing coupling partners *via* nucleophilic ring opening,[41] while maleimide-functionalized COSS could be decorated with substituted thiols through the formation of stable thio-ethers.[27] Additionally, innovative bioorthogonal coupling strategies as the inverse electron-demand Diels-Alder reaction[42] could contribute to the tool set of COSS-based bioconjugations.

3.2 Heterofunctional COSS scaffolds

Bifunctional COSS derivatives combining two selectively addressable functionalities can be generated either by stoichiometrically controlled single-corner ligation on a fully condensed particle or *via* the corner capping of incompletely condensed COSS. Resulting molecules can be used as starting point for the design of compounds with higher structural hierarchy and peculiar properties. Vinyl-modified silsesquioxanes are especially suited for the synthesis of heterobifunctional COSS constructs as vinyl groups are bioorthogonal (Fig. 3). Recently, COSS molecules bearing seven vinyl and one hydroxyethyl substituent have been synthesized by stoichiometrically controlled reactions.[43] Thus, to a single-corner hydroxy group of heptavinyl COSS a hydrophobic polymer was attached upon polymerization. Subsequent modification of the remaining seven alkenes with hydrophilic moieties such as alcohols,[44, 45] carboxylic acids,[44, 46] or carbohydrates[44] resulted in a number of amphiphilic siloxane derivatives which exhibit potentially useful biophysical properties.[44] Moreover, fluorescent dyes and amino acids have been single-corner grafted onto azide[18]- or amine[4, 47]-bearing COSS. The resulting conjugates are of particular interest for biomedical microscopic studies. [4, 47]

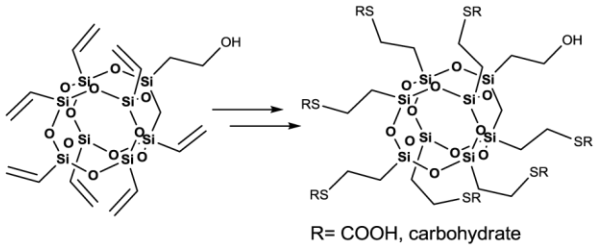

Fig. 3 Heptavinyl hydroxyethyl COSS is a heterobifunctional scaffold allowing for additional functionalization *via* thiol-ene click reactions.

Bifunctional COSS may serve as scaffolds for the oligomerization of bioactive molecules, such as peptides and carbohydrates, allowing for the additional attachment of reporter molecules. Therefore, they are well-suited for e.g. theranostic *in-vivo* studies.

The addition of functional groups to partially condensed COSS using the corner-capping approach is limited to the modification of aliphatic- and aromatic-substituted cages and results in single-corner-functionalized scaffolds bearing carboxy,[48] halogen,[48] azide,[48] amine[49] or hydroxy[48] groups. Additionally, it appeared possible to cap multiple corners of COSS with monomeric building blocks that bear functional molecules as e.g. fluorescein. Thus, cell-penetrating fluorescein-labeled, heterobifunctionalized aliphatic COSS particle comprising an additional amino or carboxy site for successive attachment of cargo molecules was examined in microscopic studies on human cancer cells.[50]

Today, incompletely condensed cages and suitable monomers bearing a broad range of functional groups are commercially available (Hybrid Plastics Inc., USA; SiKÉMIA, France). Therefore, the modular approach to the synthesis of novel heterobifunctional COSS derivatives becomes possible.

Finally, the application of heterobifunctional COSS can be extended if heterodimeric COSS conjugates are considered. Li *et al.* recently approached this strategy by fusing an aliphatic and a vinylic COSS through esterification using a dicarboxy linker.[51]

4 Hydrolytic stability of COSS particles

A remarkable feature of the COSS cage is its stability that is highly dependent on the environment. Although the rigid inorganic core endows COSS with chemical and thermal robustness,[49] the nature of its corner substituents crucially influences the stability, i.e. integrity of the whole framework. Considering the latter issue, it is essential to distinguish between cage rearrangement and its breakdown.

Rearrangement of a T_8 cage to T_{10} and T_{12} structures was observed in potassium carbonate or sodium hydroxide solutions, where the tendency to undergo such rearrangements seemed to correlate with the electronegativity of a terminal moiety X within the pendant ligands in octa(3-X-propyl) COSS (X = H < I < C_6F_6 < Br < Cl < NCS).[52]

As the inorganic core of COSS is formed upon a condensation under acidic conditions, the incubation in basic medium might cause hydrolytic decomposition of the system. Furthermore, it was shown that amines accelerate the degradation of COSS in wet solvents.[21] Therefore, it is advisable to use dry organic solvents or acidic aqueous media for silsesquioxane reactions or storage. Interestingly, the breakdown of aminopropyl-substituted siloxanes has been suggested to follow a back-bite mechanism. In this case, the amino groups themselves may intramolecularly attack the core, thus promoting decomposition.[21]

In recent years, extensive studies concerning the half-life of different monomeric COSS derivatives and their breakdown products were performed. The degradation of carbohydrate-functionalized COSS in different buffer systems under different pH was studied. Both, the buffer composition and the pH were found to influence the half-life of the COSS scaffold. In 4-(2-hydroxyethyl)-1-piperazineethanesulfonic acid (HEPES) buffer at pH 6.55 the degradation was completed within 48 hours as

Table 1 Alphabetical list of of COSS scaffolds allowing for bioconjugation.

Ligand/functionality	Precursor	Applied reaction	Yield	Subsequent conjugation chemistry	Year	Ref.
α-β unsaturated carboxylic acid	octaammonium	anhydride opening	64%	amide coupling/esterification	1999	[21]
acetophenon	octaphenyl	Friedel-Crafts reaction	n.d.	oxime ligation	2012	[26]
allyl	octaammonium	addition	90%	cross-metathesis/hydrosilylation/thiol-ene	1999	[21]
amine	monomer	condensation	93%	amide coupling/S_N	2005	[53]
amine (hydrochloride)	monomer	condensation	30%	amide coupling/S_N	1998	[54]
aminooxy	octaammonium	amide coupling	4-33%	oxime ligation	2012	[24]
aminophenyl	octaphenyl	nitration/hydrogenation	68%	amide coupling/S_N	2011	[25]
azide	octaiodo	S_N	90%	CuAAC/SPAAC/Staudinger ligation	2010	[19]
azide	octaammonium	diazotransfer	60-73%	CuAAC/SPAAC/Staudinger ligation	2010	[22, 23]
azide	Q8	Hydrosilylation/oxirane opening	90-91%	CuAAC/SPAAC/Staudinger ligation	2012	[33]
azidophenyl	octaaminophenyl	diazotation/S_N	76%	CuAAC/SPAAC/Staudinger ligation	2012	[25]
benzaldehyde	octavinyl	hydrosilylation	92%	Schiffs base formation	2001	[34]
bromo	octachloro	S_N	91%	S_N/Grignard/cross-coupling	2010	[18]
carboxylic acid	octaammonium	anhydride opening	58%	amide coupling/esterification	1999	[21]
carboxylic acid	octanitrile	hydrolysis	quant.	amide coupling/esterification	2012	[20]
carboxyphenyl	octaphenyl	Friedel-Crafts reaction	85%	amide coupling/esterification	2012	[26]
chloro	monomer	condensation	25-35%	S_N/Grignard	1995/2008	[11, 13]
epoxide	monomer	condensation	n.d.	oxirane opening	2006	[55]
epoxide	Q8	Hydrosilylation	> 80%	oxirane opening	2001	[32]
hydroxy	octaammonium	amide coupling	23%	esterification/ether bond formation/S_N	1999	[21]
hydroxy	octaiodo	nitration/hydrogenolysis	85%	esterification/ether bond formation/S_N	1999	[21]
iodo	octachloro	Finkelstein reaction	quant.	S_N/Grignard/cross-coupling	1995	[11]
iodophenyl	octaphenyl	iodination	80-90%	S_N/Grignard/cross-coupling	2010	[56]
maleimidephenyl	octaaminophenyl	dehydration	79%	thioether formation	2001	[27]
nitrile[a]	octachloro	S_N	98%	hydrolysis/hydration	2012	[20]
nitrile[a]	octahydrido	hydrosilylation	93%	hydrolysis/hydration	1995	[11]
nitrophenoxy[b]	octaepoxy	oxirane opening	99%	hydration	2012	[33]
nitrophenyl[b]	octaphenyl	nitration	90%	hydration	2001/2011	[25, 27]
sulfhydryl	monomer	condensation	> 50%	thioether/disulfide formation	1995	[11]

[a] Precursor for carboxy-functionalized COSS, [b] precursor for amine-functionalized COSS.

determined by comparison of ^{29}Si-NMR shifts. In contrast, at pH 7.20 the signal corresponding to the breakdown products was found already after 21 hours. In phosphate buffer at pH 6.35 degradation occurred much faster and was completed within 24 hours.[57] More detailed studies that extended analytics to the breakdown products of COSS were performed using silsesquioxanes decorated with macrocyclic Gd^{3+} chelates (2D ^{1}H, ^{29}Si HSQC-NMR, ESI-MS and relaxivity measurements). At pH 7.0 in deuterated water NMR signals corresponding to the completely degraded species were observed only after 7 days. Further core stability tests were based on water relaxivity measurements that quantified the rigidity of the core-attached Gd^{3+} chelates. Combination with ESI-MS measurements provided detailed insights into the degradation of the core. In aqueous solution at pH 7.0 the MS signal corresponding to the intact COSS species faded within 48 h. After 14 days a complex mixture of partially degraded COSS was formed. For complete degradation at neutral pH it was necessary to heat the mixture to 75 °C for several days.[58] A further test that was performed under physiological conditions (HEPES buffer, pH 7.4-7.6, 37 °C) with and without fetal calf serum (FCS) indicated no additional destabilization of COSS caused by enzymatic degradation.

Relaxivity measurements showed a first-order exponential decay corresponding to a half-life of 11- 18 h for these special COSS derivatives. A plateau indicating no further degradation was reached after 5 days. These experiments clearly showed that the stability of COSS famework is pH dependent as its half-life was dramatically shortened to about 55 min when measured in solution at pH 8.1 - 8.6.[58]

The tunable decomposition of COSS has been exploited for the synthesis of biodegradable polymers as poly(L-lactide),[59, 60] polycaprolactone, and polycarbonate polyurethane.[61] They were found to degrade faster when aliphatic COSS substituents have been incorporated into the framework.[59, 60] However, the presence of COSS units in these polymers was supposed to have a stabilizing effect in the case of enzyme-mediated degradation.[61]

In conclusion, the hydrolytic stability of the COSS core depends on its ligands and the chemical environment, e.g. applied solvent or buffer system. Hence, a crude estimation of the integrity of novel COSS compounds is possible, but stability tests in each particular case should be conducted.

5 Cell toxicity of COSS

As COSS derivatives are potential scaffold molecules or drug carriers for *in vivo* applications, the biocompatibility of COSS and its breakdown products is an important issue.

COSS precursors, monomeric primary silsesquioxanes, are known to possess low *in vitro* and *in vivo* toxicity.[62] Therefore, low toxicity of the silsesquioxane component of a COSS particle may be assumed. Nevertheless, the nature of ligands attached to a COSS core may influence its toxicity. For the assessment of toxicological risks of COSS derivatives from literature data it is essential to note that the direct comparison is not possible due to the distinct assay setups (choice of cell line, incubation times, etc.). Hence, we strongly recommend an independent and comprehensive evaluation of the toxicity of novel COSS compounds, as even within one cell line toxic concentrations differ depending on external stimuli as e.g. hormone concentration.[63]

Although *in vivo* toxicity of COSS derivatives has not been studied extensively to date, potential risks depending on the nature of the COSS derivative and the initial concentration may be ascertained based on *in vitro* assays. For example, the effect of 3-aminopropyl-substituted COSS on the Cos-1 cells was quantified using a cell vitability test. Incubation with COSS taken at different concentrations (0.05 mM to 1 mM) did not lead to decreased enzyme activity within 36 hours, indicating low or no toxicity.[4] However, in another study, HeLa cells were incubated with a single-corner cysteine-modified 3-aminopropyl COSS and an IC_{50} was determined as 70 µM.[47]

In addition to monomeric silsesquioxanes, the toxicity of COSS-based amphiphiles and COSS-containing polymers has been extensively analyzed. COSS-derived amphiphiles showed low toxicity in NIH/3T3 and L929 cells as indicated by an MTT cell viability test.[64, 65] Hydrido-COSS copolymers used in tissue engineering and cell culture have demonstrated low toxicity in MC3T3-E1[66] and human stem cells[67] as well. Both the copolymer and its degradation products did not affect cell growth and viability.

6 Self-assembly of COSS

Aggregation of biomolecules is supposed to play a crucial role in a number of pathologic disorders, e.g. neurodegenerative diseases. On the other hand, important biological processes, among them cell penetration, may be governed by the formation of highly ordered structures from monomeric precursors.[68, 69] The implementation of tailor-made ordering segments into bioactive molecular blocks may influence the shape of the resulting structures, thus stimulating the formation of ordered aggregates. The effect of an individual component is therefore enhanced.[70] Indeed, Bode *et al* have recently shown that aggregation of small cationic peptides multiplied their efficiency upon cell penetration.[71]

Due to their unique structure, COSS provide additional ordering effects during self-assembly. Thus, linear and dendrimer-like assemblies of silsesquioxane monomers were observed upon crystallization.[47, 72] These findings are in accordance with theoretical studies which propose a particular mode of interacion between COSS molecules resulting in face-to-face stacking.[73, 74] Being one of energetically preferable siloxane modifications, the cubic core of COSS is formed spontaneously from amorphous Si. Therefore, this modification could be essential for biological processes aiming at the construction of diverse silica frameworks.[75] Moreover, COSS can potentially serve as building blocks for the controlled assembly of nanoscale structures possessing different architectures.[76] Recent publications reported the synthesis of nanostructured hybrid materials with distinct characteristics that are attributed to the ordering effect of COSS.[51, 77] Potential applications of COSS-based amphiphilic nanostructures as drug delivery units are detailed in section 8.

7 COSS-based bioconjugations

Over the years, an increasing number of COSS-based bioconjugates has been reported that are listed in Table 2.

7.1 Carbohydrates

Molecular interactions and cell signalling in living cells involve a range of small- to medium-sized molecules, often presented in multiple copies. Therefore, COSS particles offering eight (or more) conjugation sites are viable molecular scaffolds for oligomerization of peptides and carbohydrates. Thus, the eightfold presentation of gluco- or mannosyl residues on a COSS core allowed for an efficient synthesis of glycoclusters. These spherical macromolecules enable, for example, the investigation of structural, thermodynamic, kinetic and mechanistic aspects of lectin[78]-carbohydrate interactions. Feher *et al.* reported a pioneering work in the field of COSS-based glycoclusters, having synthesized octagalactose and –maltose frameworks.[21] The reaction of carbohydrate lactones with octaamino COSS resulted in a respective glycocluster, albeit in a moderate yield (26-53%), within 24-72 h. Hence, improved synthetic routes towards the synthesis of COSS glycoclusters were established. In 2004, the photoactivated conjugation of thiol-terminated glycoside residues to the cubic silsesquioxane (66-70% yield) was reported.[79] Six years later, the research groups of Chiara and Fessner further improved coupling efficacies by using CuAAC.[19, 22, 57] Taking the sensitivity of a COSS core into account (see section 4), a biphasic

base-free $CuSO_4$/sodium ascorbate system was found to perform best (~80% yield, 2-36 h). Finally, Dondoni and coworkers could perfect the conjugation of carbohydrates and T_8 silsesquioxanes applying the photoinduced free-radical thiol-ene coupling (TEC).[39]

The bioactivity of COSS-derived glycoclusters was generally validated *via* lectin precipitation[19, 57, 80] or inhibition.[39, 57, 79] Yet, the recent contribution to this field by Trastoy *et al.*[57] allowed for further understanding of COSS-glycocluster-lectin interactions. The comparison between the lectin binding properties of two octamannosyl COSS derivatives with maximal ligand distances of ~25 Å (Fig. 4) and ~50 Å (PEG linker applied) allowed not only for an evaluation of the sterical accessibility of ligands presented on a COSS core, but also for an assessment of the increased binding affinities achieved *via* eightfold presentation of the ligands.[57]

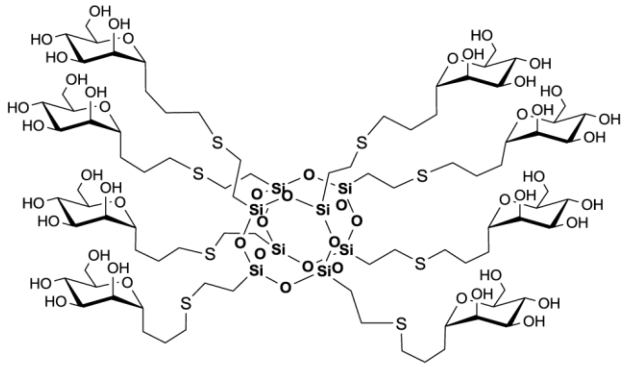

Fig. 4 Mannopyranoside glycocluster synthesized *via* photoinduced free-radical thiol-ene coupling of the respective glyco-thiol and octavinyl COSS.[39]

Although the covalent attachement of carbohydrates is most common, examples for the non-covalent presentation of sugar derivatives on cube-octameric silsesquioxanes are noteworthy. They are generally based on cyclodextrin (CD) host-guest interactions, e.g. rotaxane formation *via* complexation of PEGylated COSS with α-CDs[81] or on exploiting the interaction of adamantan silsesquioxanes[19] and β-CDs.[65] The latter allows for the formation of supramolecular amphiphiles that might be applicable in tissue engineering and cell culture by promoting adhesion and proliferation of cells.[65]

7.2 Peptides/ amino acids

The presentation of amino acids and peptides in multiple copies on a defined scaffold allows for the targeting of diverse biological functions, e.g. cell surface receptors or enzymes. They can be added to a scaffold using either a divergent or a convergent approach. The first one is usually based on amide chemistry. Thus, an excess of a benzotriazole-activated amino acid and a hindered nitrogenous base (e.g. *N*,*N*-diisopropylethylamine) in an aprotic solvent are added to an amine-functionalized COSS scaffold (water and humidity must be excluded). Straightforward examples for divergently synthesized amino acid-bearing silsesquioxane are the functionalization of COSS with single amino acids[82] and the generation of lysine dendrimers comprising cube-octameric silsesquioxanes as a core unit (see also section 7.3).[83]

For the convergent attachement of peptides directly to the nanoparticle only highly effective conjugation chemistry is applicable. Considering 85 % conversion for a single ligation, the respective overall yield for the octa-functionlization of silsesquioxanes drops to 27 %. Therefore, only reactions that allow for full conversion are recommended for the functionalization of COSS. Click reactions, as defined by Sharpless and co-workers in 2001,[84] easily comply with this requirement. Hence, it is not surprising that the first direct coupling of a biologically relevant peptide was conducted applying the CuAAC[18] on an octaazido COSS scaffold. [17-19, 22] Within the last two years not only the application of the CuAAC was optimized for the COSS conjugations,[57] but also a new set of biocompatible ligations was established. LoConte *et al.* used the photoinduced free-radical thiol-ene coupling to attach a tetrapeptide RGDC.[39] Additionally, the conjugation of a heptadecapeptide to a cysteine-bearing silsesquioxane *via* disulfide bond formation appeared possible.[47] Taking the sensitivity of COSS towards nucleophiles into account (see section 4), acid-catalyzed reactions are preferable over base-catalyzed conjugation methods. Hence, COSS bearing aminooxy functionalities were developed.[24] These particles readily react with aldehydes and allow for the multiple presentation of diverse peptide-based ligands, among them a derivative of antimicrobial peptide jelleine, a three-disulfide trypsin inhibitor MCoTI (Fig. 5), or a 35 amino acid K-coil peptide, a possible interface for non-covalent protein binding.[24] The aminooxy-based conjugation chemistry might also be exploited to decorate cubic siloxanes with cancer-targeting peptides and reporter molecules, e.g. DOTA (see section 9) promising its future pharmaceutical use as a biodegradable scaffold.

Considering the novelty of functional peptide-COSS conjugates, the actual research is focused on proof-of-principle experiments, and biological applications are limited. Noteworthy are efforts to elucidate hierarchical self-assembly processes of peptidic COSS.[24, 64, 77, 85, 86] These can be exploited to form e.g. vesicles using lipid surrogates[86] or peptisomes that mimic viral capsids[64] allowing for new approaches towards drug delivery.

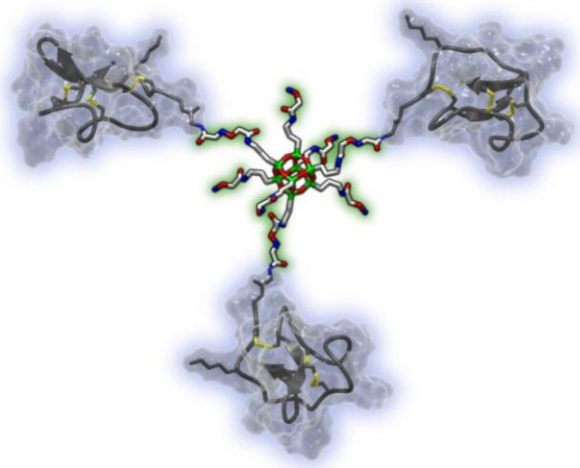

Fig. 5 Proposed model of a miniprotein-COSS conjugate (YASARA calculation; pale blue: cystine-knot peptide MCoTI with disulfide bridges depicted as yellow sticks; red: oxygen, blue: nitrogen, green: silicon, grey: carbon).For the chemical structure see table 2.[24]

Table 2 List of biofunctionalized cubic siloxanes and COSS based probes.

Ligand/ precursor for bioconjugation	COSS functionalization	Conjugation chemistry	Yield	No. Copies	Year	Ref.
δ-Lactonolactone	octaamino propyl	amide bond	53 %	8	1998/99	21, 80
δ-Maltonolactone	octaamino propyl	amide bond	26 %	8	1998/99	21, 80
Thiol modified mannosyl derivative	octavinyl	thiol radical addition	70 %	8	2004	79
Thiol modified lactosyl derivative	octavinyl	thiol radical addition	66, 73 %	8	2004	79
Propynyl-β-D-galactoside	octaazido propyl	CuAAC	~80 %	8	2010	19
Propynyl-α-D-mannoside	octaazido propyl	CuAAC	~80 %	8	2010	19
Propargyl α-D-mannopyranoside	octaazido propyl	CuAAC	≤76 %	8	2010	22
C-glucosylpropyl thiol	octavinyl	TEC	94 %	8	2012	39
C-mannosylpropyl thiol	octavinyl	TEC	93 %	8	2012	39
1-thio-β-D-glucopyranose	PEGylated octaallyl	TEC	79 %	8	2012	39
1-thio-β-D-lactopyranose	PEGylated octaallyl	TEC	50 %	8	2012	39
β-cyclodextrin oligomer	mono adamantane	non-covalent	na	1	2012	65
Single amino acids (Z-Gly, Z-Ala, Z-Pro)	octaamino propyl	amide bond	91/98/44 %	8	1998	82
Dipeptides (Z-Phe-Leu, Z-Ala-Pro)	octaamino propyl	amide bond	94/100 %	8	1998	82
Tripeptides (Z-Phe-Leu-Ala, Z-Ala-Phe-Leu)	octaamino propyl	amide bond	73/92 %	8	1998	82
$(L\text{-}Lys)_8$-$(L\text{-}Lys)_4$-$(L\text{-}Lys)_2$-$(L\text{-}Lys)_1$	octaamino propyl	amide bond	16 %	8	2007	83
$(L\text{-}Lys)_2$-$(L\text{-}Lys)_1$, ELLLLLLLLL	octaamino propyl	amide bond, non-covalent	na	--	2012	64
$(CGLIIQKNEC)_{0.25}$-(Gd or Mn-DOTA)$_{3.2}$-$(L\text{-}Lys)_4$-$(L\text{-}Lys)_2$-$(L\text{-}Lys)_1$	octaamino propyl	amide bond, CuAAC	na	8	2010-12	5, 87-89
$(L\text{-}Glu)_4$-$(L\text{-}Glu)_2$-$(L\text{-}Glu)_1$	succinic acid terminated octaamino propyl	amide bond	57 %	8	2010	6
Poly(benzyl-L-glutamate)$_{5\text{-}53}$	monoazido phenyl	CuAAC	na	1	2011	77
Propynyl poly(benzyl-L-glutamate)$_{16 \text{ and } 36}$	monothiol propyl	thiol-alkyne chemistry	73 %[a]	1	2011	86
(γ-propargyl-L-glutamate)$_{5\text{-}50}$	monoazido phenyl	CuAAC	na	na	2012	85
ECG	PEGylated octaallyl	TEC	78 %	8	2012	39
RGDC	PEGylated octaallyl	TEC	61 %	8	2012	39
Hexynyl-IPRGDYRG	octaazido propyl	CuAAC	91 %[a]	8	2010	18
Glyoxylyl-IPRGDYRKG	Boc-aminooxy derivative	oximation	90 %	8	2012	24
Glyoxylyl-LHLSLKFPG	Boc-aminooxy derivative	oximation	99 %	6	2012	24
Glyoxylyl-GVCPKILKKCRRDSDCPGACICRGNGYCG	Boc-aminooxy derivative	oximation	na	3	2012	24
Glyoxylyl-WGVCPKVLRNCRRDSDCPGACICLGNGYCG	Boc-aminooxy derivative	oximation	na	3	2012	24
Glyoxylyl-$(KVSALKE)_5$	Boc-aminooxy derivative	oximation	na	2	2012	24
Fluorescein	octaazido	CuAAC	100 %[a]	1	2010	18
BODIPY	octaamino/vinyl-heptaisobutyl	amide bond/ Heck reaction	14-88 %	1	2005/11	4, 90
Cationic oligofluorene	octavinyl	Heck reaction	45 %	8	2010	91
Trifluoro acetic acid	octaamino	amide bond	83 %	3-5	2008	92
C_{60} fullerene	heptaisobutyl hydroxyl propyl	esterfication	70 %	1	2011	93
Ferrocene carboxylic acid	octaamino	amide bond	70 %	3-5	2009	94

[a] Conversion.

7.3 Biofunctional COSS-based dendrimers

Dendrimers are a special class of branched and short-chained polymers. For biomedical applications, dendrimers based on polyamidoamine (PAMAM)[95] and polylysine[5, 64, 83, 87-89, 96] are of special interest. Due to the presentation of multiple positive surface charges, they exhibit cell-membrane-targeting properties that can result in membrane permeation or disruption.[97] These properties were utilized for the development of antimicrobial compounds[97] or to facilitate drug delivery into cells.[64, 83, 96]

In 2007, Kaneshiro *et al.*[83] demonstrated the general applicability of poly-L-lysine octaaminopropyl COSS dendrimers as drug carriers. In 2008, Chujo's research group[95] reported an increased cargo capacity of COSS-based dendrimers. These findings gave rise to a growing interest in the synthesis of cube-octameric silsesquioxane dendrimers.

Amphiphilic dendrimers allow either for an entrapment of small hydrophopic molecules in their interior or for a covalent ligand attachment to their external functionalities enabling them to act as a supramolecular scaffold. The specific chemical environment of a COSS dendrimer interior keeps trapped molecules well-dispersed and can regulate their molecular rotation.[98] This freezing effect caused not only an improvement of quantum yields and the elongation of fluorescent life-times for an *in-vivo* imaging relevant fluorophore emitting in the deep red region,[98] but also resulted in the effective inhibition of fluorescence bleaching of a rhodamin dye.[95]

Concerning the surface modification of globular COSS-based dendrimers, their functionalization with metal chelators is of special interest as it allows for magnetic resonance imaging (MRI) in tumor diagnostics. In this context, it is important to mention Lu and his co-workers who developed surface-modified polylysine dendrimers with a cube-octameric silsesquioxane core. Thus, gadolinium 1,4,7,10-tetraazacyclododecane-1,4,7,10-triacetic acid (Gd-DOTA), manganese 1,4,7-triaazacyclononane-1,4,7-triacetic acid (Mn-NOTA) and tumor targeting peptides were attached to surface-exposed lysine residues.[5, 87-89] The resulted particles have been applied in a murine animal model as MRI contrast agent targeting human breast and prostate carcinoma xenografts *via* CTL1[99] peptide-mediated interaction with extracellular abundantly present fibrin-fibronectin complexes.[87-89] The size of one of these second generation (G2) COSS dendrimers was determined as ~5.6 nm allowing for a fast renal clearance.[88] This finding is of special importance due to the toxicity of paramagnetic gadolinium (Gd) generally used for MRI studies.[100] Interestingly, Tan *et al.*[5, 89] also considered that *in-vivo* dissociation and trans-metallation of complexed Gd can result in harmful side effects e.g. nephrogenic systemic fibrosis.[100] Therefore, Gd was substituted with manganese, a less toxic paramagnetic metal.[5, 89] In summary, the development of COSS-dendrimer-based contrast agents is an advanced research field. After appropriate safety experiments, the synthesized compounds can be considered as excellent candidates for initial clinical studies. Nevertheless, approaches have been reported to evaluate the direct attachment of Gd-chelates to cubic silsesquioxanes (see also section 9).[58]

Another interesting example for surface-modified COSS dendrimers was given by Gu and colleges.[6] They designed a dendrimer skeleton on the basis of poly-L-glutamic acid with a cube-octameric silsesquioxane as a core unit. The reaction of terminal carboxylic moieties with hydrazine towards corresponding hydrazides allowed for the pH-sensitive attachment of a respective biotin derivative and doxorubicin. The biotin targeted overexpressed biotin receptors on the surface of HeLa cancer cells and doxorubicin destroyed the cells *via* DNA intercalation upon a receptor-mediated uptake.[6] Considering pharmacokinetics and, especially, the clearance of these particles in potentially upcoming animal model experiments, it is noteworthy that this glutamic acid hydrazide particles seemed to be prone to aggregation and their diameter increases of 30-50 nm.[6]

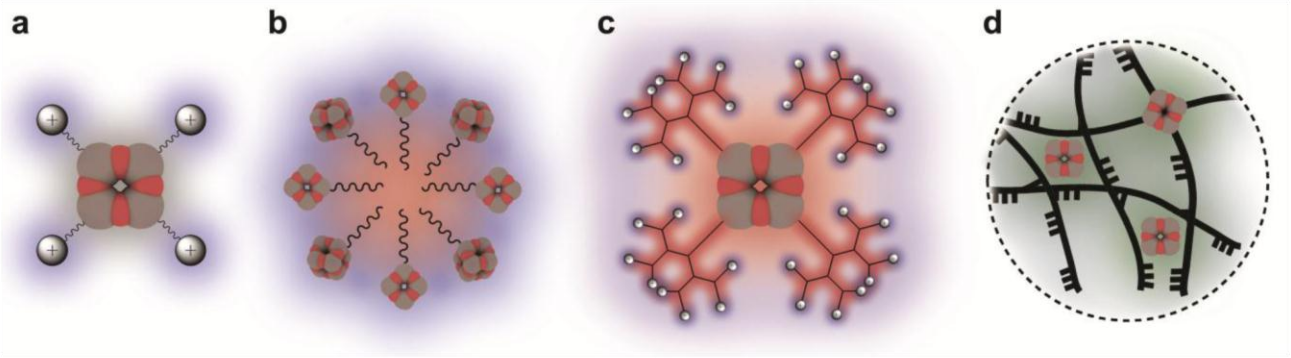

Fig. 6 Schematic depiction of COSS constructs used in drug delivery: a, direct cell penetration of e.g. polycationic octaamino COSS;[4] b, formation of nanocontainers by self-assembly of amphiphilic silsesquioxane derivatices;[44, 46, 86] c, dendrimers with highly symmetric and compact COSS core;[6, 96] d, incorporation of cubic siloxanes in cell-penetrating polymeric nanoparticles.[101, 102] (Silicon atoms are depicted in grey colour, oxygen in red; blue shadows indicate hydrophilic environement, red shadows indicate a hydrophobic milieu.)

8 COSS-mediated drug delivery

Due to their hydrophobic nature, potent drugs (e.g. paclitaxel) very often feature low solubility in aqueous systems. Furthermore, their efficacy might be limited to special body or cell compartements. In this context, DNA-intercalating drugs as doxorubicin are good examples. Accordingly, carriers are needed

to overcome these limitations. COSS-based drug delivery systems follow four general design principles (Fig. 6): (i) the particle itself facilitates cell penetration,[4, 47, 50] upon its derivatization; (ii) an amphiphil[44, 46, 64, 65, 86, 103] is formed allowing for the self-assembly of micelle-like structures; (iii) COSS constitutes the core structure of a dendrimer[6, 83, 96] (see section 7.3); (iv) it is incorporated into biocompatible polymers.[101, 104]

In the recent literature the development of COSS amphiphils gained particular attention. To highlight the structural similarities of these constructs and small molecules surfactants as e.g. sodium dodecyl sulfate (SDS), the term "giant surfactants"[46] was coined. Compact COSS cages presenting alcohols,[44] carboxylic acids[46] or carbohydrates[44] are expedient hydrophilic tenside head groups, whereas cubic silsesquioxanes bearing aliphatic ligands are also viable analogs of a tensides hydrophobic tail.[65, 86, 103] Amphiphilic COSS derivatives are able to hierarchically self-assemble.[65, 103] Thus, they are able to form nanocontainers that might host a drug.[44] Considering the cell penetration potential of micelle- and liposome-like assemblies,[105] amphiphilic COSS are promising candidates for new drug delivery studies.

COSS-based drug delivery must be considered as an expanding research field, still suffering from a difficult generalization of obtained results. Identified uptake mechanisms are not only strongly dependent on the functionalties decorating a COSS surface, but also on the used cell lines, incubation methods, etc For example, polycationic octaamino COSS are able to transport an attached cargo across a cell membrane,[4] but depending on the cell line its distribution pattern differs. Whereas in COS-1 cell the flourescein-siloxane derivative exclusively labeled the cytoplasm,[4] a similar compound showed accumulation in HeLa cell nucleoli, allowing for nuclear drug targeting.[47]

9 COSS-based molecular probes

Good water solubility, low toxicity, compact and precise 3D architecture of amine-terminated cube-octameric silsesquioxanes (see section 1 and 5) make these particles a versatile framework for the construction of environment-sensitive molecular probes.

In this context, the decoration of COSS with fluorinated ligands is intriguing. The resulting particles, often called F-POSS,[92, 106] are applicable for ^{19}F-NMR experiments[92, 94, 107, 108] and exhibit tunable melting properties relevant for polymer science.[106]

The recent literature offers two different approaches for the synthesis of fluorinated COSS. Fluoroalkyl ligands are introduced either *via* corner capping[106] or by a stoichiometrically controlled conjugation between octaamino COSS and trifluoroacetic acid.[92] Chujo and co-workers implemented F-POSS units in experimental setups allowing for the monitoring of enzymatic activities[92, 107, 108] and redox reactions.[94] The attachment of fluorinated COSS to macromolecular silica particle resulted in decreased intensity of signals in ^{19}F-NMR spectrum, due to a restricted molecular rotation.[92] Depending on the conjugation pattern, the activity of different enzyme classes was assessed. Thus, alkaline phosphatase cleaved COSS bound *via* phosphorodiamidate linker.[92, 107] Reduced glutathione generated by glutathione reductase detached disulfide-bound fluorinated silsesquioxane cages[108] from their macromolecular support. The

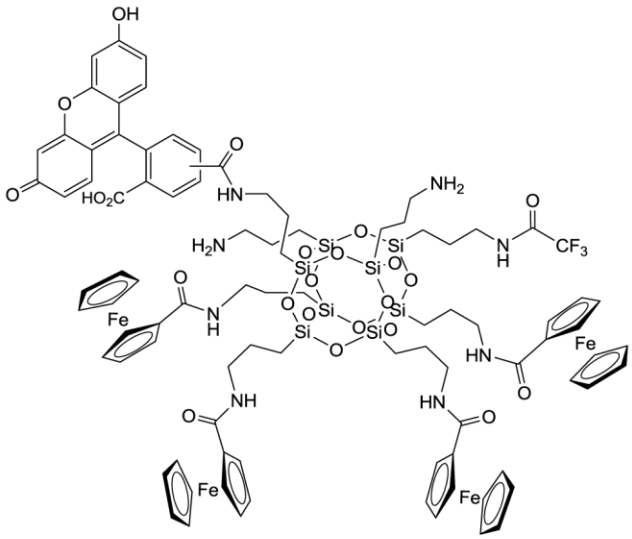

Fig. 7 Proposed structure of a bimodal probe for fluorescence microscopy and ^{19}F-NMR.[94]

respective COSS release resulted in a measurable ^{19}F-NMR signal enhancement due to the regained rotational freedom of the fluorinated ligands and allowed for the calculation of enzyme activities. COSS scaffolds bearing Fe^{3+} ferrocenyl ligands are, therefore, of interest as powerful electrochemical probes.[109] Furthermore, the addition of Fe^{3+} ferrocenyl groups to F-POSS transforms the resulting construct (Fig. 7) into a switchable redox-sensitive ^{19}F-NMR probe. Conjugation of this construct with an additional fluorescein moiety yields a versatile redox sensor that allows for bimodal measurements.[94]

It will be interesting to see if the synthesis of functional COSS cages with entrapped fluoride ions[110] is possible as these derivatives could allow for even more sophisticated F-POSS probes.

Other NMR applications of COSS exploit its octavalent framework for the development of MRI contrast agent. Apart from the already discussed dendrimeric design, the eightfold presentation of Gd^{3+} chelates reported by Hening *et al.*[58] is noteworthy. Interestingly, Gd^{3+} is not only applicable as DOTA chelates. Fullerene-encapsulated gadolinium species ($Gd@C_{82}(OH)_n$, $n > 32$)[111] allow for enhanced *in-vivo* MRI studies.[111, 112] The recent report on C_{60} fullerene-COSS conjugates[93] might allow for the development of a new class of COSS-based contrast agents.

Fluorescently labelled silsesquioxanes are common COSS-based probes. Cubic siloxanes decorated with fluorescein[18, 94] and BODIPY[4, 90, 113] allow for confocal microscopy studies on live cells. Oligoelectrolyte-polyhedral oligomeric silsesquioxanes (O-POSS) designed by Bin Liu and co-workers[91, 104, 114-116] are of interest as special fluorescent COSS particles (Fig. 8).

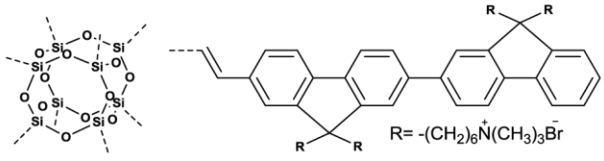

Fig. 8 Chemical structure of a water-soluble oligoelectrolyte-COSS.[91]

These water-soluble molecules feature low toxicity, whole cell permeability and high fluorescence quantum yields.[91] Hence, O-POSS were used as nuclear-staining agents[104] and as efficient Förster resonance energy (FRET) donors that enhanced the ethidium bromide labelling of DNA.[91] Further biological applications are based on O-POSS derivatives incorporated into polymeric nanoparticles that were used for for folic acid[104] or HER2 antibody-targeted[115] tumor imaging.

Finally, Xiong and co-workers[117] nicely highlighted the opto-physical properties of COSS. They demonstrated that the photoluminescence of quantum dots increased upon their surface decoration with cubic silsesquioxanes.[117] This enhancement was attributed to the special 3D structure of a COSS cage. It reflects emitted light and allows for a multiple excitation of the quantum dots.[117] In summary, light-harvesting COSS particle[91, 117] can be considered as promising agents for enhanced *in-vitro* microscopy studies.

10 Conclusions

Cube-octameric silsesquioxanes are small silica nanoparticles featuring an extremely compact structural framework, high symmetry and up to eight addressable organic ligands. Low toxicity of these molecules combined with solubility in aqueous systems and half-life under physiological conditions sufficient for *in-vivo* studies make them attractive scaffolds for the development of tailor-made bioconjugates or hybrid molecules of biologic relevance. Thus, conjugation of cubic silsesquioxanes with carbohydrates resulted in glycoclusters used to study sugar-lectin interactions. Coupling of functional peptides onto COSS scaffolds yielded oligomeric peptidic constructs without loss of bioactivity, while surface-modified silsesquioxane-based dedrimers have been used in drug delivery and MRI. Development of molecular probes comprising a COSS core is, probably, the most advanced application of these unique nanoparticles. The recently expanded arsenal of effective conjugation methods (CuAAC, TEC, oxime ligation) made COSS-based bioconjugations a rapidly growing research field with a large potential for further developments, particularly for tumor diagnostics and therapy.

11 Acknowledgement

This project was funded in part by the LOEWE Soft Control consortium.

12 References

1 J. Wu and P. T. Mather, *Polym. Rev.*, 2009, **49**, 25-63.
2 Y. Kawakami, Y. Kakihana, A. Miyazato, S. Tateyama and M. A. Hoque, *Adv. Polym. Sci.*, 2011, **235**, 185-228.
3 H. Ghanbari, A. de Mel and A. M. Seifalian, *Int. J. Nanomed.*, 2011, **6**, 775-786.
4 C. McCusker, J. B. Carroll and V. M. Rotello, *Chem. Commun.*, 2005, 996-998.
5 M. Q. Tan, Z. Ye, E. K. Jeong, X. M. Wu, D. L. Parker and Z. R. Lu, *Bioconjug. Chem.*, 2011, **22**, 931-937.
6 H. Yuan, K. Luo, Y. S. Lai, Y. J. Pu, B. He, G. Wang, Y. Wu and Z. W. Gu, *Mol. Pharm.*, 2010, **7**, 953-962.
7 A. Ladenburg, *Liebigs Ann. Chem.*, 1874, **173**, 143-166.
8 A. J. Barry, W. H. Daudt, J. J. Domicone and J. W. Gilkey, *J. Am. Chem. Soc.*, 1955, **77**, 4248-4252.
9 C. L. Frye and W. T. Collins, *J. Am. Chem. Soc.*, 1970, **92**, 5586-5588.
10 R. Weidner, N. Zellner, B. Deubzer and V. Frey, *Germany Pat. DE 383797-A1* 1990.
11 U. Dittmar, B. J. Hendan, U. Florke and H. C. Marsmann, *J. Organomet. Chem.*, 1995, **489**, 185-194.
12 A. R. Bassindale, Z. H. Liu, I. A. MacKinnon, P. G. Taylor, Y. X. Yang, M. E. Light, P. N. Horton and M. B. Hursthouse, *Dalton Trans.*, 2003, 2945-2949.
13 B. Marciniec, M. Dutkiewicz, H. Maciejewski and M. Kubicki, *Organometallics*, 2008, **27**, 793-794.
14 J. F. Brown and L. H. Vogt, *J. Am. Chem. Soc.*, 1965, **87**, 4313-4317.
15 D. B. Cordes, P. D. Lickiss and F. Rataboul, *Chem. Rev.*, 2010, **110**, 2081-2173.
16 C. H. Ni, G. Wu, C. P. Zhu and B. L. Yao, *J. Phys. Chem. C* 2010, **114**, 13471-13476.
17 V. Ervithayasuporn, X. Wang and Y. Kawakami, *Chem. Commun.*, 2009, 5130-5132.
18 S. Fabritz, D. Heyl, V. Bagutski, M. Empting, E. Rikowski, H. Frauendorf, I. Balog, W. D. Fessner, J. J. Schneider, O. Avrutina and H. Kolmar, *Org. Biomol. Chem.*, 2010, **8**, 2212-2218.
19 D. Heyl, E. Rikowski, R. C. Hoffmann, J. J. Schneider and W. D. Fessner, *Chem.-Eur. J.*, 2010, **16**, 5544-5548.
20 A. Boullanger, G. Gracy, N. Bibent, S. Devautour-Vinot, S. Clement and A. Mehdi, *Eur. J. Inorg. Chem.*, 2012, 143-150.
21 F. J. Feher, K. D. Wyndham, D. Soulivong and F. Nguyen, *Dalton Trans.*, 1999, 1491-1497.
22 B. Trastoy, M. E. Perez-Ojeda, R. Sastre and J. L. Chiara, *Chem.-Eur. J.*, 2010, **16**, 3833-3841.
23 J. R. Suarez, B. Trastoy, M. E. Perez-Ojeda, R. Marin-Barrios and J. L. Chiara, *Adv. Synth. Catal.*, 2010, **352**, 2515-2520.
24 S. Fabritz, S. Hörner, D. Könning, M. Empting, M. Reinwarth, C. Dietz, B. Glotzbach, H. Frauendorf, H. Kolmar and O. Avrutina, *Org. Biomol. Chem.*, 2012, DOI: 10.1039/c1032ob25728a.
25 H. B. Fan and R. J. Yang, *J. Appl. Polym. Sci.*, 2012, **124**, 4389-4397.
26 H. Cai, K. Xu, X. Liu, Z. Fu and M. Chen, *Dalton Trans.*, 2012, **41**, 6919-6921.
27 R. Tamaki, Y. Tanaka, M. Z. Asuncion, J. W. Choi and R. M. Laine, *J. Am. Chem. Soc.*, 2001, **123**, 12416-12417.
28 V. Abbate, A. R. Bassindale, K. F. Brandstadt and P. G. Taylor, *J. Inorg. Biochem.*, 2011, **105**, 268-275.
29 M. Frampton, R. Simionescu and P. M. Zelisko, *Silicon*, 2009, **1**, 47-56.
30 M. B. Frampton and P. M. Zelisko, *Silicon*, 2012, **4**, 51-56.
31 N. Ihara, M. Kurisawa, J. E. Chung, H. Uyama and S. Kobayashi, *Appl. Microbiol. Biotechnol.*, 2005, **66**, 430-433.
32 R. M. Laine, J. W. Choi and I. Lee, *Adv. Mater.*, 2001, **13**, 800-+.
33 M. Dutkiewicz, H. Maciejewski and B. Marciniec, *Synthesis*, 2012, **44**, 881-884.
34 B. W. Manson, J. J. Morrison, P. I. Coupar, P. A. Jaffres and R. E.

Morris, *Dalton Trans.*, 2001, 1123-1127.
35 V. V. Rostovtsev, L. G. Green, V. V. Fokin and K. B. Sharpless, *Angew. Chem. Int. Ed.*, 2002, **41**, 2596-2599.
36 J. M. Baskin, J. A. Prescher, S. T. Laughlin, N. J. Agard, P. V. Chang, I. A. Miller, A. Lo, J. A. Codelli and C. R. Bertozzi, *Proc. Natl. Acad. Sci. U. S. A.*, 2007, **104**, 16793-16797.
37 A. Dirksen, T. M. Hackeng and P. E. Dawson, *Angew. Chem. Int. Ed.*, 2006, **45**, 7581-7584.
38 K. F. Geoghegan and J. G. Stroh, *Bioconjug. Chem.*, 1992, **3**, 138-146.
39 M. Lo Conte, S. Staderini, A. Chambery, N. Berthet, P. Dumy, O. Renaudet, A. Marra and A. Dondoni, *Org. Biomol. Chem.*, 2012, **10**, 3269-3277.
40 Y. Itami, B. Marciniec and M. Kubicki, *Chem.-Eur. J.*, 2004, **10**, 1239-1248.
41 J. Choi, J. Harcup, A. F. Yee, Q. Zhu and R. M. Laine, *J. Am. Chem. Soc.*, 2001, **123**, 11420-11430.
42 E. M. Sletten and C. R. Bertozzi, *Angew. Chem. Int. Ed.*, 2009, **48**, 6974-6998.
43 F. J. Feher, K. D. Wyndham, R. K. Baldwin, D. Soulivong, J. D. Lichtenhan and J. W. Ziller, *Chem. Commun.*, 1999, 1289-1290.
44 W. B. Zhang, Y. W. Li, X. P. Li, X. H. Dong, X. F. Yu, C. L. Wang, C. Wesdemiotis, R. P. Quirk and S. Z. D. Cheng, *Macromolecules*, 2011, **44**, 2589-2596.
45 Y. Li, X.-H. Dong, H. Guo, Z. Wang, Z. Chen, C. Wesdemiotis, R. P. Quirk, W. B. Zhang and S. Z. D. Cheng, *ACS Macro Lett.*, 2012, **1**, 834−839.
46 X. F. Yu, S. Zhong, X. P. Li, Y. F. Tu, S. G. Yang, R. M. Van Horn, C. Y. Ni, D. J. Pochan, R. P. Quirk, C. Wesdemiotis, W. B. Zhang and S. Z. D. Cheng, *J. Am. Chem. Soc.*, 2010, **132**, 16741-16744.
47 S. Hörner, S. Fabritz, H. D. Herce, O. Avrutina, C. Dietz, R. W. Stark, M. C. Cardoso and H. Kolmar, 2012, DOI: 10.1039/b000000x.
48 H. Liu, M. Puchberger and U. Schubert, *Chem.-Eur. J.*, 2011, **17**, 5019-5023.
49 J. L. Zhou, Y. C. Zhao, K. C. Yu, X. P. Zhou and X. L. Xie, *New J. Chem.*, 2011, **35**, 2781-2792.
50 F. Olivero, F. Renò, F. Carniato, M. Rizzi, M. Cannas and L. Marchese, *Dalton Trans.*, 2012, **41**, 7467-7473.
51 Y. W. Li, W. B. Zhang, I. F. Hsieh, G. L. Zhang, Y. Cao, X. P. Li, C. Wesdemiotis, B. Lotz, H. M. Xiong and S. Z. D. Cheng, *J. Am. Chem. Soc.*, 2011, **133**, 10712-10715.
52 E. Rikowski and H. C. Marsmann, *Polyhedron*, 1997, **16**, 3357-3361.
53 G. Jungang, Z. Xuejian, W. Shichen and R. Mingtao, *Chemical Journal on Internet (http://www.chemistrymag.org/cji/2005/077048ne.htm)*, 2005, **7**, 48.
54 F. J. Feher and K. D. Wyndham, *Chem. Commun.*, 1998, 323-324.
55 T. L. Lu, G. Z. Liang and Z. Guo, *J. Appl. Polym. Sci.*, 2006, **101**, 3652-3658.
56 M. F. Roll, J. W. Kampf, Y. Kim, E. Yi and R. M. Laine, *J. Am. Chem. Soc.*, 2010, **132**, 10171-10183.
57 B. Trastoy, D. A. Bonsor, M. E. Pérez-Ojeda, M. L. Jimeno, A. Méndez-Ardoy, J. M. García-Fernández, E. J. Sundberg and J. L. Chiara, *Adv. Funct. Mater.*, 2012, DOI: 10.1002/adfm.201200423
58 J. Henig, E. Toth, J. Engelmann, S. Gottschalk and H. A. Mayer, *Inorg. Chem.*, 2010, **49**, 6124-6138.
59 Z. B. Qiu and H. Pan, *Compos. Sci. Technol.*, 2010, **70**, 1089-1094.
60 H. Pan and Z. B. Qiu, *Macromolecules*, 2010, **43**, 1499-1506.
61 J. Raghunath, G. Georgiou, D. Armitage, S. N. Nazhat, K. M. Sales, P. E. Butler and A. M. Seifalian, *J. Biomed. Mater. Res. Part A*, 2009, **91A**, 834-844.
62 W. H. Siddiqui and R. G. York, *Fund. Appl. Toxicol.*, 1993, **21**, 66-70.
63 V. Edwards, E. Markovic, J. Matisons and F. Young, *Biotechnol. Appl. Biochem.*, 2008, **51**, 63-71.
64 X. Xu, H. Yuan, J. Chang, B. He and Z. Gu, *Angew. Chem. Int. Ed.*, 2012, **51**, 3130-3133.
65 B. B. Jiang, W. Tao, X. Lu, Y. Liu, H. B. Jin, Y. Pang, X. Y. Sun, D. Y. Yan and Y. F. Zhou, *Macromol. Rapid Commun.*, 2012, **33**, 767-772.
66 K. Wang, L. Cai and S. F. Wang, *Polymer*, 2011, **52**, 2827-2839.
67 J. Raghunath, H. Zhang, M. J. Edirisinghe, A. Darbyshire, P. E. Butler and A. M. Seifalian, *Biotechnol. Appl. Biochem.*, 2009, **52**, 1-8.
68 C. Munch, J. O'Brien and A. Bertolotti, *Proc. Natl. Acad. Sci. U. S. A.*, 2011, **108**, 3548-3553.
69 P. H. Ren, J. E. Lauckner, I. Kachirskaia, J. E. Heuser, R. Melki and R. R. Kopito, *Nat. Cell Biol.*, 2009, **11**, 219-U232.
70 Y. B. Lim, E. Lee and M. Lee, *Angew. Chem. Int. Ed.*, 2007, **46**, 9011-9014.
71 S. A. Bode, M. Thevenin, C. Bechara, S. Sagan, S. Bregant, S. Lavielle, G. Chassaing and F. Burlina, *Chem. Commun.*, 2012, **48**, 7179-7181.
72 C. Y. Jung, H. S. Kim, H. J. Hah and S. M. Koo, *Chem. Commun.*, 2009, 1219-1221.
73 E. R. Chan, X. Zhang, C. Y. Lee, M. Neurock and S. C. Glotzer, *Macromolecules*, 2005, **38**, 6168-6180.
74 X. Zhang, E. R. Chan and S. C. Glotzer, *J. Chem. Phys.*, 2005, **123**.
75 M. Z. Asuncion, I. Hasegawa, J. W. Kampf and R. M. Laine, *J. Mater. Chem.*, 2005, **15**, 2114-2121.
76 T. T. Toth-Fejel, *IEEE Sens. J.*, 2008, **8**, 1036-1040.
77 Y. C. Lin and S. W. Kuo, *J. Polym. Sci. A Polym.*, 2011, **49**, 2127–2137.
78 Y. Kamiya, M. Yagi-Utsumi, H. Yagi and K. Kato, *Curr. Pharm. Des.*, 2011, **17**, 1672-1684.
79 Y. Gao, A. Eguchi, K. Kakehi and Y. C. Lee, *Org. Lett.*, 2004, **6**, 3457-3460.
80 F. J. Feher, K. D. Wyndham and D. J. Knauer, *Chem. Commun.*, 1998, 2393-2394.
81 J. C. Huang, X. Li, T. T. Lin, C. B. He, K. Y. Mya, Y. Xiao and J. Li, *J. Polym. Sci. Pt. B-Polym. Phys.*, 2004, **42**, 1173-1180.
82 F. J. Feher, K. D. Wyndham, M. A. Scialdone and Y. Hamuro, *Chem. Commun.*, 1998, 1469-1470.
83 T. L. Kaneshiro, X. Wang and Z. R. Lu, *Mol. Pharm.*, 2007, **4**, 759-768.
84 H. C. Kolb, M. G. Finn and K. B. Sharpless, *Angew. Chem. Int. Ed.*, 2001, **40**, 2004-2021.
85 Y. C. Lin and S. W. Kuo, *Polym. Chem.*, 2012, **3**, 162-171.
86 J. G. Ray, J. T. Ly and D. A. Savin, *Polym. Chem.*, 2011, **2**, 1536-1541.
87 M. Q. Tan, X. M. Wu, E. K. Jeong, Q. J. Chen and Z. R. Lu, *Biomacromolecules*, 2010, **11**, 754-761.
88 M. Tan, S. M. Burden-Gulley, W. Li, X. Wu, D. Lindner, S. M.

Brady-Kalnay, V. Gulani and Z. R. Lu, *Pharm. Res.*, 2012, **29**, 953-960.
89 M. Q. Tan, X. M. Wu, E. K. Jeong, Q. J. Chen, D. L. Parker and Z. R. Lu, *Mol. Pharm.*, 2010, **7**, 936-943.
90 M. Liras, M. Pintado-Sierra, F. Amat-Guerri and R. Sastre, *J. Mater. Chem.*, 2011, **21**, 12803-12811.
91 K. Y. Pu, K. Li and B. Liu, *Adv. Mater.*, 2010, **22**, 643-646.
92 K. Tanaka, N. Kitamura, K. Naka and Y. Chujo, *Chem. Commun.*, 2008, 6176-6178.
93 H. J. Sun, Y. F. Tu, C. L. Wang, R. M. Van Horn, C. C. Tsai, M. J. Graham, B. Sun, B. Lotz, W. B. Zhang and S. Z. D. Cheng, *J. Mater. Chem.*, 2011, **21**, 14240-14247.
94 K. Tanaka, N. Kitamura, Y. Takahashi and Y. Chujo, *Bioorg. Med. Chem.*, 2009, **17**, 3818-3823.
95 K. Tanaka, K. Inafuku, K. Nakab and Y. Chujo, *Org. Biomol. Chem.*, 2008, **6**, 3899-3901.
96 T. L. Kaneshiro and Z. R. Lu, *Biomaterials*, 2009, **30**, 5660-5666.
97 M. A. Mintzer, E. L. Dane, G. A. O'Toole and M. W. Grinstaff, *Mol. Pharm.*, 2012, **9**, 342-354.
98 K. Tanaka, J. H. Jeon, K. Inafuku and Y. Chujo, *Bioorg. Med. Chem.*, 2012, **20**, 915-919.
99 J. Pilch, D. M. Brown, M. Komatsu, T. A. Jarvinen, M. Yang, D. Peters, R. M. Hoffman and E. Ruoslahti, *Proc. Natl. Acad. Sci. U. S. A.*, 2006, **103**, 2800-2804.
100 J. L. Abraham and C. Thakral, *Eur. J. Radiol.*, 2008, **66**, 200-207.
101 X. J. Loh, Z. X. Zhang, K. Y. Mya, Y. L. Wu, C. B. He and J. Li, *J. Mater. Chem.*, 2010, **20**, 10634-10642.
102 M. Tarini, P. Cignoni and C. Montani, *IEEE Transactions on Visualization and Computer Graphics*, 2006, **12**, 1237-1244.
103 L. Ma, H. P. Geng, J. X. Song, J. Z. Li, G. X. Chen and Q. F. Li, *J. Phys. Chem. B*, 2011, **115**, 10586-10591.
104 D. Ding, K. Y. Pu, K. Li and B. Liu, *Chem. Commun.*, 2011, **47**, 9837-9839.
105 V. P. Torchilin, *Adv. Drug Deliv. Rev.*, 2006, **58**, 1532-1555.
106 S. C. Kettwich, S. N. Pierson, A. J. Peloquin, J. M. Mabry and S. T. Iacono, *New J. Chem.*, 2012, **36**, 941-946.
107 K. Tanaka, N. Kitamura and Y. Chujo, *Bioconjug. Chem.*, 2011, **22**, 1484-1490.
108 K. Tanaka, N. Kitamura and Y. Chujo, *Bioorg. Med. Chem.*, 2012, **20**, 96-100.
109 S. Bruna, D. Nieto, A. M. Gonzalez-Vadillo, J. Perles and I. Cuadrado, *Organometallics*, 2012, **31**, 3248-3258.
110 P. G. Taylor, A. R. Bassindale, Y. El Aziz, M. Pourny, R. Stevenson, M. B. Hursthouse and S. J. Coles, *Dalton Trans.*, 2012, **41**, 2048-2059.
111 L. Qu, W. B. Cao, G. M. Xing, J. Zhang, H. Yuan, J. Tang, Y. Cheng, B. Zhang, Y. L. Zhao and H. Lei, *J. Alloy. Compd.*, 2006, **408**, 400-404.
112 M. Mikawa, H. Kato, M. Okumura, M. Narazaki, Y. Kanazawa, N. Miwa and H. Shinohara, *Bioconjug. Chem.*, 2001, **12**, 510-514.
113 M. E. Perez-Ojeda, B. Trastoy, I. Lopez-Arbeloa, J. Banuelos, A. Costela, I. Garcia-Moreno and J. L. Chiara, *Chem.-Eur. J.* , 2011, **17**, 13258-13268.
114 K. Y. Pu, Z. T. Luo, K. Li, J. P. Xie and B. Liu, *J. Phys. Chem. C* 2011, **115**, 13069-13075.
115 K. Li, Y. T. Liu, K. Y. Pu, S. S. Feng, R. Y. Zhan and B. Liu, *Adv. Funct. Mater.*, 2011, **21**, 287-294.
116 K. Y. Pu and B. Liu, *Adv. Funct. Mater.*, 2011, **21**, 3408-3423.
117 Q. Li, L. J. Dong, X. Wang, J. Huang, H. A. Xie and C. X. Xiong, *Scr. Mater.*, 2012, **66**, 646-649.

3. Experimenteller Teil der Arbeit

3.1. Towards click bioconjugations on cube-octameric silsesquioxane scaffolds

Sebastian Fabritz , Dirk Heyl , Viktor Bagutski , Martin Empting , Eckhard Rikowski , Holm Frauendorf , Ildiko Balog , Wolf-Dieter Fessner , Jörg. J. Schneider , Olga Avrutina and Harald Kolmar

Org. Biomol. Chem., 2010,**8**, 2212-2218
DOI: 10.1039/B923393H
Received 10 Nov 2009, Accepted 18 Feb 2010
First published on the web 12 Mar 2010

Graphical Abstract:

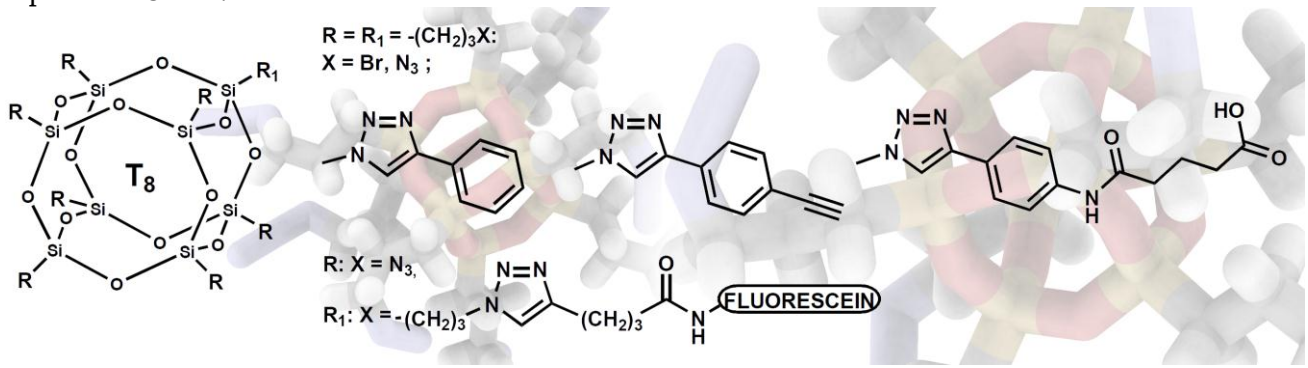

Short Summary:
Synthesis and click conjugations on octaazido octasilsesquioxane scaffold without cage rearrangements are described, including effective transformation into an octaalkyne POSS framework and an octaconjugate of a fully unprotected functional peptide.

Detailed analytical Data are given in chapter 4.1..

PAPER www.rsc.org/obc | Organic & Biomolecular Chemistry

Towards click bioconjugations on cube-octameric silsesquioxane scaffolds†

Sebastian Fabritz,[a] Dirk Heyl,[a] Viktor Bagutski,[b] Martin Empting,[a] Eckhard Rikowski,[c] Holm Frauendorf,[d] Ildiko Balog,[c] Wolf-Dieter Fessner,[a] Jörg. J. Schneider,[c] Olga Avrutina[a] and Harald Kolmar*[a]

Received 10th November 2009, Accepted 18th February 2010
First published as an Advance Article on the web 12th March 2010
DOI: 10.1039/b923393h

Cube-octameric silsesquioxane (POSS) based conjugation scaffolds for copper catalysed azide-alkyne [3+2] cycloaddition are reported. The synthetic route to octaazido and octaalkyno functionalised POSS templates without cage rearrangements is described. A set of click couplings is conducted including the first effective conjugation with a fully unprotected functional peptide towards a POSS assembled peptide octamer.

Introduction

Polyhedral oligomeric silsesquioxanes (POSS) are well defined nanosized molecules containing an inorganic silica-like core that is decorated with organic groups (Fig. 1). These hybrid nanoparticles have gained considerable research interest in recent years due to their potential application in electronics, engineering, material science and optics.[1]

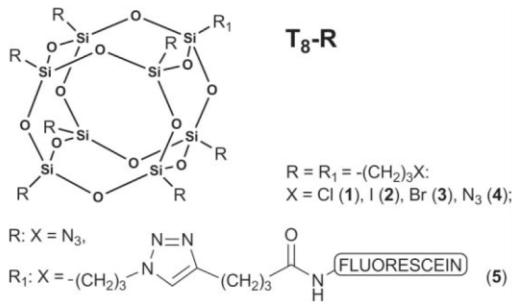

Fig. 1 Schematic representation of T_8-POSS oligomerisation scaffolds.

Though a vast number of polyhedral frameworks have been developed,[2] cube-octameric POSS bearing eight corner groups (T_8) are the most common. They form robust cage-like structures, thus allowing for a unique spatial arrangement of ligand molecules.

This siloxane core can contain either the same sort of ligands (homofunctionalised POSS)[3–7] or bear a single orthogonal function along with seven identical ligands of another type attached to the cube-octameric scaffold.[1,8–14]

Octameric POSS have been applied for the synthesis of diverse homosilsesquioxanes, were used as cores in dendrimer assembly, or employed as nanobridges.[1,15–20] Compared to gold or quantum dot nanoparticles, cube-octameric POSS have a significantly smaller inorganic core (0.5–0.7 nm),[21] thereby providing a compact scaffold enabling the display of up to eight ligand molecules in close proximity.

Despite their biocompatibility,[8,22,23] they have attracted comparably little attention for biomedical applications mainly due to the lack of robust and versatile strategies for conjugation of POSS nanoparticles with biorelevant ligands as *e.g.* peptides. Only one synthetic approach towards peptidyl silsesquioxanes has been reported to date.[24,25] This route of synthesis that is based on the acylation of octaamino or octaalcohol functionalised POSS has serious limitations concerning the choice of the ligand, thus narrowing the scope of conjugation counterparts to single amino acids or short peptides lacking reactive side chains.[24,25]

The copper-catalysed azide–alkyne cycloaddition (CuAAC) is a reliable and robust method widely used for conjugation of a variety of molecules covering almost all classes of chemical substances, including peptides.[26–31] It can be performed in various solvents and in the presence of diverse functional groups leading to the formation of a triazole ring, playing the role of a stable and rigid linker interconnecting the respective conjugation partners.[32–35] Several synthetic routes to click functionalised silsesquioxanes have been reported to date for azido substituted POSS. Monosubstituted azido-POSS were synthesised by the ring opening of epoxides using azide group as a nucleophile, or by nucleophilic substitution *via* azide/chloride exchange, respectively, from commercially available monosubstituted precursors.[36,37] Octasubstituted azidophenyl-POSS has been synthesised from the corresponding aminophenyl precursor *via* its diazonium salt,[38] and octakis(3-azidopropyl)-POSS—by azidation of a corresponding chloride.[37,39]

Though the introduction of a single azide function *via* a chlorosubstituted precursor is clean and quantitative, extensive rearrangements of T_8 cage have been reported for the synthesis of fully converted octaazide-POSS under azidation at elevated temperature.[37] Thus, only about 25% of pure octakis(3-azidopropyl)-POSS was isolated from a mixture of T_8, T_{10} and T_{12} cages.[37]

Herein, we report an easy and efficient procedure for the preparation of an octaazido functionalised octasilsesquioxane scaffold and conjugations thereupon without cage rearrangements, including octamerisation of an unprotected peptide ligand

[a]*Clemens Schöpf Institute of Organic Chemistry and Biochemistry, Technische Universität Darmstadt, Petersenstr. 22, 64287, Darmstadt, Germany*
[b]*School of Chemistry, Bristol University, Cantock's Close, Bristol, UK BS8 1TS*
[c]*Eduard Zintl Institute of Inorganic Chemistry, Technische Universität Darmstadt, Petersenstr. 22, 64287, Darmstadt, Germany*
[d]*Institute of Organic and Biomolecular Chemistry, Georg-August Universität Göttingen, Tamannstraße 2, 37077, Göttingen, Germany*

† Electronic supplementary information (ESI) available: **NMR** data of: **2–7**; **ESI-MS** data of: **1–9**; **IR** spectra of: **3**, **4**, **6**, **7**; **RP-HPLC** of: **5**, **6**, **8**, **9**; **TG analysis** of **1–4**, **6**. See DOI: 10.1039/b923393h

as well as effective transformation into an octaalkyne cube-octameric framework.

Results and discussion

Synthesis of octakis(3-azidopropyl)-POSS scaffold

We investigated the azidation of different octakis(3-haloalkyl)-POSS in order to find optimal conditions in terms of safety, efficacy, and formation of a fully substituted sole octaazide-POSS (Scheme 1). Octachloropropyl substituted precursor **1** was prepared using a two-step procedure by acid catalysed hydrolysis of trichloro- or trialkoxysilanes to silanols followed by condensation to siloxanes with successive substitution of terminal halogens (Scheme 1a,b).[40,41]

Although the synthesis of primary alkyl azides from their halide precursors is a well developed routine procedure,[42] initial attempts to apply it for the synthesis of **4** turned out to be problematic due to incomplete conversion, low reaction rate and sensitivity of the siloxane cage towards strong nucleophiles. Indeed, only 65% of octasubstituted T_8-POSS have been obtained in the product blend in the case of 95% conversion for an individual transformation.[43] Our observations corroborated reported rearrangements from T_8 to T_{10} and T_{12} cages;[37] in the worst case, formation of polymeric products was observed under attempted treatment of octakis(3-halopropyl)-POSS with strong nucleophiles in highly polar aprotic solvents commonly used for S_N2 reactions, particularly at elevated temperatures.[44,45] Since the reaction of **1** with NaN_3 in DMF at ambient temperature was very slow and thus could not be accomplished in one week, initially the starting POSS **1** was replaced by **2**[40] bearing a better leaving group.[46] Due to the poor solubility of $T_8[(CH_2)_3I]_8$ in polar aprotic solvents like DMF or DMSO, the azide substitution was conducted in chloroform using soluble *N*,*N*′-tetramethylguanidinium azide (TMGA)[47-49] as an azide source. In view of the concomitant formation of hazardous azidomethanes,[50] a safe alternative approach to the synthesis of **4** from corresponding halides was required.

Table 1 Preparation of $T_8[(CH_2)_3N_3]_8$

T_8 alkyl halide	Azide source	Reaction conditions	Yield (%)
1	NaN_3	DMF, rt, 1 week	n. d.
1	TMGA	$CHCl_3$, TBAI, reflux, 48 h	86[a]
2	TMGA	$CHCl_3$, reflux, 24 h	90[a,b]
3	TMGA	$C_2H_5NO_2$, 40 °C, 36 h	80
3	NaN_3	DMF, rt, 20 h	89

[a] Ref. 46 [b] Conversion.

We found that the synthesis of azide **4** from the corresponding bromide **3** using sodium azide in dry, amine-free DMF is optimal as no elevated temperatures and no chromatographic purification were required. Formed POSS azide **4** was isolated by simple water precipitation from the concentrated DMF solution, followed by washing and successive lyophilisation, in very good yield (Table 1).

^{1}H NMR studies proved excellent quality of formed azide **4**. ^{29}Si NMR used to provide information about the cage symmetry and the coordination sphere of Si atoms showed that mild synthesis conditions did not affect the unique architecture of the siloxane core, as exclusively the shift attributed to T_8 cage has been detected (Fig. 2).

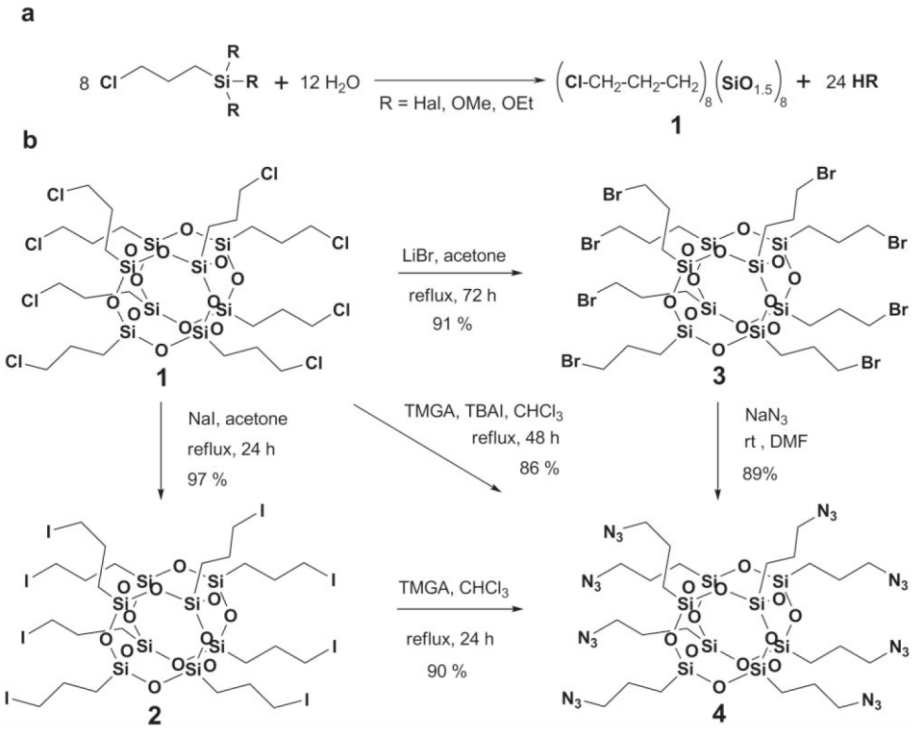

Scheme 1 Synthetic approaches to octakis(3-azidopropyl)-POSS **4**; **a**, hydrolytic condensation towards **1**; **b**, substitution of halide precursors yielding scaffold **4**.

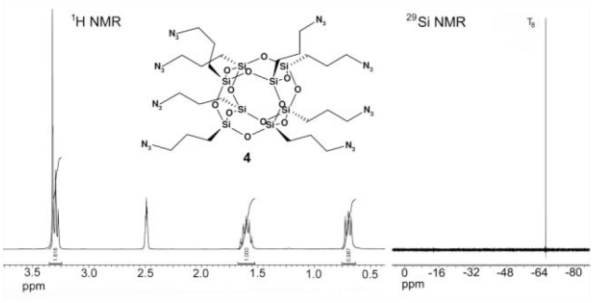

Fig. 2 ^{1}H and ^{29}Si NMR spectra of octakis(3-azidopropyl)-POSS **4**.

In our hands, ESI-FTICR MS proved to be a powerful tool for the characterisation of halide, azide, and alkyne POSS derivatives (Table 2). Intensive quasimolecular ions $[M+NH_4]^+$ were formed upon ionization of modified nanoparticles with ammonium without significant fragmentation. These studies showed that the silsesquioxane framework stabilised an ammonium ion very well, forming singly charged adducts. Therefore, ammonium acetate in solution can be used successfully for ionisation of silsesquioxanes if exclusively poorly ionisable side chain modifications are present.

Infrared (IR) spectroscopy that has been applied to study many silsesquioxane structures[51] is a useful analytical method for azide functionalised POSS. Thus, the IR spectrum of **4** shows Si–O–Si asymmetric stretching absorptions near 1112 cm^{-1}, the absorption bands of the azide group (2097 cm^{-1}, 1277 cm^{-1}), the aliphatic C–H stretching bands (2938 and 2876 cm^{-1}), and deformational vibrations of the silicon–oxygen framework in the region between 360 and 600 cm^{-1}. The broad band around 3400 cm^{-1} corresponds to physically adsorbed water (see the ESI†).[52,53]

Although POSS **4** nearly matches the so-called "rule of six",[26,54,55] and thus is expected to be fairly stable against spontaneous decomposition, the thermal behaviour of this octaazide scaffold was additionally studied by thermogravimetry coupled with mass spectrometry (TG-MS). This method provides extensive information on temperature dependent degradation pathways and has been widely used for the analysis of diverse saturated aliphatic and aromatic silsesquioxanes.[56–58] TG-MS studies demonstrated acceptable stability of **4**.[46]

Click conjugations on octakis(3-azidopropyl)-POSS scaffold

Synthesised azido-POSS template **4** was subjected to the coupling with several small molecule alkyne ligands as well as alkyne functionalised fully deprotected peptide bearing reactive groups in its side chains (Scheme 2, Fig. 3).

It is well known for siloxanes to undergo decomposition under aqueous alkaline conditions.[44,59] On the other hand, the most popular protocol for CuAAC usually requires factors potentially harmful for a POSS cage. Therefore, we focused our efforts on development of such a version of this reaction which would afford the required octaconjugated POSS derivatives under neutral media in aprotic solvent. Indeed, we found that elemental copper turned out to be a proper catalyst for the desired transformation in polar aprotic solvents like DMF, DMSO or acetonitrile. These mild conditions are appropriate for the coupling of bioligands.

Conjugates bearing hydrophobic aromatic substituents (**6**, **7**) were easily isolated by precipitation, though significant loss of reaction products occurred due to their partial solubility in reaction media as well as in the solvent used for washing.

Our subsequent study revealed that click coupling could be successfully performed in a biphasic system with both click partners dissolved in DCM, and under Sharpless conditions, namely, aqueous copper sulfate and sodium ascorbate. In this case, target conjugate **6** was isolated chromatographically in good yield.

Octasubstituted conjugates bearing phenyl (**6**), *p*-ethynylphenyl (**7**), and *p*-carboxybutanamido phenyl (**8**) residues connected with a scaffold through a stable and robust triazole linker were successfully synthesised as well as an asymmetric template bearing seven functional trimethyleneazide groups and one fluorescein derived substituent (**5**). Introduction of this chromophore into optically transparent octaazide octasilsesquioxane scaffold allowed us to trace the reaction progress by monitoring UV absorption and therefore made possible its HPLC analysis and isolation (see the ESI†). Experiments on cell penetration[60] using non-cationic fluorescein labeled POSS **5** by measures of confocal microscopy are currently on the way.

Data of IR spectroscopy for click POSS derivatives showed along with a strong band associated with asymmetric stretching of a siloxane framework (1123 cm^{-1}) the disappearance of a characteristic absorption band corresponding to the azide group in the region of 2100 cm^{-1}. For the complete information refer to the ESI.†

Evidence for exhaustive ligation of all eight azide groups of octaazide **4** is provided by ^{1}H NMR spectroscopy (Table 3). Thus, the characteristic triplet of an N–CH_2 group was shifted downfield by ~1.25 ppm together with the emergence of a triazole singlet at >7.9 ppm, after 1,3-dipolar cycloaddition of terminally

Table 2 Data of high resolution ESI MS for synthesised compounds

Compound	Monoisotopic mass (calc.)	ESI-FTICR MS *m/z* (found)	ESI-FTICR MS *m/z* (calc.)
1	1031.88	1049.9145 $[M+NH_4]^+$	1049.9146 $[M+NH_4]^+$
2	1767.35	1785.4020 $[M+NH_4]^+$	1785.3996 $[M+NH4]^+$
3	1383.48	1403.5091 $[M+NH_4]^+$	1403.5085 $[M+NH_4]^+$
4	1088.20	1106.2369 $[M+NH_4]^+$	1106.2376 $[M+NH_4]^+$
5	1529.33	765,6700 $[M+2H]^{2+}$	765,6698 $[M+2H]^{2+}$
6	1904.58	953.2965 $[M+2H]^{2+}$	953.2970 $[M+2H]^{2+}$
7	2096.58	1049.2968 $[M+2H]^{2+}$	1049.2970 $[M+2H]^{2+}$
8	2936.92	979.9802 $[M+3H]^{3+}$	979.9806 $[M+3H]^{3+}$
9	9300.40	1163.6817 $[M+8H]^{8+}$, 1034.6096 $[M+9H]^{9+}$	1163.5574 $[M+8H]^{8+}$, 1034.3852 $[M+9H]^{9+}$

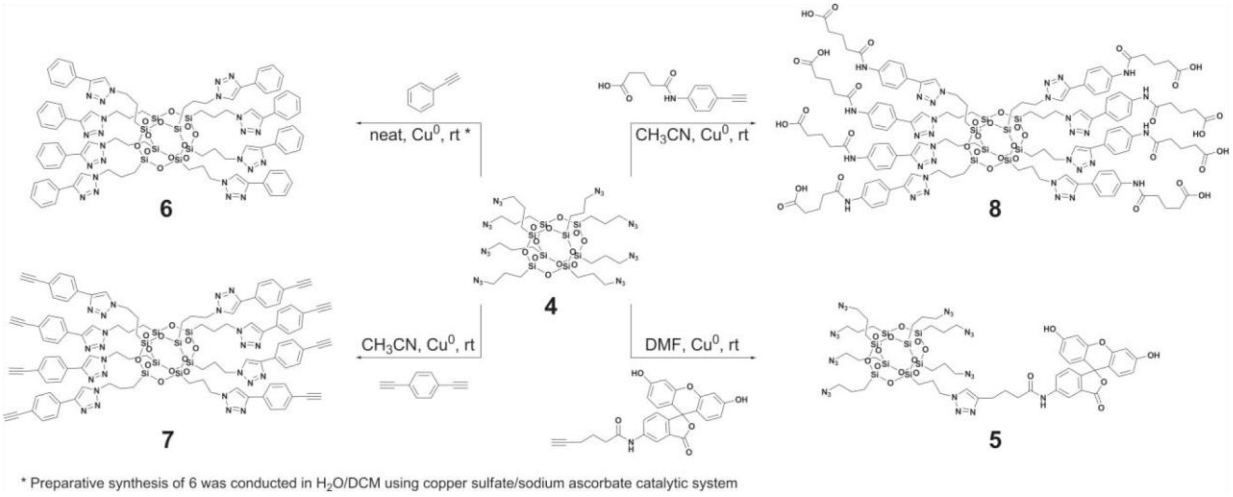

Scheme 2 Click conjugations of small molecules on octakis(3-azidopropyl)-POSS scaffold **4**.

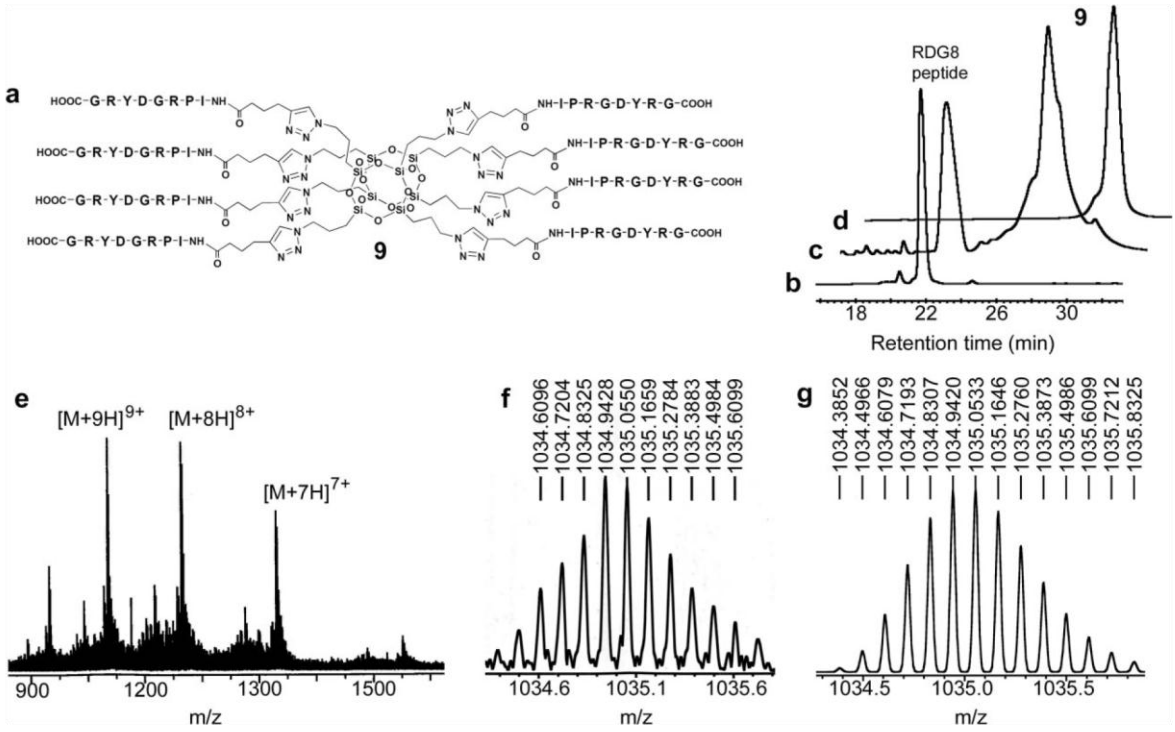

Fig. 3 Click conjugation of alkyne bearing RGD octapeptide. **a**, POSS-peptide octaconjugate; **b**, HPLC trace of the peptide ligand at 220 nm; **c**, HPLC trace of the click reaction mixture after 6 weeks (peptide ligand in excess) at 220 nm; **d**, HPLC trace of the octameric POSS-peptide conjugate **9** at 220 nm; **e**, ESI-MS analysis of the octameric POSS-peptide conjugate **9**; **f**, HR ESI-MS: isotopic pattern for ninefold charged quasimolecular ion $[M+9H]^{9+}$ of **9**; **g**, simulated isotopic pattern for $[C_{392}H_{617}N_{136}O_{116}Si_8]^{9+}$.

substituted alkyne had been accomplished. It should be noted, however, that in general proton spectroscopy cannot serve as evidence of the structural integrity of a POSS-cage, since its decomposition causes either none or only slight changes (*e.g.*, line broadening), keeping major coupling and shift patterns unaffected. Therefore, the structural integrity of the POSS cage was unambiguously confirmed by ^{29}Si NMR spectroscopy showing a sharp sole peak at -66 ± 1 ppm.

The synthesis of POSS-peptide conjugates has been reported for aminopropyl or hydroxypropyl substituted scaffolds and implies coupling of protected ligands (amino acids, di- or tripeptides) under standard activation conditions.[24,25] This method has serious limitations as stepwise coupling needs a deprotection step after each chain elongation, and convergent synthesis requires either fully protected peptides, or those without reactive groups in their side chains. Couplings are generally characterised by long

Table 3 Chemical shifts of selected POSS scaffolds and conjugates[a]

Compound	δ_H (δ_C), ppm											δ_{Si}
	1-CH_2		2-CH_2		–C≡CH		3-CH_2		Triazole		$C_{Ar\text{-}triazole}$	
3	0.75	(11.2)	1.90	(26.9)	—		3.36	(36.5)	—		—	–67.2
4	0.73	(9.0)	1.70	(22.5)	—		3.28	(53.4)	—		—	–66.5
6	0.64	(8.6)	2.02	(24.0)	—		4.35	(52.2)	7.90	(120.2)	147.7	–66.3
									—	(130.6)		
7[b]	0.61	(7.9)	1.89	(23.2)	4.22	(83.3)	4.32	(51.4)	8.54	(120.9)	145.5	–66.1
					—	(81.3)			—	(131.1)		

[a] NMR spectra were recorded in $CDCl_3$. [b] NMR spectra were recorded in DMSO-d_6.

reaction times ranging from days to weeks, and often incomplete substitutions are observed. In the present study, an integrin binding RGD peptide with a sequence IPRGDYRG[61] was taken as a model ligand for coupling onto scaffold **4**. This ligand was N-terminally modified with hexynoic acid and contained unprotected side chains of arginine, tyrosine and aspartic acid, as well as the C-terminal carboxy group. Click reaction was conducted in acetonitrile–DMF (3 : 1) at room temperature using copper wire as a catalyst. Though the reaction rate was slow, about 91% conversion into desired octamer was observed after 6 weeks. Reaction success was proved by high resolution ESI-MS (Fig. 3 and ESI†).

Conclusions

We have synthesised sterically defined frameworks for the introduction of molecules with the potential to interfere with biologic systems by copper catalysed click cycloaddition, which combine a highly symmetric siloxane inorganic core with functional azide or alkyne substituents, and demonstrated their utility in Sharpless-type couplings. Mild reaction conditions, though leading to extended reaction duration ensured the inalterability of the midmost siloxane cage for all octaconjugates of small molecular ligands.

For the first time conjugation of POSS with an RGD octapeptide bearing fully unprotected side chains was conducted leading to an eightfold presentation of a peptide ligand. It will be interesting to see to what extent the integrin binding activity of the RGD peptide is modulated upon oligomerisation on the scaffold. Detailed studies concerning conjugation of peptides of different size, polarity and biological activity using azide and alkyne bearing POSS frameworks are currently ongoing.

In conclusion, the constructs described here are promising templates for the assembly of various ligands including small molecules, sugars, peptides or proteins.

Experimental

1,3,5,7,9,11,13,15-Octakis(3-bromopropyl)pentacyclo-[9.5.1.1^{3,9}.1^{5,15}.1^{7,13}]octasiloxane (3)

$T_8[(CH_2)_3Cl]_8$[40,41] (5 g, 4.8 mmol) and anhydrous lithium bromide (25 g, 287 mmol, 60 equiv.) were dissolved in anhydrous acetone (200 mL) and the resulting mixture was heated under reflux for three days. Then, water (150 mL) and CH_2Cl_2 (300 mL) were added to the vigorously stirred reaction mixture. The organic layer was separated, washed with water (4 × 100 mL) and dried *in vacuo*. The resulting crude product was submitted to another four cycles of the procedure described above to ensure complete conversion. Finally, the pale-yellow crude material was dissolved in CH_2Cl_2 and purified by flash chromatography on Merck Silica gel 60 (0.04–0.063 mm) eluting with CH_2Cl_2, to afford 6.13 g (91.5%) of **3** as a white solid after removal of the solvent *in vacuo*.

^{1}H NMR (300 MHz, $CDCl_3$): δ 0.75 (t, $^3J_{H,H}$ = 8.1 Hz, 16H), 1.90 (mult., 16H), 3.36 (t, $^3J_{H,H}$ = 6.7 Hz, 16H) ppm; ^{13}C NMR (75 MHz, $CDCl_3$): δ 11.20, 26.86, 36.46 ppm; ^{29}Si NMR (59.6 MHz, $CDCl_3$): δ–67.2 (s) ppm; IR (KBr) [cm^{-1}] ν 2958 m (C–H), 2853w, 1098vs (Si–O), 540w (O–Si–O); 475 m (Si–O). TG-MS: see the ESI.† Anal.: calc. for $C_{24}H_{48}Br_8O_{12}Si_8$ C, 20.70; H, 3.47; meas. C, 20.88; H, 3.448. HR-MS: calc. for $C_{24}H_{52}NBr_8O_{12}Si_8$ (+1): 1403.5085, meas. 1403.5091 $[M+NH_4]^+$.

1,3,5,7,9,11,13,15-Octakis(3-azidopropyl)pentacyclo-[9.5.1.1^{3,9}.1^{5,15}.1^{7,13}]octasiloxane (4)

Method A (analytic scale). POSS-bromide **3** (50 mg, 0.036 mmol) and NaN_3 (26 mg, 0.4 mmol, 11 equiv.) were dissolved in anhydrous DMF (1.5 mL). The mixture was stirred for 20 h at room temperature and concentrated *in vacuo* to a total volume of ~0.5 mL. Crude product, precipitated as a viscous oil after addition of H_2O (1 mL), was separated from supernatant solution by centrifugation and decantation, washed with water (3 × 1 mL), dissolved in CH_3CN (2 mL) and finally subjected to lyophilic drying to yield 35 mg (89%) of pure azide **4** as a colourless viscous oil.

Method B (preparative scale). POSS bromide **3** (1 g, 0.718 mmol) and NaN_3 (1 g, 15.3 mmol, 21.3 equiv., 2.7-fold excess) were dissolved in anhydrous DMF (20 mL). After stirring for 36 h at room temperature the mixture was diluted with ethylacetate (100 mL), washed with water (3 × 100 mL) and brine (100 mL). The organic layer was dried over $MgSO_4$. Solvent evaporation yielded **4** (700 mg, 89%) as a pale-yellow oil which solidified in a fridge.

^{1}H NMR (400 MHz, $CDCl_3$, TMS): δ 0.70–0.76 (m, 16H), 1.66–1.74 (m, 16H), 3.28 (t, $^3J_{H,H}$ = 6.8 Hz, 16H) ppm; ^{13}C NMR (100 MHz, $CDCl_3$): δ 9.0, 22.5, 53.4 ppm; ^{29}Si NMR (59.6 MHz, $CDCl_3$): δ–66.5 (s); IR (neat) [cm^{-1}] ν 2938 m (C–H), 2876w, 2097vs (N_3), 1112vs (Si–O), 556w (O–Si–O); 486w (Si–O). TG-MS: see the ESI.† Anal.: calc. for $C_{24}H_{48}N_{24}O_{12}Si_8$ C, 26.46; H, 4.44; N, 30.86; meas. C, 26.01; H, 4.343; N, 29.05. HR-MS: calc. for $C_{24}H_{52}N_{25}O_{12}Si_8$ (+1): 1106.2376, meas. 1106.2369 $[M+NH_4]^+$

1-(3-(4-(4-(3′,6′-Dihydroxy-3-oxo-3*H*-spiro[isobenzofuran-1,9′-xanthene]-5-ylamino)-4-oxobutyl)-1*H*-1,2,3-triazol-1-yl)propyl), 3,5,7,9,11,13,15-heptakis(3-azidopropyl)penta-cyclo-[9.5.1.1^{3,9}.1^{5,15}.1^{7,13}]octasiloxane (5)

POSS azide **4** (5 mg, 0.0046 mmol, 8 equiv.) and fluorescein alkyne[62] (0.25 mg, 0.00057 mmol, 1 equiv.) were dissolved in 0.5 mL of anhydrous DMF and added to a HNO_3-preactivated Cu^0 turnings (~15 mg). The mixture was shaken at room temperature until full conversion of the starting material has been achieved (~3 weeks). Reaction progress was monitored at 220 and 485 nm by reverse phase HPLC on a Waters Symmetry 100 C8 column (150 × 3.9 mm, 5 µm) using a linear gradient of 90% aq. CH_3CN in 0.1% aq. TFA (20→100% in 30 min) at flow rate of 1 mL min^{-1}. t_R = 33.8 min.

HR-MS: calc. for $C_{50}H_{69}N_{25}O_{18}Si_8$ (+2): 765.6698, meas. 765.6700 $[M+2H]^{2+}$. t_R = 9.47 min (column: Shim-pack XR- C8, 50 × 2 mm, 2.2 µm, flow rate 0.2 mL min^{-1}, 40→100% CH_3CN).

1,3,5,7,9,11,13,15-Octakis[3-(1-phenyltriazol-4-yl)propyl]-pentacyclo-[9.5.1.1^{3,9}.1^{5,15}.1^{7,13}]octasiloxane (6)

Method A (analytic scale). Scaffold **4** (5 mg, 4.6 µmol) was dissolved in 500 µL of phenylacetylene and added to HNO_3-preactivated Cu^0 turnings (~15 mg). The mixture was then shaken at room temperature for 72 h. Formed precipitate was isolated by centrifugation, washed with CH_3CN (4 × 1 mL), and resubjected to the above procedure using fresh catalyst. Subsequent work-up followed by lyophilic drying, afforded 2.1 mg (23%) of pure **6** as a pale-yellow solid.

Method B (preparative scale). To a rapidly stirred solution of **4** (200 mg, 0.184 mmol) and phenylacetylene (450 mg, 4.41 mmol, 24 equiv.) in 10 mL CH_2Cl_2, 4 mL H_2O, 2 mL 1M aq. $CuSO_4$ and 4 mL 1M aq. sodium ascorbate were added. After 36 h the reaction mixture was diluted with 50 mL CH_2Cl_2 and 50 mL H_2O. The organic layer was washed with saturated aq. NH_4Cl (100 mL), filtered through a celite pad, dried over $MgSO_4$ and evaporated to dryness. The crude product was purified by DCVC[63] (0→100% acetone in toluene) yielding 300 mg (86%) of **6** as a white solid.

^{1}H NMR (500 MHz, $CDCl_3$, TMS): δ 0.62–0.65 (m, 16H), 1.99–2.05 (m, 16H), 4.35 (t, $^3J_{H,H}$ = 6.9 Hz, 16H), 7.31 (tt, $^3J_{H,H}$ = 7.4 Hz, $^4J_{H,H}$ = 1.2 Hz, 8H, H-Ph$_{para}$), 7.35–7.39 (m, 16H, H-Ph$_{meta}$), 7.81–7.83 (m, 16H, H-Ph$_{ortho}$), 7.90 (s, 8H) ppm; ^{13}C NMR (125 MHz, $CDCl_3$): δ 8.6 (8CH_2), 24.0 (8CH_2), 52.2 (8CH_2), 120.2 (8CH, triazole), 125.6 (16CH, Ph$_{ortho}$), 128.1 (8CH, Ph$_{para}$), 128.9 (16CH, Ph$_{meta}$), 130.6 (8C$_{quat}$, triazole), 147.7 (8C$_{quat}$, Ph) ppm; ^{29}Si NMR (59.6 MHz, $CDCl_3$): δ –67.3 (s); IR (KBr) [cm^{-1}] ν 3088 m (C–H, aromatic), 2948 m (C–H, alkyl), 1123vs (Si–O), 766 s (C–H, triazole), 490w (Si–O). TG-MS: see the ESI.† HR-MS: calc. for $C_{88}H_{98}N_{24}O_{12}Si_8$ (+2): 953.2970, meas. 953.2965 $[M+2H]^{2+}$. t_R = 9.25 min (column: Shim-pack XR- C8, 50 × 2 mm, 2.2 µm, flow rate 0.2 mL min^{-1}, 40→100% CH_3CN).

1,3,5,7,9,11,13,15-Octakis{3-[1-(4-ethynylphenyl)triazol-4-yl]propyl}pentacyclo-[9.5.1.1^{3,9}.1^{5,15}.1^{7,13}]octasiloxane (7)

To a reaction flask containing **4** (7.5 mg, 6.9 µmol) and HNO_3-preactivated Cu^0-turnings (~15 mg) 600 µL of saturated at 50 °C solution of 1,4-diethynylbenzene in acetonitrile was added. Then the reaction mixture was shaken for 96 h at room temperature. After the dilution with 0.5 mL CH_3CN a brown-yellow precipitate was isolated by centrifugation and the entire cycle was repeated. After washing of the solid (6 times with 1.5 mL CH_3CN), 14.9 mg precipitate were isolated as an intercalation product with diethynyl benzene.

^{1}H NMR (500 MHz, DMSO-d_6): δ = 0.59–0.62 (m, 16H), 1.86–1.92 (m, 16H), 4.22 (s, 8H, –C≡C*H*); 4.32 (t, $^3J_{H,H}$ = 6.8 Hz, 16H), 7.47–7.50 (m, 16H), 7.76–7.79 (m, 2H), 8.54 (s, 8H, triazole-C*H*) ppm; ^{13}C NMR (125 MHz, DMSO-d_6): δ 7.9 (8CH_2), 23.2 (8CH_2), 51.4 (8CH_2), 83.3 (8CH, –C≡*C*H), 81.3 (8C$_{quat}$, –C≡CH), 120.9 (8CH, triazole), 121.8 (8C$_{quat}$, Ar–C≡CH), 125.2 (16CH, Ar), 131.1 (8C$_{quat}$, triazole), 132.2 (16CH, Ar), 145.5 (8C$_{quat}$, Ar-triazole) ppm; ^{29}Si NMR (59.6 MHz, DMSO-d_6): δ = 66.1 (s) ppm; IR (KBr) [cm^{-1}] ν 3268 s (C–H, alkyne), 2925 m (C–H, alkyl), 2105w (C≡C), 1102vs (Si–O), 829 s (C–H, triazole). HR-MS: calc. for $C_{104}H_{98}N_{24}O_{12}Si_8$ (+2): 1049.2970, meas. 1049.2968 $[M+2H]^{2+}$.

1,3,5,7,9,11,13,15-Octakis {3-[4-(4-(4-carboxybutanamido)phenyl)-1*H*-1,2,3-triazol-1-yl]propyl} pentacyclo-[9.5.1.1^{3,9}.1^{5,15}.1^{7,13}]octasiloxane (8)

To a reaction flask containing **4** (5 mg, 4.6 µmol) and HNO_3-preactivated Cu^0-turnings (~15 mg) 500 µL of saturated at 50 °C solution of 5-(4-ethynylphenylamino)-5-oxopentanoic acid in acetonitrile was added. Then the reaction mixture was shaken for 96 h at room temperature. After the dilution with 0.5 mL CH_3CN a pale-green precipitate was isolated by centrifugation, redissolved in water–acetonitrile mixture and subjected to reverse phase HPLC on a Waters Symmetry 100 C8 column (150 × 3.9 mm, 5 µm) using a linear gradient of 90% aq. CH_3CN in 0.1% aq. TFA (20→100% in 35 min) at flow rate of 1 mL min^{-1}. HPLC analysis of crude reaction product has shown that 55.2% of the starting material were converted into an octamer **8**. t_R = 14.97 min

HR-MS: calc. for $C_{128}H_{155}N_{32}O_{36}Si_8$ (+3): 979.9806, meas. 979.9802 $[M+3H]^{3+}$. t_R = 6.51 min (column: Shim-pack XR- C8, 50 × 2 mm, 2.2 µm, flow rate 0.2 mL min^{-1}, 40→100% CH_3CN).

T_8-(IPRGDYRG)$_8$ (9)

To a reaction flask containing **4** (1.6 mg, 1.5 µmol, 1 equiv.) and HNO_3-preactivated Cu^0-turnings (~15 mg) 1 mL CH_3CN and 300 µL DMF, alkyne derivatised RDG8 peptide (25 mg, 23.95 µmol, 16 equiv.) was added. Then the reaction mixture was shaken at room temperature, and reaction progress was monitored by RP HPLC. After 6 weeks 91.3% conversion into the desired product was achieved, and the product was isolated by HPLC using Waters Symmetry 100 C8 column (150 × 3.9 mm, 5 µm) and linear gradient of 90% aq. CH_3CN in 0.1% aq. TFA (10→35% in 30 min) at a flow rate of 1 mL min^{-1}. t_R = 27.6 min.

HR-MS: calc. for $C_{392}H_{616}N_{136}O_{116}Si_8$ (+8): 1163.5574, meas. 1163.6817 $[M+8H]^{8+}$, calc. for $C_{392}H_{617}N_{136}O_{116}Si_8$ (+9): 1034.3852, meas. 1034.6096 $[M+9H]^{9+}$.

Acknowledgements

This work was supported by the Deutsche Forschungsgemeinschaft through grant KO 1390/9-1 and by BMBF.

The visualization of the molecular images was conducted with QuteMol.[64]

References

1 G. Li, L. Wang, H. Ni and C. U. Pittman Jr, *J. Inorg. Organomet. Polym.*, 2001, **11**, 123–154.
2 R. H. Baney, M. Itoh, A. Sakakibara and T. Suzuki, *Chem. Rev.*, 1995, **95**, 1409–1430.
3 A. Provatas and J. G. Matisons, *Trends Polym. Sci.*, 1997, **5**, 327–332.
4 C. Zhang and R. M. Laine, *J. Am. Chem. Soc.*, 2000, **122**, 6979–6988.
5 P. P. Pescarmona and T. Maschmeyer, *Aust. J. Chem.*, 2001, **54**, 583–596.
6 F. J. Feher and T. A. Budzichowski, *Polyhedron*, 1995, **14**, 3239–3253.
7 M. G. Voronkov and V. I. Lavrent'yev, *Top. Curr. Chem.*, 1982, **102**, 199–236.
8 J. D. Lichtenhan, *Comments Inorg. Chem.*, 1995, **17**, 115–130.
9 J. D. Lichtenhan, N. Q. Vu, J. A. Carter, J. W. Gilman and F. J. Feher, *Macromolecules*, 1993, **26**, 2141–2142.
10 T. S. Haddad, H. W. Oviatt, J. J. Schwab, P. T. Mather, K. P. Chaffee and J. D. Lichtenhan, *Polym. Prepr. (Am. Chem. Soc. Div. Polym. Chem.)*, 1998, **39**, 611–612.
11 J. D. Lichtenhan, Y. A. Otonari and M. J. Carr, *Macromolecules*, 1995, **28**, 8435–8437.
12 J. W. Gilman, D. S. Schlitzer and J. D. Lichtenhan, *J. Appl. Polym. Sci.*, 1996, **60**, 591–596.
13 *Polymeric Materials Encyclopedia*, ed. J. D. Lichtenhan, CRC Press, New York, 1996.
14 F. J. Feher and K. J. Weller, *Organometallics*, 1990, **9**, 2638–2640.
15 K. Naka, M. Sato and Y. Chujo, *Langmuir*, 2008, **24**, 2719–2726.
16 B. Hong, T. P. S. Thoms, H. J. Murfee and M. J. Lebrun, *Inorg. Chem.*, 1997, **36**, 6146–6147.
17 M. F. Roll, M. Z. Asuncion, J. Kampf and R. M. Laine, *ACS Nano*, 2008, **2**, 320–326.
18 N. R. Vautravers, P. André and D. J. Cole-Hamilton, *Dalton Trans.*, 2009, 3413–3424.
19 N. R. Vautravers, P. André, A. M. Z. Slawin and D. J. Cole-Hamilton, *Org. Biomol. Chem.*, 2009, **7**, 717–724.
20 G. Cheng, N. R. Vautravers, R. E. Morris and D. J. Cole-Hamilton, *Org. Biomol. Chem.*, 2008, **6**, 4662–4667.
21 H. Mori, Y. Miyamura and T. Endo, *Langmuir*, 2007, **23**, 9014–9023.
22 F. J. Feher and K. J. Weller, *Inorg. Chem.*, 1991, **30**, 880–882.
23 I. Lacatusu, R. Nita, N. Badea, D. Bojin and A. Meghea, *Mater. Res. Innovations*, 2009, **13**, 330–333.
24 F. J. Feher, K. D. Wyndham, M. A. Scialdone and Y. Hamuro, *Chem. Commun.*, 1998, 1469–1470.
25 T. L. Kaneshiro, X. Wang and Z.-R. Lu, *Mol. Pharmaceutics*, 2007, **4**, 759–768.
26 H. C. Kolb, M. G. Finn and K. B. Sharpless, *Angew. Chem., Int. Ed.*, 2001, **40**, 2004–2021.
27 A. J. Dirks, S. S. van Berkel, N. S. Hatzakis, J. A. Opsteen, F. L. van Delft, J. J. L. M. Cornelissen, A. E. Rowan, J. C. M. van Hest, F. P. J. T. Rutjes and R. J. M. Nolte, *Chem. Commun.*, 2005, 4172–4174.
28 J.-F. Lutz, *Angew. Chem., Int. Ed.*, 2007, **46**, 1018–1025.
29 W. H. Binder and R. Sachsenhofer, *Macromol. Rapid Commun.*, 2007, **28**, 15–54.
30 R. A. Evans, *Aust. J. Chem.*, 2007, **60**, 384–395.
31 O. Avrutina, M. Empting, S. Fabritz, M. Daneschdar, H. Frauendorf, U. Diederichsen and H. Kolmar, *Org. Biomol. Chem.*, 2009, **7**, 4177–4185.
32 C. W. Tornoe, C. Christensen and M. Meldal, *J. Org. Chem.*, 2002, **67**, 3057–3064.
33 V. V. Rostovtsev, L. G. Green, V. V. Fokin and K. B. Sharpless, *Angew. Chem., Int. Ed.*, 2002, **41**, 2596–2599.
34 D. T. S. Rijkers, G. W. van Esse, R. Merkx, A. J. Brouwer, H. J. F. Jacobs, R. J. Pieters and R. M. J. Liskamp, *Chem. Commun.*, 2005, 4581–4583.
35 B. Jagadish, R. Sankaranarayanan, L. Xu, R. Richards, J. Vagner, V. J. Hruby, R. J. Gillies and E. A. Mash, *Bioorg. Med. Chem. Lett.*, 2007, **17**, 3310–3313.
36 L. Petraru and W. H. Binder, *Polym. Prepr.*, 2005, **46**, 841–842.
37 V. Ervithayasupron, X. Wang and Y. Kawakami, *Chem. Commun.*, 2009, 5130–5132.
38 M. Ak, B. Gacal, B. Kiskan, Y. Yagci and L. Toppare, *Polymer*, 2008, **49**, 2202–2210.
39 Z. Ge, L. Wang, Y. Zhou, H. Liu and S. Liu, *Macromolecules*, 2009, **42**, 2903–2910.
40 U. Dittmar, B. J. Hendan, U. Flörke and H. C. Marsmann, *J. Organomet. Chem.*, 1995, **489**, 185–194.
41 S. Lücke, K. K. Stoppek-Langner, B. Krebs and M. Läge, *Z. Anorg. Allg. Chem.*, 1997, **623**, 1243–1246.
42 S. Bräse, C. Gil, K. Knepper and V. Zimmermann, *Angew. Chem.*, 2005, **117**, 5320–5374.
43 F. J. Feher, K. D. Wyndham, D. Soulivong and F. Nguyen, *J. Chem. Soc., Dalton Trans.*, 1999, 1491–1497.
44 E. Rikowski and H. C. Marsmann, *Polyhedron*, 1997, **16**, 3357–3361.
45 F. J. Feher and T. A. Budzichowski, *J. Organomet. Chem.*, 1989, **379**, 33–40.
46 D. Heyl, E. Rikowski, R. C. Hoffmann, J. J. Schneider and W.-D. Fessner, *Chem. Eur. J.*, 2010, DOI: 10.1002/chem.201000488.
47 A. J. Papa, *J. Org. Chem.*, 1966, **31**, 1426–1430.
48 C. Li, A. Arasappan and P. L. Fuchs, *Tetrahedron Lett.*, 1993, **34**, 3535–3538.
49 C. Li, T. Shih, J. U. Jeong, A. Arasappan and P. L. Fuchs, *Tetrahedron Lett.*, 1994, **35**, 2645–2646.
50 R. E. Conrow and W. D. Dean, *Org. Process Res. Dev.*, 2008, **12**, 1285–1286.
51 E. S. Park, H. W. Ro, C. V. Nguyen, R. L. Jaffe and D. Y. Yoon, *Chem. Mater.*, 2008, **20**, 1548–1554.
52 O. Cozar, L. David, V. Chis, G. Damian, M. Todica and C. Agut, *J. Mol. Struct.*, 2001, **563–564**, 371–375.
53 E. Lieber, C. N. R. Rao, T. S. Chao and C. W. W. Hoffman, *Anal. Chem.*, 1957, **29**, 916–918.
54 S. Bräse, C. Gil, K. Knepper and V. Zimmermann, *Angew. Chem., Int. Ed.*, 2005, **44**, 5188–5240.
55 M. Peer, *Spec. Chem.*, 1998, **18**, 256–263.
56 C. Bolln, A. Tsuchida, H. Frey and R. Mülhaupt, *Chem. Mater.*, 1997, **9**, 1475–1479.
57 A. Fina, D. Tabuani, F. Carniato, A. Frache, E. Boccaleri and G. Camino, *Thermochim. Acta*, 2006, **440**, 36–42.
58 Z. Zhang, G. Liang and T. Lu, *J. Appl. Polym. Sci.*, 2007, **103**, 2608–2614.
59 F. J. Feher and K. D. Wyndham, *Chem. Commun.*, 1998, 323–324.
60 C. McCusker, J. B. Carroll and V. M. Rotello, *Chem. Commun.*, 2005, 996–998.
61 S. Reiss, M. Sieber, V. Oberle, A. Wentzel, P. Spangenberg, R. Claus, H. Kolmar and W. Loesche, *Platelets*, 2006, **17**, 153–157.
62 Synthesis of *N*-(3′,6′-dihydroxy-3-oxo-3*H*-spiro[isobenzofuran-1,9′-xanthene]-5-yl)hex-5-ynamide is given in the ESI†.
63 D. S. Pedersen and C. Rosenbohm, *Synthesis*, 2001, 2431–2434.
64 M. Tarini, P. Cignoni and C. Montani, *IEEE Transactions on Visualization and Computer Graphics*, 2006, **12**, 1237–1244.

3.2. From pico to nano: biofunctionalization of cube-octameric silsesquioxanes by peptides and miniproteins

Sebastian Fabritz , Sebastian Hörner , Doreen Könning , Martin Empting , Michael Reinwarth , Christian Dietz , Bernhard Glotzbach , Holm Frauendorf , Harald Kolmar and Olga Avrutina

Org. Biomol. Chem., 2012,**10**, 6287-6293
DOI: 10.1039/C2OB25728A
Received 13 Apr 2012, Accepted 11 Jun 2012
First published on the web 13 Jun 2012

Graphical Abstract:

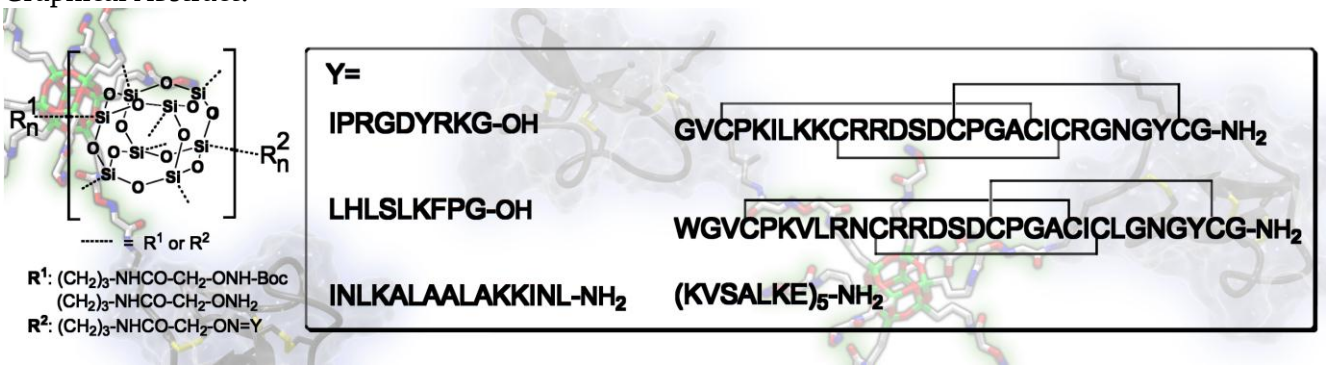

Short Summary:
Conjugation of bioorthogonal aminooxy cube-octameric silsesquioxanes with bioactive peptides and miniproteins as well as AFM analysis of resulting constructs are given.

Detailed analytical Data are given in chapter 4.2..

View Online / Journal Homepage
Dynamic Article Links

Organic & Biomolecular Chemistry

Cite this: DOI: 10.1039/c2ob25728a

www.rsc.org/obc

PAPER

From pico to nano: biofunctionalization of cube-octameric silsesquioxanes by peptides and miniproteins†

Sebastian Fabritz,‡[a] Sebastian Hörner,‡[a] Doreen Könning,[a] Martin Empting,[a] Michael Reinwarth,[a] Christian Dietz,[b] Bernhard Glotzbach,[a] Holm Frauendorf,[c] Harald Kolmar*[a] and Olga Avrutina*[a]

Received 13th April 2012, Accepted 11th June 2012
DOI: 10.1039/c2ob25728a

Polyhedral silsesquioxanes are considered valuable conjugation scaffolds. Nevertheless, only a few examples of silsesquioxane-assembled peptide oligomers have been reported to date. We developed a new bioorthogonal cube-octameric silsesquioxane (COSS) scaffold bearing eight aminooxy coupling sites allowing for the conjugation of diverse peptides *via* oxime ligation. We found that the coupling efficacy depends on the ligand in view of steric hindrance and electrostatic repulsion. For the first time scaffold-based conjugation of cystine-knot miniproteins having a backbone of about thirty amino acids was successfully accomplished without loss of bioactivity. Atomic force microscopy (AFM) provided further knowledge on the size of COSS verifying them as picoscaffolds growing upon bioconjugation to nano-dimension.

Introduction

Combining several ligands on a single scaffold often results in improved characteristics of a formed oligomer compared to its individual constituents. Nature extensively uses this phenomenon known as multivalency to effect biomolecular interactions[1] in living organisms by enhancing affinity and specificity of binding.[2] This inspires research efforts towards creation of synthetic molecules in which the benefits of simultaneous multiple contacts are achieved through the oligomerization of bioactive modules – small molecules,[3] carbohydrates,[4] peptides,[5] and proteins.[1] Properties of scaffold-grafted molecular blocks are often governed by the peculiar architecture that implies shape, size, and valency of the framework, as well as spatial orientation of ligands.[6]

In recent years, cube-octameric silsesquioxanes (COSS)[7,8] have been brought into focus as promising oligomerization scaffolds due to their unique characteristics. These monodisperse particles with a core size of 0.5 nm[9] are considered the smallest known nanoscaffolds with a high degree of symmetry. Their hybrid molecules are composed of a siloxane inorganic core decorated with organic ligands which combine an aliphatic linker with a terminal active group. From a broad repertoire of functionalized COSS molecules reported to date, amine,[10] azide,[11–13] alkyne,[12] thiol,[14] aldehyde[15] or maleimide bearing[16] particles are potentially applicable for bioconjugations.

To date, several COSS-based bioconjugates have been reported, among them lysine dendrimers for drug delivery,[17,18] oligomers of peptides[12,19] and carbohydrates,[13,20] as well as macrocyclic Gd^{3+} chelates as potential magnetic resonance imaging contrast agents.[21]

The convergent synthesis of peptidic COSS is limited to homopolypeptides where one amino acid unit with a protected or non-reactive side chain is propagated,[22,23] or to rather short (up to 8 residues) RGD oligomers.[12] In these bioconjugations, copper-catalyzed azide–alkyne cycloaddition (CuAAC) is currently the established method to obtain a linkage between an azide-bearing silsesquioxane and an alkyne-modified peptidic ligand usually added in stoichiometric excess.[24,25] Due to the instability of a COSS core in the presence of aqueous nucleophiles,[21,26] CuAAC with silsesquioxanes is generally performed in water-free DMF.[12,27,28] In this aprotic solvent, the copper catalyst often appeared to be coordinated by an amide backbone[29] or functional side chains[30] of peptides leading to a drastic decrease of active catalytic species and, as a consequence, to prolonged reaction times (up to several weeks) and low yields.[12] Very recently, an elegant alternative approach to silsesquioxane-based peptide conjugations has been reported which utilized the photo-induced free-radical thiol–ene coupling and resulted in eightfold presentation of the tripeptide glutathione on a COSS scaffold.[31,32] Interestingly, for a tetrapeptide RGDC complete

[a]*Clemens-Schöpf Institute of Organic Chemistry and Biochemistry, Technische Universität Darmstadt, Petersenstr. 22, 64287 Darmstadt, Germany.*
E-mail: Kolmar@Biochemie-TUD.de; Avrutina@Biochemie-TUD.de
[b]*Center of Smart Interfaces, Technische Universität Darmstadt, Petersenstr. 32, 64287 Darmstadt, Germany*
[c]*Institute of Organic and Biomolecular Chemistry, Georg-August Universität Göttingen, Tamannstraße 2, 37077 Göttingen, Germany*
†Electronic supplementary information (ESI) available: ^{1}H-NMR and ^{29}Si-NMR data of **2**, **3**; ESI-MS data of **2–9**; IR spectra of **2**, **3**. See DOI: 10.1039/c2ob25728a
‡These authors contributed equally to this work.

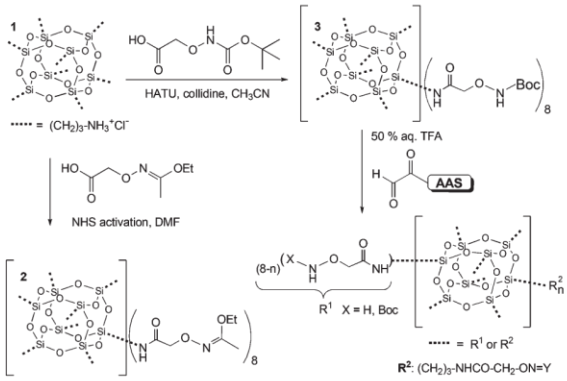

Peptidic Ligands

Amino Acid Sequence (AAS)	Precursor	Conjugate	
IPRGDYRKG-OH	p4	4	8
LHLSLKFPG-OH	p5	5	8
INLKALAALAKKINL-NH_2	p6	6	6
GVCPKILKKCRRDSDCPGACICRGNGYCG-NH_2	p7	7	3
WGVCPKVLRNCRRDSDCPGACICLGNGYCG-NH_2	p8	8	3
$(KVSALKE)_5$-NH_2	p9	9	2

Scheme 1 Synthetic approaches to protected aminooxy COSS **2** and **3**. Octakis (Boc-aminooxy) COSS was used as a scaffold for bioconjugation. Ligands: an octapeptide with an RGD motif (**p4**), a derivative of the antimicrobial peptide Jelleine 1 (**p5**), mastoparan (**p6**), MCoTI-based miniproteins (**p7**, **p8**) and Kcoil, a basic α-helical coil (**p9**), were chosen.

hydrothiolation of vinyl coupling sites was achieved only after the introduction of elongation linkers.[31]

Herein, we report bioconjugation on a COSS scaffold in acidic aqueous media based on the oxime ligation[33,34] between an aldehyde and an aminooxy functionality (Scheme 1). This approach provides several advantages compared to other methods reported for COSS–peptide conjugations[12,27,28,31,32] as it ensures both stability of the silsesquioxane core and good solubility of biological ligands. The introduction of aldehyde moieties into biomolecules is well-established and can easily be achieved *via* periodate oxidation of an N-terminal serine residue.[35] Moreover, building blocks for solid phase peptide synthesis[36,37] containing a masked side-chain aldehyde function enable the generation of this moiety at any desired sequence position. Aminooxy functionality can be easily introduced in peptides by N-acylation of side-chain or terminal amines by butoxycarbonyl (Boc)[38] or ethoxyethylidene (Eei)[39,40] protected aminooxy acetic acid. Protection is essential to avoid side reactions and overacylation of target compounds. In the present research, the applicability of the oxime ligation to the synthesis of hybrid COSS–peptide conjugates was studied highlighting the benefits and the limitations of the method.

Table 1 Reaction conditions for the synthesis of **3**

No.	Solvent	Base equiv. (collidine)	Activator (8 × 5.2 equiv.)	Overacylated 0	×1	×2	×3
1	DMF	85	HBTU	X	X	X	X
2	DMF	43	HBTU	X	X	nd	nd
3	DMF	53	HATU	X	X	nd	nd
4	MeCN	53	HATU	X	X	X	X
5	MeCN	20	HATU	X	nd	nd	nd
6	DMF	20	HATU	X[a]	nd	nd	nd

X: detected; nd: not detected.[a] Reaction showed incomplete conversion. Heptameric Boc-aminooxy COSS species were detected *via* LC-MS analysis.

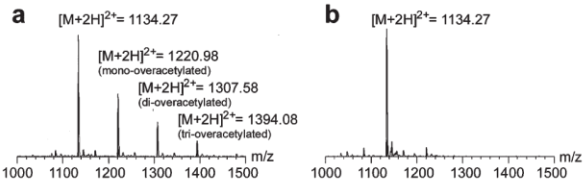

Fig. 1 ESI-MS spectra for the synthesis of **3**. (a) Reaction in DMF using HBTU and 85 equiv. collidine; (b) reaction in MeCN using HATU and 20 equiv. collidine.

Results and discussion

As a conjugation scaffold an octaaminopropyl-COSS **1** was used. The reaction with commercially available mono-Boc aminooxy acetic acid towards **3** appeared strongly dependent on the activation conditions leading to overacylated species (Table 1).

Decostaire *et al*. have recently reported[38] that the control over these undesired processes could be achieved by the proper choice of used activator, base, and solvent as well as their excess. Corroborating the reported data,[38] 2-(7-aza-1*H*-benzotriazole-1-yl)-1,1,3,3-tetramethyluronium hexa-fluoro-phosphate (HATU) activation in the presence of collidine was found to be the optimal reaction conditions, and 20 equivalents of the base per silsesquioxane octamer were used (Fig. 1). Although no overacylated COSS species have been found in both acetonitrile- and DMF-based reaction mixtures (Table 1, entries 5 and 6), dry acetonitrile appeared to be the solvent of choice as no complete conversion was observed in DMF after an overnight reaction. Contrary to this procedure, reaction of **1** with *N*-hydroxysuccinimide-activated 2-(1-ethoxy-ethylidene-aminooxy) acetic acid[40] resulted in octakis Eei-protected aminooxy-COSS **2** without overacylation. Due to the instability of COSS in the presence of aqueous nucleophiles,[21,26] the cage integrity of **2** and **3** was verified by ^{29}Si-NMR and IR spectroscopy (see ESI Fig. S3, S4 and S6†). The NMR spectra showed exclusively the shifts corresponding to COSS cages **2** and **3** (δ −66.87 and δ −66.75, respectively). The IR spectra showed a Si–O–Si stretch characteristic band at 1115 cm^{-1}. Both Boc and Eei groups were cleaved in 50% aqueous trifluoroacetic acid (TFA) within 3 hours, and one-pot conjugation with aldehyde functionalized peptides[35] succeeded. In our study, ligands with diverse primary

and secondary structures and different bioactivity were used (Scheme 1).

For the initial experiment, an integrin-binding octapeptide bearing an RGD functional motif (**p4**) was chosen.[41,42] It was shown previously that this ligand could be coupled onto the COSS scaffold in eightfold copies *via* CuAAC.[12] We found that oxime ligation had obvious benefits compared to CuAAC as the reaction time needed for full conversion was drastically reduced – from several weeks to an overnight reaction at room temperature. LC-MS monitoring of the reaction progress showed the presence of COSS species bearing both protected aminooxy coupling sites and oxime-ligated peptides (see ESI Fig. S8†), indicating that Boc cleavage was the rate-determining step. Nevertheless, as soon as full deprotection was achieved, the steric hindrance and electrostatic repulsion caused by the growing number of peptidic ligands seemed to have a major influence on the reaction progress.

Consequently, we explored the ligand-dependent limitations of the proposed COSS-based oximation. It is obvious that direct coupling of bulky peptide ligands onto constrained COSS scaffolds can be hindered due to steric reasons. On the other hand, often the oligomerization of peptides and full-size proteins is desirable without implementation of elongation linkers. Therefore, in a series of coupling experiments the size of bioactive peptidic ligands was progressively increased from eight (**p4**) to 35 (**p9**) amino acid residues.

To that end, a derivative of natural antimicrobial peptide Jelleine 1[43,44] from the royal jelly of honey bees (**p5**) was used. The successful eightfold presentation of this octapeptide on the COSS scaffold encouraged us to approach more sophisticated ligands. Thus, an α-helical calmodulin[45] binding peptide mastoparan (**p6**)[46] comprising 14 residues, trypsin inhibitors[47] **p7** and **p8** having 29 and 30 residues, respectively, and the inherent Kcoil part of a heterodimeric coiled coil (**p9**)[48–50] with a length of 35 amino acids were used. Moreover, miniproteins[51] **p7** and **p8** contained a characteristic tri-disulfide pattern known as a cystine knot[52] that is absolutely essential for the function; the damage of this motif results in the loss of three-dimensional structure and, as a consequence, of bioactivity.[52]

All peptidic ligands contained, compared to their parent sequences, an additional N-terminal serine and were assembled by standard microwave-assisted Fmoc-SPPS as previously described.[53] After chain assembling and cleavage from the support, sodium periodate oxidation resulted in peptide aldehydes.[35] In the case of miniproteins **p7** and **p8**, oxidative folding[54] into a cystine knot preceded the formation of an N-terminal glyoxal.

One-step deprotection of **3** followed by conjugation with peptidic ligands **p5**–**p9** was performed in 50% aqueous TFA as described above. The LC-MS monitoring of the conjugation reaction with cystine-free ligands revealed the formation of COSS–peptide intermediates after 10 min. Within 12 hours the reactions were completed. The formation of miniprotein–COSS conjugates **7** and **8** was only observed after an overnight reaction. This might be attributed to a hindered accessibility of the miniprotein aldehyde functionalities.

The amount of ligand copies attached to the COSS core correlated with the primary structure of the peptides and the increasing steric demand. Thus, the conjugation with the Jelleine-derived octapeptide **p5** yielded an octameric product. Mastoparan **p6** with just 6 additional amino acids formed a hexameric conjugate. In miniproteins **p7** and **p8** the amount of amino acids is doubled compared to **p6** resulting in a decreased coupling efficacy. Accordingly, only di- as well as trimeric constructs were observed for these ligands (Fig. 2). Finally, the pronounced steric hindrance as well as the possibility of strong electrostatic

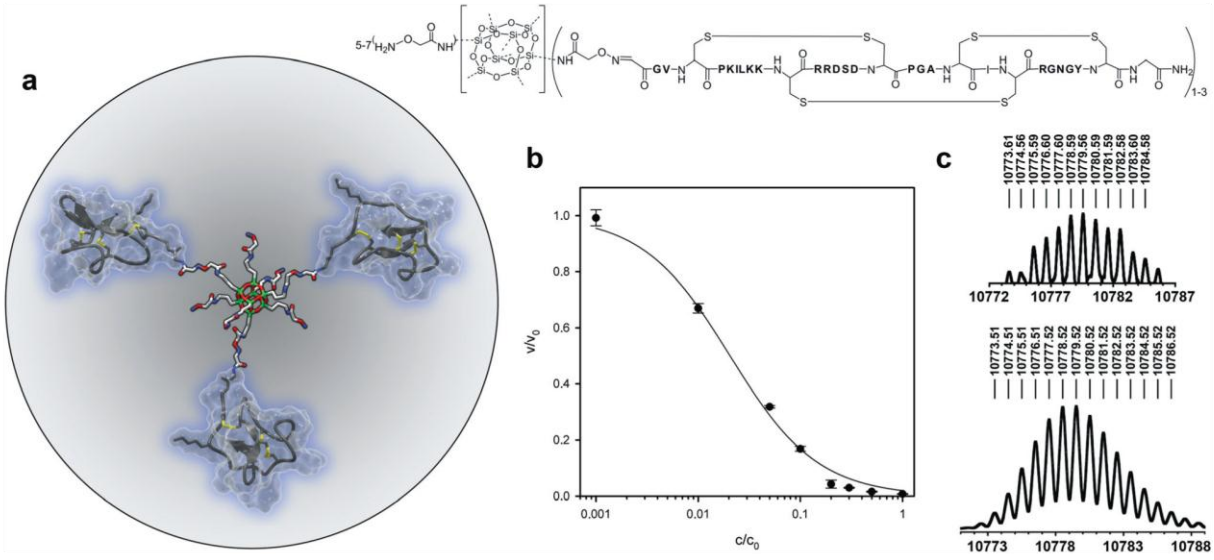

Fig. 2 (a) Proposed YASARA model of a miniprotein–COSS conjugate (pale blue: MCoTI miniproteins with disulfide bridges depicted as yellow sticks; red: oxygen; blue: nitrogen; green: silicon; grey: carbon) and its chemical structure. (b) Inhibition of trypsin-catalyzed proteolysis of chromogenic substrate *Boc*-QAR-*pNA* by conjugate **7**. Trypsin fractional activity is plotted as a function of inhibitor concentration on a log scale.[56] (c) Observed (top) and simulated (bottom) HR-MS spectra of **7**.

repulsion allowed only for the formation of mono- and dimeric products with the α-helical Kcoil peptide **p9**.

To the best of our knowledge, to date the dimerization of miniproteins was only facilitated *via* chemical cross-linking using a bis-succinimidyl suberate.[55] Herein, we present the first scaffold-based approach to the oligomerization of miniproteins. To examine whether cystine knot protease inhibitors retained their unique three-dimensional structure after conjugation, we studied the bioactivity of formed hybrid molecules. To that end, an RP-HPLC fraction containing conjugate **7** and lower substituted COSS–**p7** conjugates was tested for inhibitory activity against trypsin (Fig. 2).[56] Although a precise determination of inhibitor concentrations in the mixture of tri-, bi- and monoconjugated miniproteins was not possible and corresponding inhibition constants were not calculated, the concentration-dependent inhibition of trypsin-mediated proteolysis provided clear evidence that the bioactivity of **p7** was preserved under oximation conditions.

The bioactivity and toxicity of nanoparticles as well as their potential for drug delivery is greatly dependent on the size. Therefore, we conducted atomic force microscopy (AFM) experiments using the particles **1**, **4**, and **5**. We considered mica (negatively charged sheet silica) an optimal substrate, as the eight amino groups of **1** and the peptidic side chains of **4** and **5** promised a good binding to this surface. The dropcasting of an acidic solution of **1** (~1 ng mL^{-1}) allowed us to visualize singular particles. The enumeration of 60 particles (see ESI Fig. S7† and Fig. 3d) resulted in an average particle size of 743 ± 211 pm. This value is in good accordance with the literature stating ~500 pm for the POSS core.[8,9] For further measurements a mica substrate was dipcoated with an RP-HPLC fraction containing **4**. An analysis of the particle size distribution revealed an average size of 1810 ± 300 pm. Hence, the peptidic shell induced a measurable size increase of 1050 pm. On a first glance, this value seemed to be rather small compared to a rough simulation of **4** predicting 6.42 ± 0.69 nm as its maximal diameter in solution (see ESI Fig. S12†). However, it has to be taken into account that the particle is absorbed on a mica surface and might adopt a pancake-like structure. Furthermore, the recorded topography of a sample always depends on several parameters. Being operated in tapping mode, the AFM *z*-piezo detects changes upon the interaction of its tip with an analyzed sample keeping the amplitude of the vibrating cantilever constant. If attractive van der Waals forces change due to differences in the Hamaker constant[57] between two materials, the *z*-piezo will compensate this difference by varying the mean distance between the tip and the sample. On soft materials, compared to the sample substrate, an additional difference of the indentation depth of the tip into the material is compensated by the *z*-piezo. As a consequence, even for atomically flat surfaces a non-negligible height profile can be measured for inhomogeneous samples.[58] Hence, the measured height differences should only be used to classify the nanoparticle dimension.

The subsequent analysis of **5** revealed, in accordance with the expectations, particles with a similar height profile. Therefore, we chose a random particle and continuously increased its mapping resolution using bimodal atomic force microscopy. Fig. 4a shows the high resolution phase image of the second eigenmode. Phase images in AFM are related to mechanical properties of the sample. Three regions with a distinctive phase shift between cantilever oscillation and excitation were identified. The difference in phase values of mica ($\Delta\varphi_2$ = 120°) and the main body of the particle ($\Delta\varphi_2$ = 119°) can be attributed to the mechanical dissimilarity of the materials. A region with a relatively low phase shift ($\Delta\varphi_2$ = 110°) was found in the right part of the particle (Fig. 4b). An image artefact can be excluded since the same area was successively scanned several times depicting comparable contrast. We presume that this region might visualize the position of the mica-adsorbed silsesquioxane core surrounded by randomly oriented peptide chains (Fig. 4d).

Conclusion

A new bioorthogonal COSS scaffold was developed comprising a highly symmetric silsesquioxane core decorated with aminooxy functional modules. We demonstrated the applicability of this scaffold for the oligomerization of aldehyde-bearing peptidic ligands through oxime ligation. Our scheme has an obvious advantage as all involved reactions proceed in an acidic medium that does not affect the COSS core known to be extremely unstable in the presence of nucleophiles. We found that the coupling efficacy depends on the ligand in view of steric hindrance and electrostatic repulsion. Thus, octapeptide derivatives were eightfold presented on a COSS scaffold, whereas for more bulky ligands lower oligomers were detected. Nevertheless, for the first time the scaffold-based conjugation of miniproteins comprising a backbone of about thirty amino acids with a structure-defining cystine knot was successfully accomplished without the loss of ligand bioactivity.

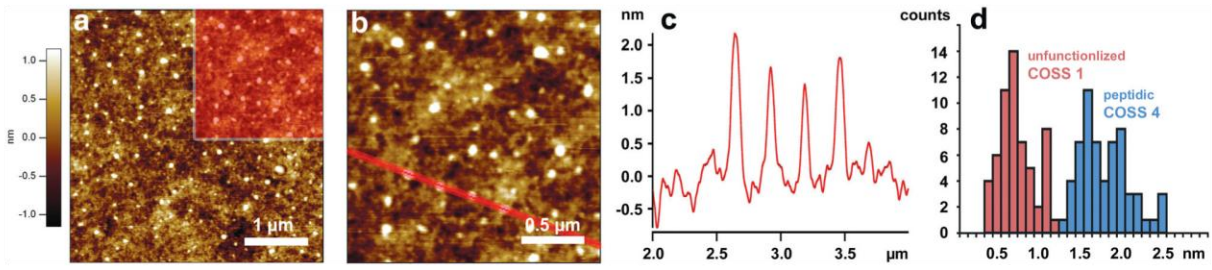

Fig. 3 (a) AFM topography image of a uniformly distributed COSS–peptide particle **3** on a mica surface; (b) image extension displaying the trend of the section line; (c) profile of four adjacent particles; (d) comparative histogram depicting the size distribution of **1** and **4**.

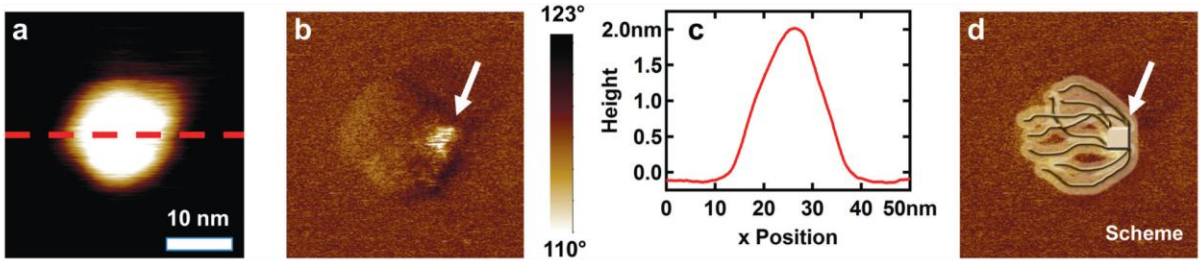

Fig. 4 High-resolution image of a single COSS–peptide particle **4** using bimodal atomic force microscopy. (a) Topography image and (b) profile of a single particle. (c) Corresponding second eigenmode phase image. The image reveals a bright region at the right area of the particle. (d) Schematic structure of the particle deduced from the phase image shown in (b).

AFM experiments conducted in the present study provided further knowledge on the size of COSS allowing us to consider them as picoscaffolds growing upon bioconjugation to nano-dimension.

Detailed studies concerning the bioactivity of COSS-assembled conjugates are currently ongoing, with constructs **6** and **9** being of particular interest. They can provide an interface for the non-covalent oligomerization of proteins fused either to a complementary Ecoil or to calmodulin. Thus, oligomerization can occur *via* the formation of a Kcoil/Ecoil leucine zipper,[48] or through tight binding to mastoparan,[46] respectively.

Experimental

Peptide synthesis

Microwave-assisted Fmoc-SPPS of peptide ligands was performed on a CEM *liberty*® peptide synthesizer equipped with a CEM *discover*® SPS microwave (CEM GmbH). As solid supports 2-CT-resin-Gly-OH from Iris Biotech GmbH (**p4** and **p5**), AmphiSphere™ 40 RAM resin from Varian Inc. (**p6**, **p7** and **p8**) and NovaSyn®TGR resin from Merck KGaA (**p8**) were used. After cleavage, cysteine-free crude products were oxidized using 10 equiv. of sodium periodate in PBS buffer for 10 min. The reaction product was isolated by RP-HPLC using a Varian 940-LC equipped with a YMC Europe GmbH C18 column (250 × 20 mm; S- 4 µm, 8 nm). Oxidative folding[59] of hexathiol precursors was followed by RP-HPLC purification. The resulting cystine knots were submitted to the above-described periodate oxidation procedure.

Synthesis of octa(aminopropyl) COSS 1

The synthesis of **1** was performed according to the reported procedure.[10]

Synthesis of scaffold 2

10 mg (1 equiv., 0.009 mmol) of **1**, 90 mg (5 equiv. per ammonium group, 0.35 mmol) of Eei protected and NHS activated aminooxyacetic acid[40] and 240 µL (20 equiv. per ammonium group, 178.1 mg, 1.38 mmol) of dry DIEA were dissolved in 3 mL of dry DMF. After 12 hours of stirring, full conversion of **1** into **2** was confirmed by LC-MS monitoring. Subsequently, the solvent and base were removed *in vacuo*. The resulting crude product was purified *via* RP-HPLC using a semi-preparative C4 column (300 × 20 mm, 5 µ, PSS Polymer Standards Service GmbH) and a linear gradient of 90% aq. MeCN (10 → 100% B in 63 min) preceded by 10 min isocratic 10% B at a flow rate of 10 mL min^{-1} with t_R = 48.0 min. Yield after RP-HPLC purification: 5.7 mg (33%).

HR-MS: calc. for $C_{72}H_{136}N_{16}O_{36}Si_8$ (+2): 1013.3801, meas. 1013.3800 $[M + 2H]^{2+}$, 1024.3710 $[M + H + Na]^{2+}$, 1035.3622 $[M + 2Na]^{2+}$; ATR-IR: *ν* 702 w, 1114 vs, 1308 m, 1378 w, 1540 w, 1651 m, 2933 vw, 3332 vw cm^{-1}, ^{29}Si NMR IGATED (99 MHz, $CDCl_3$): δ −66.85.

Synthesis of scaffold 3

50 mg (1 equiv., 0.043 mmol) of **1**, 347 mg Boc-aminooxy acetic acid (5.3 equiv. per ammonium group, 1.815 mmol), 674 mg HATU (5.2 equiv. per ammonium group, 1.773 mmol) and 112.5 µL dry collidine (120.8 mg, 2.9 equiv. per ammonium group, 0.997 mmol) were dissolved in 8 mL dry MeCN. After 12 hours of stirring full conversion of **1** into **3** was confirmed *via* LC-MS monitoring. Subsequently, the solvent and base were removed *in vacuo*. The resulting crude product was purified *via* RP-HPLC using a semi-preparative C8 column (250 × 20 mm, 5 µ, Phenomenex Inc.) and a linear gradient of 90% aq. MeCN in 0.1% aq. TFA (40 → 100% B in 20 min) preceded by 5 min isocratic 40% B at a flow rate of 18 mL min^{-1} with t_R = 16.5 min. Yield after RP-HPLC purification: 3.6 mg (4%).

HR-MS: calc. for $C_{80}H_{154}N_{16}O_{44}Si_8$ (+2): 1133.4224, meas. 1133.4216 $[M + 2H]^{2+}$; ATR-IR: *ν* 1115 vs, 1286 m, 1371 w, 1567 w, 1661 m, 1729 m, 2944 vw, 2989 vw, 3327 vw, ^{29}Si NMR (99 MHz, $CDCl_3$): δ −66.90.

Conjugation of peptidic ligands on aminooxy COSS 3

0.1 mg (1 equiv., 0.041 µmol) of **3** were dissolved in 500 µL 50% aq. TFA and 9 equiv. (0.39 µmol) of a corresponding peptidic ligand were added. The reaction process was monitored for 12 hours by LC-MS. The conjugates were isolated *via* RP-HPLC using an analytical C4 column (50 × 1 mm, 5 µ, Phenomenex Inc.) and a linear gradient of MeCN in 0.1% aq. formic acid (2 → 100% in 10 min) at a flow rate of 0.2 mL min^{-1}.

HR-MS: calc. for **4** $C_{424}H_{689}N_{144}O_{140}Si_8$ (+9): 1140.4375, meas. 1140.4393 $[M + 9H]^{9+}$ (see Fig. S9 and S10†), calc. for **5**

$C_{448}H_{705}N_{112}O_{124}Si_8$ (+9): 1096.0051, meas. 1096.0042 $[M + 9H]^{9+}$ (see ESI Fig. S14 and S15†), calc. for **6** $C_{472}H_{862}N_{130}O_{124}Si_8$: 10 565.34, meas. 10 565.37 (see ESI Fig. S17 and S18†), calc. for **7** $C_{418}H_{697}N_{145}O_{139}S_{18}Si_8$: 10 773.51, meas. 10 773.61 (see ESI Fig. S20 and S21†), calc. for **8** $C_{308}H_{496}N_{104}O_{106}S_{12}Si_8$: 7957.15, meas. 7957.22 (see ESI Fig. S23 and S24†), calc. for **9** $C_{384}H_{700}N_{108}O_{130}Si_8$: 9132.97, meas. 9132.98 (see ESI Fig. S26 and S27†).

Yields based on the integration of HPLC traces at 220 nm: 90% (conjugate **4**) and 99% (conjugate **5**).

See the ESI† for full LC-MS and HR-MS data.

Trypsin inhibition assay

The trypsin inhibition assay of **7** was performed according to the reported procedure.[56]

High resolution imaging of COSS–peptide particles using bimodal atomic force microscopy

Tapping mode atomic force microscopy measurements were performed on COSS–peptide particles randomly distributed on a mica surface. The resonance frequency of the cantilever (PPP-ZEIHR and PPP-NCH from NanoandMore GmbH, Wetzlar, Germany) was f_1 = 120–320 kHz and a free amplitude of $A_{01} \approx 10$ nm was chosen. We paid careful attention to operate the AFM in the net attractive regime where van der Waals forces dominate the tip–sample interaction by keeping the free amplitude low and using a relatively high setpoint amplitude $A_1/A_{01} \approx 0.9$. This operation regime is comparably gentle to the sample surface avoiding excessive indentation of the tip apex into the surface structure.

High-resolution images on single COSS–peptide particles were accomplished using bimodal atomic force microscopy.[60–66] Compared to the conventional tapping mode, the cantilever was excited simultaneously at the first two flexural eigenmodes. The amplitude of the first eigenmode was kept constant varying the distance between a tip and a sample (as in conventional tapping). Additionally, the amplitude and phase shift of the second eigenmode sensed compositional variations of the sample with very high accuracy. The cantilevers' resonance frequencies (PPP-ZEIHR Cantilever) were as follows: f_1 = 127 kHz and f_2 = 781 kHz for the first and second oscillations, respectively. The free amplitude of the oscillating cantilever was excited to A_{01} = 5 nm and A_{02} = 0.5–1 nm.

AFM image processing

All topography images were 1st order flattened in order to remove image tilt. A Gauss filter was applied to enhance the signal-to-noise ratio.

Acknowledgements

We acknowledge the collaboration with Prof. Dr Robert Stark (Center of Smart Interfaces, Technische Universität Darmstadt) with respect to AFM measurements in the frame of the LOEWE Soft Control consortium. We thank Volker Schmidts (Clemens-Schöpf Institute of Organic Chemistry and Biochemistry, Technische Universität Darmstadt) for the performance of ^{29}Si-NMR experiments on **3**.

References

1 P. H. Ehrlich, *J. Theor. Biol.*, 1979, **81**, 123–127.
2 S. M. Deyev and E. N. Lebedenko, *Bioassays*, 2008, **30**, 904–918.
3 D. Wright and L. Usher, *Curr. Org. Chem.*, 2001, **5**, 1107–1131.
4 R. J. Pieters, *Org. Biomol. Chem.*, 2009, **7**, 2013–2025.
5 S. P. Liu, L. Zhou, R. Lakshminarayanan and R. W. Beuerman, *Int. J. Pept. Res. Ther.*, 2010, **16**, 199–213.
6 J. E. Gestwicki, C. W. Cairo, L. E. Strong, K. A. Oetjen and L. L. Kiessling, *J. Am. Chem. Soc.*, 2002, **124**, 14922–14933.
7 J. F. Brown, L. H. Vogt and P. I. Prescott, *J. Am. Chem. Soc.*, 1964, **86**, 1120–1125.
8 D. B. Cordes, P. D. Lickiss and F. Rataboul, *Chem. Rev.*, 2010, **110**, 2081–2173.
9 H. Mori, Y. Miyamura and T. Endo, *Langmuir*, 2007, **23**, 9014–9023.
10 F. J. Feher and K. D. Wyndham, *Chem. Commun.*, 1998, 323–324.
11 V. Ervithayasuporn, X. Wang and Y. Kawakami, *Chem. Commun.*, 2009, 5130–5132.
12 S. Fabritz, D. Heyl, V. Bagutski, M. Empting, E. Rikowski, H. Frauendorf, I. Balog, W.-D. Fessner, J. J. Schneider, O. Avrutina and H. Kolmar, *Org. Biomol. Chem.*, 2010, **8**, 2212–2218.
13 B. Trastoy, M. Eugenia Perez-Ojeda, R. Sastre and J. Luis Chiara, *Chem.–Eur. J.*, 2010, **16**, 3833–3841.
14 U. Dittmar, B. J. Hendan, U. Flörke and H. C. Marsmann, *J. Organomet. Chem.*, 1995, **489**, 185–194.
15 B. W. Manson, J. J. Morrison, P. I. Coupar, P. A. Jaffres and R. E. Morris, *J. Chem. Soc., Dalton Trans.*, 2001, 1123–1127.
16 R. Tamaki, Y. Tanaka, M. Z. Asuncion, J. W. Choi and R. M. Laine, *J. Am. Chem. Soc.*, 2001, **123**, 12416–12417.
17 T. L. Kaneshiro, X. Wang and Z.-R. Lu, *Mol. Pharm.*, 2007, **4**, 759–768.
18 K. Tanaka, K. Inafuku, K. Nakab and Y. Chujo, *Org. Biomol. Chem.*, 2008, **6**, 3899–3901.
19 F. J. Feher, K. D. Wyndham, M. A. Scialdone and Y. Hamuro, *Chem. Commun.*, 1998, 1469–1470.
20 D. Heyl, E. Rikowski, R. C. Hoffmann, J. J. Schneider and W.-D. Fessner, *Chem.–Eur. J.*, 2010, **16**, 5544–5548.
21 J. Henig, E. Toth, J. Engelmann, S. Gottschalk and H. A. Mayer, *Inorg. Chem.*, 2010, **49**, 6124–6138.
22 Y.-C. Lin and S.-W. Kuo, *Polym. Chem.*, 2012, **3**, 162–171.
23 S.-W. Kuo, H.-F. Lee, W.-J. Huang, K.-U. Jeong and F.-C. Chang, *Macromolecules*, 2009, **42**, 1619–1626.
24 V. V. Rostovtsev, L. G. Green, V. V. Fokin and K. B. Sharpless, *Angew. Chem., Int. Ed.*, 2002, **41**, 2596–2599.
25 O. Avrutina, M. Empting, S. Fabritz, M. Daneschdar, H. Frauendorf, U. Diederichsen and H. Kolmar, *Org. Biomol. Chem.*, 2009, **7**, 4177–4185.
26 E. Rikowski and H. C. Marsmann, *Polyhedron*, 1997, **16**, 3357–3361.
27 S.-W. Kuo and H.-T. Tsai, *Polymer*, 2010, **51**, 5695–5704.
28 Y.-C. Lin and S.-W. Kuo, *J. Polym. Sci., Part A: Polym. Chem.*, 2011, **49**, 2127–2137.
29 H. Sigel and R. B. Martin, *Chem. Rev.*, 1982, **82**, 385–426.
30 A. Jancso, K. Andras, B. Gyurcsik, N. V. Nagy and T. Gajda, *J. Inorg. Biochem.*, 2009, **103**, 1634–1643.
31 M. Lo Conte, S. Staderini, A. Chambery, N. Berthet, P. Dumy, O. Renaudet, A. Marra and A. Dondoni, *Org. Biomol. Chem.*, 2012, **10**, 3269–3277.
32 A. Dondoni, A. Massi, P. Nanni and A. Roda, *Chem.–Eur. J.*, 2009, **15**, 11444–11449.
33 A. Dirksen, T. M. Hackeng and P. E. Dawson, *Angew. Chem., Int. Ed.*, 2006, **45**, 7581–7584.
34 O. Renaudet, D. Boturyn and P. Dumy, *Bioorg. Med. Chem. Lett.*, 2009, **19**, 3880–3883.
35 K. F. Geoghegan and J. G. Stroh, *Bioconjugate Chem.*, 1992, **3**, 138–146.
36 J. C. Spetzler and T. Hoeg-Jensen, *Tetrahedron Lett.*, 2002, **43**, 2303–2306.
37 T. Groth and M. Meldal, *J. Comb. Chem.*, 2001, **3**, 34–44.
38 I. P. Decostaire, D. Lelievre, H. Zhang and A. F. Delmas, *Tetrahedron Lett.*, 2006, **47**, 7057–7060.

39 S. Foillard, M. O. Rasmussen, J. Razkin, D. Boturyn and P. Dumy, *J. Org. Chem.*, 2008, **73**, 983–991.
40 V. Dulery, O. Renaudet and P. Dumy, *Tetrahedron*, 2007, **63**, 11952–11958.
41 R. O. Hynes, *Cell*, 1992, **69**, 11–25.
42 R. H. Kimura, A. M. Levin, F. V. Cochran and J. R. Cochran, *Proteins*, 2009, **77**, 359–369.
43 R. Fontana, M. A. Mendes, B. M. de Souza, K. Konno, L. M. M. Cesar, O. Malaspina and M. S. Palma, *Peptides*, 2004, **25**, 919–928.
44 A. Romanelli, L. Moggio, R. C. Montella, P. Campiglia, M. Iannaccone, F. Capuano, C. Pedone and R. Capparelli, *J. Pept. Sci.*, 2011, **17**, 348–352.
45 A. R. Means and J. R. Dedman, *Nature*, 1980, **285**, 73–77.
46 D. A. Malencik and S. R. Anderson, *Biochem. Biophys. Res. Commun.*, 1983, **114**, 50–56.
47 O. Avrutina, H. U. Schmoldt, D. Gabrijelcic-Geiger, D. Le Nguyen, C. P. Sommerhoff, U. Diederichsen and H. Kolmar, *Biol. Chem.*, 2005, **386**, 1301–1306.
48 B. Tripet, L. Yu, D. L. Bautista, W. Y. Wong, R. T. Irvin and R. S. Hodges, *Protein Eng.*, 1996, **9**, 1029–1042.
49 B. Steinmann, A. Christmann, T. Heiseler, J. Fritz and H. Kolmar, *Appl. Environ. Microbiol.*, 2010, **76**, 5563–5569.
50 B. Apostolovic, M. Danial and H.-A. Klok, *Chem. Soc. Rev.*, 2010, **39**, 3541–3575.
51 C. P. Sommerhoff, O. Avrutina, H.-U. Schmoldt, D. Gabrijelcic-Geiger, U. Diederichsen and H. Kolmar, *J. Mol. Biol.*, 2010, **395**, 167–175.
52 A. Heitz, O. Avrutina, D. Le-Nguyen, U. Diederichsen, J.-F. Hernandez, J. Gracy, H. Kolmar and L. Chiche, *BMC Struct. Biol.*, 2008, 8.
53 I. Coin, M. Beyermann and M. Bienert, *Nat. Protocols*, 2007, **2**, 3247–3256.
54 L. Moroder, D. Besse, H. J. Musiol, S. RudolphBohner and F. Siedler, *Biopolymers*, 1996, **40**, 207–234.
55 S. Krause, H.-U. Schmoldt, A. Wentzel, M. Ballmaier, K. Friedrich and H. Kolmar, *FEBS J.*, 2007, **274**, 86–95.
56 M. Empting, O. Avrutina, R. Meusinger, S. Fabritz, M. Reinwarth, M. Biesalski, S. Voigt, G. Buntkowsky and H. Kolmar, *Angew. Chem., Int. Ed.*, 2011, **50**, 5207–5211.
57 J. N. Israelachvili, *Intermolecular and Surface Forces*, Elsevier Inc., 2011.
58 A. Knoll, R. Magerle and G. Krausch, *Macromolecules*, 2001, **34**, 4159–4165.
59 O. Avrutina, H. U. Schmoldt, H. Kolmar and U. Diederichsen, *Eur. J. Org. Chem.*, 2004, 4931–4935.
60 T. R. Rodriguez and R. Garcia, *Appl. Phys. Lett.*, 2004, **84**, 449–451.
61 S. Patil, N. F. Martinez, J. R. Lozano and R. Garcia, *J. Mol. Recognit.*, 2007, **20**, 516–523.
62 R. W. Stark, N. Naujoks and A. Stemmer, *Nanotechnology*, 2007, **18**, 065502.
63 N. F. Martinez, J. R. Lozano, E. T. Herruzo, F. Garcia, C. Richter, T. Sulzbach and R. Garcia, *Nanotechnology*, 2008, **19**, 163118.
64 C. Dietz, M. Zerson, C. Riesch, A. M. Gigler, R. W. Stark, N. Rehse and R. Magerle, *Appl. Phys. Lett.*, 2008, **92**, 143107.
65 J. W. Li, J. P. Cleveland and R. Proksch, *Appl. Phys. Lett.*, 2009, **94**, 163118.
66 C. Dietz, E. T. Herruzo, J. R. Lozano and R. Garcia, *Nanotechnology*, 2011, **22**, 125708.

3.3. Cube-octameric silsesquioxane-mediated cargo peptide delivery into living cancer cells

Sebastian Hörner,‡ Sebastian Fabritz,‡ Henry D. Herce,* Olga Avrutina, Christian Dietz, Robert W. Stark, M. Cristina Cardoso and Harald Kolmar*

‡ These authors contributed equally to this work.

Org. Biomol. Chem., 2013,**11**, 2258-2265.
DOI: 10.1039/C2OB26808F
Received 14 Sep 2012, Accepted 06 Dec 2012
First published on the web 06 Dec 2012

Graphical Abstract:

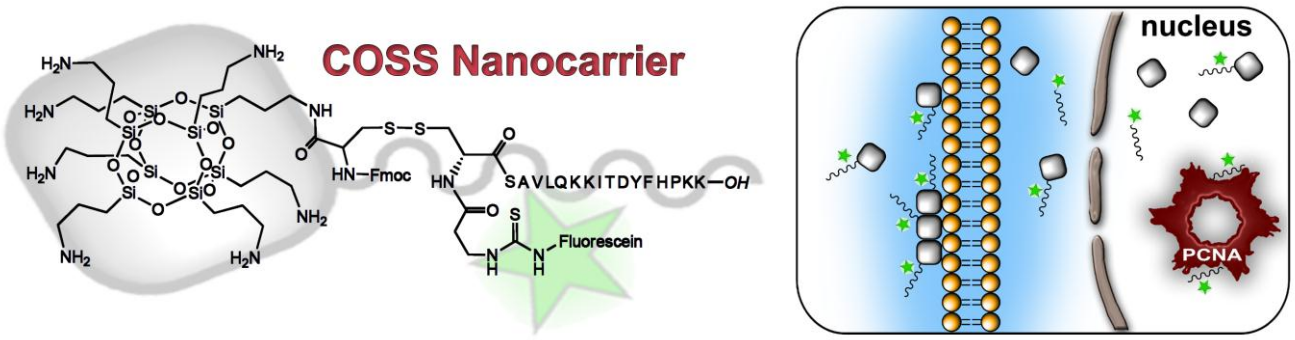

Short Summary:
A COSS-based delivery system which allows for nuclear drug targeting in living HeLa cells is described and the binding of a delivered cargo peptide to Proliferating-Cell-Nuclear-Antigen (PCNA) was demonstrated.

Detailed experimental Data are given in chapter 4.3..

PAPER

Cube-octameric silsesquioxane-mediated cargo peptide delivery into living cancer cells

Sebastian Hörner,‡[a] Sebastian Fabritz,‡[a] Henry D. Herce,*[b,c] Olga Avrutina,[a] Christian Dietz,[d] Robert W. Stark,[d] M. Cristina Cardoso[c] and Harald Kolmar*[a]

Received (in XXX, XXX) Xth XXXXXXXXX 20XX, Accepted Xth XXXXXXXXX 20XX
DOI: xx.xxxx/b000000x

Abstract

Cube octameric silsequioxanes (COSS) are among the smallest nanoparticles known to date with a diameter of only 0.7 nm. We describe a COSS-based delivery system which allows for the drug targeting in human cells. It comprises a siloxane core with seven pendant aminopropyl groups and a fluorescently labeled peptidic ligand attached to one cage corner *via* a reversible disulfide bond to ensure its intracellular release. Bimodal amplitude-modulated atomic force microscopy (AFM) experiments revealed the formation of dendritic COSS structures by a self-assembly of single particles on negatively charged surfaces. Nuclear targeting was demonstrated in HeLa cells by selective binding of released $p21^{Cip1/Waf1}$-derived cargo peptide to PCNA, a protein involved in DNA replication and repair.

Introduction

Nanomaterials and nanoparticles with tailor-made functionalities attract growing interest in the fields of gene therapy,[1] DNA protection,[2] or cancer targeting (the topics are reviewed in [1-3]). In molecular oncology, they enable cell penetration acting as modules for drug delivery into tumor cells. *In vivo*, the enhanced permeability and retention effect[4, 5] as well as the leaky vasculature of cancer cells result in a passive targeting of nanoparticle-delivered drugs.[6, 7] Size, shape, surface charge, and the functional groups of a nanoparticle control its interaction with biological systems.[8, 9] Thus, the functionality but also the toxicity of nanoparticle-based delivery units strongly depend on their design.[10, 11] Therefore, it is essential to ensure a balance between the desired biological function and cytotoxicity due to e.g. reactive oxygen species[10] or vasculature obstruction resulting in organ-associated toxicity.[11] Considering these requirements, a wide range of cell membrane-permeable nanoparticles has been developed, among them core-shell fluorescent,[12] mesoporous dye-doped,[13, 14] and TAT[15]-peptide-conjugated[16, 17] silica nanoparticles (SNP).

Cube-octameric silsesquioxanes (COSS)[18] can be considered as special members of the SNP family. They are highly symmetric molecules of pico dimension comprising a 500 pm silica core that is decorated with organic ligands.[19] COSS with pendant azide,[20-22] aminooxy,[19] vinyl,[23] thiol[24] or amine[25] functionalities allow for the presentation of biomolecules such as carbohydrates,[22, 23, 26, 27] peptides,[19, 20] and miniproteins[19] using the respective conjugation chemistry. Thus, up to eight ligands can be covalently attached to the silsesquioxane scaffold (Scheme 1a).

Modified silsesquioxanes demonstrate unique properties in biological systems. Among others, COSS carrying either lysine dendrimers[28] or poly(2-dimethlyamino)ethyl methacrylate chains,[29] respectively, have been reported as DNA delivery systems into cells. Nanodots composed of a COSS cage surrounded by cationic-conjugated electrolyte arms could be targeted to the cell nucleus upon folic acid functionalization.[30]

In addition to nanoparticles that contain large and branched side chains extending from the inorganic silica core, cell-penetrating COSS derivatives have been described that bear relatively short arms, i.e. an isobutyl[31] or aminopropyl side chain.[32] Interestingly, McCusker *et al.* have demonstrated that fluorescently labeled water-soluble ammonium-functionalized COSS penetrated the outer membrane of Cos-1 cells[33] while exhibiting very low toxicity.[32] Based on these findings, the general applicability of

[a] *Clemens-Schöpf Institute of Organic Chemistry and Biochemistry, Technische Universität Darmstadt, Petersenstr. 22, 64287 Darmstadt, Germany. E-mail: Kolmar@Biochemie-TUD.de*
[b] *Department of Physics, Rensselaer Polytechnic Institute, Center for Biotechnology and Interdisciplinary Studies, building 3237, 110 8th Street, Troy, NY 12180 E-mail: hdherce@gmail.com*
[c] *Fachbereich Biologie, Technische Universität Darmstadt, Schnittspahnstraße 10, 64287 Darmstadt, Germany*
[d] *Center of Smart Interfaces, Technische Universität Darmstadt, Petersenstr. 32, 64287 Darmstadt, Germany.*
† *Electronic **Supplementary Information (ESI) available: RP-HPLC** spectra of **2, 2a**, **3**, **4**, **5**, **5a**; **ESI-MS** data of **2**, **3**, **5**, **5a**, **5b**; **HR-MS** data of **2a**, **4**; **IR** spectrum of **4** See DOI: xxxxx/b000000x/*
‡ *These authors contributed equally to this work.*

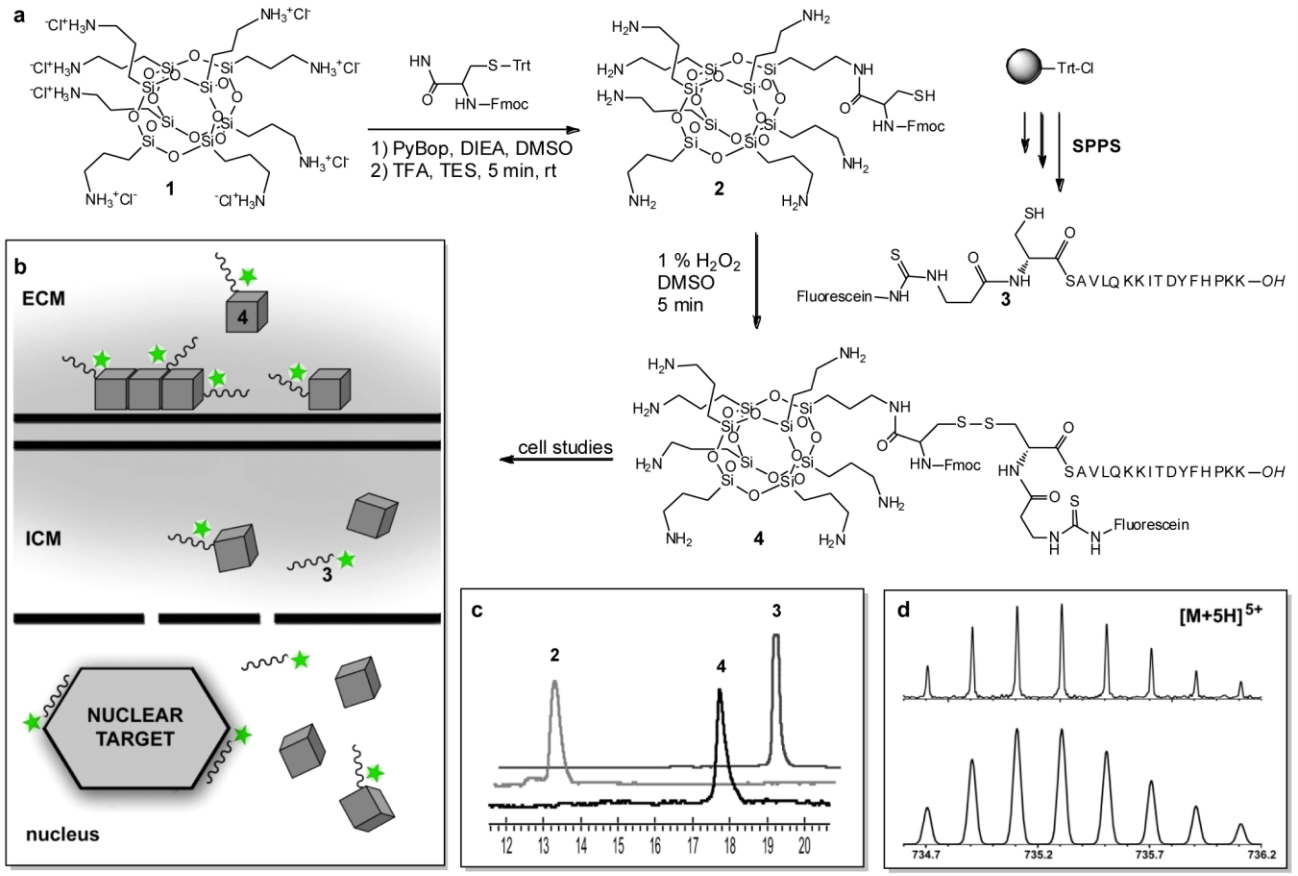

Scheme 1 (a) Synthesis of a biodegradable COSS-peptide conjugate **4**. The sequence of a $p21^{Cip1/Waf1}$ -based peptide cargo is shown using a one-letter code; SPPS – solid phase peptide synthesis; (b) Studies in HeLa cells using **4** are depicted as cartoon. **4** was applied to the extracellular medium (ECM) and penetrated the cell outer membrane. In the intracellular medium (ICM) the nanoparticle was accumulated in the nucleoli allowing for the targeting of the nucleus abundant protein PCNA; (c) HPLC traces (220 nm, 25% → 50% aq. CH_3CN in 20 min) recorded upon the synthesis of **4**; (d) High-resolution mass spectrometric isotopic pattern; calc. for **4** $C_{158}H_{246}N_{35}O_{45}S_3Si_8$ (5+): 734.7065, meas. 734.7077.

octaamino COSS as a very small nanoparticle drug carrier was postulated, albeit an experimental proof is still missing.[32] Herein, we investigated the applicability of octaamino COSS nanoparticles as a delivery system for targeting a peptidic cargo molecule to the nucleus of human HeLa[34] cancer cells.

As a model peptide for cargo delivery a 16-mer peptide SAVLQKKITDYFHPKK[35] was chosen that is known to bind an abundant nuclear protein, the proliferating cell nuclear antigen (PCNA).[36] PCNA is an essential component of the DNA replication and repair machinery and plays a fundamental role in cell proliferation and genome stability.[35-37] Tumor theranostic-related research in this field is concentrated on the development of a cancer biomarker based on the immunostaining of cancer-associated PCNA isoforms[38] and the inhibition of DNA replication *via* binding of peptidic ligands to PCNA.[35] The peptide mentioned above is derived from protein $p21^{Cip1/Waf1}$ that is known to bind PCNA,[39] thus playing a crucial role in regulating its activity.[40] An oligopeptide comprising the PCNA binding sequence of $p21^{Cip1/Waf1}$ was delivered into C2C12[41] mouse myoblast cells *via* TAT-mediated transduction. It caused cell cycle arrest indicating direct interference with protein/protein interaction that is crucial for DNA replication and repair.[42]

Results and Discussion

For initial experiments, a single corner of the octaamino COSS particle was modified with a C-terminally fluorescein-labeled Cys-*β*Ala dipeptide (Fig. 1a) and human HeLa cells were incubated with the resulting conjugate (20 µM) for 30 min. Confocal microscopy studies revealed the distinct accumulation of silsesquioxanes in the multiple nucleoli of HeLa cells and also, to a lower extent, throughout the nucleoplasm and cytoplasm (Fig. 1b-d). Due to the small size of COSS derivatives, their transit through the nuclear pore complex with internal diameter of about 50 nm[43] might be achieved by passive diffusion. The observed accumulation in the nucleoli could be enhanced *via* electrostatic interactions of positively charged SNPs and phosphate-rich RNA. Providing clear evidence that amino silsesquioxanes are accumulated in the nucleoli of HeLa cells, our data differ from the reported lack of nuclear uptake of octaammonium COSS in a Cos-1 cell assay.[32]

After having confirmed intracellular and nuclear accumulation of COSS, the p21-derived peptide was covalently attached to a single-corner cysteine-modified octaamino COSS through a

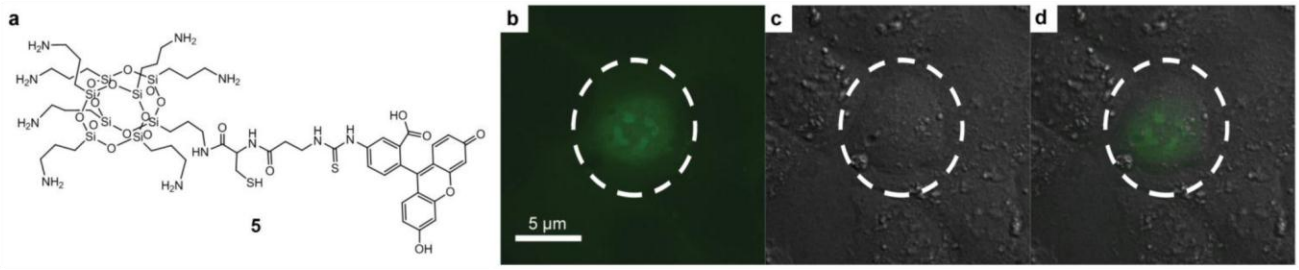

Fig. 1 Cellular uptake of fluorescein-labeled octaamino COSS **5** (a). The nanoparticle was added to the extracellular medium (final concentration of 20 µM) and after 30 min incubation the cells were washed with phosphate buffered saline and imaged. (b) fluorescence image, (c) contrast image, (d) overlay. The location of the nucleus is indicated by a dotted circle.

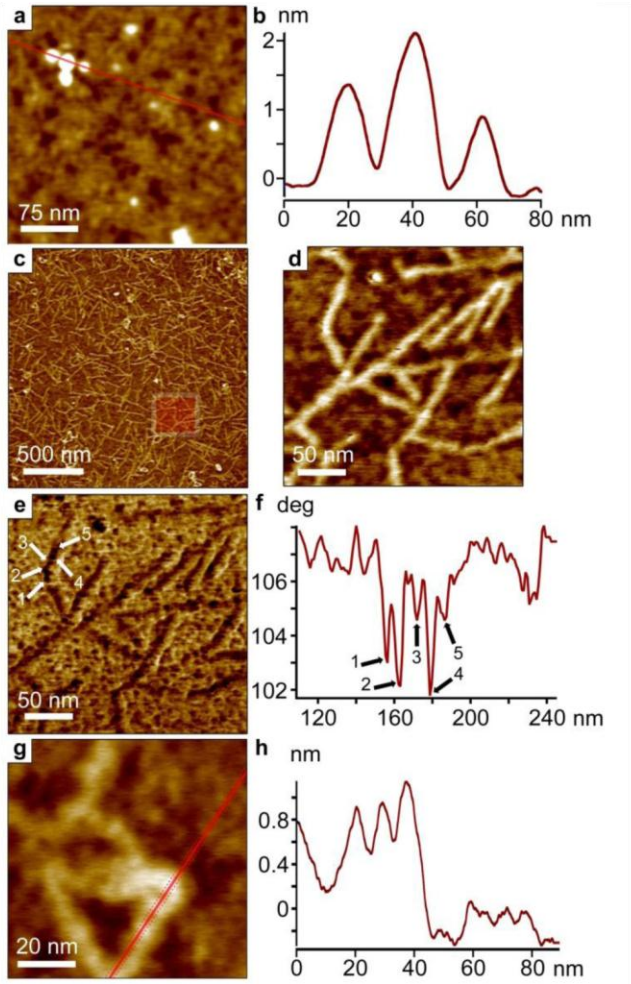

Fig. 2 (a) AFM topography image of singular and globular COSS-peptide particles **4**; (b) particle profile along the red line in (a); (c) and (d) AFM topography image of self-assembled SNP **4**; (e) second eigenmode phase image corresponding to (d). The image allows for the detection of single particles within the dentritic structure; (g) high resolution frequency modulated AFM image of self-assembled **4**; (h) corresponding particle profile.

reversible disulfide bond (Scheme 1). Being sensitive to reducing conditions inside living cells,[44] the disulfide bond is well known to dissociate after cell penetration thereby releasing the attached cargo molecule from the carrier.[44] An additional fluorescein moiety was introduced into this hybrid construct allowing for live-cell confocal[45] microscopy studies.

As cell penetration, toxicity and nuclear targeting depend on the size and shape of the applied SNPs, bimodal amplitude-modulated atomic force microscopy (AFM)[46-48] was used to further characterize particle **4**. Depending on the particle concentration in the initial solution, we observed two types of particle arrangements on a mica surface: globular particle assembly (Fig. 2a – b) and dendritic structures (Fig. 2c – h). Fig. 2a shows an amplitude-modulated AFM topography image of solitary and assembled COSS particle **4**. The cross-section analysis (Fig. 2a and 2b) reveals three distinctive heights: ≈ 700 pm, 1400 pm and 2100 pm, suggesting a single particle size of 700 pm and multiples of it. At higher concentrations dendritic structures of **4** can be seen in the topographical image of Fig. 2c. Here, bimodal AFM was applied to enhance the lateral resolution of the phase images, giving the height of the ordered structures as ≈ 700 - 800 pm (Fig. 2d). The corresponding second eigenmode phase image (Fig. 2e) clearly depicts the arrangement of single particles within one chain. Particles appear as dark dots (phase shift ≈ 102-104°) whereas the mica substrate shows a phase shift of ≈ 108°. In the profile (Fig. 2f) these particles are well separated. This leads to the conclusion that the dendritic structures are formed by a self-assembly of single SNPs **4** arranged next to each other. Frequency-modulated AFM topography images (Fig. 2g and Fig. 2h) corroborated these findings. Because this technique is extremely sensitive to topographical variations, even single particles were distinguished in the height profile.

A similar self-assembly of silsesquioxane monomers may occur on a cell surface as well. However, the issue remains open whether the monomeric octaammonium COSS or self-assembled polymers are preferably involved in uptake and cell penetration. We suppose that the difference between heptalysine which lacks membrane permeability[49] and cell-penetrating octaamino silsesquioxanes could be explained by the higher charge density within COSS and its shape-dependent self-assembly.[50-52] It might allow these cube-octameric SNPs to act as polycationic polymers (e.g. polylysine or polyethyleneimine) which are known to penetrate cell membranes.[53] It will be interesting to see, whether variation of the spatial arrangement and nature of the cationic groups has an influence on cellular uptake of COSS and on the uptake mechanism, which has to be elucidated yet. It remained to be investigated, whether the COSS-bound cargo peptide displays biological activity which, in this experimental setting, is binding to PCNA. To address this question, co-localization experiments were performed involving FITC-labeled peptide **3** and PCNA, that was expressed as a fusion protein with red fluorescent protein (mRFP)[54] *via* transient transfection of HeLa cells with a mammalian expression plasmid coding for mRFP-tagged PCNA. PCNA is known to accumulate at sites of DNA damage that can be induced locally *via* UV-microbeam irradiation (Fig. 3 and S18).[55] To this end, a spot in a nucleus of a HeLa cell treated with

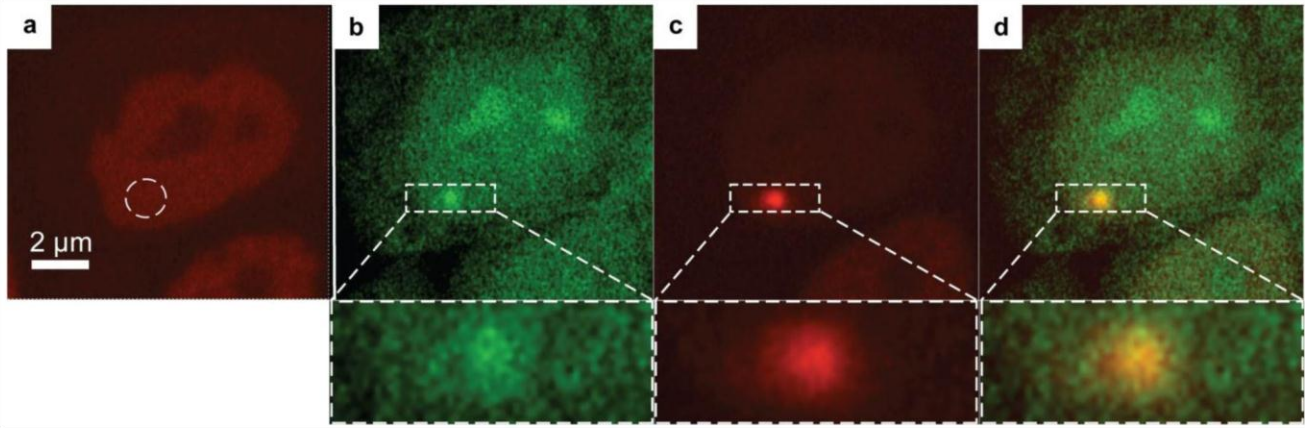

Fig. 3 (a) Micro-irradiation at the circle position (1.2 sec) of a HeLa cell using a 405 nm laser; (b)- (d); Co-localization of **3** and PCNA. PCNA is recruited to repair micro-irradiated damaged DNA;(b) Fluorescence signal of **3** (green); (c) Fluorescence signal of red fluorescent protein labeled PCNA; (d) Overlay of (b) and (c).

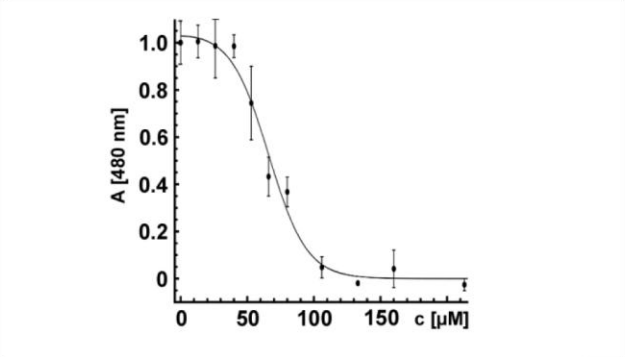

Fig. 4 Cell viability test using a single-corner cysteine-modified octaamino COSS. At a nanoparticle concentration of ~70 µM half of the observed cell population died whereas a concentration of ~120 µM killed all cells within 12 hours.

a 20 µM solution of **4** was micro-irradiated for 1.2 seconds. Within 20 min RFP-labeled PCNA could be visualized at the site of DNA damage.[55] Co-localization of the fluorescent signal of **3** provided evidence of its accumulation at the DNA repair site (Fig. 3b and 3d). This clearly demonstrates that a significant portion of the cargo is able to freely address a target site in a HeLa cell nucleus.

Release of a peptide from a disulfide-bound cell-penetrating peptide carrier in the reducing milieu of a cell is a process that occurs relatively fast.[44, 56] This is corroborated by our finding that the fluorescently labeled nanoparticle **5** is predominantly found in the nucleus while the COSS-bound labeled peptide **3** is also detected in the cytoplasm 30 min after incubation (Fig. S18), which indicates a release from the carrier. Hence, it is most likely the liberated peptide **3** that interacts with PCNA rather than the COSS-peptide complex **4**.

For drug delivery, interactions of the carrier with a biological system that may eventually result in cell toxic effects are not desired, except those important for directed transit. Indeed, non-porous SNPs presenting primary amines at their surface have been reported to exhibit low toxicity[11, 32] and degrade[57, 58] under physiological conditions.[26, 59] Here we corroborate these findings for amino-functionalized COSS with a cell viability assay based on the enzymatic reduction of the tetrazole XTT[60] using a single-corner cysteine-modified octaamino COSS. Within 12 hours, a SNP solution with a concentration of ~70 µM was needed to kill half of the cell population, which sufficiently exceeds the SNP concentration used for the delivery of the PCNA targeting peptide (Fig. 4).

Conclusion

In conclusion, a COSS derivative was synthesized which comprised a siloxane core with seven pendant aminopropyl groups and a peptidic ligand attached to one cage corner through a reversible disulfide bond. This architecture allowed for the penetration of human cells and peptide accumulation in the cell nucleus. Nuclear drug targeting was demonstrated in HeLa cells using a fluorescently labeled $p21^{Cip1/Waf1}$-derived peptide as a COSS cargo, which selectively bound PCNA, a protein involved in DNA replication and repair. In perspective, it might be interesting to study the octaamino COSS uptake mechanism in further detail by AFM and fluorescence microscopy studies on artificial lipid membranes[61, 62] and cells. Finally, it remains to be elucidated whether silsesquioxane-based cargo delivery allows for the targeting of other proteins both in the nucleus and cytoplasm.

Experimental

HPLC analysis and purification

For RP-HPLC analysis a Varian 940-30 LC equipped with a Phenomenex Luna C_{18} column (5u, 100 A, 250×4.60 mm, 5 µm) was used at a flow rate of 1 mL min^{-1}. For isolation of products by RP-HPLC a C_{18} column (250 × 20 mm; S-4 µm, 8 nm) was employed at a flow rate of 18 mL min^{-1}. Eluent A: 0.1% aq. trifluoroacetic acid (TFA), eluent B: 90 % aq. MeCN in 0.1% aq. TFA. 5 min of isocratic flow (starting concentration of eluent B) was followed by 20 min of gradient flow.

Compound 1

Synthesis of octaammonium COSS

According to a modified procedure reported by Feher *et al,*[63] 25 mL (23.7 g, 0.107 mol) 3-(triethoxysilyl)-1-propanamine were dissolved in 600 mL methanol. 34.0 mL concentrated

hydrochloric acid (HCl) were added and the reaction was stirred at room temperature. After 4 weeks, a colorless precipitate was formed. The suspension was stirred additional two weeks. The colorless precipitate was separated by filtration, washed 2 times with ice-cold acetone and dried in a desiccator. 3.08 g of colorless solid were obtained (23.0%).
^{1}H NMR [300.0 MHz, (DMSO-d_6, room temp.] δ 8.25 (s, NH_3, 24 H), 2.79 (t, CH_2NH_3, 16 H), 1.74 (m, $SiCH_2CH_2$, 16 H), 0.74 (t, $SiCH_2$, 16 H). ^{13}C NMR [300.0 MHz, DMSO-d_6, room temp.] δ 41.44 (s, CH_2NH_3), 21.03 (s, $SiCH_2CH_2$), 8.87 (s, $SiCH_2$). ^{29}Si NMR [59.6 MHz, DMSO-d_6, room temp.] δ -66.41. ESI-MS calc. for **1** $C_{24}H_{64}N_8O_{12}Si_8$ m/z: 881.5, meas. 881.5 ($[M+H]^+$); calc. 441.8, meas. 441.8 ($[M+2H]^{2+}$).

Compound 2

Synthesis of Fmoc-S-trityl-L-cysteine heptaamino-COSS (2a)

To a mixture of 10.5 mg (0.018 mmol, 2.1 eq.) of Fmoc-S-trityl-L-cysteine and 8.9 µL dry DIEA (6.6 mg, 0.051 mmol, 6.0 eq.) in 1 mL dry DMSO, 8.9 mg (0,017 mmol, 2.0 eq.) of (benzotriazol-1-yloxy)tripyrrolidinophosphonium hexafluorophosphate (PyBOP) in 1 mL dry DMSO were added dropwise. The mixture was incubated for 10 min at room temperature and afterwards diluted with dry DMSO to a volume of 12 mL.
10 mg (0,0085 mmol, 1.0 eq.) of **1** were dissolved in 0.5 mL dry DMSO and vigorously stirred. The previously described mixture was added slowly using a peristaltic pump (flow: 0,05 mL min^{-1}). After complete addition, the mixture was stirred for 1 hour at room temperature. The solvent was removed by lyophilization. The resulting oil was suspended in 5 mL of 0,01 M HCl and again lyophillized. The colorless powder was suspensed in dry acetonitrile and the insolble part was washed two times with dry acetonitrile. The precipitate was dried *in vacuo* and purified by semipreparative RP-HPLC. After lyophilization, 3.0 mg of colorless solid were obtained (24.4%).
RP-HPLC, 10 → 80% B, t_R = 20.1 min. HR-MS calc. for **2a** $C_{24}H_{79}N_9O_{15}SSi_8$ m/z: 724.7406, meas. 724.7409 $[M+2H]^{2+}$ (see Fig. S2 and S3).

Deprotection of Fmoc-S-trityl-L-cysteine heptaamino-COSS

3.0 mg of Fmoc-S-trityl-L-cysteine heptaamino-COSS were dissolved in 500 µL TFA and 5 µL (1 vol%) triethylsilane (TES) were added. The mixture was shaken for 30 min at room temperature and the solvent was removed *in vacuo*. The colorless residue was dissolved in deionized water and the solvent was removed by lyopilization. The colorless residue was used without further purification.
RP-HPLC 10 → 80% B, t_R = 16.7 min. ESI-MS calc. for **2** $C_{42}H_{79}N_9O_{15}SSi_8$ m/z: 1206.9, meas. 1206.6 ($[M+H]^+$); calc. 604.4, meas. 604.4 ($[M+2H]^{2+}$); calc. 403.3, meas. 403.3 ($[M+3H]^{3+}$) (see Fig. S4).

Compound 3

Synthesis of fluorescein-labeled PCNA binding peptide

Microwave-assisted Fmoc-SPPS of PCNA binding peptide **3** was performed on 2-chorotrityl resin (*Iris Biotech* GmbH) (0.25 mmol) using a CEM *liberty*® peptide synthesizer equipped with a CEM *discover*® SPS microwave (CEM GmbH). All amino acids were coupled by triple coupling using 4.0 eq. of the amino acid, 3.9 eq. of *O*-(benzotriazol-1-yl)-*N,N,N′,N′*-tetramethyluronium hexafluorophosphate (HBTU) (*Iris Biotech* GmbH), and 8 eq. base (DIEA for all amino acids except cysteine; for coupling of Fmoc-S-trityl-L-cysteine, collidine (*Sigma-Aldrich*) was used) in *N,N'*-dimethylformamide (DMF). Triple coupling (30 W, 50 °C, 15 min) and double deprotection (30 W, 50 °C, 5 min) of the amino acids was performed upon microwave assistance. Fluorescein isothiocyanate (FITC) was coupled manually to the resin-bound peptide. 194.7 mg (0.50 mmol, 2 eq.) FITC and 87.2 µL (64.7 mg, 4.0 eq.) dry DIEA were dissolved in 5 mL dry DMF and the solution was added to the resin-bound peptide. The mixture was heated 3 times in a microwave (30 W, 50 °C, 30 min). Afterwards, the mixture was shaken at room temperature overnight. The peptide was cleaved from the resin and purified by semi-preparative RP-HPLC yielding 37.0 mg of a yellow solid after lyophilization (6.0%).
RP-HPLC, 30 → 40% B, t_R = 20.0 min. ESI-MS calc. for **3** $C_{116}H_{164}N_{26}O_{30}S_2$ m/z: 1234.4, meas. 1234.5 ($[M+2H]^{2+}$); calc. 823.3, meas. 823.3 ($[M+3H]^{3+}$); calc. 617.7, meas. 617.8 ($[M+4H]^{4+}$); calc 494.4, meas. 494.5 ($[M+5H]^{5+}$) (see Fig. S6 and S7).

Compound 4

Coupling of PCNA binding peptide to 2

1.6 mg (0.0014 mmol, 1 eq.) of **2** and 10.0 mg (0.0040 mmol, 3 eq.) of compound **3** were dissolved in 200 µL dimethylsulfoxide (DMSO). 10 µL 30 vol% aqueous hydrogen peroxide were mixed with 100 µL DMSO and quickly added to the mixture resulting in a 1 vol% solution of hydrogen peroxide. The probe was vigorously shaken for 5 min at room temperature. Immediately, 1 mL of deionized water was added and the probe was frozen in liquid nitrogen. The solvent was removed by lyophilization and the resulting solid was purified by RP-HPLC. After lyophilization, 1.4 mg of yellow solid were obtained (23.0%).
RP-HPLC, 27 → 40% B, t_R = 17.8 min. HR-MS calc. for **4** $C_{158}H_{241}N_{35}O_{45}S_3Si_8$ m/z: 734.7065, meas. 734.7077 $[M+5H]^{5+}$. IR: 2912, 1629, 1530, 1104 cm^{-1} (see Fig. S9, S10, and S11).

Compound 5

Synthesis of Cys-(S-Trt)-beta-Ala-FITC (5a)

Microwave-assisted Fmoc-SPPS of dipeptide Cys-(S-Trt)-beta-Ala-FITC was performed at 0.10 mmol scale on 2-chorotrityl resin (*Iris Biotech* GmbH). 58.6 mg (0.10 mmol, 1 eq.) Fmoc-S-trityl-L-cysteine (*IRIS Biotech* GmbH) and 52.9 µL (48.5 mg, 0.40 mmol, 4 eq.) collidine (*Sigma-Aldrich*) were dissolved in 3 mL dry DCM and the solution was added to the resin and shaken for 2 hours at room temperature. The

Fmoc protecting group was removed by double deprotection using a CEM *discover*® SPS microwave (CEM GmbH) (30 W, 50 °C, 5 min). Coupling of Fmoc-β-alanine (*IRIS Biotech* GmbH) was performed as a triple coupling using 4.0 eq. Fmoc-β-alanine, 3.9 eq. HBTU, and 8 eq. DIEA in DMF in a microwave (30 W, 50 °C, 15 min). 78.0 mg (0.20 mmol, 2 eq.) FITC and 69.5 µL (51.6 mg, 4.0 eq.) dry DIEA were dissolved in 2 mL dry DMF and the solution was added to the resin-bound dipeptide. The mixture was heated 3 times (30 W, 50 °C, 30 min) in a microwave. Afterwards, the mixture was shaken at room temperature overnight. For cleavage of the peptide, 5.0 mL of a mixture of acetic acid, methanol, and DCM (5:1:4, *v*:*v*:*v*) were added. The mixture was shaken for 3 hours at room temperature. Afterwards the solution was added dropwise to 45.0 mL of ice-cold methyl *tert*.-butyl ether (MTBE). The yellow precipitate purified by semi-preparative RP-HPLC. Lyophilization gave 52.4 mg of a yellow solid (63.6%).

RP-HPLC, 10 → 100% B, t_R = 23.7 min. ESI-MS calculated for **5a** $C_{46}H_{37}N_3O_8S_2$ m/z: 823.9, meas. 824.4 ($[M+H]^+$) (see Fig. S13 and S14).

Synthesis of Cys-(S-Trt)-β-Ala-FITC hepataamino-COSS (5b)

7.7 mg (0.0094 mmol, 1.1 eq.) of the dipeptide Cys-(S-Trt)-beta-Ala-FITC, 1,6 mg (0.0085 mmol, 1 eq.) 1-ethyl-3-(3-dimethylaminopropyl)carbodiimide (DIC) and 6 µL (4.4 mg, 0.034 mmol, 4 eq.) of dry DIEA were dissolved in 500 µL dry DMSO. The mixture was shaken for 10 min at room temperature and 10.0 mg (0.0085 mmol, 1 eq.) of compound **1** dissolved in 500 µL dry DMSO were added. The mixture was shaken for 4 days in the dark and poured into 12 mL of dry acetonitrile. The yellow precipitate was washed two times with dry acetonitrile. It was purified by semi-preparative RP-HPLC. After lyophilization, 4.4 mg of colorless solid were obtained (27.8%).

RP-HPLC, 10 → 100% B, t_R = 16.0 min. ESI-MS calc. for **5b** $C_{70}H_{99}N_{11}O_{19}S_2Si_8$ m/z: 844.7, meas. 844.8 ($[M+2H]^{2+}$); calc. 563.5, meas. 563.5 ($[M+3H]^{3+}$); calc. 422.9, meas. 422.9 ($[M+4H]^{4+}$) (see Fig. S16).

Deprotection of Cys-(S-Trt)-β-Ala-FITC hepataamino-COSS

4.4 mg of Cys-(S-Trt)-β-Ala-FITC hepataamino-COSS were dissolved in 0.5 mL TFA and 5 µl (1 vol%) triethylsilane (TES) (*Alfa Aesar*) were added. The mixture was shaken for 30 min at room temperature and the solvent was removed *in vacuo*. The yellow residue was purified by semi-preparative RP-HPLC. After lyophilization, 2.0 mg of colorless solid were obtained (53.0%).

RP-HPLC, 10 → 100% B, t_R = 14.0 min. ESI-MS calc. for **5** $C_{51}H_{85}N_{11}O_{19}S_2Si_8$ m/z: 723.6, meas. 723,5 ($[M+2H]^{2+}$); calc. 482.7, meas. 482.7 ($[M+3H]^{3+}$) (see Fig. S17).

Atomic force microscopy

We conducted atomic force microscopy experiments on air using a Cypher AFM (*Asylum Research*, Santa Barbara, CA, USA) and PPP-ZEIHR cantilevers (*NanoandMore* GmbH, Wetzlar, Germany). Bimodal AFM was done with the first two eigenfrequencies at $f_1 \approx 130$ kHz and $f_2 \approx 820$ kHz.The free oscillation amplitudes were driven to $A_{01} \approx 10$ nm and $A_{02} \approx 1$ nm, respectively. A high amplitude setpoint ratio $A_{sp}/A_{01} \approx 0.9$ was chosen ensuring that the AFM is operated in the net attractive regime where mechanical repulsion is minimized and hence, the impact of the tip on the sample is small.

High resolution frequency-modulated AFM measurements were accomplished using the same type of cantilever. For tracking the frequency, an external phase-locked-loop PLLPro2 (*RHK Technology*, Troy, MI, USA) was integrated into the feedback loop of the AFM. We kept the cantilever vibrating at a constant frequency shift of Δf = 50 Hz with respect to the free oscillation and the amplitude was maintained at $A_0 \approx 10$ nm. Images (512 x 512 pixel) were obtained with a scan speed of 500 nm/s.

Cell culture and FITC-labeled COSS cellular uptake

HeLa cells were seeded at 80% confluency into 24-well microscope observation chambers (*Ibidi*, Munich, Germany) and the growth medium (Dulbecco's modified Eagle medium; PAA) DMEM supplemented with 10% fetal calf serum (*Life Technologies*) and gentamycin was exchanged against the COSS solutions. COSS were diluted to 20 µM final concentration in 400 µl DMEM and incubated with the HeLa cells for 30 min at 37°C prior to imaging.

Cell viability assay

HeLa cells were seeded at 70% confluency in 24-well plates and incubated for one hour at different COSS concentrations. The media was subsequently exchanged for DMEM without COSS and the cells were incubated for 12 hours. Then the media was exchanged with serum-free DMEM and 0.3mg/ml of XTT (2,3-bis(2-methoxy-4-nitro-5-sulfophenyl)-2H-tetrazolium-5-carbox-anilide) and incubated for three hours. The XTT enzymatic reduction was measured by reading the absorbance at 490 nm, with a reference wavelength of 630 nm. This procedure was repeated four times for each concentration.

HeLa cells expressing RFP labeled PCNA

HeLa cells were plated on 24 wells optical dishes (*Ibidi*, Munich, Germany) and transfected with a mammalian expression plasmid coding for mRFP-tagged PCNA[54] using polyethylenimine (PEI). Time lapse microscopy was performed on an UltraView spinning disc confocal microscopy system (*PerkinElmer*, UK) equipped with temperature, humidity and CO_2 incubation controller (*Olympus*) and a 63x/1.4 Plan-Fluor oil immersion lens (*Nikon*).

Microirradiation and confocal microscopy

COSS compound **4** was added at 20 µM concentration to the HeLa cells expressing RFP-labeled PCNA. After 30 min of

incubation, a cell was first imaged and then irradiated at the micrometer spot within the nucleus for 1.2 sec using a 405 nm laser. The same cell was imaged after 5 min using a laser excitation of 488 nm to detect the fluorescein-labeled peptide and 561 nm to detect the RFP labeled PCNA.

Acknowledgements

We thank Dr. Holm Frauendorf (Georg-August University, Göttingen) for the HR-MS measurements. We acknowledge the collaboration with Prof. Dr. Robert Stark (Center of Smart Interfaces, Technische Universität Darmstadt) with respect to AFM measurements in the frame of the LOEWE Soft Control consortium.

References

1 M. Mahmood, D. Casciano, Y. Xu and A. S. Biris, *J. Appl. Toxicol.*, 2011, **32**, 10-19.
2 K. Ariga, Q. M. Ji, M. J. McShane, Y. M. Lvov, A. Vinu and J. P. Hill, *Chem. Mat.*, 2012, **24**, 728-737.
3 M. R. Longmire, M. Ogawa, P. L. Choyke and H. Kobayashi, *Bioconjug. Chem.*, 2011, **22**, 993-1000.
4 J. Fang, H. Nakamura and H. Maeda, *Adv. Drug Deliv. Rev.*, 2011, **63**, 136-151.
5 V. Torchilin, *Adv. Drug Deliv. Rev.*, 2011, **63**, 131-135.
6 F. Danhier, O. Feron and V. Preat, *J. Control. Release*, 2010, **148**, 135-146.
7 M. Das, C. Mohanty and S. K. Sahoo, *Expert Opin. Drug Deliv.*, 2009, **6**, 285-304.
8 A. E. Nel, L. Madler, D. Velegol, T. Xia, E. M. Hoek, P. Somasundaran, F. Klaessig, V. Castranova and M. Thompson, *Nat. Mater.*, 2009, **8**, 543-557.
9 A. Verma and F. Stellacci, *Small*, 2010, **6**, 12-21.
10 D. Napierska, L. C. Thomassen, D. Lison, J. A. Martens and P. H. Hoet, *Part. Fibre Toxicol.*, 2010, **7**, 39.
11 T. Yu, K. Greish, L. D. McGill, A. Ray and H. Ghandehari, *ACS Nano*, 2012, **6**, 2289-2301.
12 J. E. Fuller, G. T. Zugates, L. S. Ferreira, H. S. Ow, N. N. Nguyen, U. B. Wiesner and R. S. Langer, *Biomaterials*, 2008, **29**, 1526-1532.
13 S. W. Bae, W. Tan and J. I. Hong, *Chem. Commun.*, 2012, **48**, 2270-2282.
14 V. Lebret, L. Raehm, J. O. Durand, M. Smaihi, C. Gerardin, N. Nerambourg, M. H. V. Werts and M. Blanchard-Desce, *Chem. Mat.*, 2008, **20**, 2174-2183.
15 M. Green and P. M. Loewenstein, *Cell*, 1988, **55**, 1179-1188.
16 S. Santra, H. Yang, D. Dutta, J. T. Stanley, P. H. Holloway, W. Tan, B. M. Moudgil and R. A. Mericle, *Chem. Commun.*, 2004, 2810-2811.
17 L. Pan, Q. He, J. Liu, Y. Chen, M. Ma, L. Zhang and J. Shi, *J. Am. Chem. Soc.*, 2012, **134**, 5722-5725.
18 D. B. Cordes, P. D. Lickiss and F. Rataboul, *Chem. Rev.*, 2010, **110**, 2081-2173.
19 S. Fabritz, S. Hörner, D. Könning, M. Empting, M. Reinwarth, C. Dietz, B. Glotzbach, H. Frauendorf, H. Kolmar and O. Avrutina, *Org. Biomol. Chem.*, 2012, DOI: 10.1039/C1032OB25728A.
20 S. Fabritz, D. Heyl, V. Bagutski, M. Empting, E. Rikowski, H. Frauendorf, I. Balog, W. D. Fessner, J. J. Schneider, O. Avrutina and H. Kolmar, *Org. Biomol. Chem.*, 2010, **8**, 2212-2218.
21 Y. C. Lin and S. W. Kuo, *Poly. Chem.*, 2012, **3**, 162-171.
22 B. Trastoy, M. E. Perez-Ojeda, R. Sastre and J. L. Chiara, *Chem.-Eur. J.*, 2010, **16**, 3833-3841.
23 M. Lo Conte, S. Staderini, A. Chambery, N. Berthet, P. Dumy, O. Renaudet, A. Marra and A. Dondoni, *Org. Biomol. Chem.*, 2012, **10**, 3269-3277.
24 U. Dittmar, B. J. Hendan, U. Florke and H. C. Marsmann, *J. Organomet. Chem.*, 1995, **489**, 185-194.
25 F. J. Feher, K. D. Wyndham, M. A. Scialdone and Y. Hamuro, *Chem. Commun.*, 1998, 1469-1470.
26 B. Trastoy, D. A. Bonsor, E. M. Pérez-Ojeda, L. M. Jimeno, A. Méndez-Ardoy, J. M. García-Fernándes, E. J. Sundberg and J. L. Chiara, *Adv. Funct. Mater.*, 2012, DOI: 10.1002/adfm.201200423.
27 D. Heyl, E. Rikowski, R. C. Hoffmann, J. J. Schneider and W. D. Fessner, *Chem.-Eur. J.*, 2010, **16**, 5544-5548.
28 T. L. Kaneshiro, X. Wang and Z. R. Lu, *Mol. Pharm.*, 2007, **4**, 759-768.
29 X. J. Loh, Z. X. Zhang, K. Y. Mya, Y. L. Wu, C. B. He and J. Li, *J. Mater. Chem.*, 2010, **20**, 10634-10642.
30 D. Ding, K. Y. Pu, K. Li and B. Liu, *Chem. Commun.*, 2011, **47**, 9837-9839.
31 F. Olivero, F. Reno, F. Carniato, M. Rizzi, M. Cannas and L. Marchese, *Dalton Trans.*, 2012, **41**, 7467-7473.
32 C. McCusker, J. B. Carroll and V. M. Rotello, *Chem. Commun.*, 2005, 996-998.
33 Y. Gluzman, *Cell*, 1981, **23**, 175-182.
34 W. F. Scherer, J. T. Syverton and G. O. Gey, *J. Exp. Med.*, 1953, **97**, 695-710.
35 D. I. Zheleva, N. Z. Zhelev, P. M. Fischer, S. V. Duff, E. Warbrick, D. G. Blake and D. P. Lane, *Biochemistry*, 2000, **39**, 7388-7397.
36 T. Paunesku, S. Mittal, M. Protic, J. Oryhon, S. V. Korolev, A. Joachimiak and G. E. Woloschak, *Int. J. Radiat. Biol.*, 2001, **77**, 1007-1021.
37 S. M. Görisch and M. C. Cardoso, in *Proliferating Cell Nuclear Antigen*, ed. H. Lee and M. Szyf, Research SignPost, 2006, pp. 51-70.
38 L. H. Malkas, B. S. Herbert, W. Abdel-Aziz, L. E. Dobrolecki, Y. Liu, B. Agarwal, D. Hoelz, S. Badve, L. Schnaper, R. J. Arnold, Y. Mechref, M. V. Novotny, P. Loehrer, R. J. Goulet and R. J. Hickey, *Proc. Natl. Acad. Sci. U. S. A.*, 2006, **103**, 19472-19477.
39 J. Cmielova and M. Rezacova, *J. Cell Biochem.*, 2011, **112**, 3502-3506.
40 J. M. Gulbis, Z. Kelman, J. Hurwitz, M. O'Donnell and J. Kuriyan, *Cell*, 1996, **87**, 297-306.
41 D. Yaffe and O. Saxel, *Nature*, 1977, **270**, 725-727.
42 G. Tunnemann, R. M. Martin, S. Haupt, C. Patsch, F. Edenhofer and M. C. Cardoso, *Faseb J.*, 2006, **20**, 1775-1784.
43 W. Yang, J. Gelles and S. M. Musser, *Proc. Natl. Acad. Sci. U. S. A.*, 2004, **101**, 12887-12892.
44 G. Saito, J. A. Swanson and K. D. Lee, *Adv. Drug Deliv. Rev.*, 2003, **55**, 199-215.

45 *Handbook of Biological Confocal Microscopy*, Springer Science+Business Media, LLC, 3rd edn., 2006.
46 T. R. Rodriguez and R. Garcia, *Appl. Phys. Lett.*, 2004, **84**, 449-451.
47 C. Dietz, E. T. Herruzo, J. R. Lozano and R. Garcia, *Nanotechnology*, 2011, **22**, 125708.
48 R. Garcia and E. T. Herruzo, *Nat. Nanotechnol.*, 2012, **7**, 217-226.
49 G. Tunnemann, G. Ter-Avetisyan, R. M. Martin, M. Stockl, A. Herrmann and M. C. Cardoso, *J. Pept. Sci.*, 2008, **14**, 469-476.
50 W. A. Zhang, J. Y. Yuan, S. Weiss, X. D. Ye, C. L. Li and A. H. E. Muller, *Macromolecules*, 2011, **44**, 6891-6898.
51 X. Zhang, E. R. Chan and S. C. Glotzer, *J. Chem. Phys.*, 2005, **123**, 184718.
52 Y. C. Lin and S. W. Kuo, *J. Polym. Sci. Pol. Chem.*, 2011, **49**, 2127-2137.
53 H. J. Ryser, *Nature*, 1967, **215**, 934-936.
54 A. Sporbert, P. Domaing, H. Leonhardt and M. C. Cardoso, *Nucleic Acids Res.*, 2005, **33**, 3521-3528.
55 P. Perucca, O. Cazzalini, O. Mortusewicz, D. Necchi, M. Savio, T. Nardo, L. A. Stivala, H. Leonhardt, M. C. Cardoso and E. Prosperi, *J. Cell. Sci.*, 2006, **119**, 1517-1527.
56 M. Hallbrink, A. Floren, A. Elmquist, M. Pooga, T. Bartfai and U. Langel, *BBA Biomembranes*, 2001, **1515**, 101-109.
57 E. Rikowski and H. C. Marsmann, *Polyhedron*, 1997, **16**, 3357-3361.
58 F. J. Feher, K. D. Wyndham, D. Soulivong and F. Nguyen, *J Chem. Soc. Dalton*, 1999, 1491-1497.
59 J. Henig, E. Toth, J. Engelmann, S. Gottschalk and H. A. Mayer, *Inorg. Chem.*, 2010, **49**, 6124-6138.
60 D. A. Scudiero, R. H. Shoemaker, K. D. Paull, A. Monks, S. Tierney, T. H. Nofziger, M. J. Currens, D. Seniff and M. R. Boyd, *Cancer Res.*, 1988, **48**, 4827-4833.
61 P. R. Leroueil, S. Hong, A. Mecke, J. R. Baker, Jr., B. G. Orr and M. M. Banaszak Holl, *Acc. Chem. Res.*, 2007, **40**, 335-342.
62 P. R. Leroueil, S. A. Berry, K. Duthie, G. Han, V. M. Rotello, D. Q. McNerny, J. R. Baker, Jr., B. G. Orr and M. M. Holl, *Nano Lett.*, 2008, **8**, 420-424.
63 F. J. Feher and K. D. Wyndham, *Chem. Commun.*, 1998, 323-324.

3.4. A sensitive method for rapid detection of alkyl halides and dehalogenase activity using a multistep enzyme assay

Sebastian Fabritz†, Franziska Maaß†, Olga Avrutina, Tim Heiseler, Björn Steinmann and Harald Kolmar*

†Equal contributors

AMB Express 2012, 2:51
DOI: 10.1186/2191-0855-2-51
Received: 10 August 2012, Accepted: 16 September 2012
Published: 24 September 2012

Graphical Abstract:

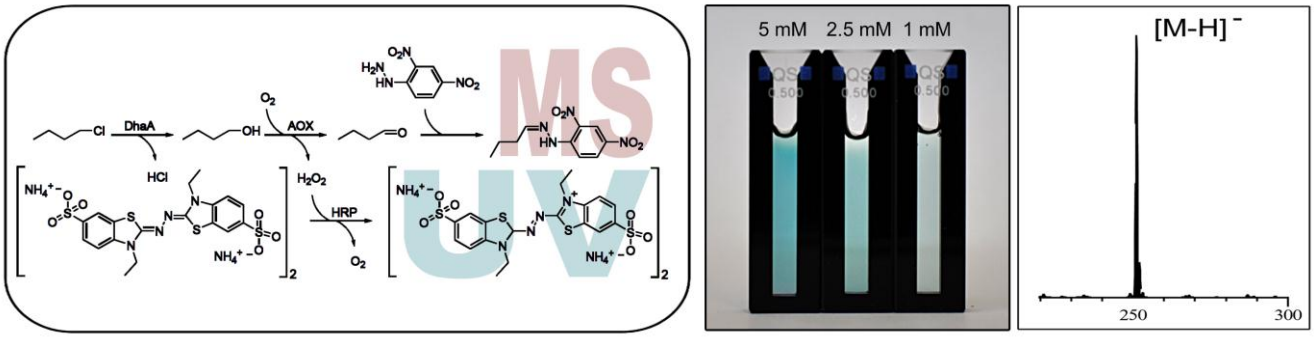

Short Summary:
A method for the detection of haloalkane conversion to the corresponding alcohols based on a multistage enzyme reaction is described. The assay offers a high sensitivity (0.025 mM, 0.43 ppm for 1,3-dibromopropane), low expenditure and the ability of handling a large number of samples in parallel.

http://www.amb-express.com/content/2/1/51

Fabritz *et al. AMB Express* 2012, **2**:51
http://www.amb-express.com/content/2/1/51

AMB Express
a SpringerOpen Journal

ORIGINAL ARTICLE Open Access

A sensitive method for rapid detection of alkyl halides and dehalogenase activity using a multistep enzyme assay

Sebastian Fabritz[†], Franziska Maaß[†], Olga Avrutina, Tim Heiseler, Björn Steinmann and Harald Kolmar[*]

Abstract

A method for the detection of haloalkane conversion to the corresponding alcohols by haloalkane dehalogenases is described. It is based on a multistage enzyme reaction which allows for the analysis of alkyl halides in buffered systems. Irreversible hydrolytic dehalogenation catalyzed by haloalkane dehalogenase DhaA from *Rhodococcus erythropolis* transfers an alkyl halide into a corresponding alcohol that is further oxidized by alcohol oxidase AOX from *Pichia pastoris* yielding a respective aldehyde and hydrogen peroxide easily detectable via the horseradish peroxidase catalyzed oxidation of chromogenic molecules. Due to its high sensitivity (0.025 mM, 0.43 ppm for 1,3-dibromopropane), low expenditure and the ability of handling a large number of samples in parallel, this method is an attractive alternative to existing procedures for the monitoring of both haloalkanes and dehalogenases.

Keywords: Alcohol oxidase, Haloalkane dehalogenase, Haloalkanes, Horseradish peroxidase, Multistage enzyme reaction

Introduction

Haloalkanes are toxic (Akers et al., 1999, Koch and Strobel 1981, Weber et al., 2003) and mutagenic (Brem et al., 1974) environmental contaminants (Koch and Tunger 1981, Yen et al., 2002). Many bacterial species that are able to degrade such compounds have been described to date. Some of them can even utilize haloalkanes as a sole carbon source (Manickam et al., 2008, Mattes et al., 2008, Torz et al., 2007). Bioremediation based on the capability of certain microorganisms to dispose halogenated pollutants is a promising and cost-effective technology (Beeman and Bleckmann 2002, Marzorati et al., 2006, Megharaj et al., 2011, Vlieg et al., 2000). Therefore, convenient methods are required to determine the activity of dehalogenases in enrichment cultures and to detect alkyl halides in environmental samples.

Methods for the determination of halogenated content in various samples have been established since the early 1950s (Iwasaki et al., 1952). A common method for the analysis of haloalkanes is gas chromatography combined with flame-ionization/electron capture or mass spectrometric detection (Arbon and Grimsrud 1990, Curragh et al., 1994, Phillips et al., 2001, van Wijk et al., 2011). These methods, although providing detailed information about the nature and composition of haloalkanes present in a sample, are technically demanding. More recently, procedures for haloalkane detection and degradation have been reported which rely on enzyme-catalyzed dehalogenation yielding free protons and halides (van Pee and Unversucht 2003). Therefore, the majority of current haloalkane assays is focused on the monitoring of proton or halide release. Several pH dependent detection systems rely on chromatic (Holloway et al., 1998, Phillips et al., 2001) or fluorescent indicators (Bidmanova et al., 2010) that require weakly buffered or unbuffered aqueous systems. Alternatively, methods enabling direct estimation of halide concentration have been developed as e.g. the classic colorimetric mercury-iron-thiocyanate method (Cirello-Egamino and Brindle 1995, Iwasaki et al., 1952, Zall et al., 1956), iodide detection via starch incorporation (Kurtovic et al., 2007) or quenching of fluorophores by halides (Marchesi 2003).

* Correspondence: Kolmar@Biochemie-TUD.de
[†]Equal contributors
Institute of Organic Chemistry and Biochemistry, Technische Universität Darmstadt, Petersenstrasse 22, D-64287 Darmstadt, Germany

Herein, we report an alternative biochemical approach to haloalkane detection based on a set of coupled enzyme reactions. At the first step, a haloalkane is converted into a corresponding aliphatic alcohol by a hydrolytic dehalogenation that is catalyzed by a microbial haloalkane dehalogenase (DhaA) (Figure 1A) (Curragh et al., 1994, Koudelakova et al., 2011, Kulakova et al., 1997, Stsiapanava et al., 2008). Then, an alcohol is oxidized by an alcohol oxidase (AOX) (Couderc and Baratti 1980, Sahm et al., 1982, Van der Klei et al., 1990) to an aldehyde yielding H_2O_2 as a detectable by-product (Figure 1B) (Ukeda et al., 1999). Finally, hydrogen peroxide is used by horseradish peroxidase (HRP) as a redox substrate for the oxidation of different chromogens (Braithwaite 1976, Delincée and Radola 1975, Welinder 1979), where 2,2'-azino-di-(3-ethyl-benzthiazoline-6-sulphonic acid) (ABTS) is known to be the most sensitive one (Figure 1C and 1D) (Childs and Bardsley 1975, Porstmann et al., 1981). In addition, the aliphatic aldehyde formed during AOX oxidation of an alcohol readily reacts with 2,4-dinitrophenylhydrazine (2,4-DNPH, Figure 1E) and

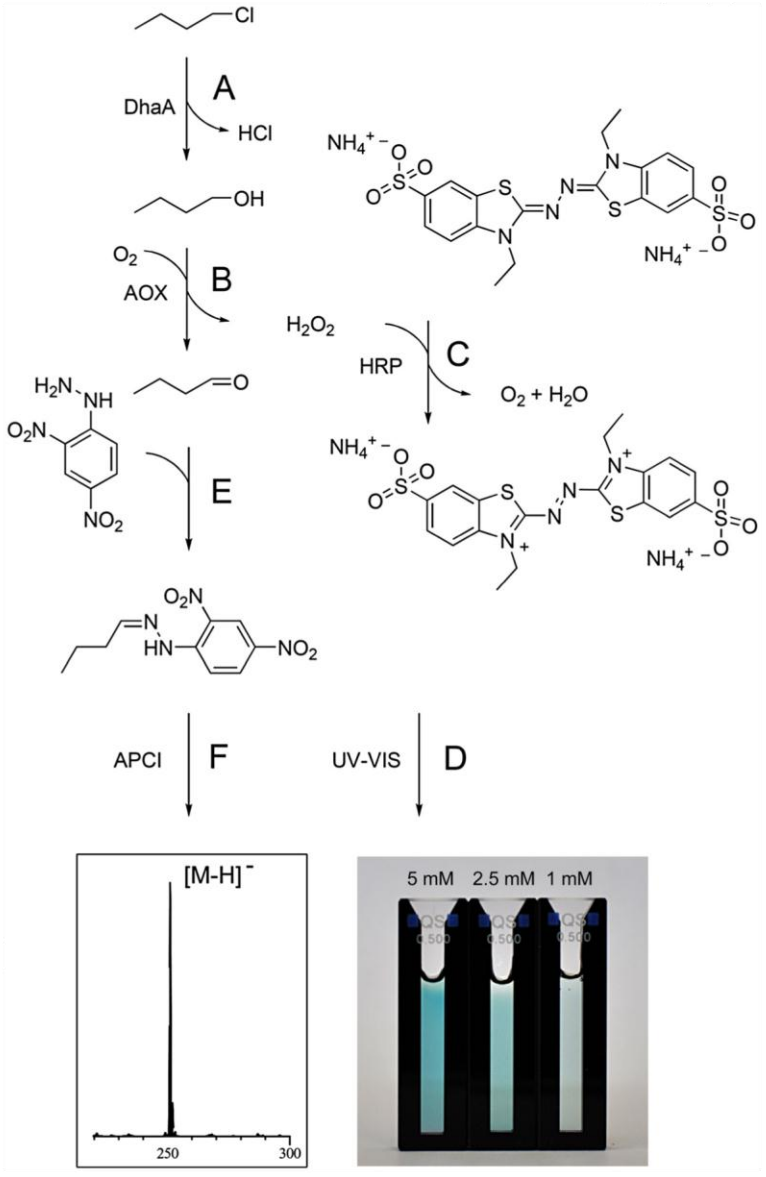

Figure 1 General scheme of an enzymatic multistep assay for the detection of haloalkanes. The alcohol formed via dehalogenation (**A**) undergoes an enzymatic oxidation and H_2O_2 is liberated (**B**). Afterwards a peroxide-HRP complex oxidizes the chromogen ABTS (**C**) resulting in a measureable increase of absorbance at 405 nm (**D**). The enzymatic formation of primary aldehydes can alternatively be proven by precipitation with 2,4-DNPH (**E**) and a subsequent APCI-MS measurement of the resulting hydrazones (**F**).

therefore allows for both photometric and mass-spectrometric detection of the resulting hydrazone (Figure 1F).

Materials and methods

Chemicals and enzymes

The chemicals and enzymes were of analytical grade and used without further purification. Alcohol oxidase (AOX) from *Pichia pastoris* (solution in phosphate-buffered 30% sucrose, 10-40 U/mg) and peroxidase (HRP) from horseradish type VI-A (950-2000 U/mg) were obtained from Sigma-Aldrich (USA). 2,2′-Azino-bis (3-ethylbenzothiazoline-6-sulfonic acid) diammonium salt (ABTS) was purchased from Fluka. Ampicillin sodium salt, isopropyl-β-D-thiogalactopyranoside (IPTG), potassium dihydrogen phosphate and dipotassium hydrogen phosphate were obtained from Carl Roth (Germany).

Expression and purification of haloalkane dehalogenase

The haloalkane dehalogenase gene (*dhaA*) from *Rhodococcus erythropolis* DSM 16550 (Gray and Thornton 1928) has been deposited in the GenBank database under accession no. AF060871.1. The gene was isolated by polymerase chain reaction (PCR) and cloned into the pET21d expression vector (Novagen) to yield pET21d-DhaA. The expression vector was transferred into *E. coli* BL21(DE3). Transformed *E. coli* cells were cultured in 3 liters of dYT medium (1% yeast extract, 1.6% Bacto tryptone, 0.5% NaCl) supplemented with 100 μg/mL ampicillin at 37°C and 180 rpm. Expression was induced with 1 mM IPTG when bacterial growth reached an A_{600} of 0.5 and performed for 18 h at 30°C. The cells were harvested by centrifugation, resuspended in potassium phosphate buffer (0.1 M, pH 7.5) and the cell suspension was stored at -80°C for 1 h. Cells were thawed and disrupted using a high-pressure cell disruption system from Constant Systems Limited (United Kingdom). The suspension was centrifuged at 19650 × g for 30 min at 4°C. The enzyme was purified from the supernatant by immobilized metal ion chromatography using Ni-loaded IMAC Sepharose 6 Fast Flow (GE Healthcare) and a step gradient of imidazole as eluent. Purified enzyme was dialyzed against potassium phosphate buffer (0.1 M, pH 7.5) and frozen in aliquots at -80°C until needed.

Detection of haloalkanes

A quartz cuvette with a path length of 5 mm (type: 104B-QS; Hellma Analytics, Germany) was filled with 500 μL potassium phosphate buffer (0.1 M, pH 7.5) containing the corresponding halogenated compound in desired concentration. 5 μL of ABTS solution in *aqua bidest* (10 mM), 1 μL AOX dissolved in phosphate buffer containing 30% sucrose (1500 U/mL) and 1 μL of a HRP solution in *aqua bidest* (15 kU/mL) was added successively. After an equilibration time of 15 min, 20 μL of purified DhaA in potassium phosphate buffer (~0.32 U/mL) were

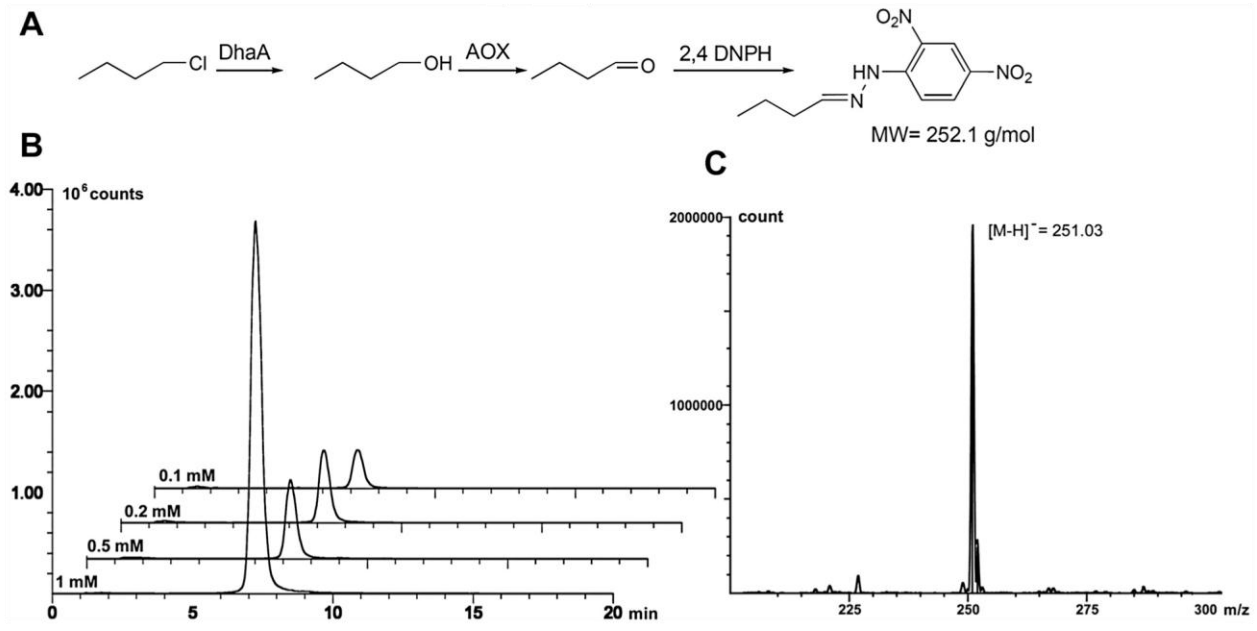

Figure 2 Detection of haloalkanes via formation of LC-MS (APCI) detectable hydrazones. General reaction pathway for the hydrazone formation using 2,4-DNPH (**A**), isolated ion currents of the formed hydrazones. The initial 1-chlorobutane concentrations are given (**B**), APCI-MS spectrum of the measured hydrazone (**C**).

added. The absorbance was measured at 405 nm using a Shimadzu UV–vis spectrophotometer UV-1650PC over 5 min at ambient temperature.

The enzymatic conversion of halogenated compounds into corresponding aldehydes was additionally verified using atmospheric pressure chemical ionisation mass spectrometry (APCI-MS, Figure 2). To that end, the reaction mixture of the enzymatic assay was allowed to stand for 2 h and was subsequently acidified with 75 μL concentrated hydrochloric acid to precipitate the enzymes. After 20 min, the suspension was centrifuged and 75 μL of a saturated solution of 2,4-DNPH in concentrated hydrochloric acid was added to 400 μL of the supernatant. After a reaction time of 30 min, 100 μL acetonitrile were added to assure the solubility of the formed hydrazones. 40 μL of the resulting solution were analyzed using a Shimadzu Mass Spectrometer LC-MS 2020 (gradient: 20 to 80% acetonitrile with 0.1% formic acid over 8 min).

Results

For the detection of haloalkanes or haloalkane dehalogenase, respectively, activity via a multistep bioassay, the haloalkane dehalogenase DhaA from *R. erythropolis* was used as a model enzyme. The His-tagged protein was produced via expression in *E. coli*, purified by immobilised metal ion affinity chromatography (IMAC) and analyzed by SDS-polyacrylamide gel electrophoresis (SDS-PAGE, Figure 3, A-E) and electrospray ionization mass spectrometry (ESI-MS, Figure 3G).

Addition of DhaA together with commercially available and inexpensive AOX and HRP to haloalkanes allows for the subsequent oxidation of the alcohol (generated by DhaA-catalyzed halide abstraction) into a corresponding carbonyl derivative and utilization of the resultant hydrogen peroxide as a cosubstrate of HRP with subsequent formation of an analytical signal by ABTS oxidation. Formation of aldehydes by coupled reaction of the dehalogenase and the alcohol oxidase was confirmed via APCI-MS monitored conversion of the aldehydes to hydrazones using 2,4-dinotrophenylhydrazine (Figure 2). Likewise, the increase of H_2O_2 liberation was detected by HRP and ABTS as a substrate (Figure 4A). In principle, DhaA activity and halide content can be measured via endpoint determination or by the rate of chromophore formation. For quantification of dehalogenase activity it is essential that the DhaA-controlled dehalogenation towards a corresponding alcohol is a rate-determining step. Therefore, a set of parallel experiments to compare reaction rates of DhaA- and AOX-catalyzed transformations was performed with 1 mM 1-chlorobutane and butan-1-ol, respectively. Kinetic assays confirmed that the AOX-driven reaction has proceeded enormously fast compared to the DhaA-mediated dehalogenation using 1.5 U AOX and 6.4 mU DhaA (Figure 4B). Since HRP was used in significant excess, its influence on the overall velocity was negligible (data not shown).

To develop appropriate experimental conditions under which the initial reaction velocity of the coupled three-step enzyme reaction directly corresponds to the initial substrate concentration, 1-chlorobutane was used as a model substrate at different concentrations. To obtain reliable values, measurements were performed in triplicate and the initial reaction rates were determined from the reaction progress curve using a time-frame ranging from 2 to 4 minutes. After substrate addition the samples were preincubated (15 min) as an initial delay in reaction progress has been observed.

To evaluate the feasibility of this method, a set of haloalkane substrates for *R. erythropolis* DhaA was chosen (Koudelakova et al., 2011). They varied in the length of the alkyl chain (C_3 and C_4) as well as the character (Cl, Br), position (primary, secondary), and amount (mono-, disubstituted) of halogen atoms. As expected, the enzyme displayed the highest activity with short- chain mono- and dibromo derivatives while the secondary haloalkane compound was only slowly converted into the corresponding alcohol (Figure 5).

Although 2-bromopropane could only be detected at 5 mM concentration (85.4 ppm), the assay was sensitive

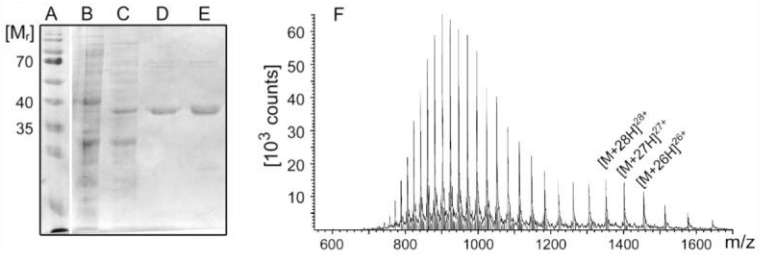

Figure 3 (A-E) SDS Page of DhaA purification via IMAC. (**A**) Prestained Protein Ladder, (**B**) potassium phosphate buffer wash, (**C**) IMAC column elution with 20 mM imidazole, (**D**) IMAC column elution with 40 mM imidazole, (**E**) IMAC column elution with 500 mM imidazole; (**F**) ESI-MS of purified DhaA, measured m/z: 1351.17 [M + 28 H]28+, 1401.07 [M + 27 H]27+, 1454.98 [M + 26 H]26+, calculated mass using ApE - a plasmid editor: 37668 g mol^{-1}, measured deconvoluted mass 37805.59 g mol^{-1}.

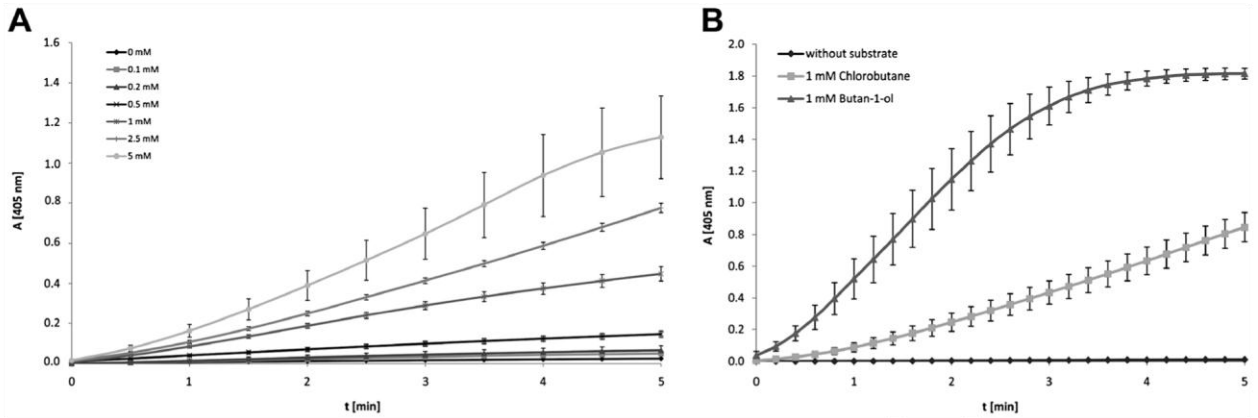

Figure 4 (A) Kinetic measurement of ABTS oxidation product formation at 405 nm. Experiments were performed in triplicate. (**B**). Comparison of reaction rates of DhaA/AOX/HRP mediated formation of ABTS using 1-chlorobutane or butan-1-ol as substrate, respectively. Experiments were performed in triplicate with 1 mM 1-chlorobutane and butan-1-ol.

enough to analyze the content of primary monosubstituted and disubstituted haloalkanes. The fastest turnover and highest detection sensitivity was found for 1,3-dibromopropane that was measured in micromolar concentrations (0.025 mM, 0.43 ppm, Figure 5 and 6).

Discussion

Haloalkane dehalogenases have been isolated from a number of species and also form uncultivated environmental samples using polymerase chain reaction (Kotik and Famerova 2012). Each specific dehalogenase can be expected to have its own characteristic substrate specificity, enantioselectivity and product inhibition properties. For detection of various haloalkanes we have chosen the *R. erythropolis* DhA since it is well characterized and it has been reported to display broadened substrate specificity (Koudelakova et al., 2011, Pavlova et al., 2009). Moreover, this parameter can be further extended even towards acceptance of mono-, di-, and trichloro-substituted substrates by enzyme engineering (Banas et al., 2006, Pavlova et al., 2009).

The coupled triple enzyme reaction described here allows fast simple and sensitive detection of haloalkanes but depending on the nature of the sample to be analysed several potentially limiting conditions have to be carefully considered. It has been reported that certain dehalogenases are inhibited by halides (Schindler et al., 1999). In the case when *R. erythropolis* DhaA is used, presence of halide salts in concentrations up to 80 mM should not disturb the reaction (Schindler et al., 1999). It should also be noted that the signal generation in our method can similarly be triggered by traces of alcohols in the sample. In this case, it may be advisable to preincubate the analyte solution with AOX and a catalase to oxidize the alcohol to the corresponding aldehyde and to remove the hydrogen peroxide generated.

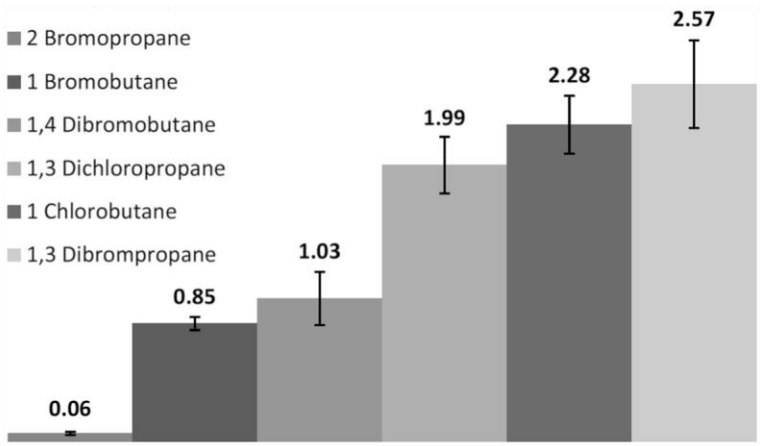

Figure 5 Comparison of reaction velocities of ABTS oxidation product formation as a result of dehalogenation using various haloalkane substrates at 1 mM concentration. The numbers are the initial reaction rate in nmol/min with error bars from three measurements.

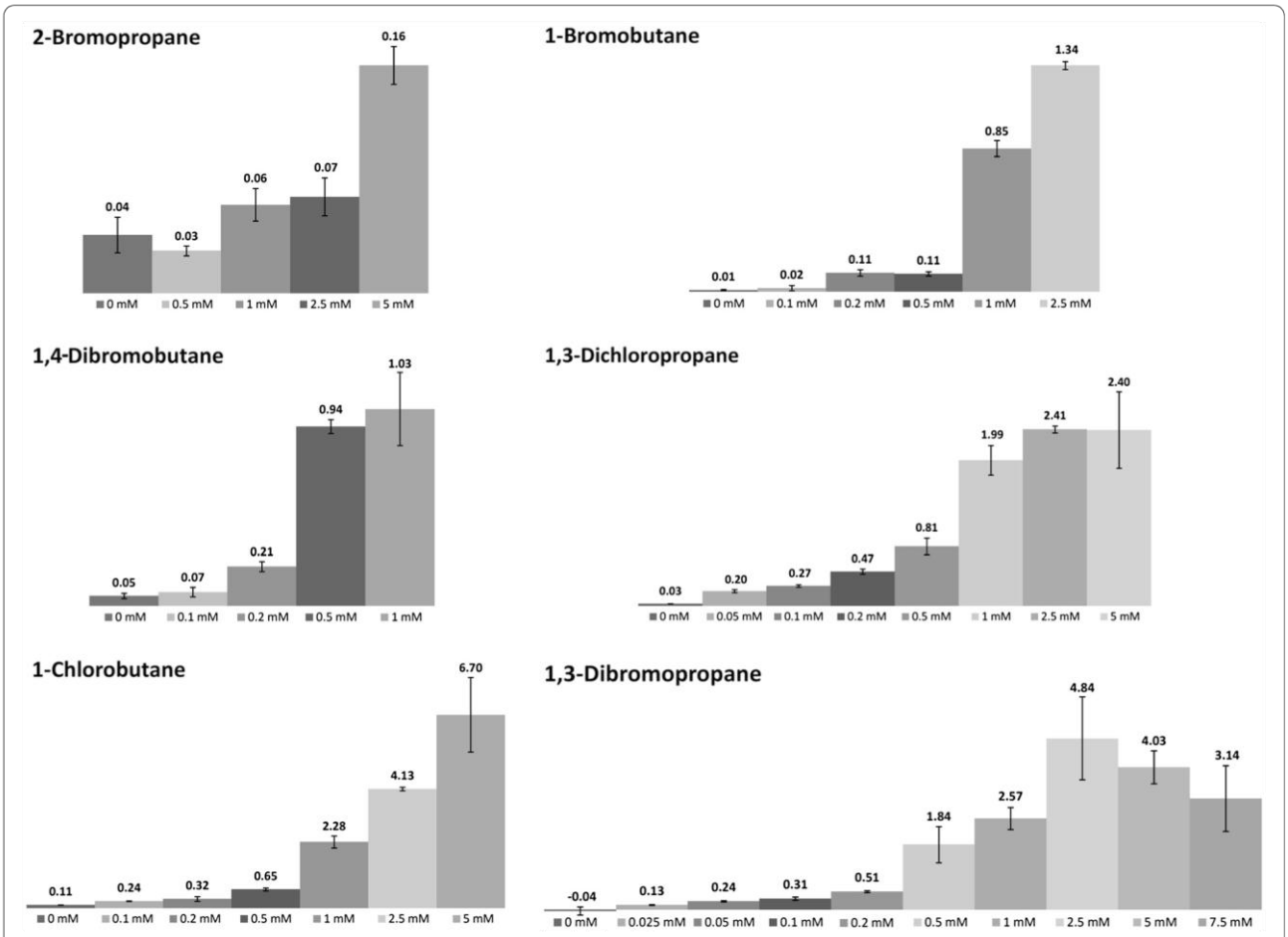

Figure 6 Concentration dependent initial velocities of ABTS oxidation product formation of different substrates. Numbers indicate the reaction rate of dehalogantion in nmol/min with error bars from three measurements.

Subsequent inactivation of catalase, e.g. by addition of 3-amino-1,2,4-triazole or 4-hydroxypyrazole (MacDonald and Pispa 1980, Margoliash et al., 1960), allows one to apply the standard procedure described above. Like other methods relying on the determination of halide content (Holloway et al., 1998, Kurtovic et al., 2007, Marchesi 2003), this assay does not allow to distinguish between individual alkyl halides if a multicomponent mixture of haloalkanes is present in a sample. Since different halogenated alkanes give rise to distinct sensitivity and reaction rates, knowledge of the haloalkane composition of a sample would be required. It can be obtained by using e.g. GC-MS analytics via the generation of an equivalent reference sample for calibration purposes.

It should also be noted that with this triple enzyme assay no linear correlation exists between analyte content and initial velocity of ABTS formation over the range of 0 to 5 mM substrate concentration (Figure 6). Several reasons may account for this finding. At low haloalkane concentration, the accuracy of the measurement may be limited due to the fact that a fraction of the primary aldehydes could react with primary amines of the enzymes present in the reaction mixture via Schiff base formation (Shan and Hammock 2001) which would impede oxidation by HRP.

Obviously, besides measurement of haloalkane content in a sample, the coupled assay can also be used for the determination of haloalkane dehalogenase activity, e.g. in an enrichment culture, using halogenated hydrocarbon substrates for which the enzyme of interest displays the highest catalytic efficiency. The detection system we report here is nontoxic, works in a buffered system, is rapid and, due to the enzyme-mediated chromophore formation, highly sensitive. The assay does not require sophisticated machinery (chlorimeter, special electrodes, etc.), and the enzymes apart from haloalkane dehalogenases are inexpensive and commercially available. Furthermore, the established multistage enzyme reaction can be considered as a modular system for haloalkane detection. The usage of different haloalkane dehalogenases (Janssen 2004, Koudelakova et al., 2011) or DhaA variants that have been optimized by directed evolution (Pavlova et al.,

2009) should result in an extension of accepted substrates if required.

Recently, an enzyme-based method for the detection of halogenated hydrocarbons that relies on an enzymatic fibre-optic biosensor has been reported with similar detection limits (Bidmanova et al., 2010). The assembly of such a device needs special equipment and fine-tuned immobilisation chemistry. Nevertheless, it has the inherent capability of continuous *in situ* measurement. Another interesting approach was developed by Marchesi (Marchesi 2003). The assay is based on the fluorescence quenching of 6-methoxy-*N*-(3-sulfopropyl)-quinolinium by halides. This elegant methodology that allows one to detect halide concentrations in the range of 1-500 mM is restricted to the samples where halide salts are absent since they quench the fluorophore. The approach described here is at least as sensitive as other methods and, depending on the nature of the haloalkane substrate and enzyme, may allow for an even lower detection limit.

In conclusion, we have developed a fast, simple and sensitive detection of haloalkanes and haloalkane dehalogenase activity based on coupled enzymatic reactions. This method may be useful for the detection of halogenated pollutants in environmental samples or for the detection of haloalkane dehalogenase activity e.g. in enrichment cultures or to control dehalogenase activity during bioremediation. Using DhaA from *R. erythropolis* as a model enzyme, we showed that the rate-determing step of the multistep assay was dehalogenation of a haloalkanes substrate. Detection can be conducted either "on-bench", with green colour of a sample indicating the enzymatic conversion of haloalkanes, or, more precisely, by photometric monitoring of the formation of an ABTS oxidation product. Our method allows for the detection of enzyme-mediated haloalkane conversion in buffered systems and, depending on the dehalogenase used, in samples that may contain inorganic halides. High sensitivity (0.025 mM, 0.43 ppm for 1,3-dibromopropane), low expedition, and possibilities to vary haloalkane dehalogenase towards broadened substrate tolerance makes this method a versatile alternative to existing procedures.

Competing interests
The authors declare that they have no competing interests.

Acknowledgement
This work was supported by BMBF through grant Nanokat.

Received: 10 August 2012 Accepted: 16 September 2012
Published: 24 September 2012

References

Akers KS, Sinks GD, Schultz TW (1999) Structure-toxicity relationships for selected halogenated aliphatic chemicals. Environ Toxicol Pharmacol 7:33–39

Arbon RE, Grimsrud EP (1990) Selective detection of iodinated hydrocarbons by the electron-capture detector with negative-ion hydration and photodetachement. Anal Chem 62:1762–1768

Banas P, Otyepka M, Jerabek P, Petrek M, Damborsky J (2006) Mechanism of enhanced conversion of 1,2,3-trichloropropane by mutant haloalkane dehalogenase revealed by molecular modeling. J Comput Aided Mol Des 20:375–383

Beeman RE, Bleckmann CA (2002) Sequential anaerobic-aerobic treatment of an aquifer contaminated by halogenated organics: field results. J Contam Hydrol 57:147–159

Bidmanova S, Chaloupkova R, Damborsky J, Prokop Z (2010) Development of an enzymatic fiber-optic biosensor for detection of halogenated hydrocarbons. Anal Bioanal Chem 398:1891–1898

Braithwaite A (1976) Unit cell dimensions of crystalline horseradish peroxidase. J Mol Biol 106:229–230

Brem H, Stein AB, Rosenkranz HS (1974) The mutagenicity and DNA-modifying effect of haloalkanes. Cancer Res 34:2576–2579

Childs RE, Bardsley WG (1975) The steady-state kinetics of peroxidase with 2,2'-azino-di-(3-ethyl-benzthiazoline-6-sulphonic acid) as a chromogen. Biochem J 145:93–103

Cirello-Egamino J, Brindle ID (1995) Determination of chloride ions by reaction with mercury thiocyanate in the absence of iron(III) using a UV-photometric, flow injection method. Analyst 120:183–186

Couderc R, Baratti J (1980) Oxidation of methanol by the yeast. Pichia pastoris. Purification and properties of the alcohol oxidase. Agr Biol Chem 44:2279–2289

Curragh H, Flynn O, Larkin MJ, Stafford TM, Hamilton JTG, Harper DB (1994) Haloalkane degradation and assimilation by *Rhodococcus rhodochrous* NCIMB 13064. Microbiology-Uk 140:1433–1442

Delincée H, Radola B (1975) Fractionation of horseradish peroxidase by preparative isoelectric focusing, gel chromatography and ion-exchange chromatography. Eur J Biochem 52:321–330

Gray PHH, Thornton HG (1928) Soil bacteria that decompose certain aromatic compounds. Zentralbl Bakterio Parasitenkd Infektionskr Hyg Abt I 73:74–96

Holloway P, Trevors JT, Lee H (1998) A colorimetric assay for detecting haloalkane dehalogenase activity. J Microbiol Methods 32:31–36

Iwasaki I, Utsumi S, Ozawa T (1952) New colorimetric determination of chloride using mercuric thiocyanate and ferric ion. Bull Chem Soc Jpn 25:226–226

Janssen DB (2004) Evolving haloalkane dehalogenases. Curr Opin Chem Biol 8:150–159

Koch R, Strobel K (1981) Ökochemische und toxikologische Daten für ausgewählte Halogenalkane und ihre Bewertung. Acta Hydrochim Hydrobiol 9:227–246

Koch R, Tunger A (1981) Kontamination von Wässern mit Halogenalkanen und -alkenen. Acta Hydrochim Hydrobiol 9:471–475

Kotik M, Famerova V (2012) Sequence diversity in haloalkane dehalogenases, as revealed by PCR using family-specific primers. J Microbiol Methods 88:212–217

Koudelakova T, Chovancova E, Brezovsky J, Monincova M, Fortova A, Jarkovsky J, Damborsky J (2011) Substrate specificity of haloalkane dehalogenases. Biochem J 435:345–354

Kulakova AN, Larkin MJ, Kulakov LA (1997) The plasmid-located haloalkane dehalogenase gene from *Rhodococcus rhodochrous* NCIMB 13064. Microbiology-Uk 143:109–115

Kurtovic S, Jansson R, Mannervik B (2007) Colorimetric endpoint assay for enzyme-catalyzed iodide ion release for high-throughput screening in microtiter plates. Arch Biochem Biophys 464:284–287

MacDonald E, Pispa JP (1980) Inhibition of catalase *in vitro* and *in vivo* by 4-hydroxypyrazole, a metabolite of pyrazole. FEBS Lett 120:61–64

Manickam N, Reddy MK, Saini HS, Shanker R (2008) Isolation of hexachlorocyclohexane-degrading Sphingomonas sp. by dehalogenase assay and characterization of genes involved in gamma-HCH degradation. J Appl Microbiol 104:952–960

Marchesi JR (2003) A microplate fluorimetric assay for measuring dehalogenase activity. J Microbiol Methods 55:325–329

Margoliash E, Novogrodsky A, Schejter A (1960) Irreversible reaction of 3-amino-1:2:4-triazole and related inhibitors with the protein of catalase. Biochem J 74:339–348

Marzorati M, Borin S, Brusetti L, Daffonchio D, Marsilli C, Carpani G, de Ferra F (2006) Response of 1,2-dichloroethane-adapted microbial communities to *ex-situ* biostimulation of polluted groundwater. Biodegradation 17:41–56

Mattes TE, Alexander AK, Richardson PM, Munk AC, Han CS, Stothard P, Coleman NV (2008) The genome of *Polaromonas* sp strain JS666: Insights into the evolution of a hydrocarbon- and xenobiotic-degrading bacterium, and

features of relevance to biotechnology. Appl Environ Microbiol 74:6405–6416
Megharaj M, Ramakrishnan B, Venkateswarlu K, Sethunathan N, Naidu R (2011) Bioremediation approaches for organic pollutants: A critical perspective. Environ Int 37:1362–1375
Pavlova M, Klvana M, Prokop Z, Chaloupkova R, Banas P, Otyepka M, Wade RC, Tsuda M, Nagata Y, Damborsky J (2009) Redesigning dehalogenase access tunnels as a strategy for degrading an anthropogenic substrate. Nat Chem Biol 5:727–733
Phillips TM, Seech AG, Lee H, Trevors JT (2001) Colorimetric assay for Lindane dechlorination by bacteria. J Microbiol Methods 47:181–188
Porstmann B, Porstmann T, Nugel E (1981) Comparison of chromogens for the determination of horseradish peroxidase as a marker in enzyme immunoassay. J Clin Chem Clin Biochem 19:435–439
Sahm H, Schutte H, Kula MR (1982) Alcohol oxidase from *Candida boidinii*. Methods Enzymol 89:424–428
Schindler JF, Naranjo PA, Honaberger DA, Chang CH, Brainard JR, Vanderberg LA, Unkefer CJ (1999) Haloalkane dehalogenases: steady-state kinetics and halide inhibition. Biochemistry 38:5772–5778
Shan G, Hammock BD (2001) Development of sensitive esterase assays based on alpha-cyano-containing esters. Anal Biochem 299:54–62
Stsiapanava A, Koudelakova T, Lapkouski M, Pavlova M, Damborsky J, Smatanova IK (2008) Crystals of DhaA mutants from *Rhodococcus rhodochrous* NCIMB 13064 diffracted to ultrahigh resolution: crystallization and preliminary diffraction analysis. Acta Crystallogr F-Struct Biol Cryst Commun 64:137–140
Torz M, Wietzes P, Beschkov V, Janssen DB (2007) Metabolism of mono- and dihalogenated C1 and C2 compounds by *Xanthobacter autotrophicus* growing on 1,2-dichloroethane. Biodegradation 18:145–157
Ukeda H, Ohira M, Sawamura M (1999) Immobilized enzyme-based microtiter plate assay for ethanol in alcoholic beverages. Anal Sci 15:447–450
Van der Klei IJ, Bystrykh LV, Harder W (1990) Alcohol oxidase from *Hansenula polymorpha* CBS 4732. Methylortophy 188:420
van Pee KH, Unversucht S (2003) Biological dehalogenation and halogenation reactions. Chemosphere 52:299–312
van Wijk AM, Beerman B, Niederlander HA, Siebum AH, de Jong GJ (2011) A new approach for generic screening and quantitation of potential genotoxic alkylation compounds by pre-column derivatization and LC-MS/MS analysis. Anal Bioanal Chem 400:1375–1385
Vlieg J, Poelarends GJ, Mars AE, Janssen DB (2000) Detoxification of reactive intermediates during microbial metabolism of halogenated compounds. Curr Opin Microbiol 3:257–262
Weber LWD, Boll M, Stampfl A (2003) Hepatotoxicity and mechanism of action of haloalkanes: Carbon tetrachloride as a toxicological model. Crit Rev Toxicol 33:105–136
Welinder KG (1979) Amino acid sequence studies of horseradish peroxidase. Eur Biochem 96:483–502
Yen JH, Lin KH, Wang YS (2002) Acute lethal toxicity of environmental pollutants to aquatic organisms. Ecotox Environ Safe 52:113–116
Zall DM, Fisher D, Garner MQ (1956) Photometric determination of chlorides in water. Anal Chem 28:1665–1668

doi:10.1186/2191-0855-2-51
Cite this article as: Fabritz *et al.*: A sensitive method for rapid detection of alkyl halides and dehalogenase activity using a multistep enzyme assay. *AMB Express* 2012 **2**:51.

4. Zusätzliche analytische und experimentelle Daten

4.1. Analytische und experimentelle Daten der Verbindungen aus Teil 3.1.

Die Nummerierung der Verbindungen entspricht: Fabritz et al., Org. Biomol. Chem., 2010, **8**, 2212-2218.

Instrumental Data

HPLC

Either a Varian 920-LC system (*Varian Deutschland GmbH*, Darmstadt, Germany) equipped with a Waters Symmetry 100 C8 column (150×3.9 mm, 5 µm) or a SHIMADZU LC-MS 2020 system (*Shimadzu Deutschland GmbH*, Duisburg, Germany) with a Shim-pack XR –C8 column (50×2 mm, 2.2 µm) was used for RP HPLC.

IR SPECTROSCOPY

Infrared spectra were obtained using a Perkin Elmer FT-IR spectrometer Paragon 1000 PC (*Perkin Elmer*, Waltham, Massachusetts, USA)

MASS SPECTROMETRY

Analysis of **1**, **2**, **3** and **4**: Solutions of the analytes were prepared in tetrahydrofuran/methanol containing 10 mM ammonium acetate (1:1).

Analysis of **5**, **6**, **7** and **8**: An HPLC fraction of sample **6** was diluted with tetrahydrofuran and 10 mM ammonium acetate in methanol. The sample **5** was dissolved in tetrahydrofuran/methanol containing 10 mM ammoinium acetate (1:1) and **7** was dissolved in a mixture of tetrahydrofuran/0.2 % formic acid in methanol. **8** was measured directly from an HPLC fraction and as a solution of the pellet in methanol containing 0.2 % formic acid.

High-resolution mass spectrometry was performed using a 7 T-FTICR-MS instrument (APEX IV, Bruker Daltonics, Billerica, USA) equipped with an APOLLO electrospray ion source and a syringe pump (74900 series, Cole-Parmer, Vernon Hills, USA) with a flow rate of 2 µL min^{-1} for sample injection.

Electrospray Ionisation was performed in the positive ion mode with a capillary voltage of 4.2 kV and a capillary exit voltage of 100 V. Nitrogen was used as nebulising gas (pressure 30 psi) and as drying gas (temperature 250°C). For external and internal calibration ESI tuning mix (Agilent Technologies) was applied.

NMR SPECTROSCOPY

NMR spectra were recorded on Varian VNMRS500 or Jeol ECP(Eclipse) 300.

Synthesis of N-(3',6'-dihydroxy-3-oxo-3H-spiro[isobenzofuran-1,9'-xanthene]-5-yl)hex-5-ynamide.

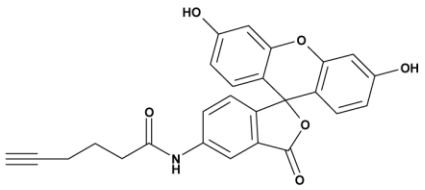

Molecular Weight =441,44
Molecular Formula =C26H19NO6

5-Hexynoic acid (45.2 mg, 0.8062 mmol, 8 equiv.) was incubated with DIC (25.4 mg, 0.4031 mmol, 4 equiv.) in 5 ml of DMF-DCM (4:1, v:v) mixture for 15 min at room temperature, and fluorescein amine (35 mg, 0.1008 mmol, 1 equiv.) dissolved in 1 ml of DMF-DCM (4:1, v:v) was added. The mixture was stirred at room temperature for 2 h. Then the solvent was evaporated under reduced pressure and the raw product was suspended in water (3 mL). The aqueous layer was extracted with MTBE (3×2mL) and dried. After evaporation of the solvent, 32 mg (71.9 %) of a fluorescein derivative bearing an alkyne moiety was obtained as an orange solid. (ESI MS: calc. 441.45, meas. 442.3 $[M+H]^+$; HPLC: Rt = 14.68 min, Waters Symmetry 100 C8 column (150×3.9 mm, 5 µm) using a linear gradient of 80% aq. CH_3CN in 0.1 % aq. TFA (20→100% in 30 min)).

Synthesis of the alkyne derivatised RDG8 peptide

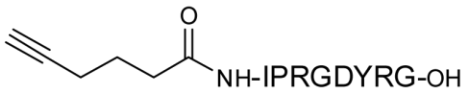

$C_{46}H_{70}N_{14}O_{13}$
Exact Mass: 1026,525
Mol. Wt.: 1027,134

The alkyne functionalized octapeptide was synthesized *via* MW-assisted Fmoc SPPS on a Wang resin with a binding capacity of 0.61 mmol/g preloaded with Fmoc-Gly (0.5 g, 0.305 mmol, 1eq.). Coupling conditions were as follows: 15 min, 50 °C, 20 W of microwave energy. Arginine and proline were attached through double coupling. Then hexynoic acid was coupled using the same conditions as described. The assembled octapeptide derivative was cleaved from the resin using a cleavage cocktail containing 92 % TFA, 4 % H_2O, 2 % anisole and 2 % TES (v:v:v:v), precipitated and washed with MTBE. The crude peptide was then purified *via* RP-HPLC yielding 89 mg of a white powder (87 µmol, 29 %).

Analytical data:

RP HPLC, C8 column, gradient: 10% → 35% B (90% aq. CH_3CN + 0.1% TFA), R_t = 21.88 min

ESI-MS: m/z: 1027.8 $[M+H]^+$, 1049.6 $[M+Na]^+$.

Analytical Data

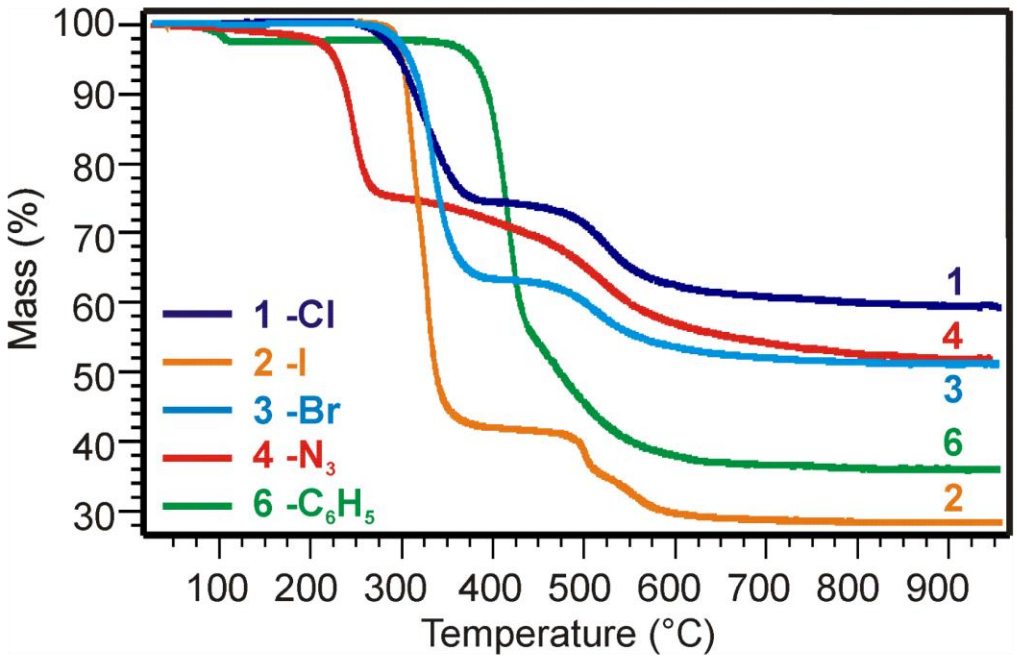

Fig. S1: Thermogravimetric analysis of **1**, **2**, **3**, **4** and **6**

Compound	Residual Mass (measured %)	Ceramic Yield (calculated % for SiO_2)
1- POSS-Cl	59.26*	46.35
2- POSS-I	28.27	27.18
3- POSS-Br	51.07*	34.51
4- POSS-N_3	52.07*	44.11
5- POSS-C_6H_5	35.81	35.08

* The difference in measured residual masses and ceramic yield can be explained by the fact that SiO_2 is not a final decomposition product for the marked substances in the given temperature interval.

Tab. 1: Comparison of measured residual masses of various POSS with different substituents and corresponding ceramic yields assuming complete conversion to SiO_2.

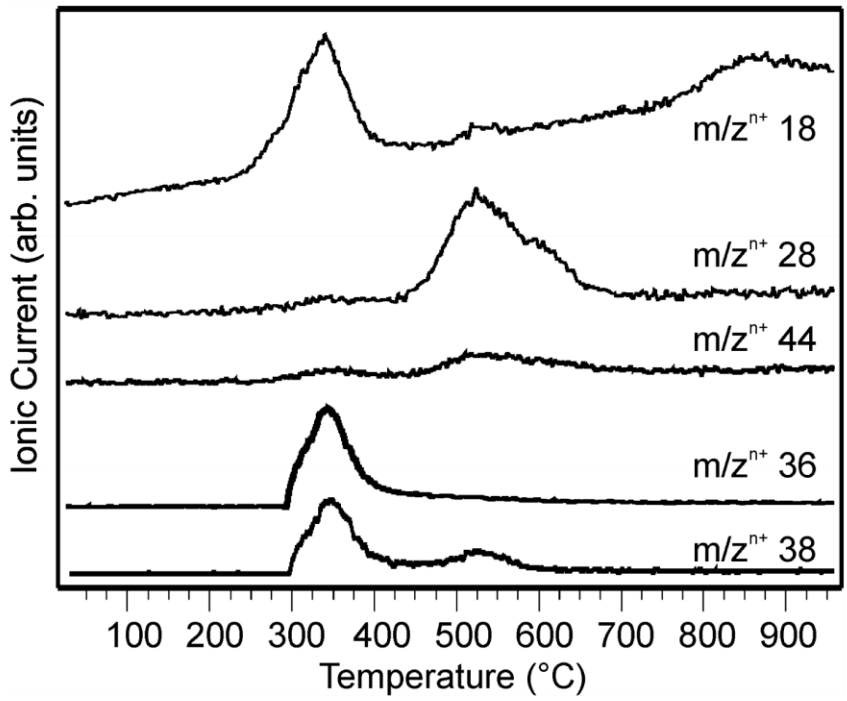

Fig. S2: TG-MS traces of **1**

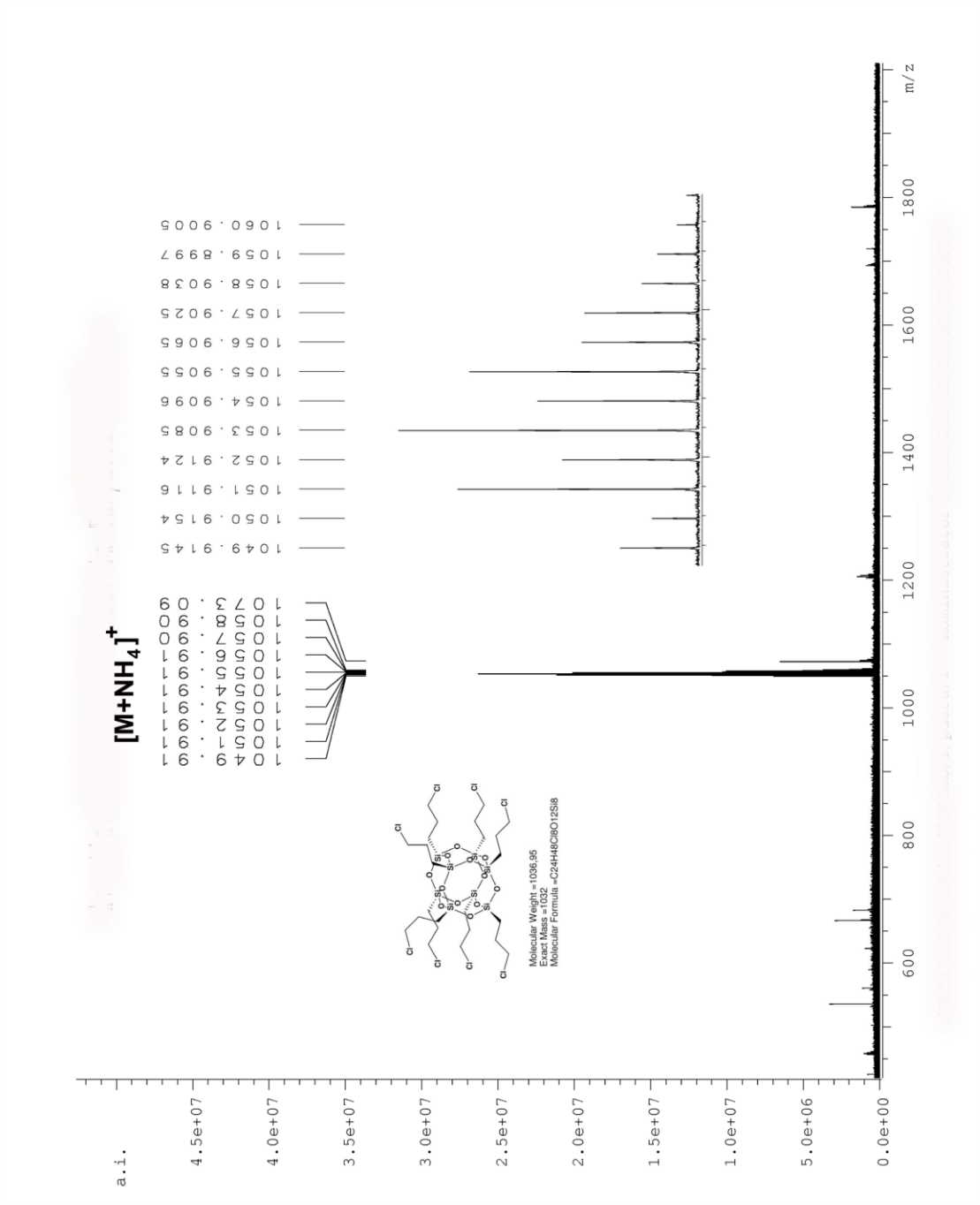

Fig. S3: ESI-MS spectrum of **1**

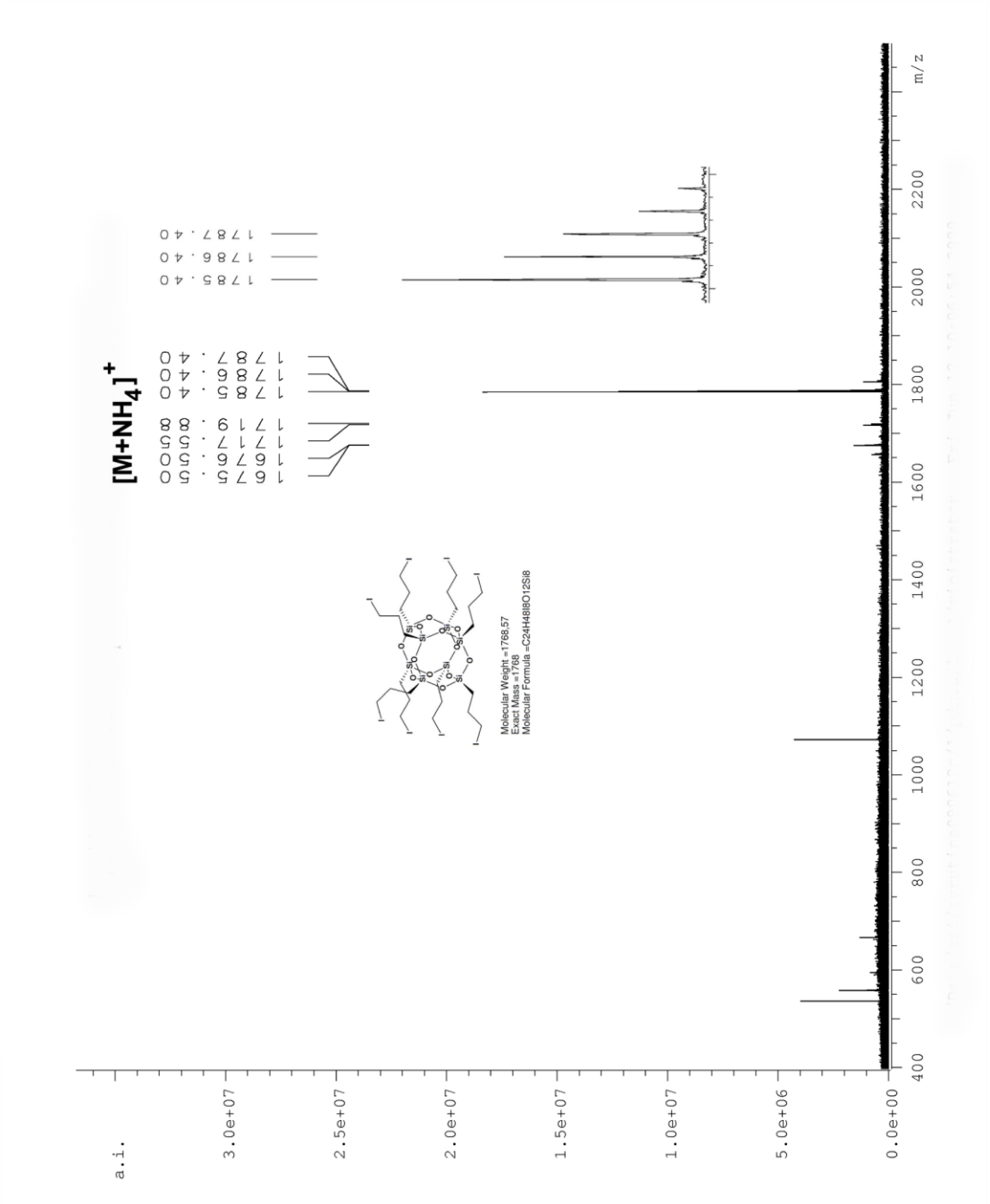

Fig. S4: ESI MS spectrum of **2**

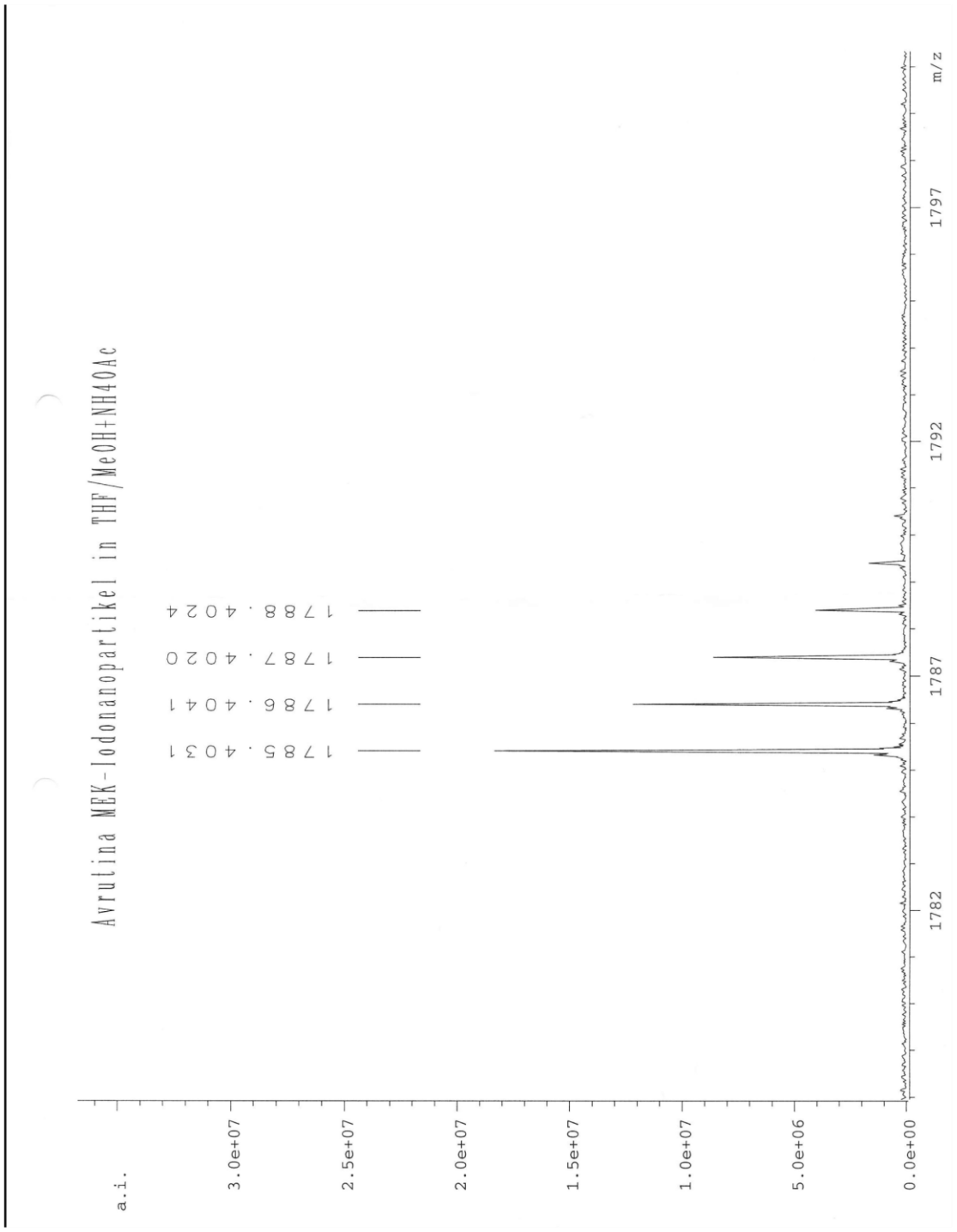

Fig. S5: HRMS, isotopic peak pattern of **2**

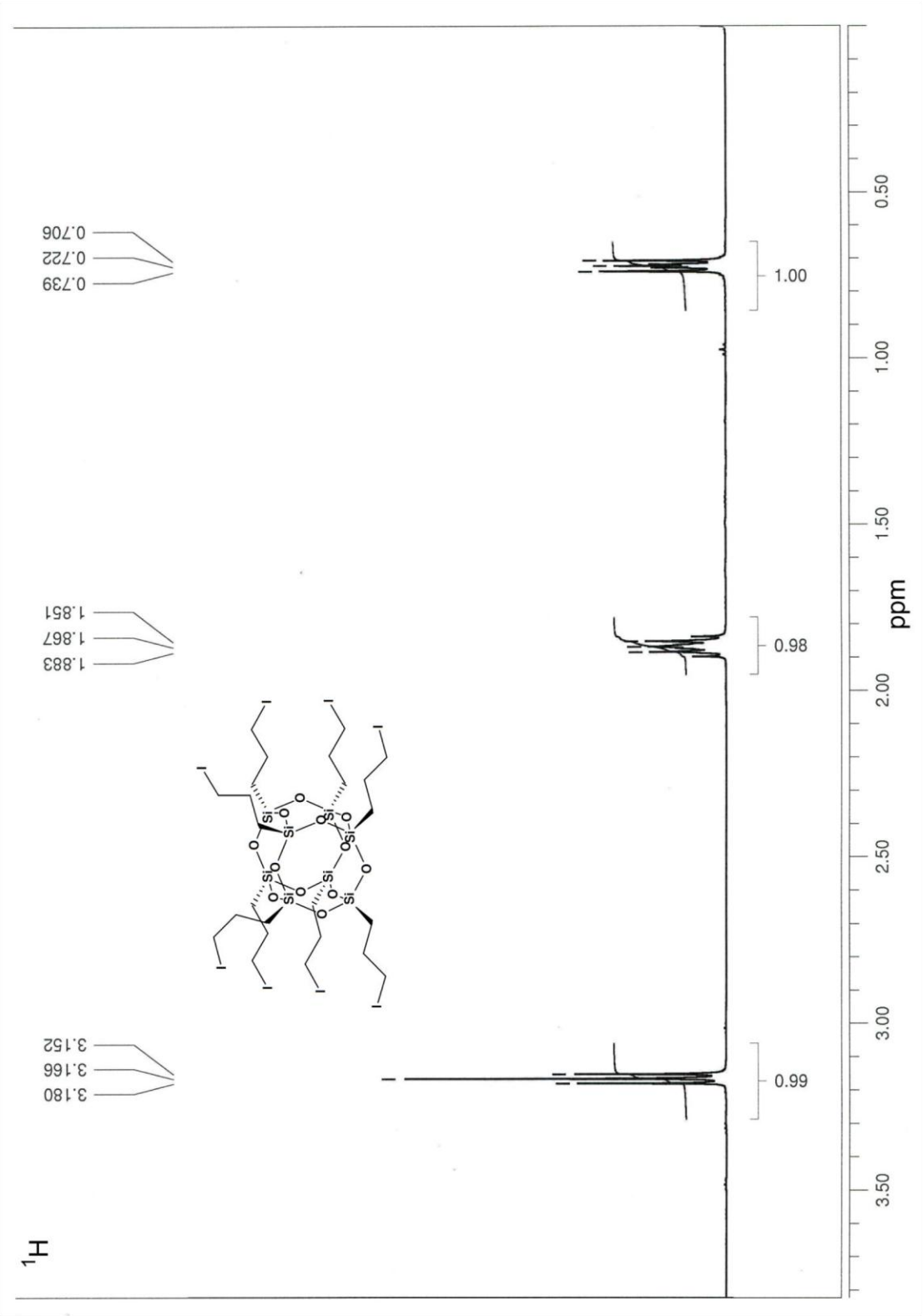

Fig. S6: ^{1}H NMR of **2**

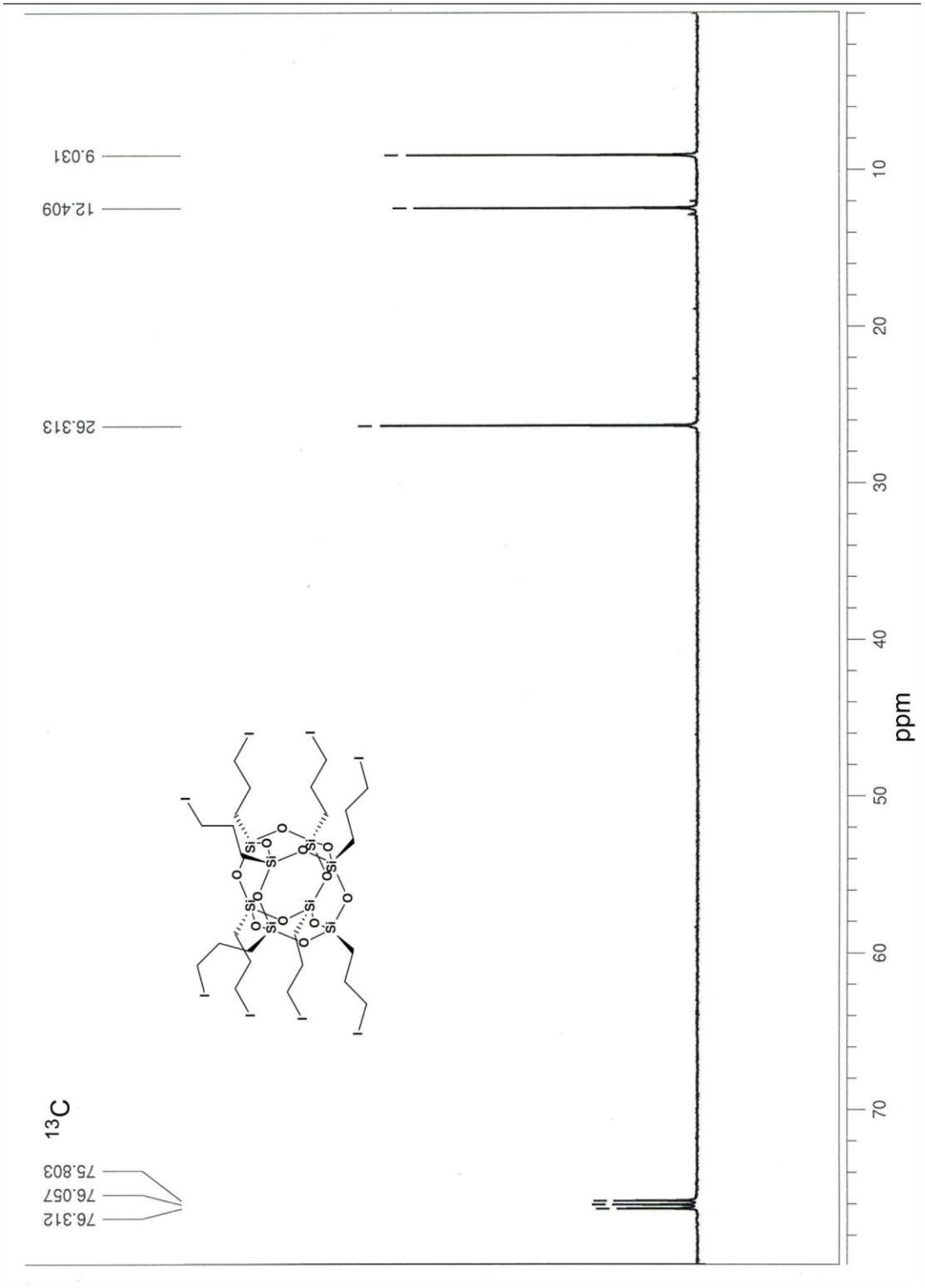

Fig. S7: ^{13}C NMR of **2**

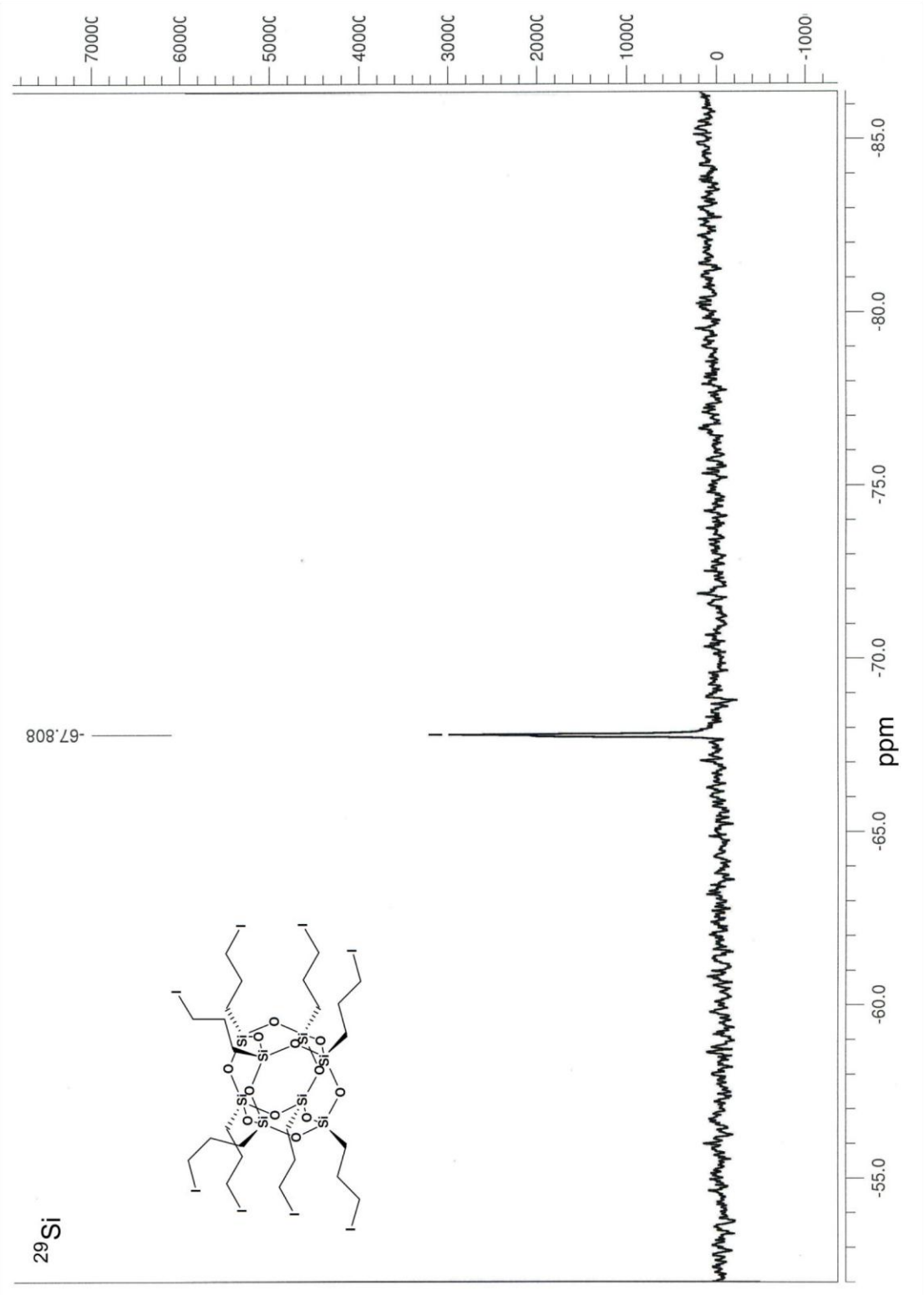

Fig. S8: ^{29}Si NMR of **2**

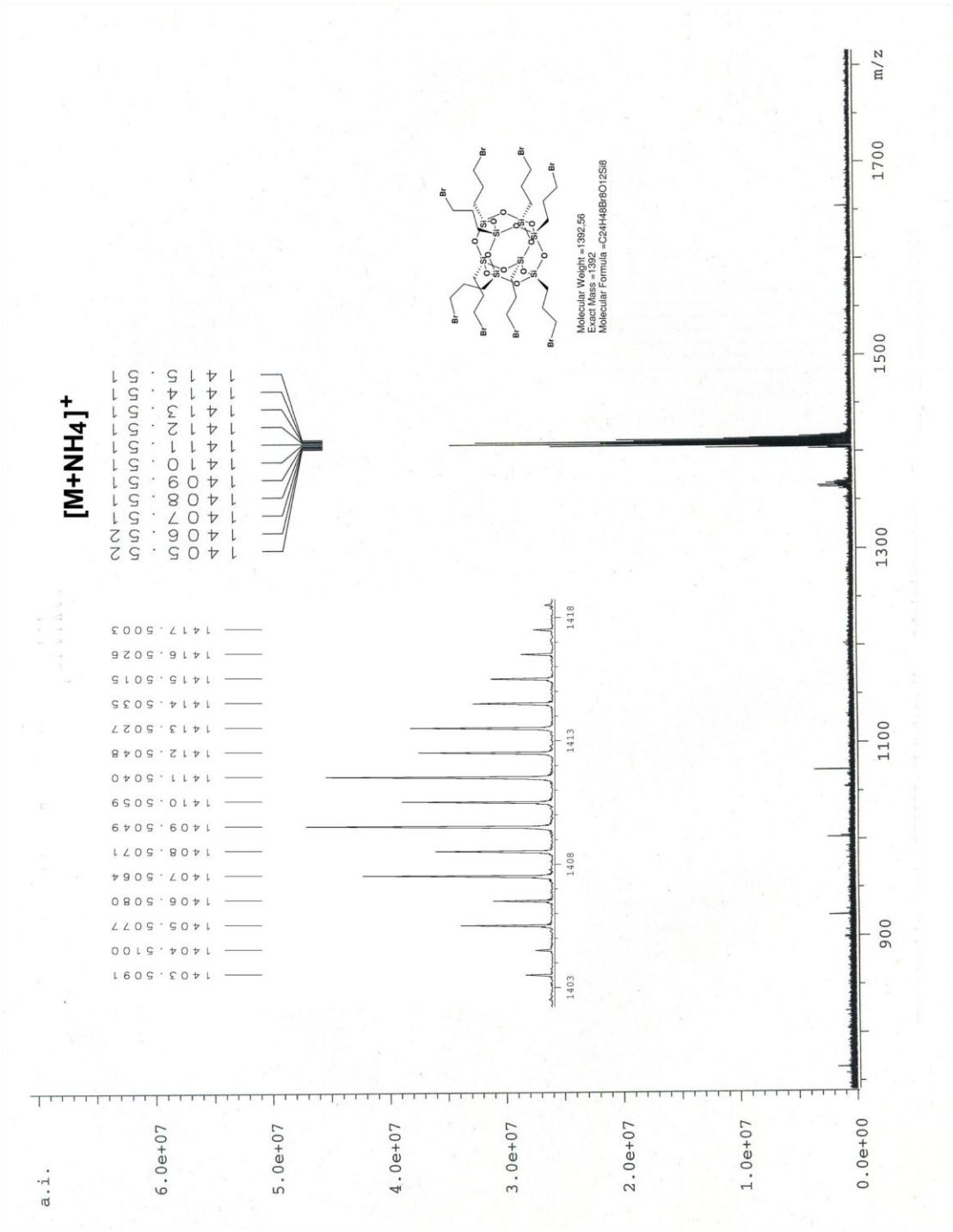

Fig. S9: ESI-MS spectrum of **3**

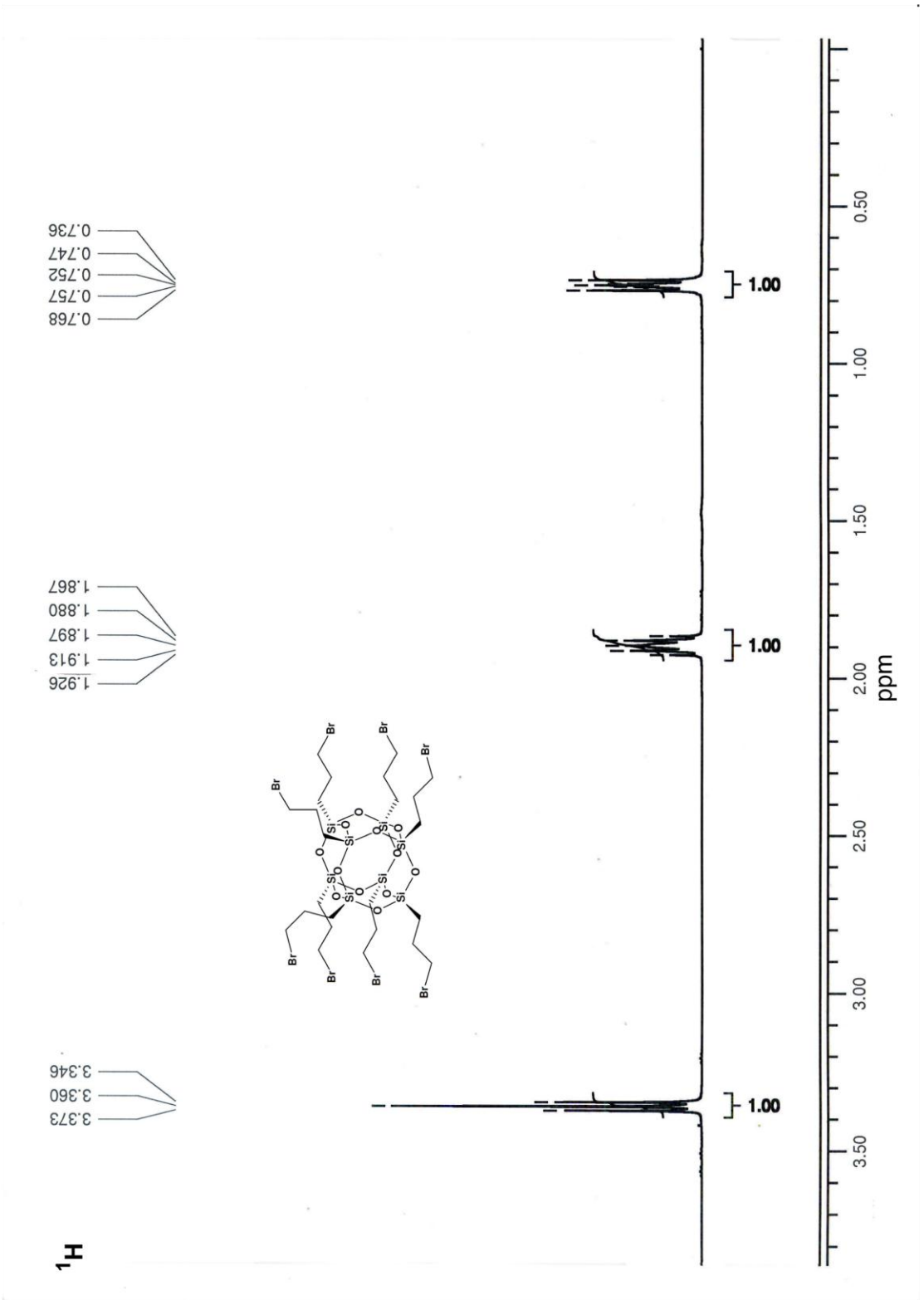

Fig. S10: ^{1}H NMR of **3**

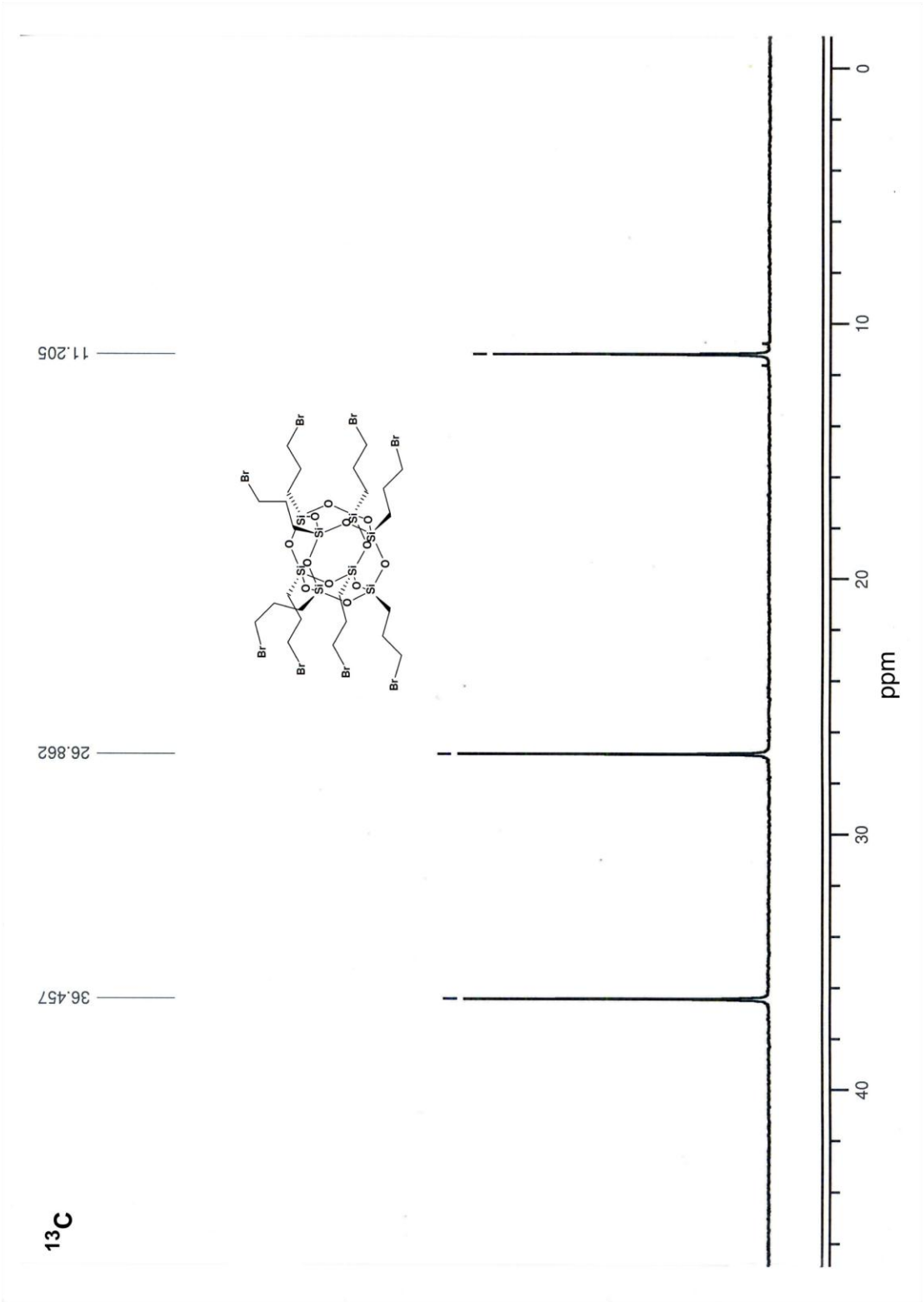

Fig. S11: ^{13}C NMR of **3**

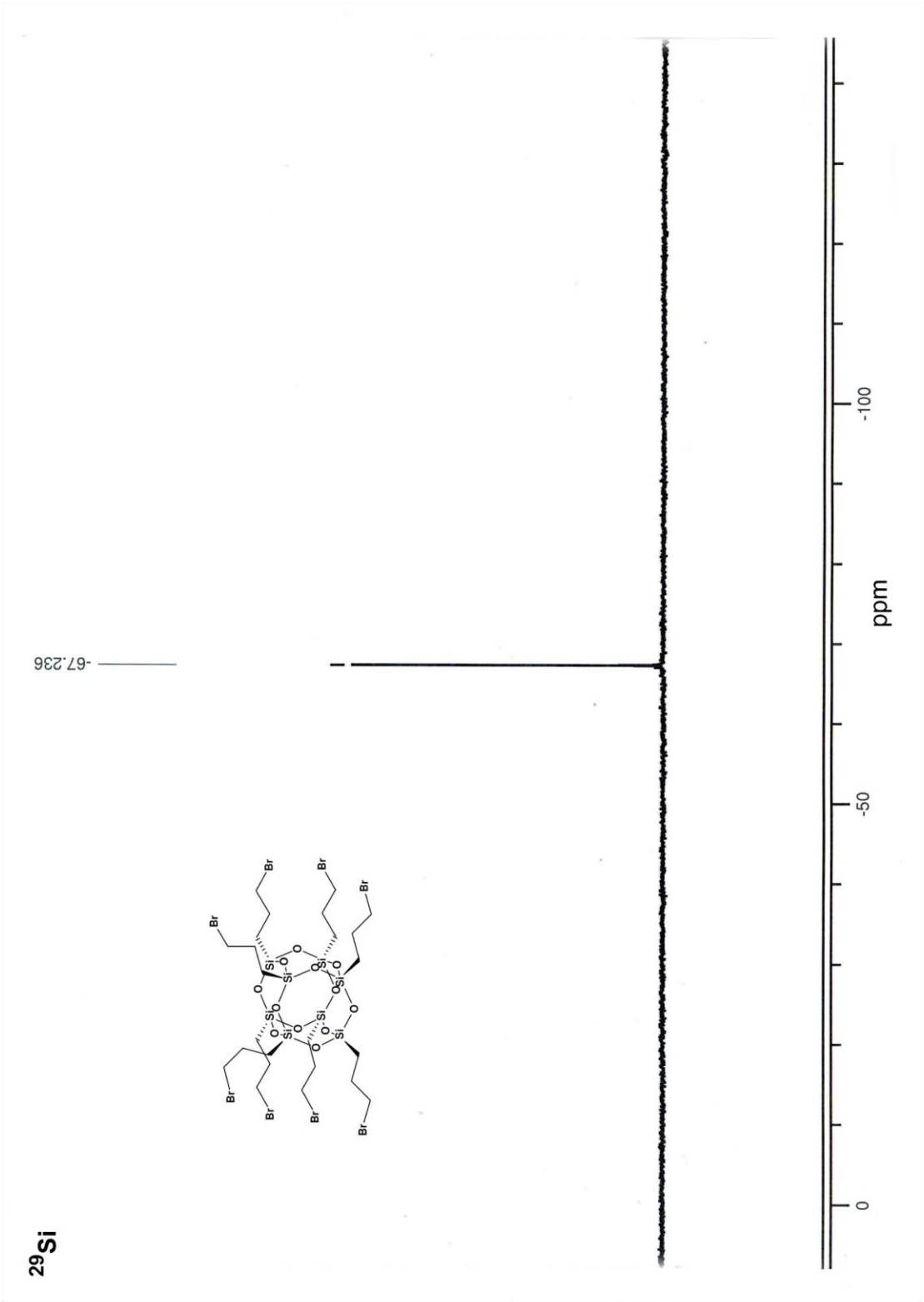

Fig. S12: ^{29}Si NMR of **3**

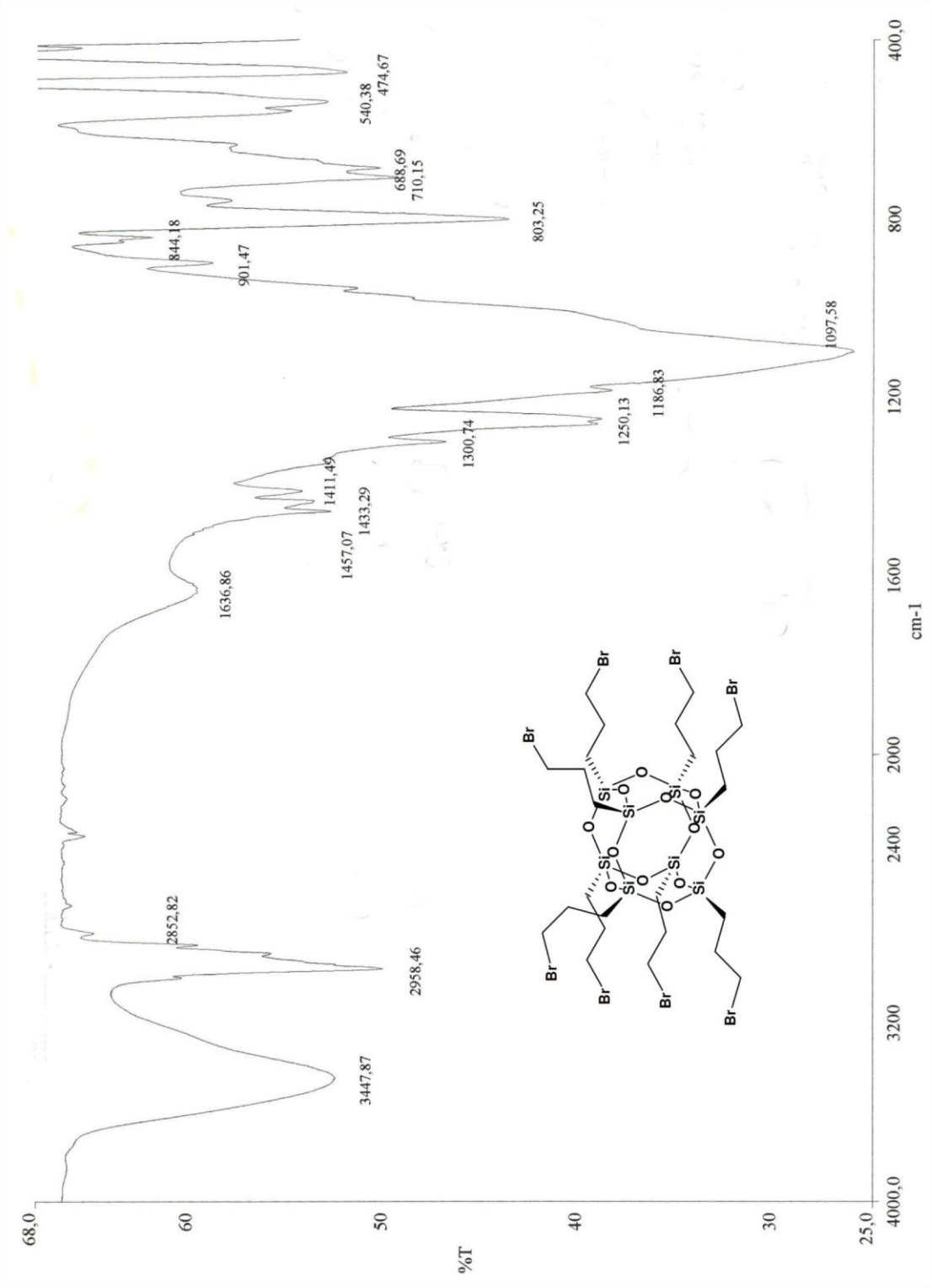

Fig. S13: IR spectrum of **3**

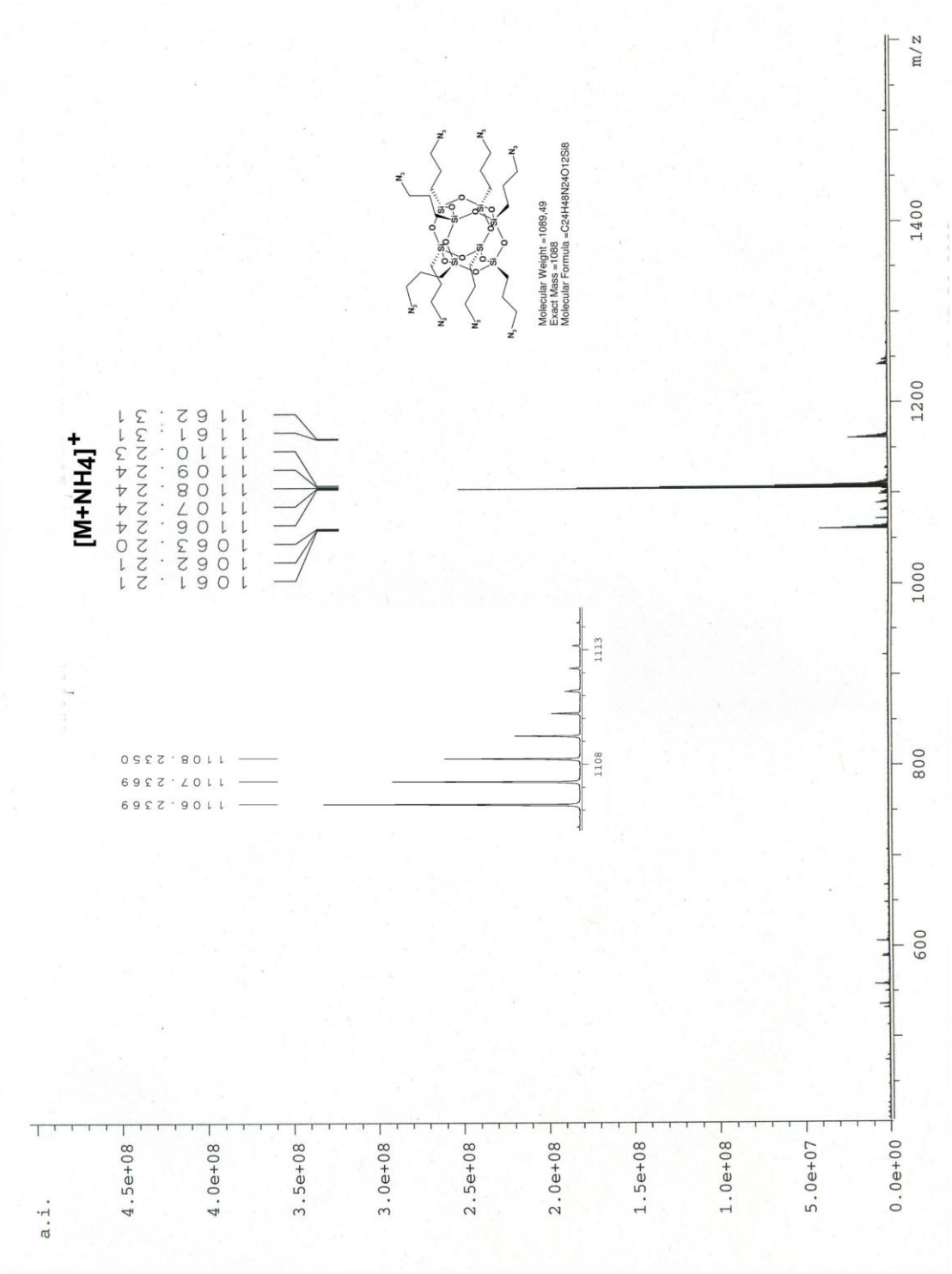

Fig. S14: ESI-MS spectrum of **4**

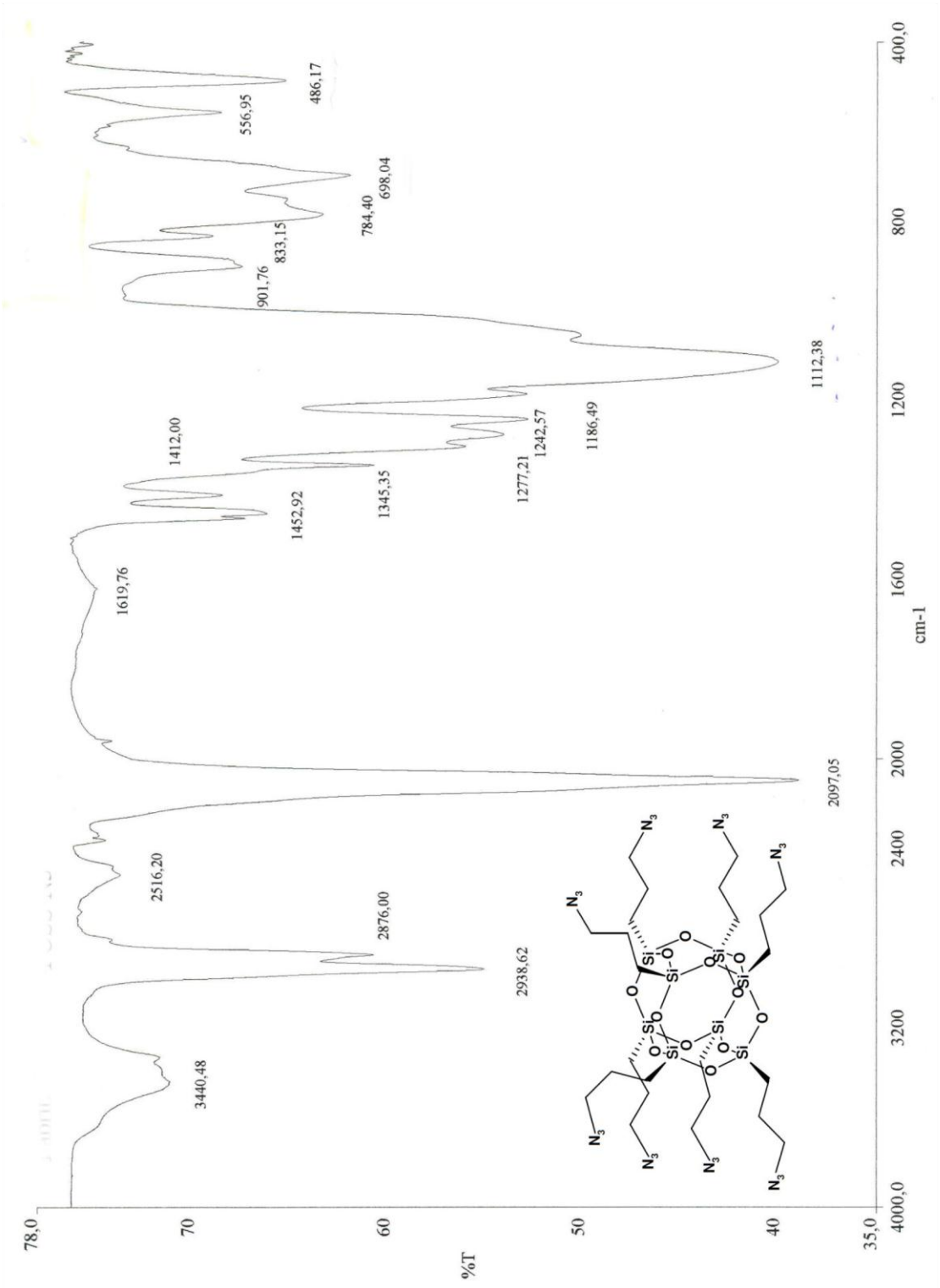

Fig. S15: IR spectrum of **4**

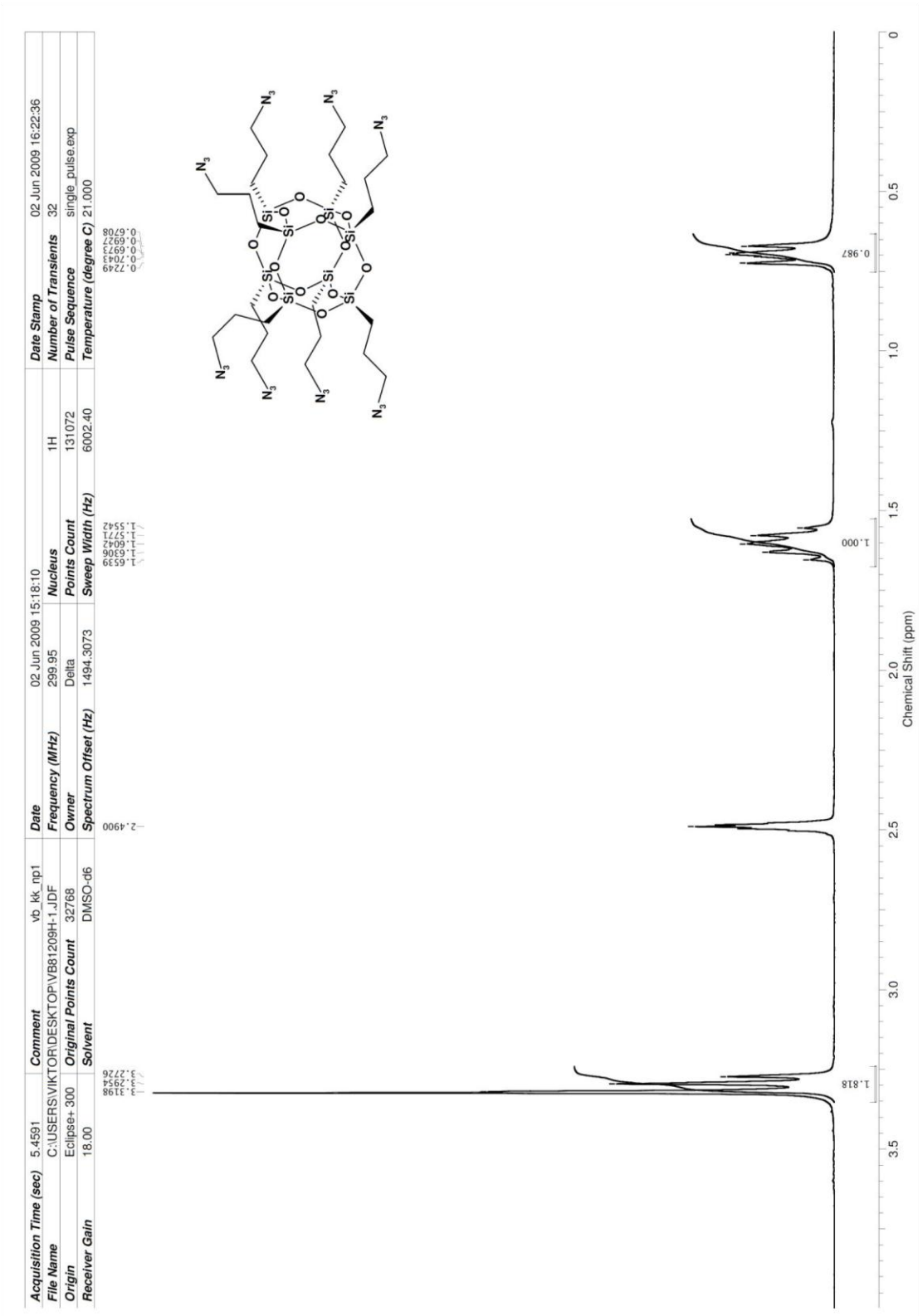

Fig. S16: ^{1}H NMR of **4**

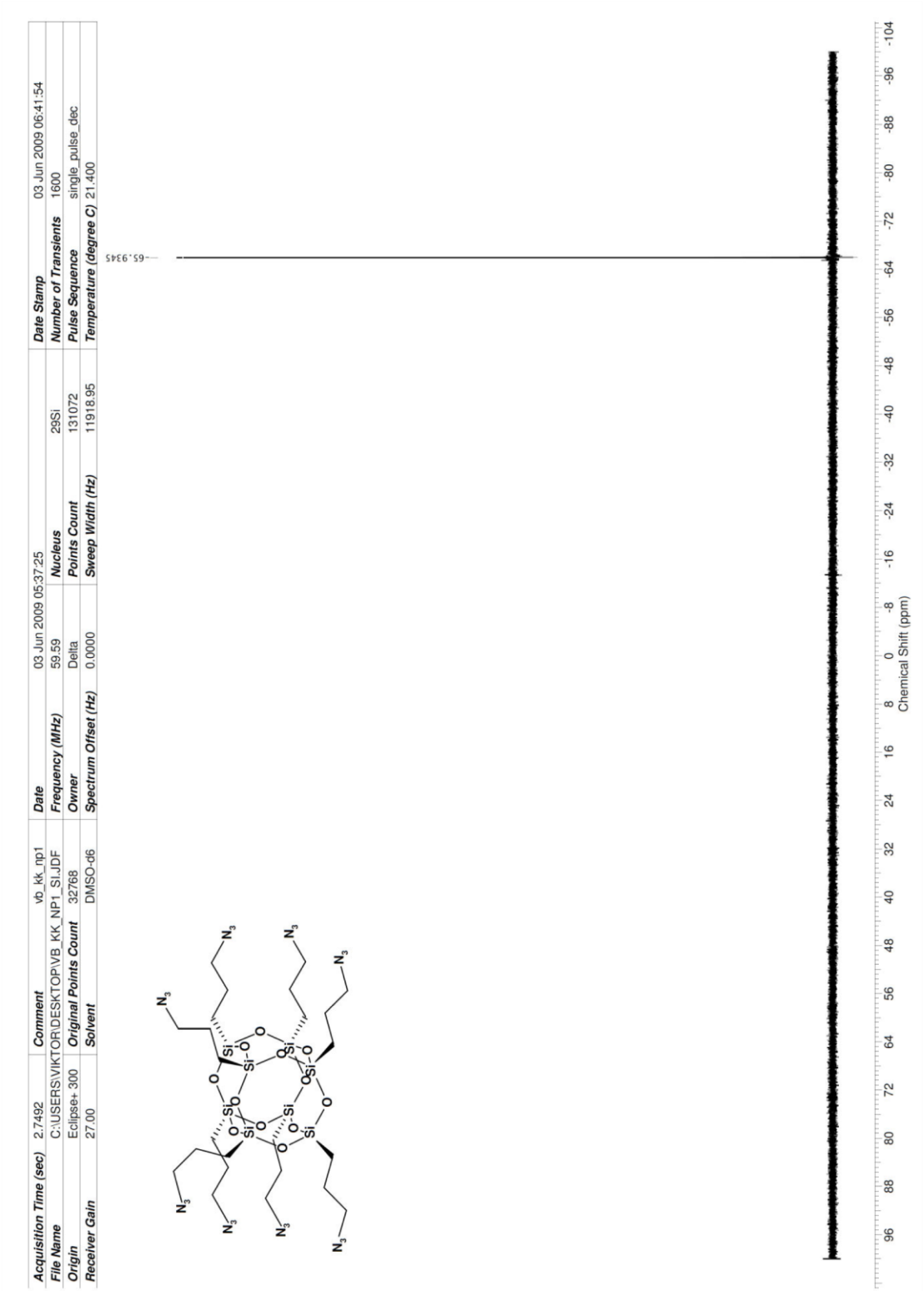

Fig. S17: ^{29}Si NMR of **4**

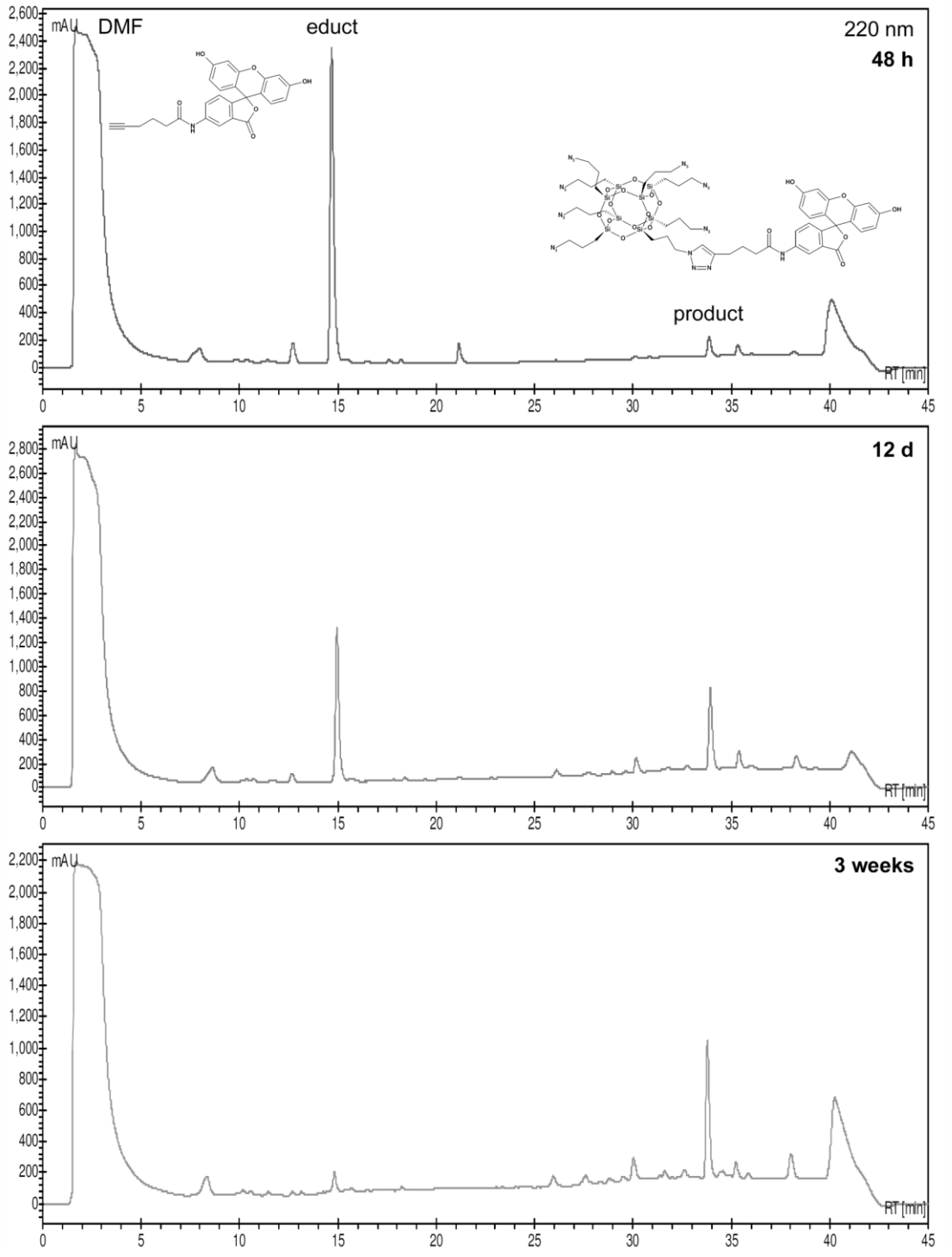

RP HPLC, C8 column, gradient: 20% → 100% B (90% aq. CH_3CN + 0.1% TFA)

Fig. S18: HPLC monitoring of the synthesis of **5**

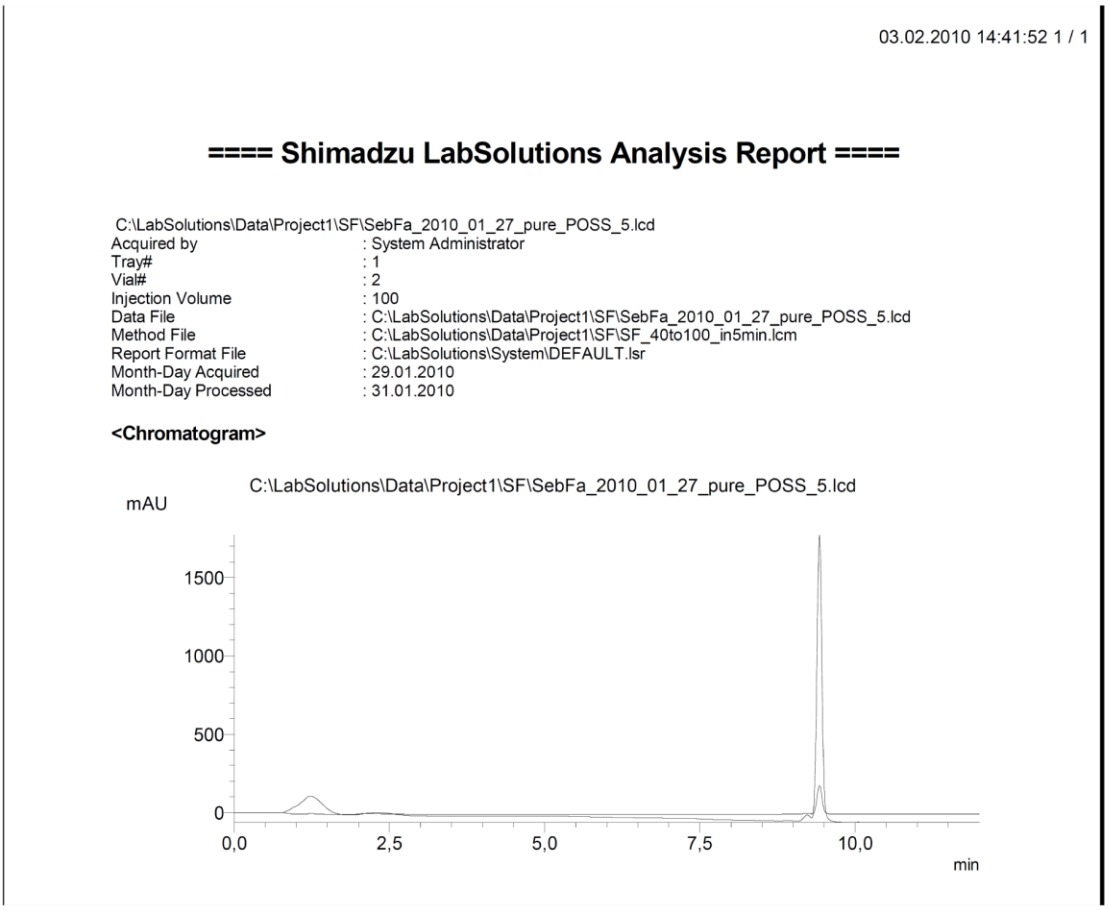

RP HPLC, C8 column, gradient: 40% → 100% B (100% aq. CH_3CN + 0.1% TFA)

Fig. S19: Analytical HPLC of **5**

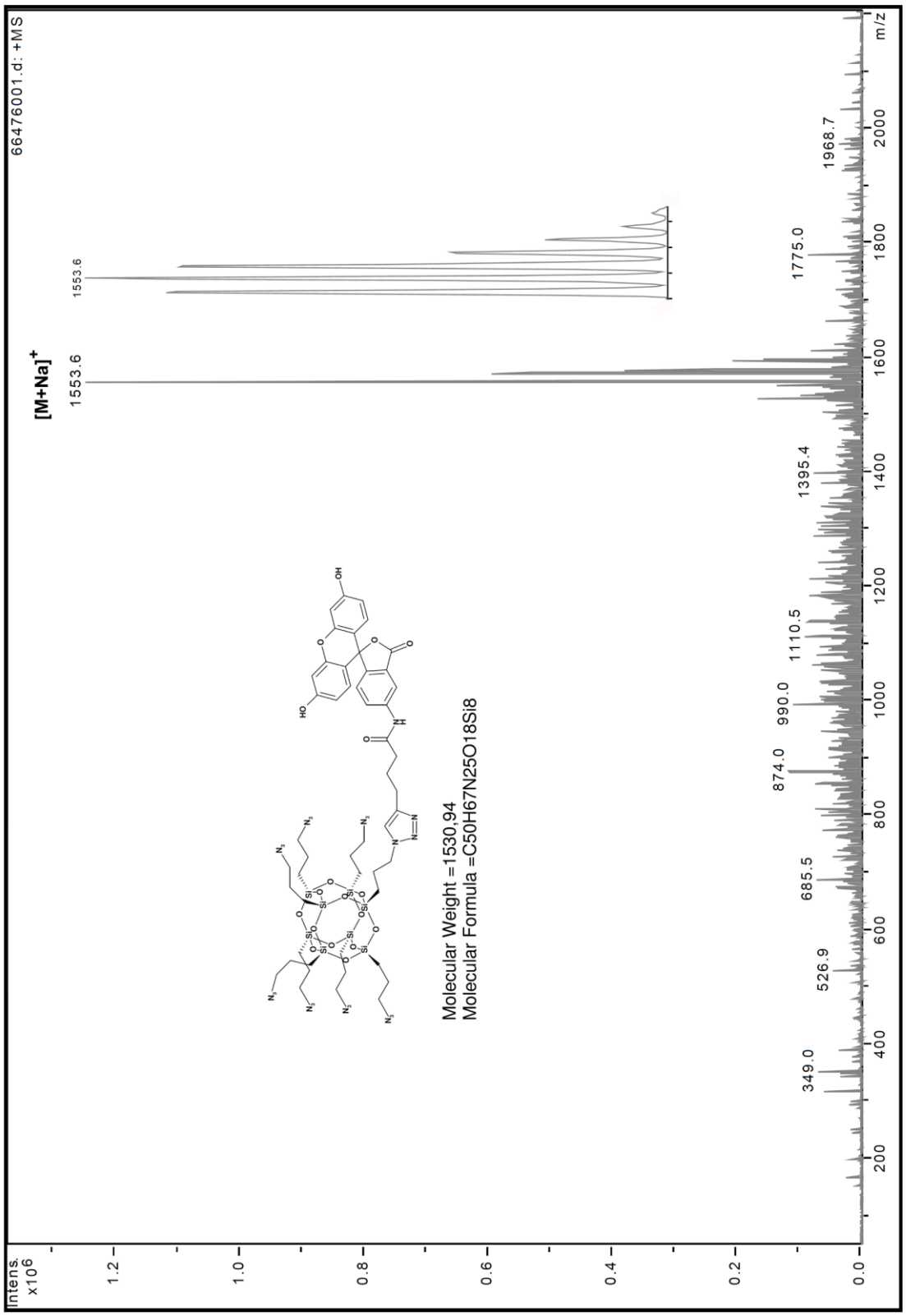

Fig. S20: ESI-MS spectrum of **5**

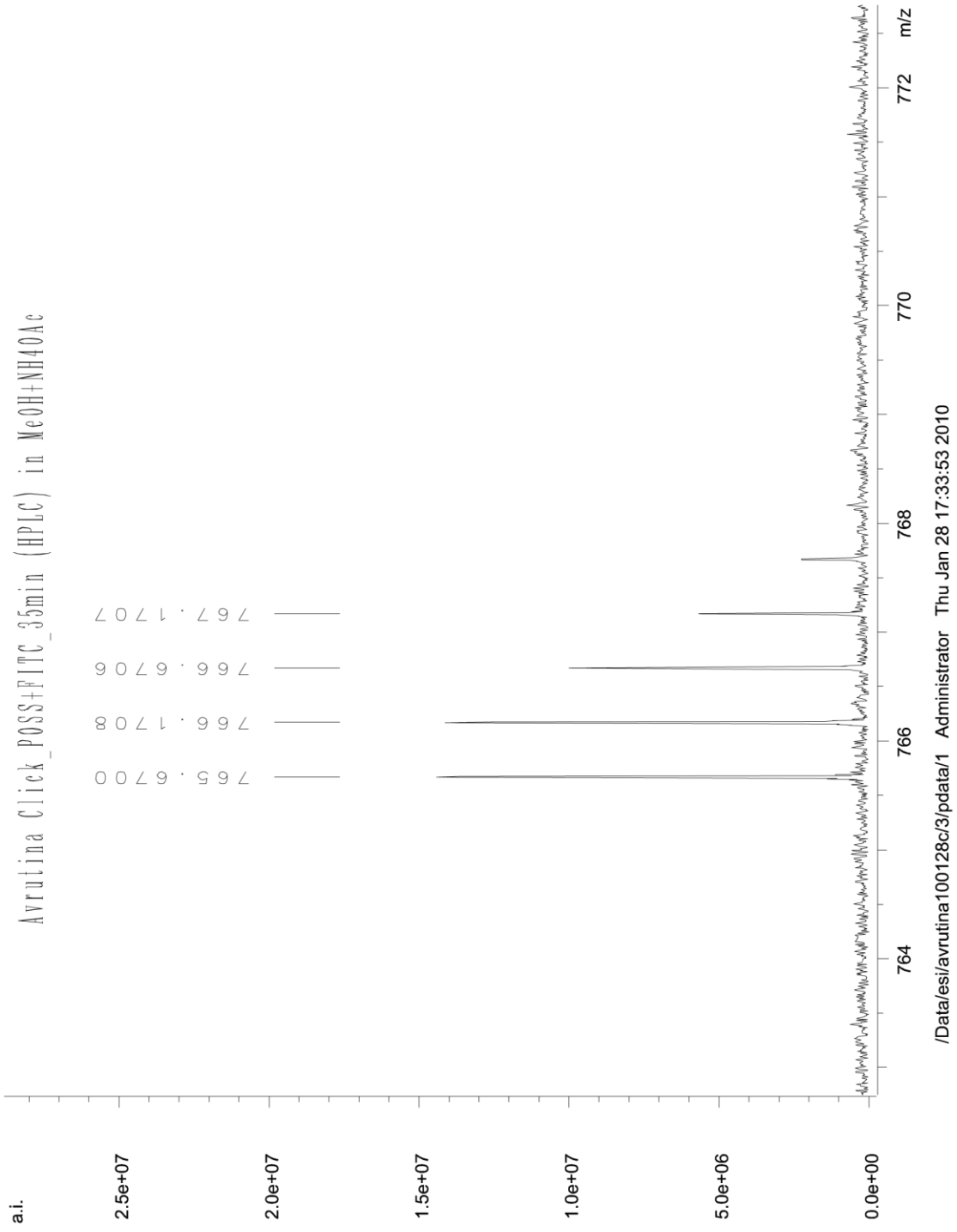

Fig. S21: HRMS, isotopic peak pattern of **5**

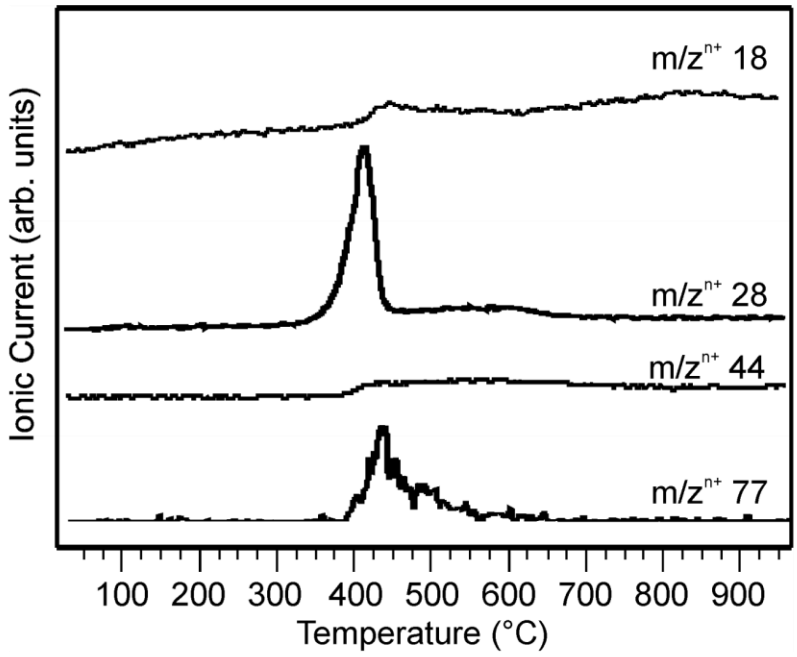

Fig. S22: TG-MS traces of **6**

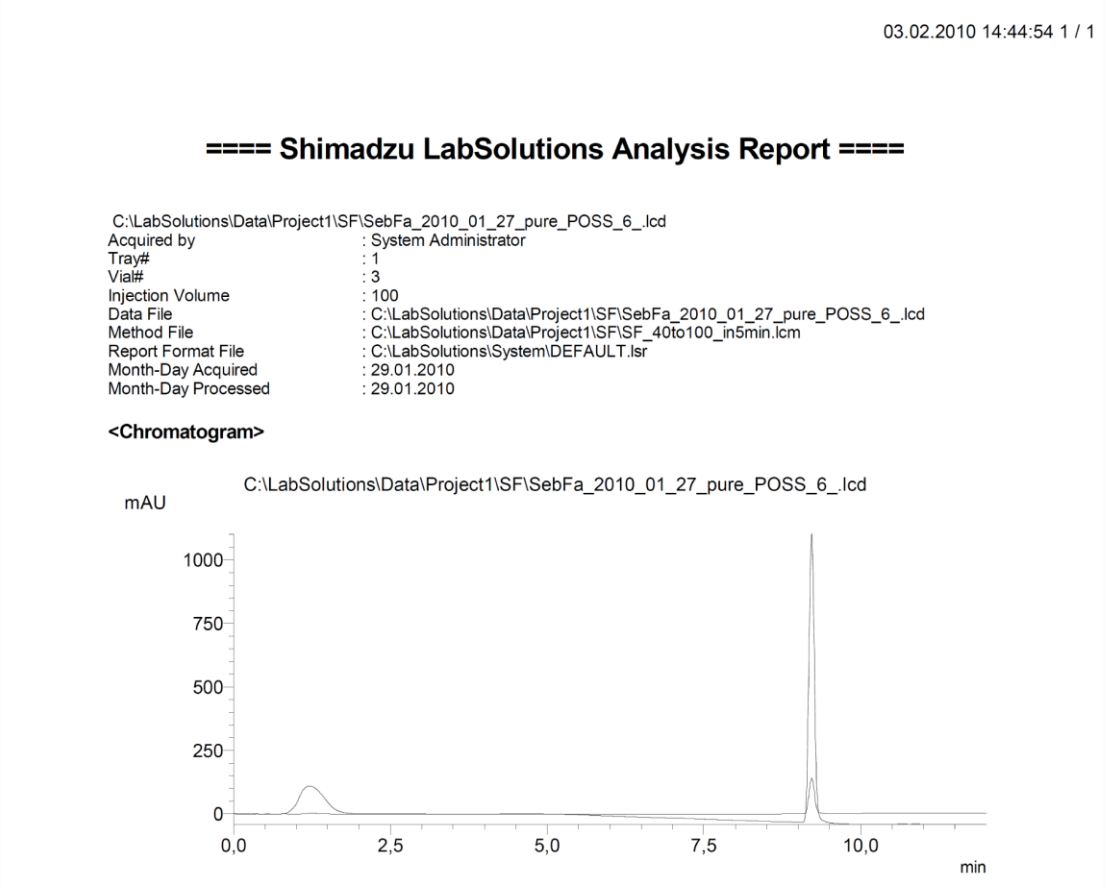

RP HPLC, C8 column, gradient: 40% → 100% B (100% aq. CH_3CN + 0.1% TFA)

Fig. S23: Analytical HPLC of **6**

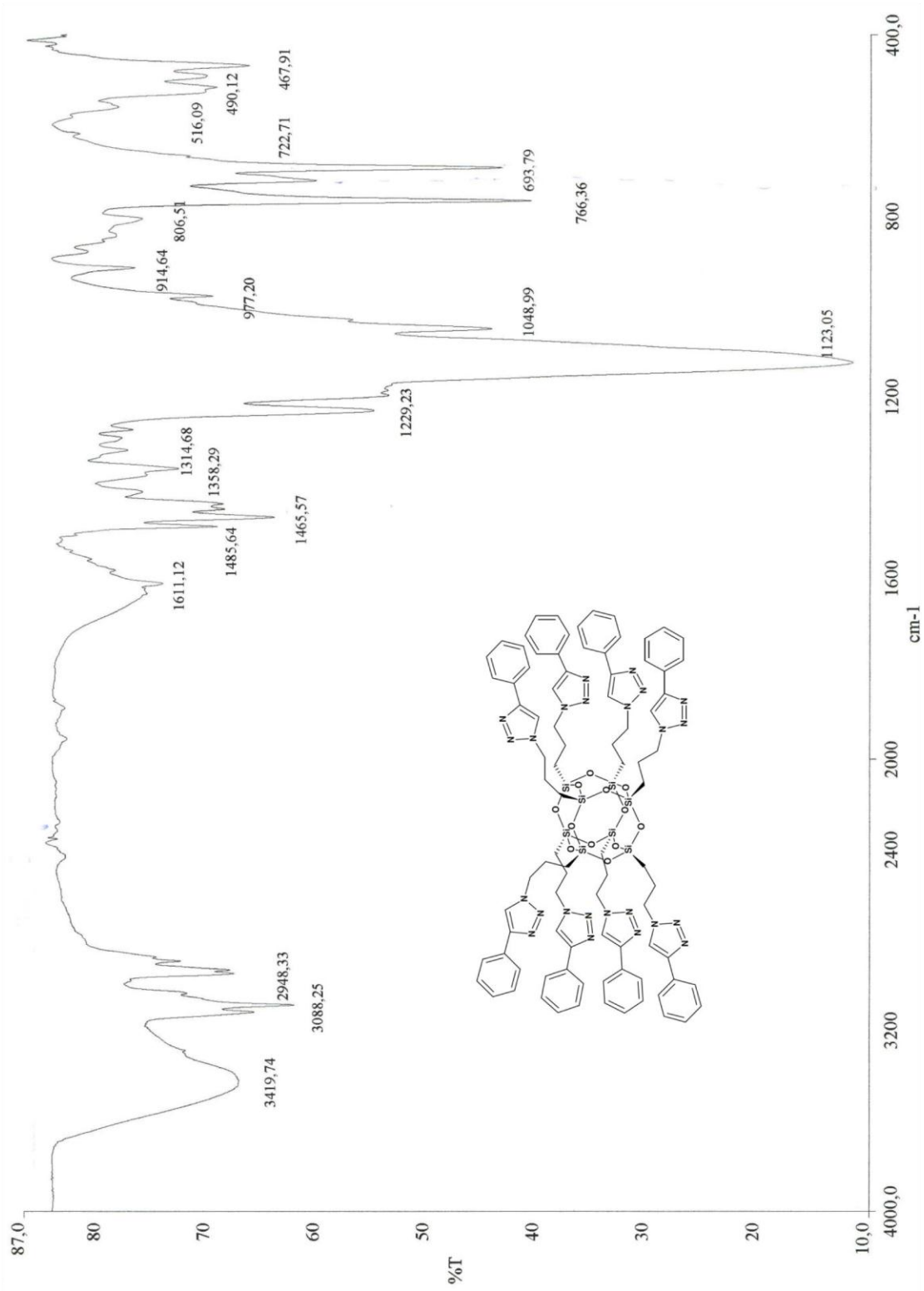

Fig. S24: IR spectrum of **6**

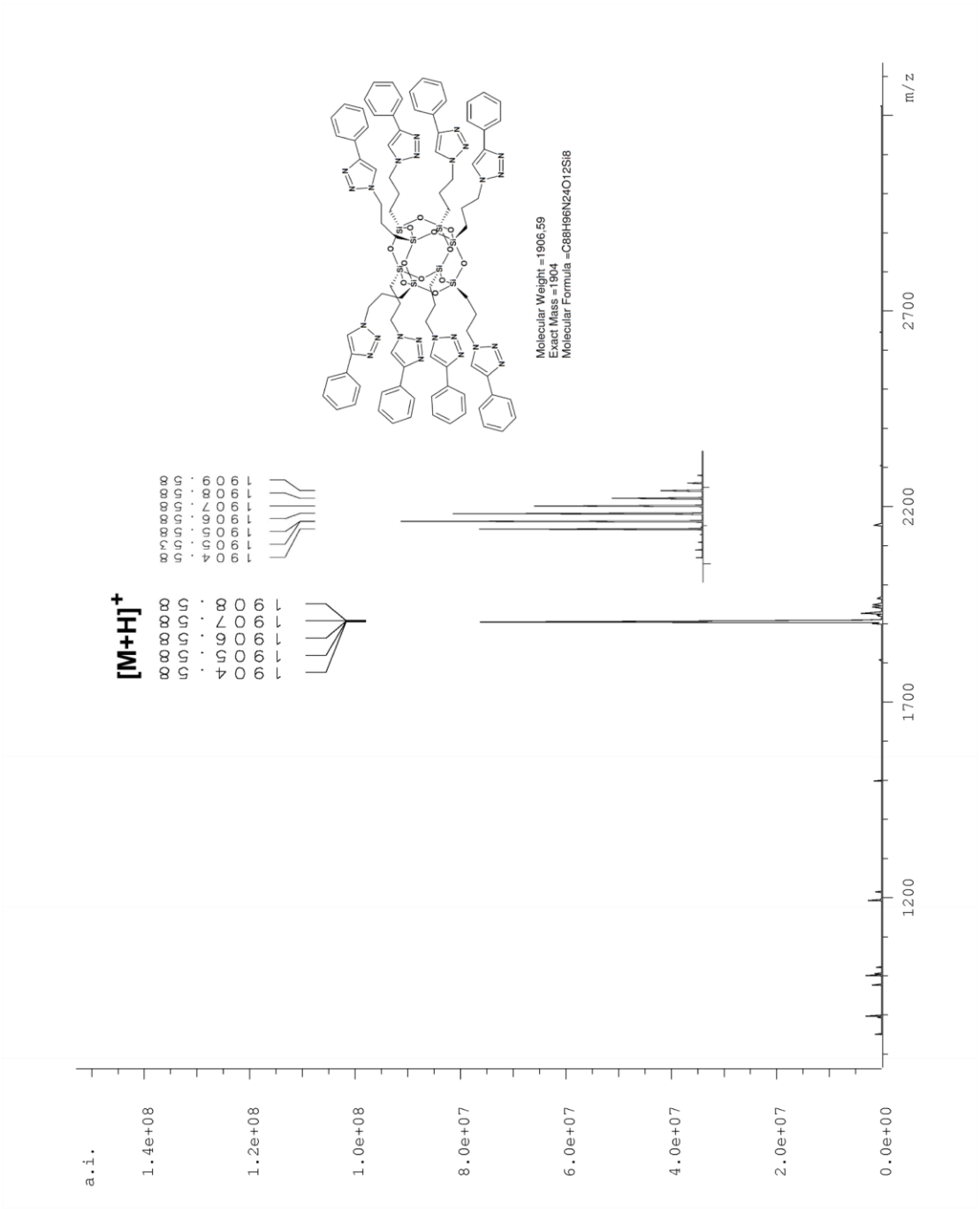

Fig. S25: ESI-MS spectrum of **6**

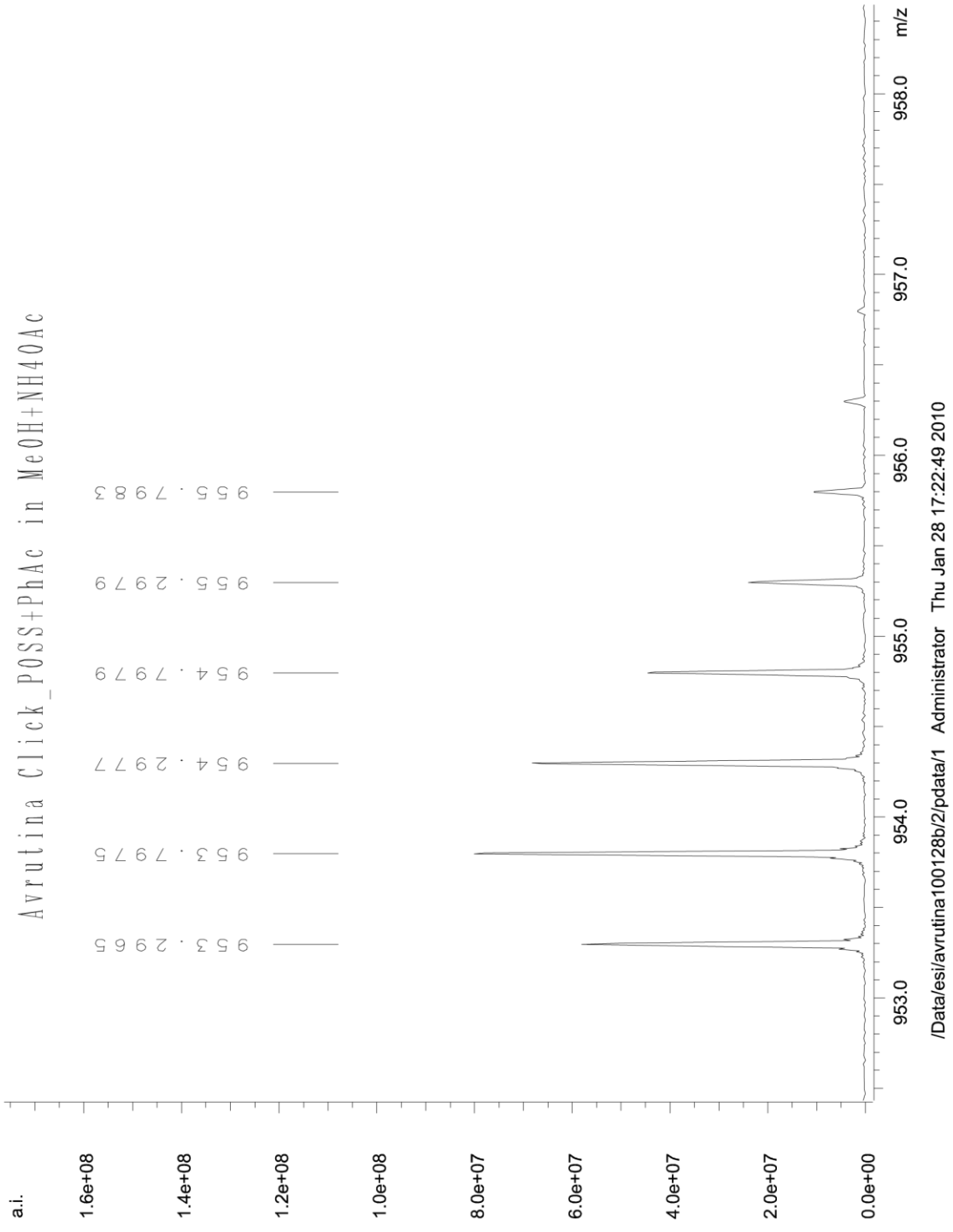

Fig. S26: HRMS, isotopic peak pattern of **6**

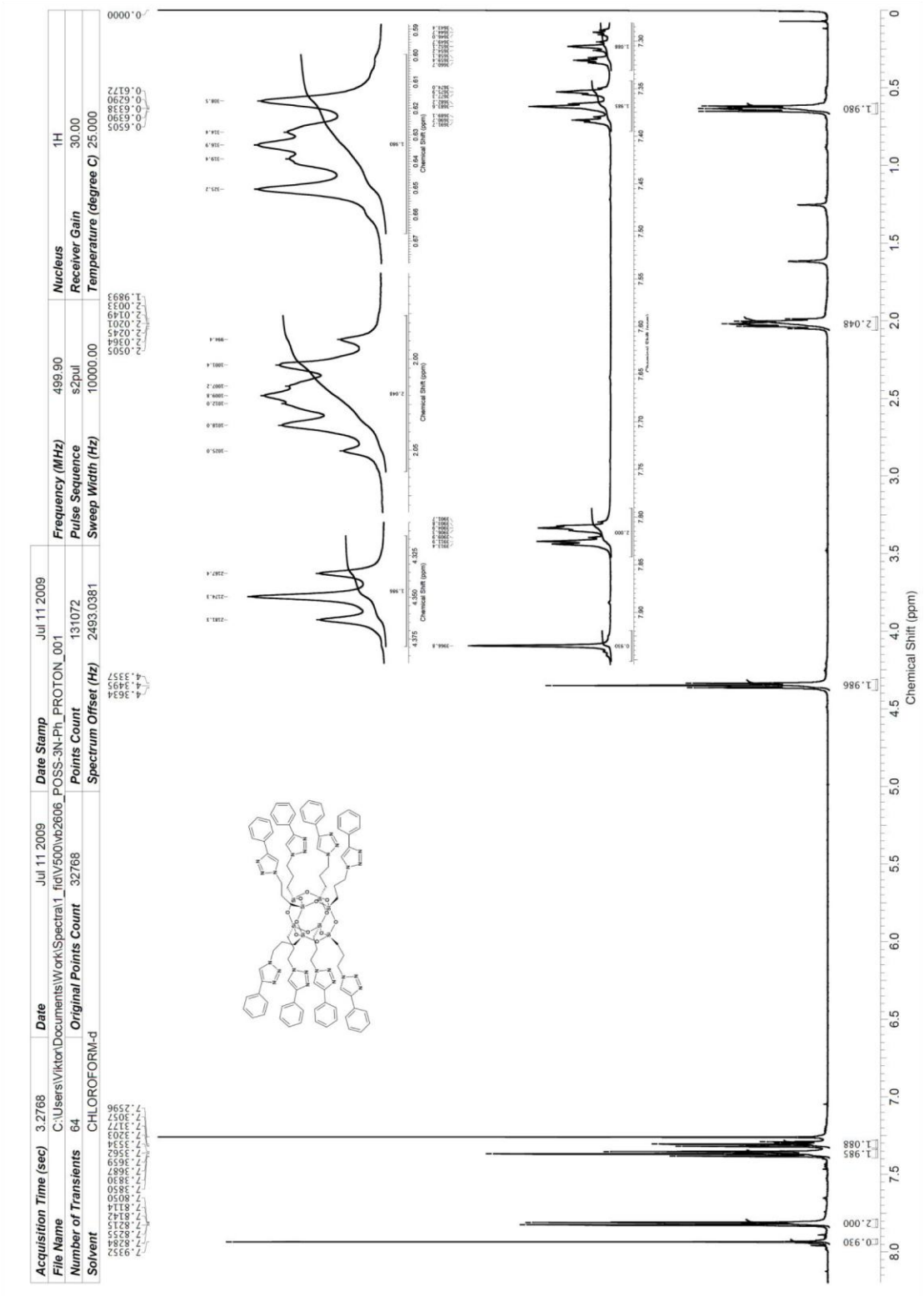

Fig. S27: ^{1}H NMR of **6**

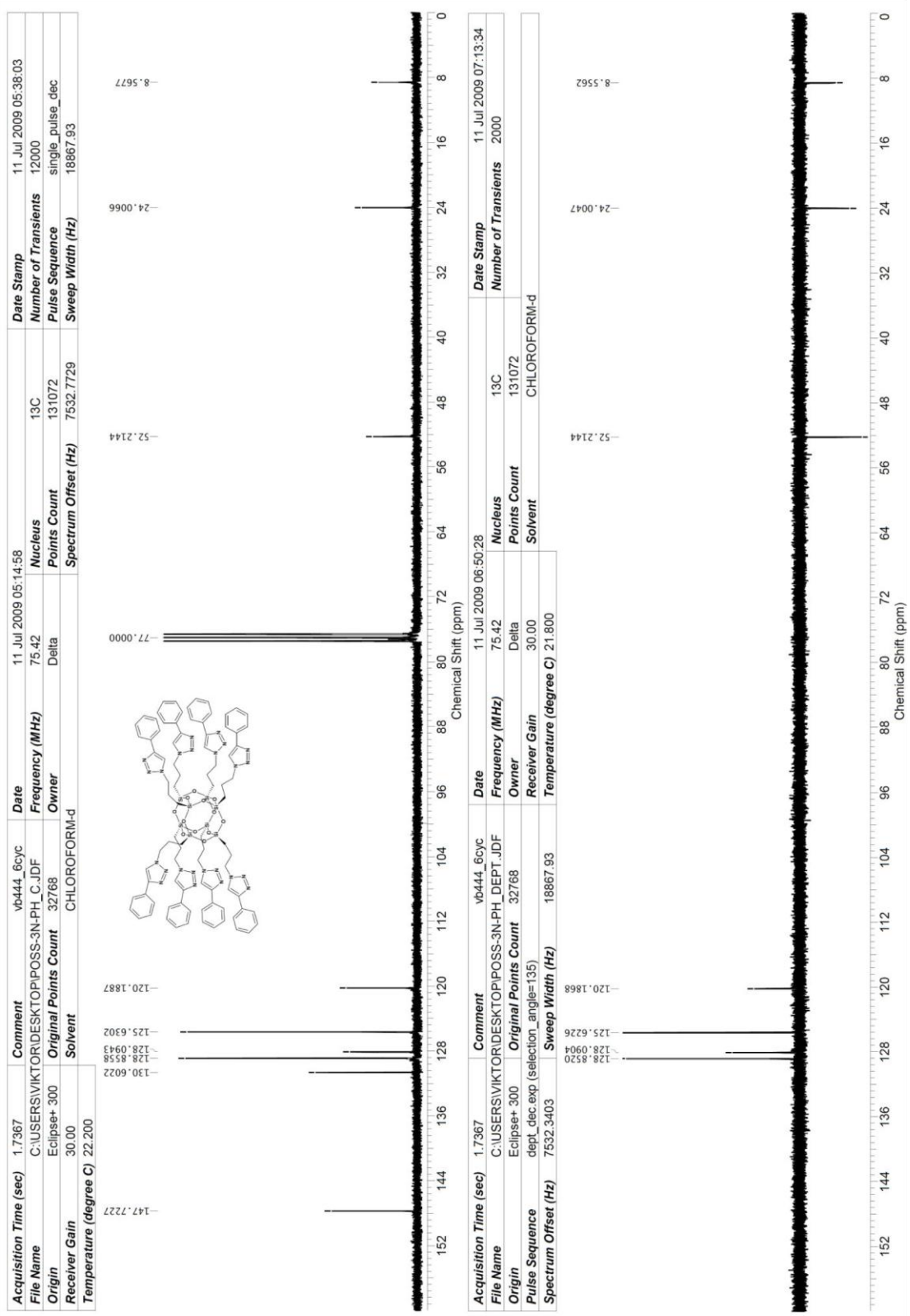

Fig. S28: ^{13}C and Dept spectra of **6**

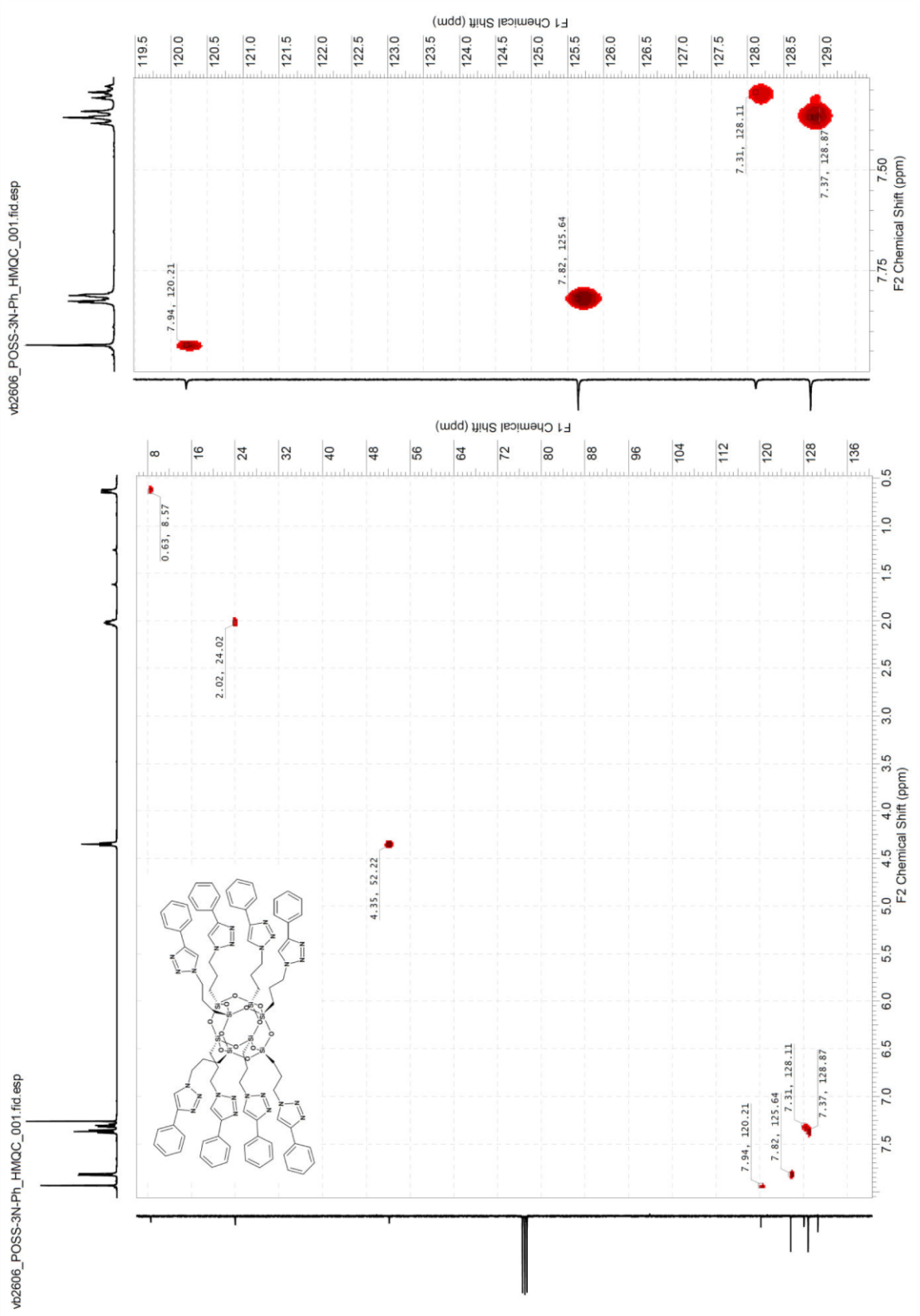

Fig. S29: HMQC spectra of **6**

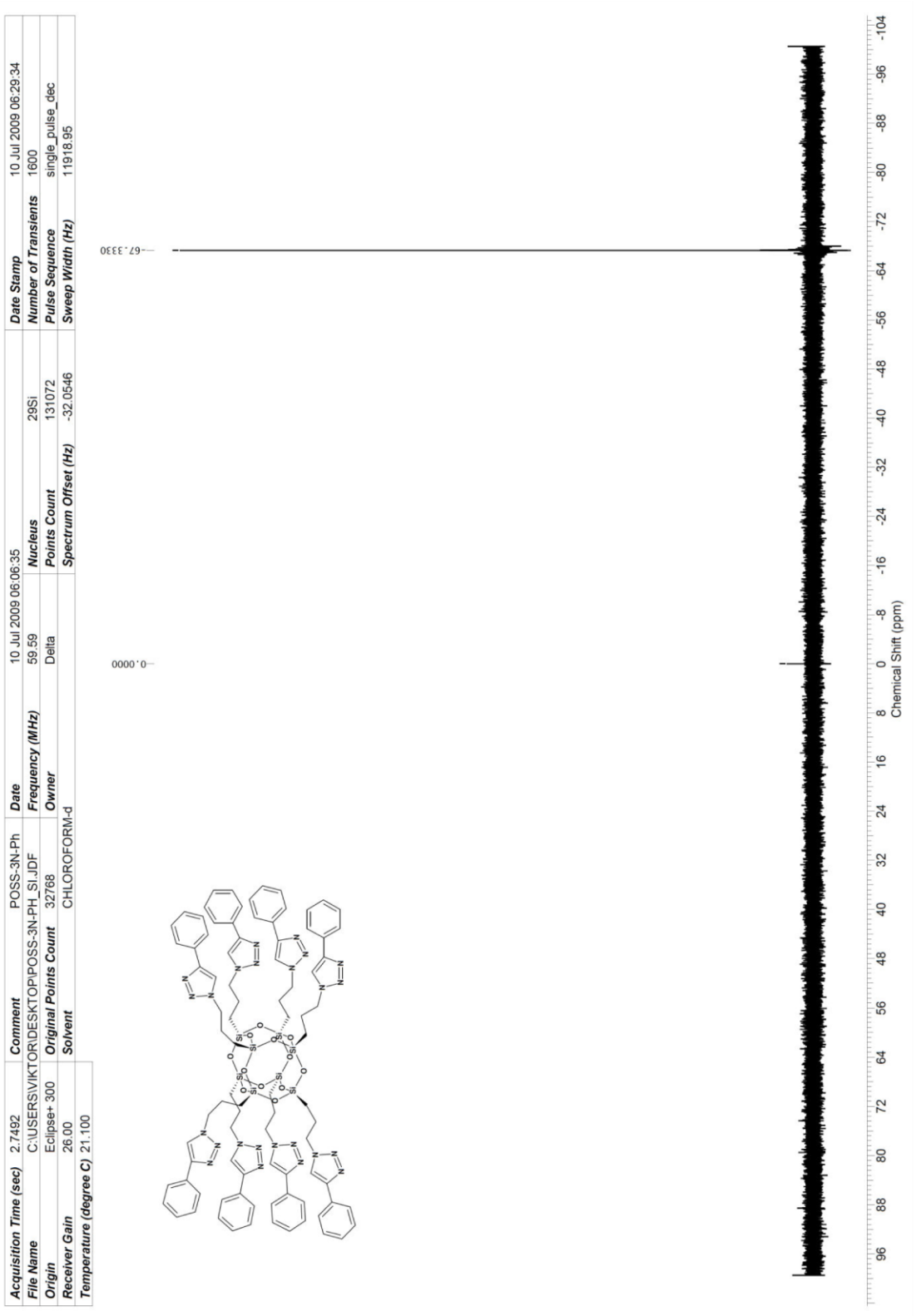

Fig. S30: ^{29}Si NMR of **6**

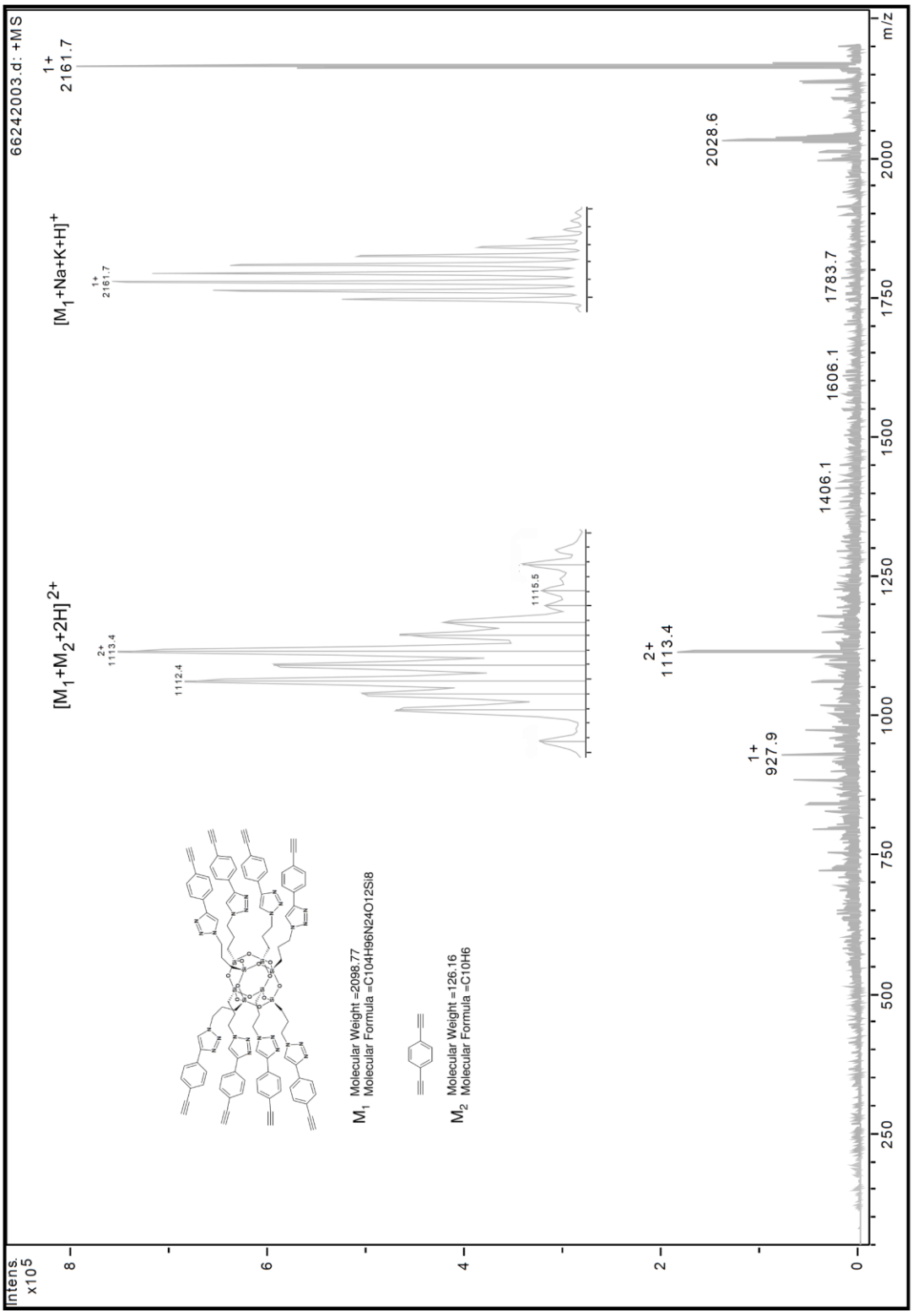

Fig. S31: ESI-MS spectrum of **7**

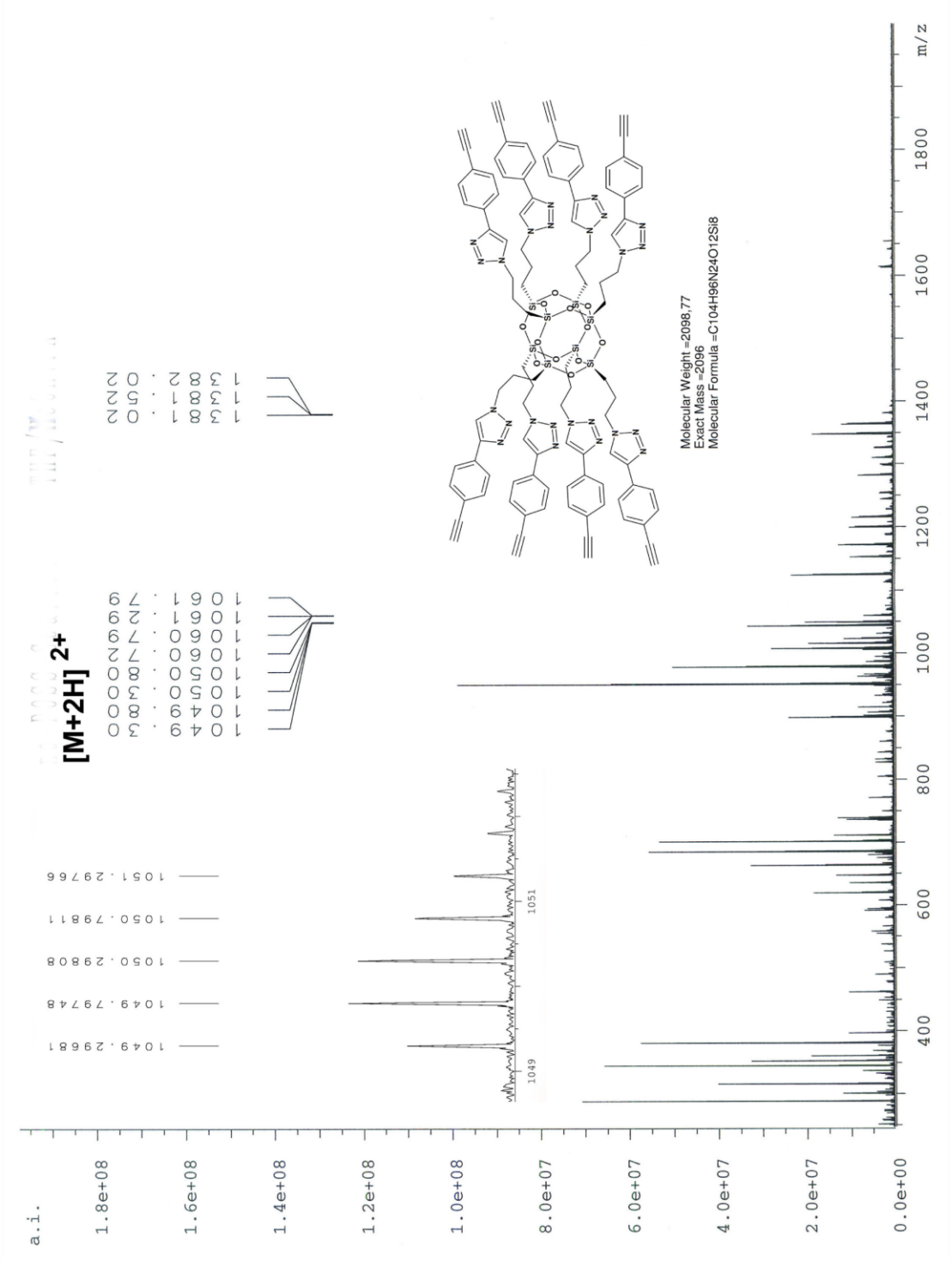

Fig. S32: HR-MS spectrum of **7**

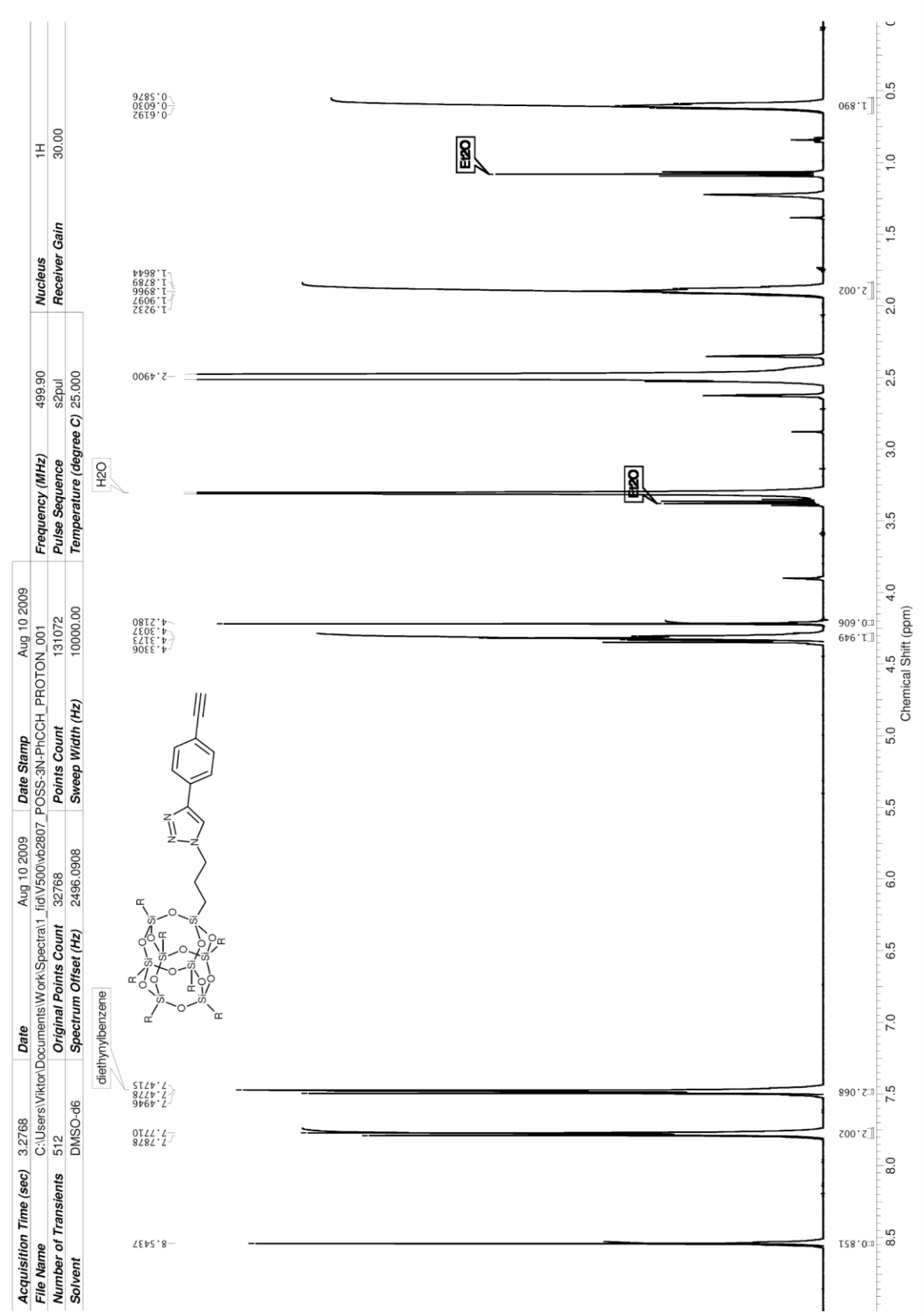

Fig. S33: ^{1}H NMR of **7**

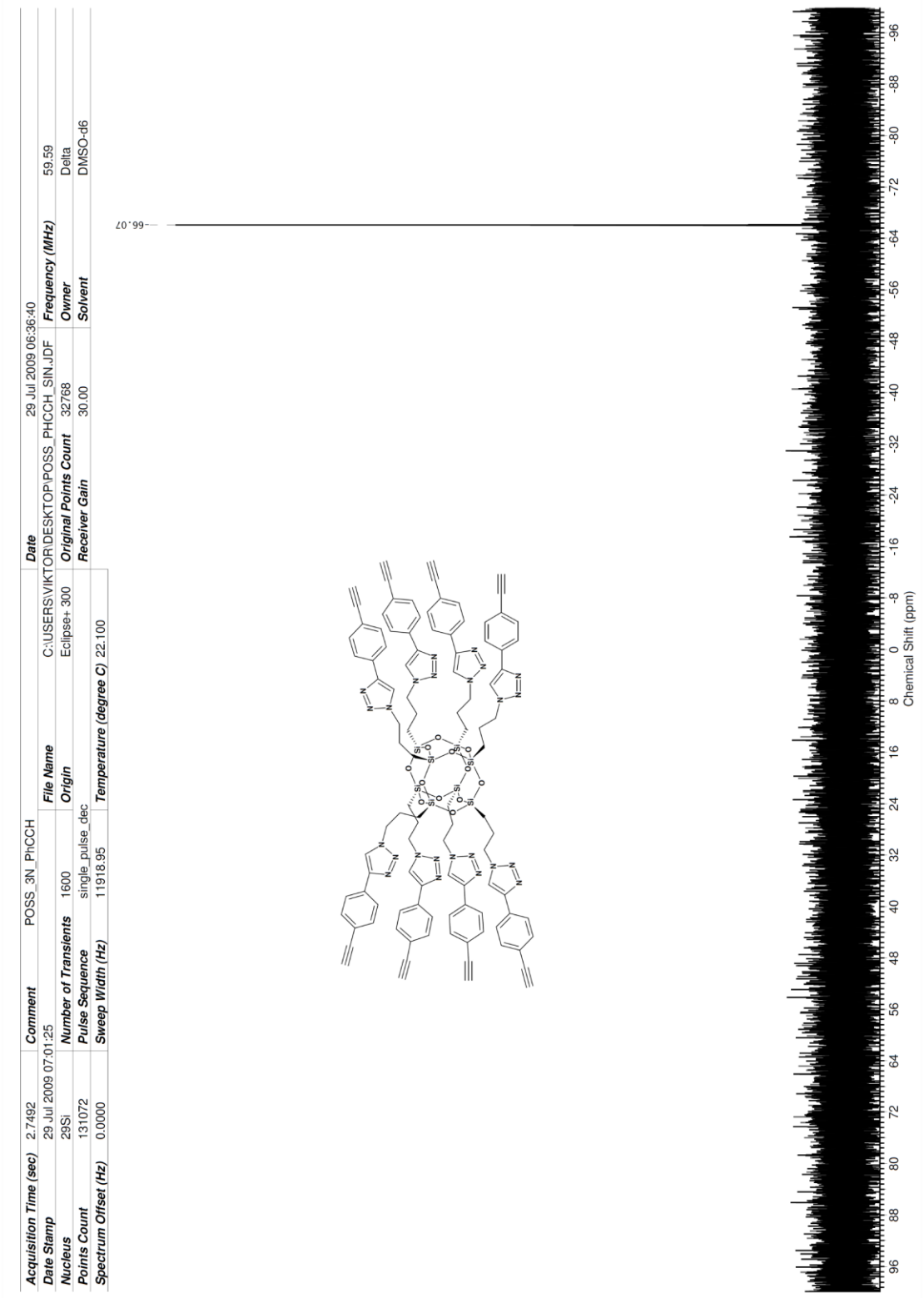

Fig. S34: ^{29}Si NMR of **7**

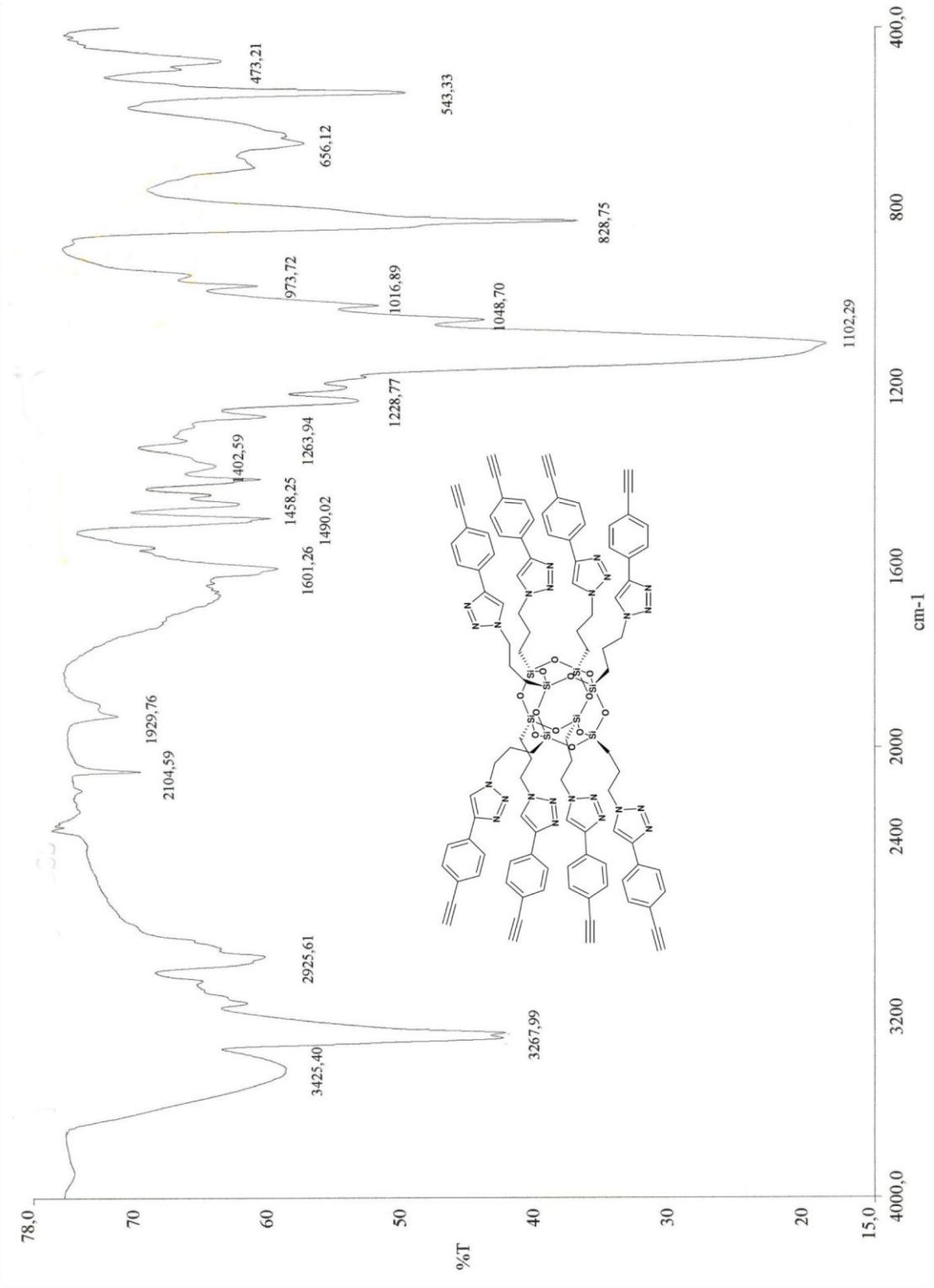

Fig. S35: IR spectrum of **7**

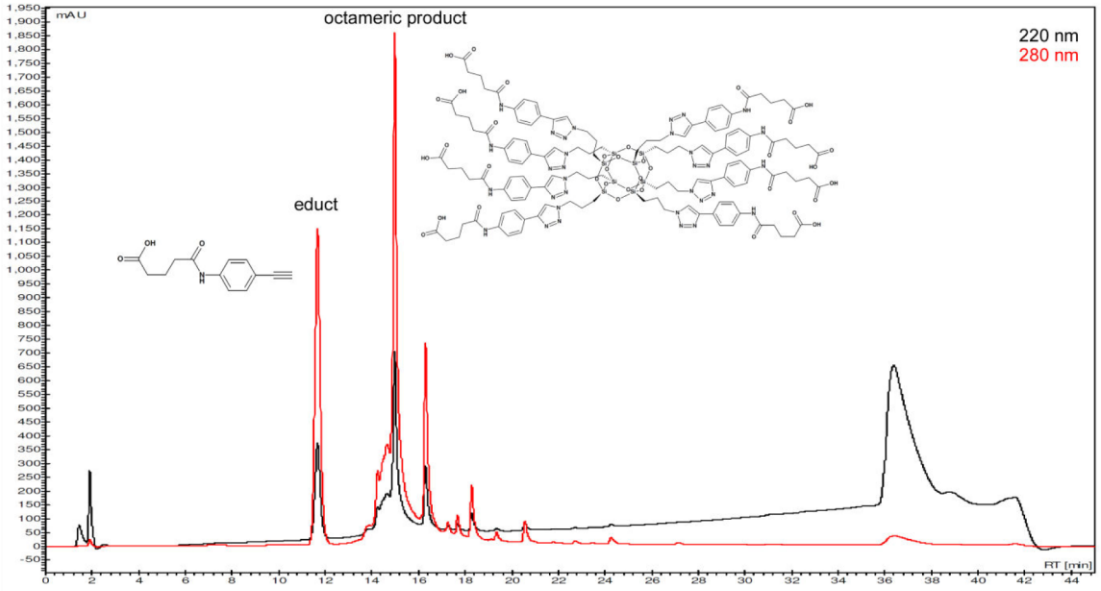

RP HPLC, C8 column, gradient: 20% → 100% B (90% aq. CH_3CN + 0.1% TFA)

Fig. S36: HPLC monitoring of synthesis of **8**

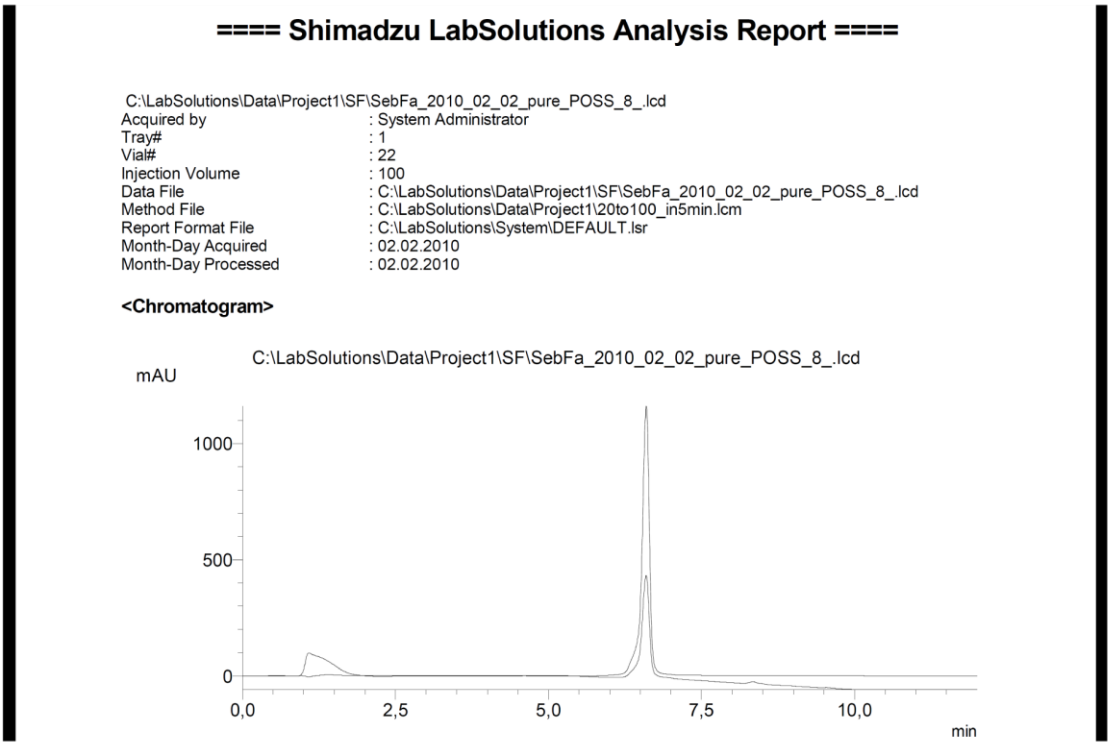

RP HPLC, C8 column, gradient: 40% → 100% B (100% aq. CH_3CN + 0.1% TFA)

Fig. S37: Analytical HPLC of **8**

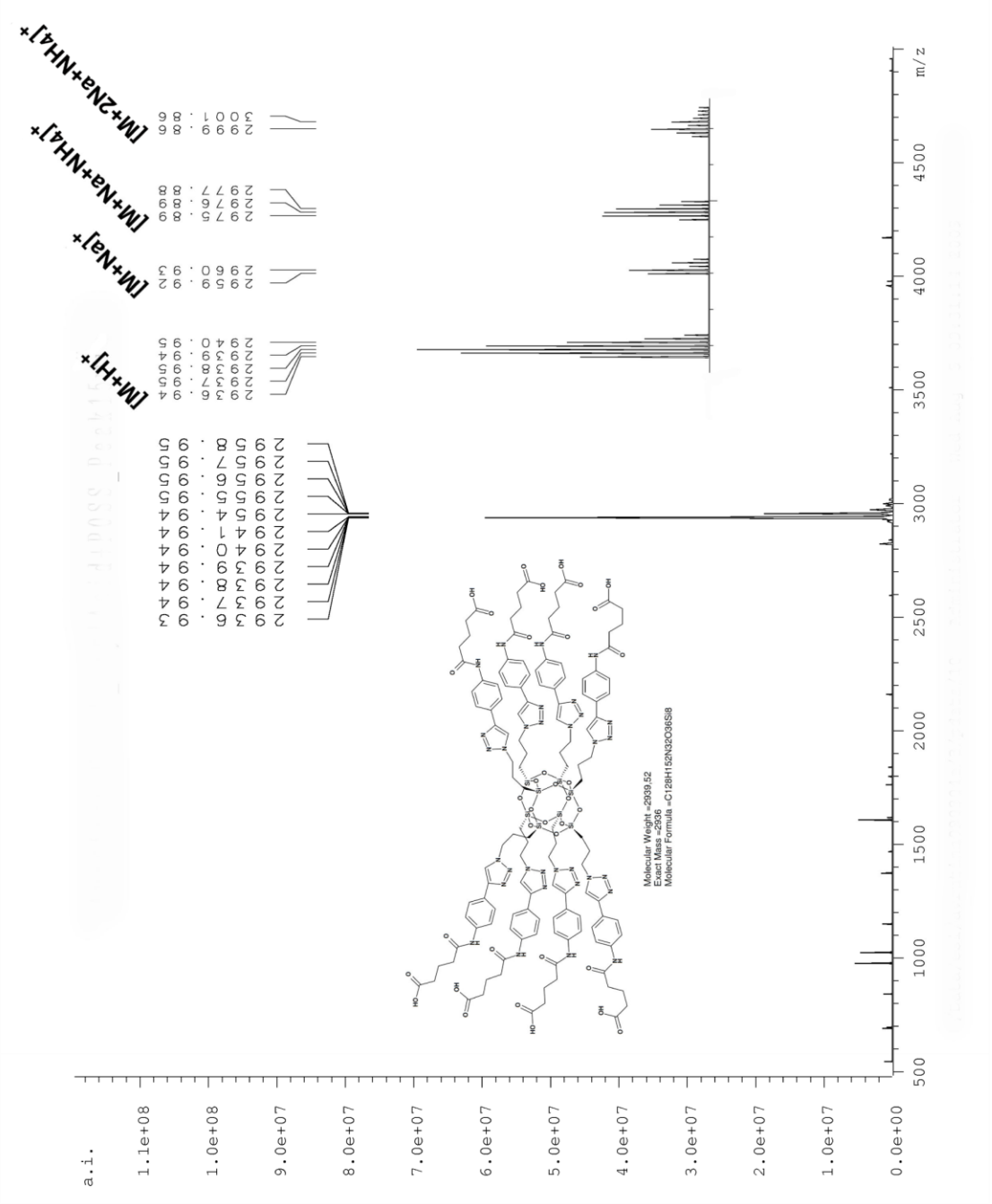

Fig. S38: ESI-MS spectrum of **8**

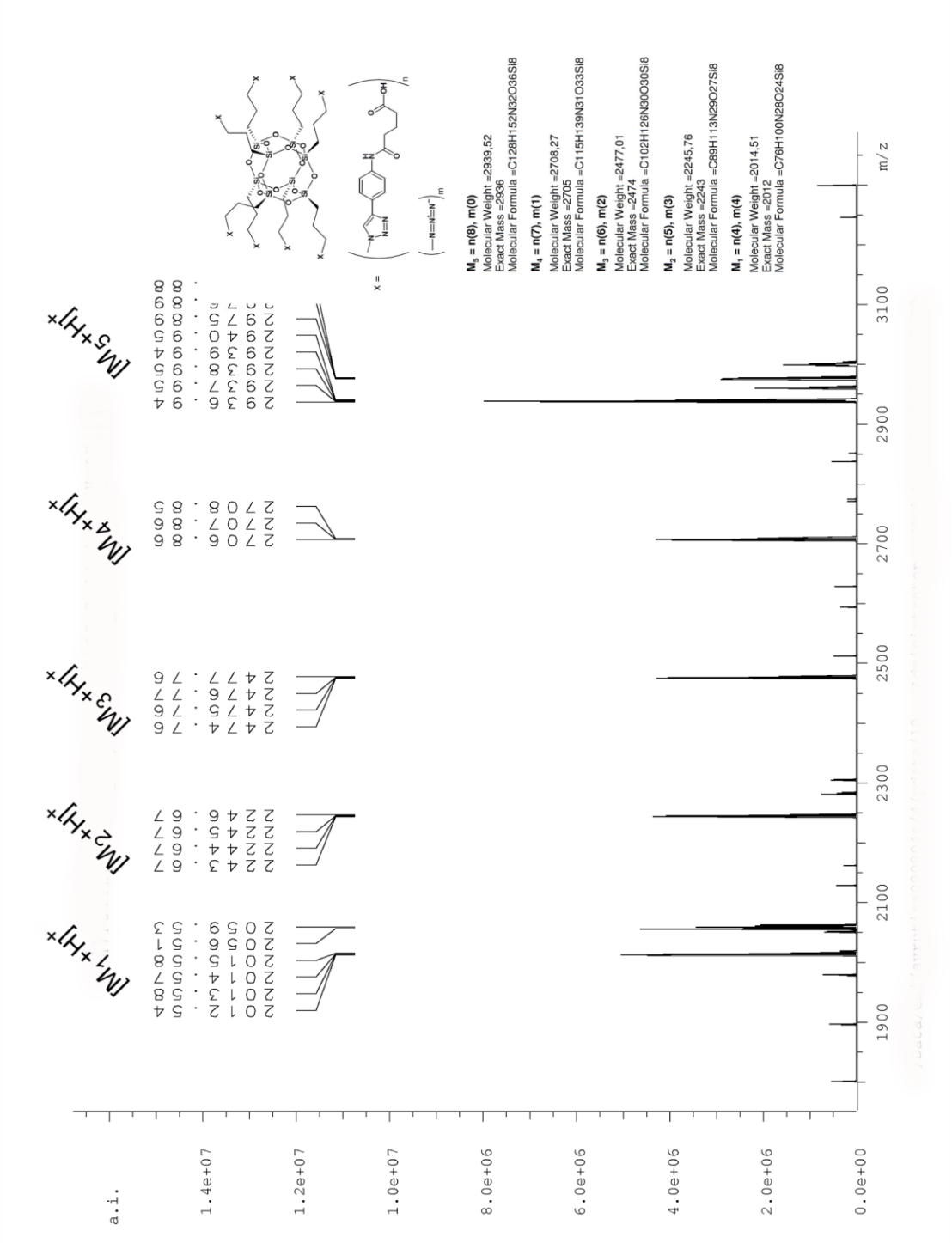

Fig. S39: ESI-MS spectrum of reaction mixture **8**

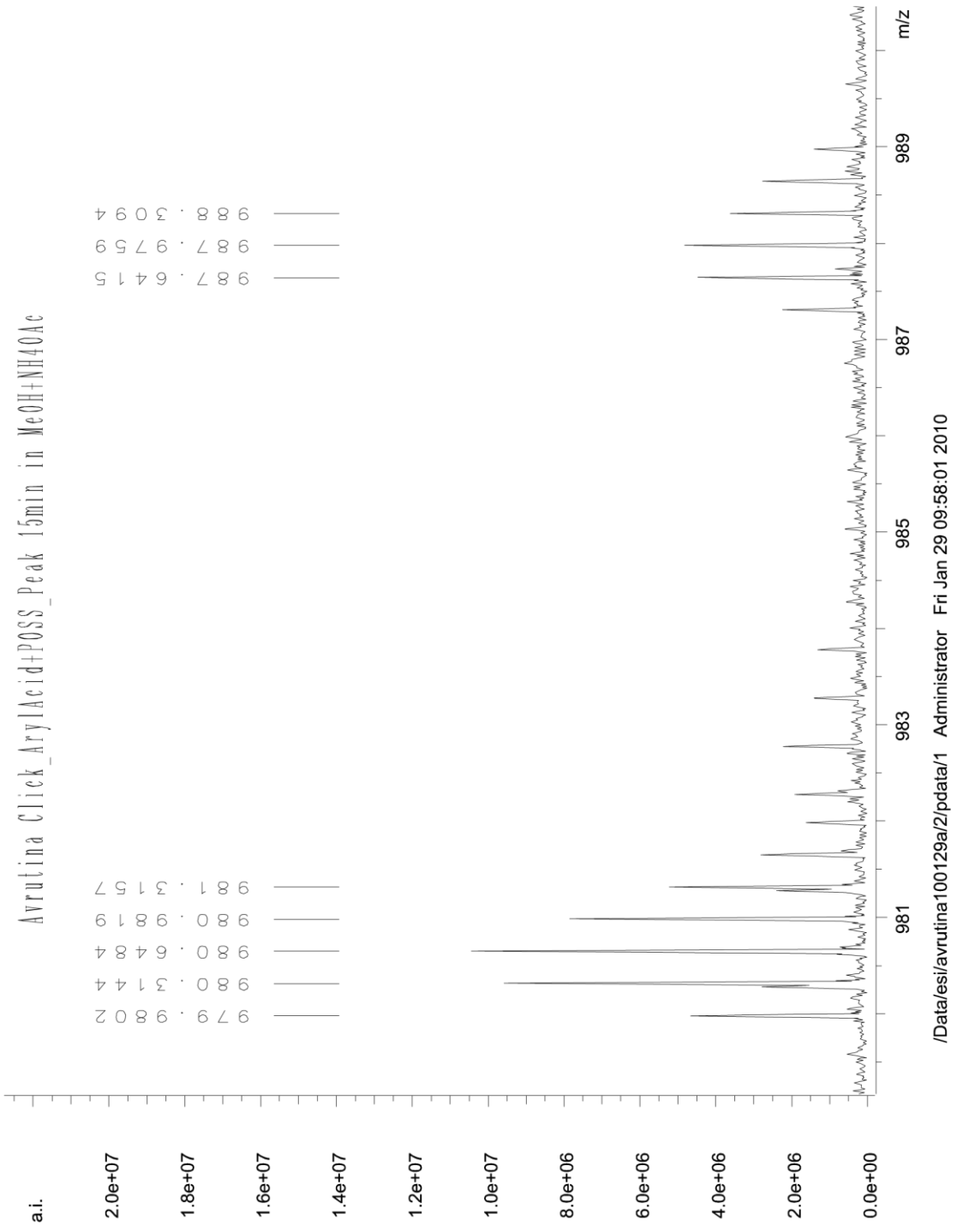

Fig. S40: HRMS, isotopic peak pattern of **8**

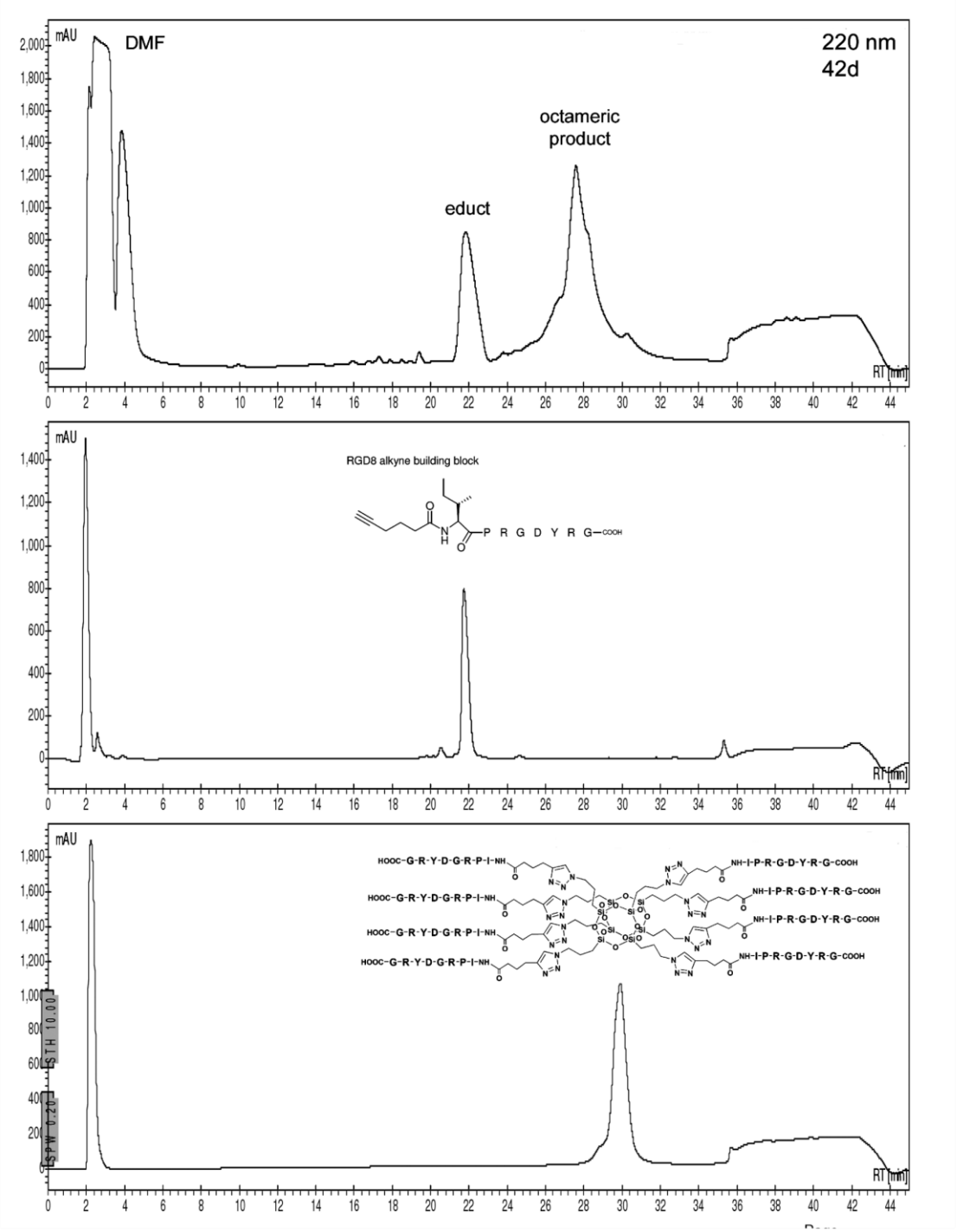

RP HPLC, C8 column, gradient: 10% → 35% B (90% aq. CH_3CN + 0.1% TFA)

Fig. S41: HPLC monitoring of synthesis of **9** and subsequent purification

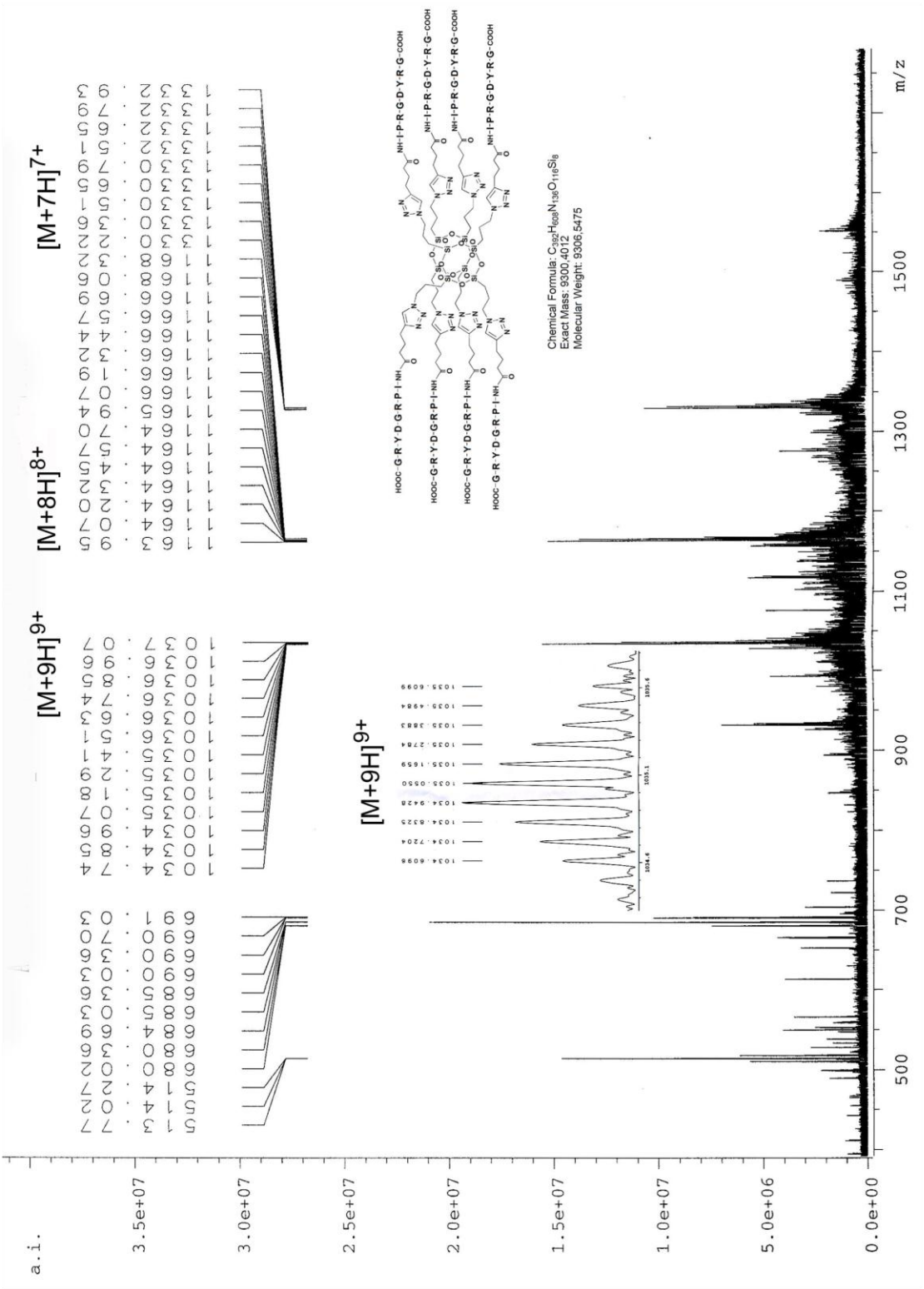

Fig. S42: ESI-MS spectrum of **9**

4.2. Analytische Daten der Verbindungen aus Teil 3.2.

Die Nummerierung der Verbindungen entspricht: Fabritz et al., Org. Biomol. Chem., 2012, **10**, 6287-6293.

Fig. S1: HR-MS spectrum of **2**.

Fig. S2: HR-MS spectrum of **3**.

Fig. S3: ATR-IR spectrum of **2**.

Fig. S4: ATR-IR spectrum of **3**.

Fig. S5: (a) ^{1}H-NMR of **2**, (b) ^{1}H-NMR of **3**.

Fig. S6: (a) ^{29}Si-NMR of **2**, (b) ^{29}Si-NMR of **3**, the NMR spectra were base-line corrected using MestReNova.

Fig. S7: AFM image of aggregated and randomly distributed COSS particles **1**.

Fig. S8: (a) proposed structure of reaction intermediates in the synthesis of **6**. (b) ESI-MS spectrum of the reaction mixture after 30 min.

Fig. S9: (a) unprotected aminooxy COSS particle, (b) periodate oxidized **p4**, (c) possible conjugation products **4**.

Fig. S10: LC-MS monitoring of the synthesis of **4**: analysis after overnight reaction.

Fig. S11: Synthesis of **4**: deconvoluted ESI MS spectrum of the reaction mixture.

Fig. S12: 3D representation (sticks) of compound **4**.

Fig. S13: (a) unprotected aminooxy COSS particle, (b) periodate oxidized **p5**, (c) possible conjugation products **5**.

Fig. S14: LC-MS monitoring of the synthesis of **5**: analysis after overnight reaction.

Fig. S15: Synthesis of **5**: deconvoluted ESI MS spectrum of the reaction mixture.

Fig. S16: (a) unprotected aminooxy COSS particle, (b) periodate oxidized **p6**, (c) possible conjugation products **6**.

Fig. S17: LC-MS monitoring of the synthesis of **6**: analysis after overnight reaction.

Fig. S18: Synthesis of **6**: deconvoluted ESI MS spectrum of the reaction mixture.

Fig. S19: (a) unprotected aminooxy COSS particle, (b) periodate oxidized **p7**, (c) possible conjugation products **7**.

Fig. S20: LC-MS monitoring of the synthesis of **7**: analysis after overnight reaction.

Fig. S21: Synthesis of **7**: deconvoluted ESI MS spectrum of the reaction mixture.

Fig. S22: (a) unprotected aminooxy COSS particle, (b) periodate oxidized **p8**, (c) possible conjugation products **8**.

Fig. S23: LC-MS monitoring of the synthesis of **8**: analysis after overnight reaction.

Fig. S24: Synthesis of **8**: deconvoluted ESI MS spectrum of the reaction mixture.

Fig. S25: (a) unprotected aminooxy COSS particle, (b) periodate oxidized **p9**, (c) possible conjugation products **9**.

Fig. S26: LC-MS monitoring of the synthesis of **9**: analysis after overnight reaction.

Fig. S27: Synthesis of **9**: deconvoluted ESI MS spectrum of the reaction mixture.

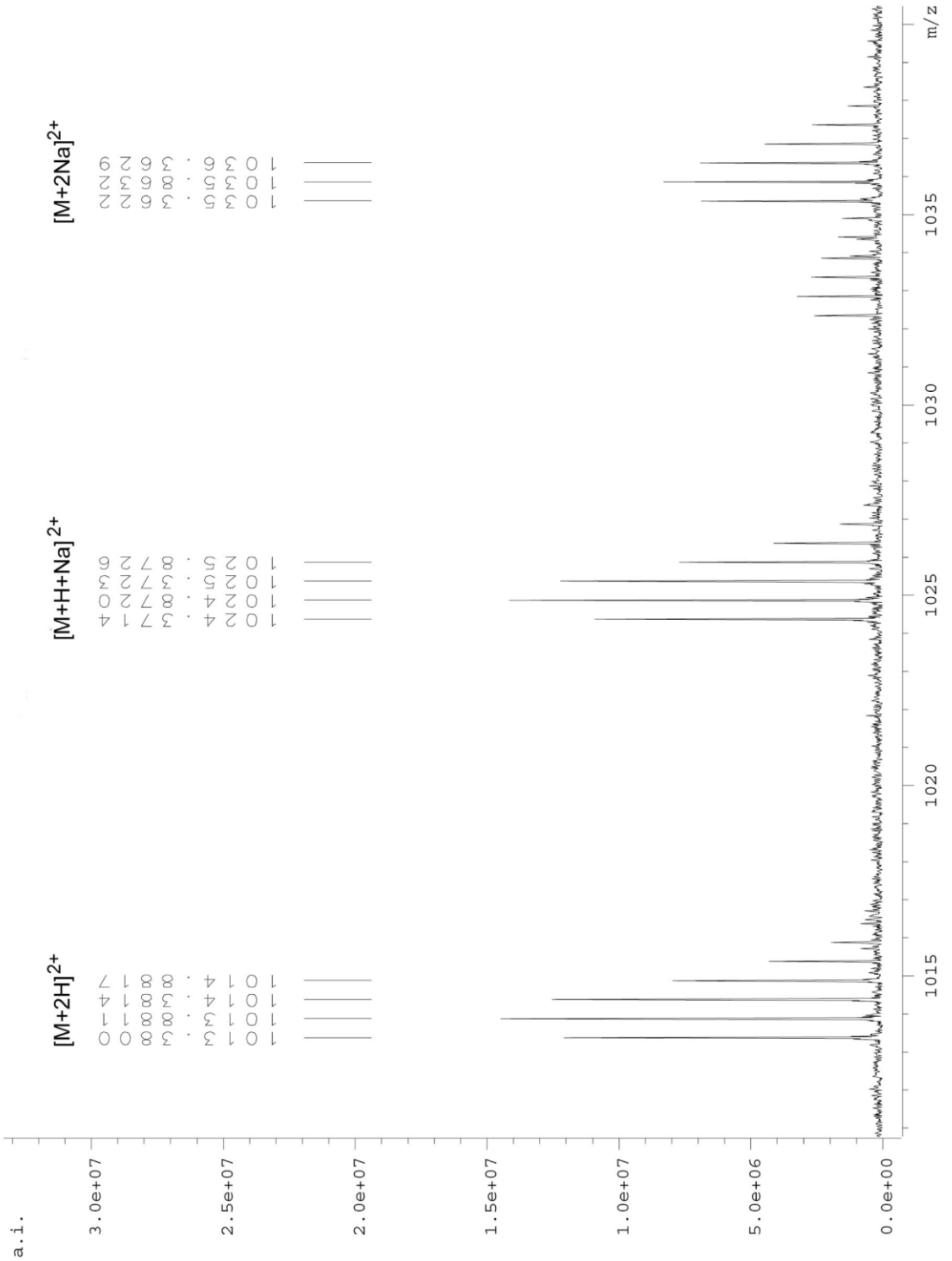

Fig. S1: HR-MS spectrum of **2**.

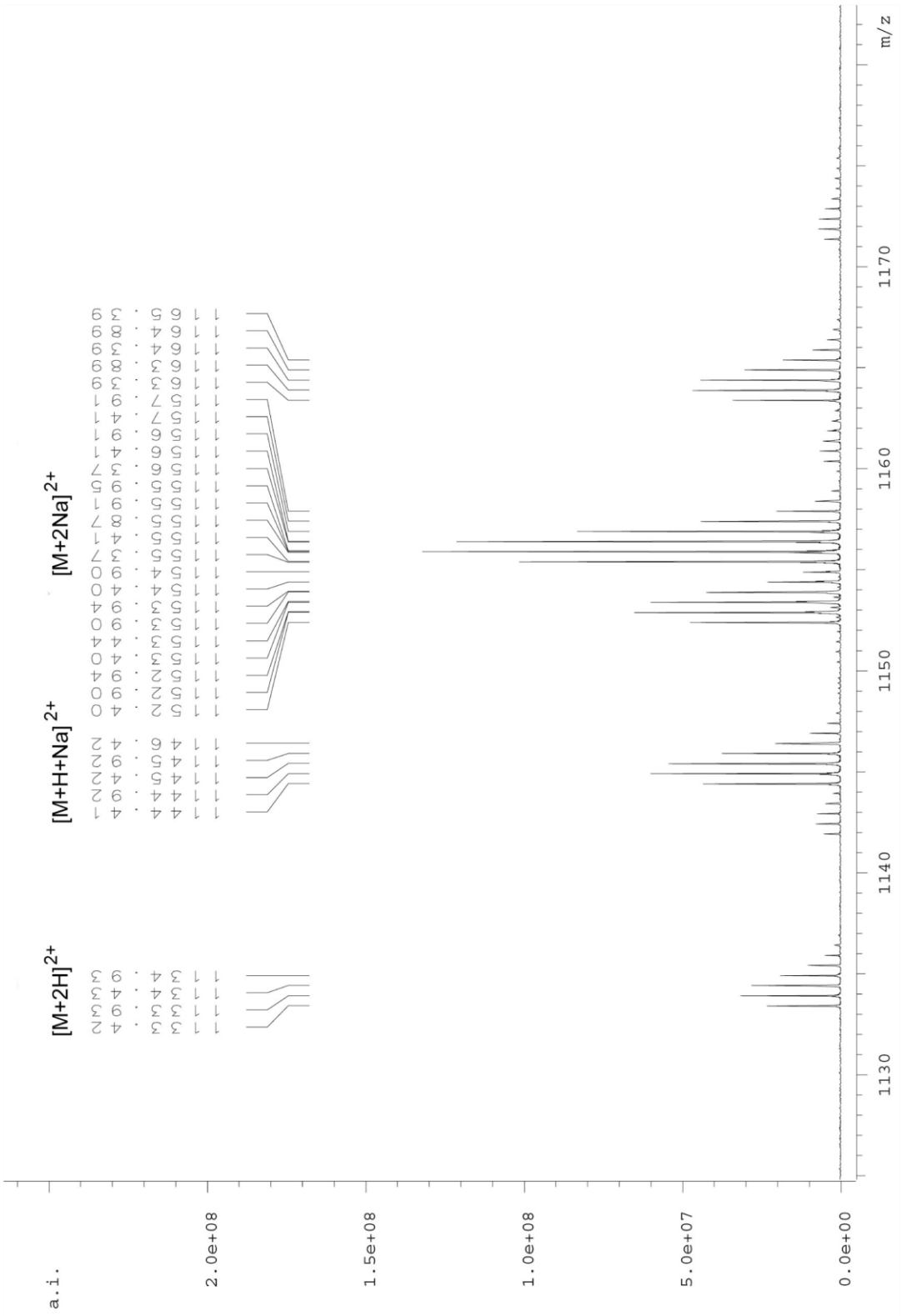

Fig. S2: HR-MS spectrum of **3**.

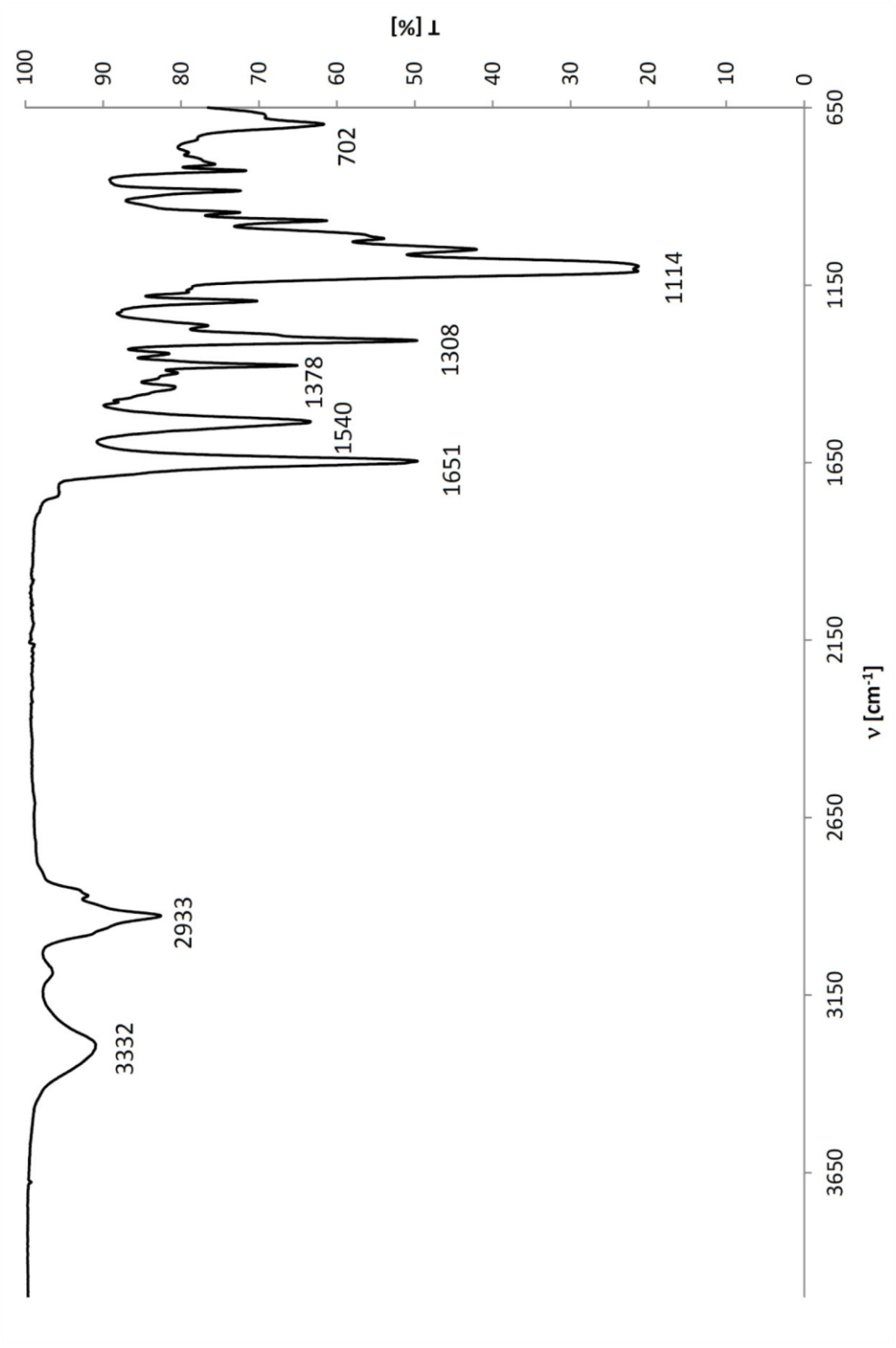

Fig. S3: ATR-IR spectrum of **2**

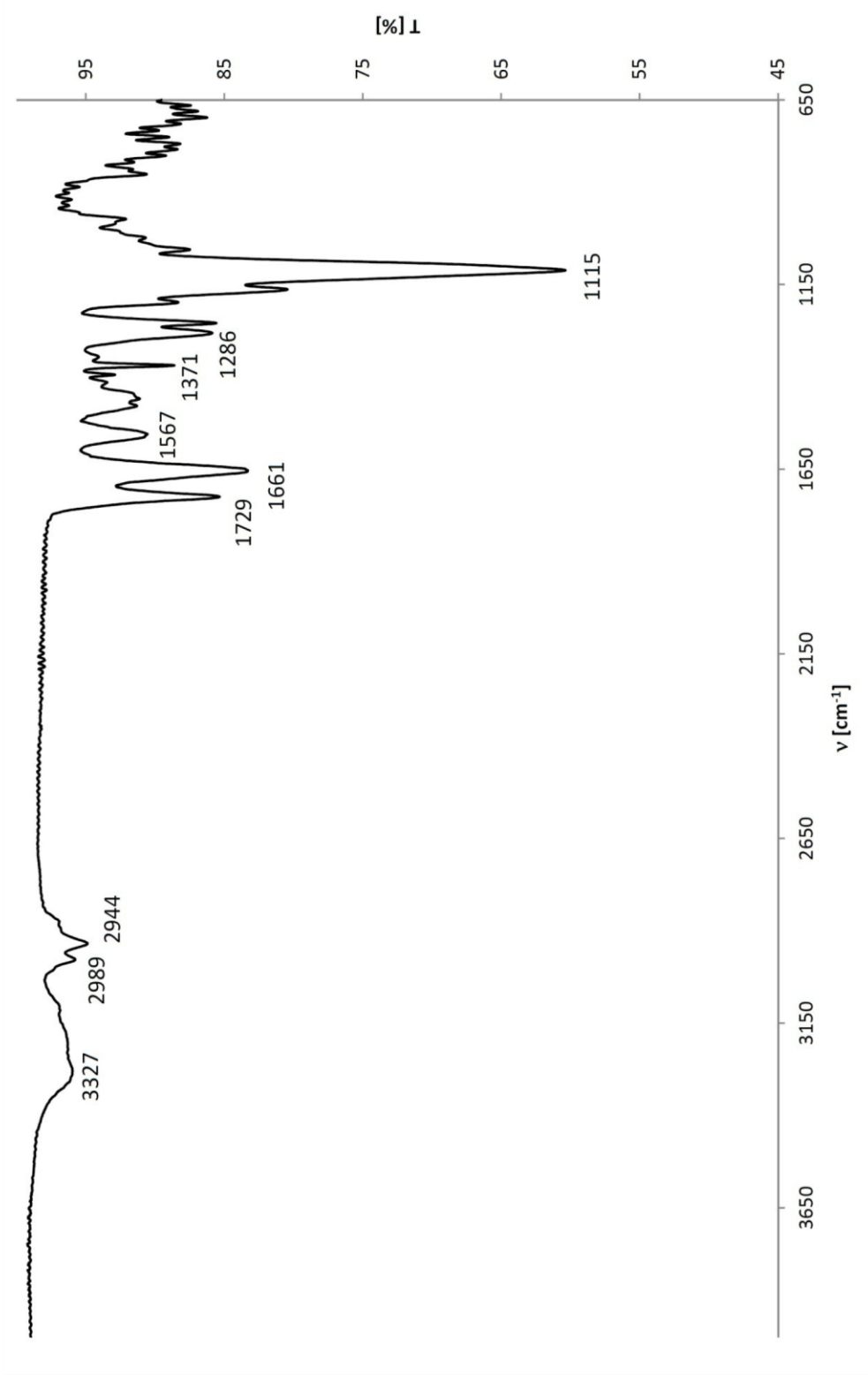

Fig. S4: ATR-IR spectrum of **3**.

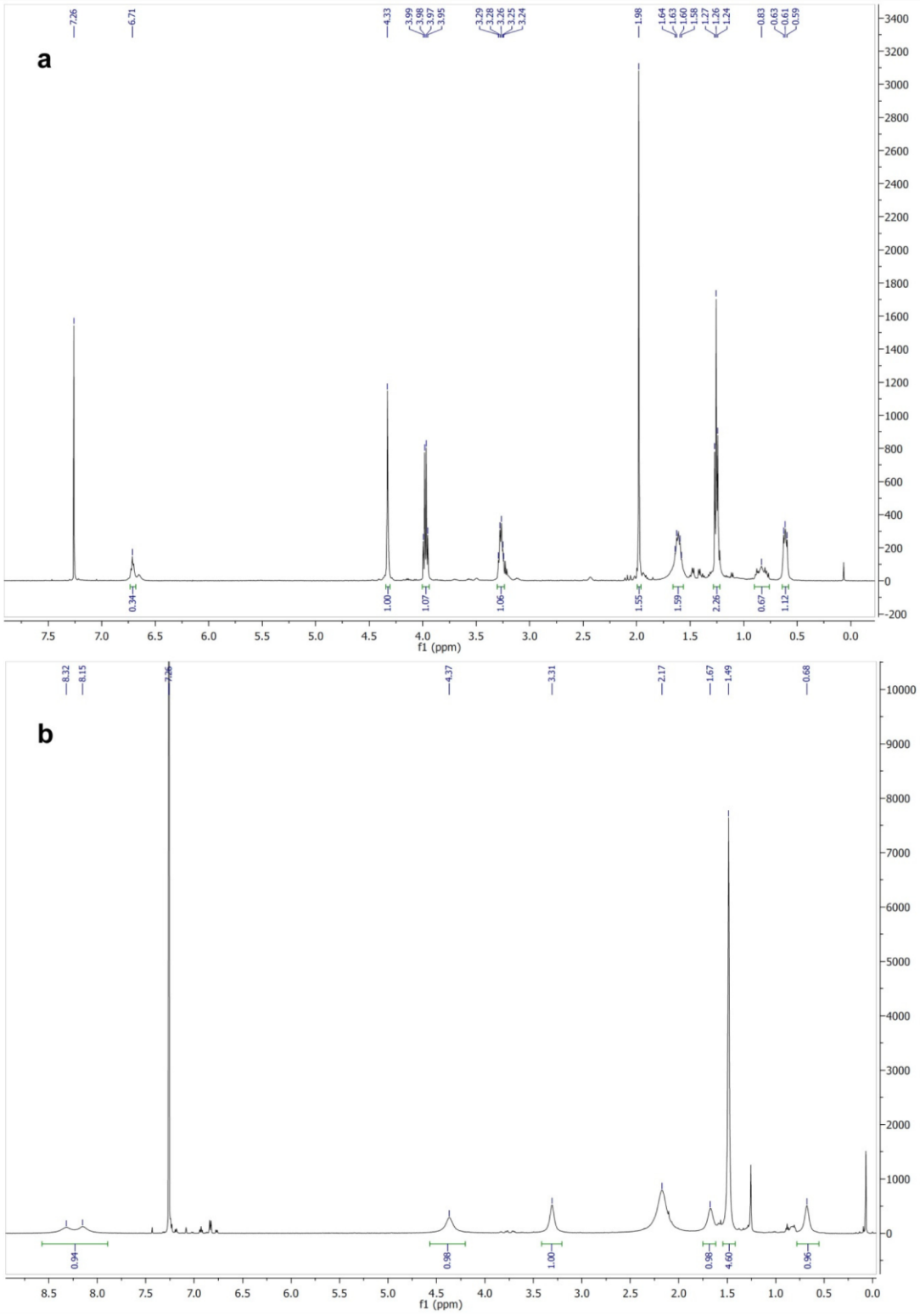

Fig. S5: (a) ^{1}H-NMR of **2**, (b) ^{1}H-NMR of **3**.

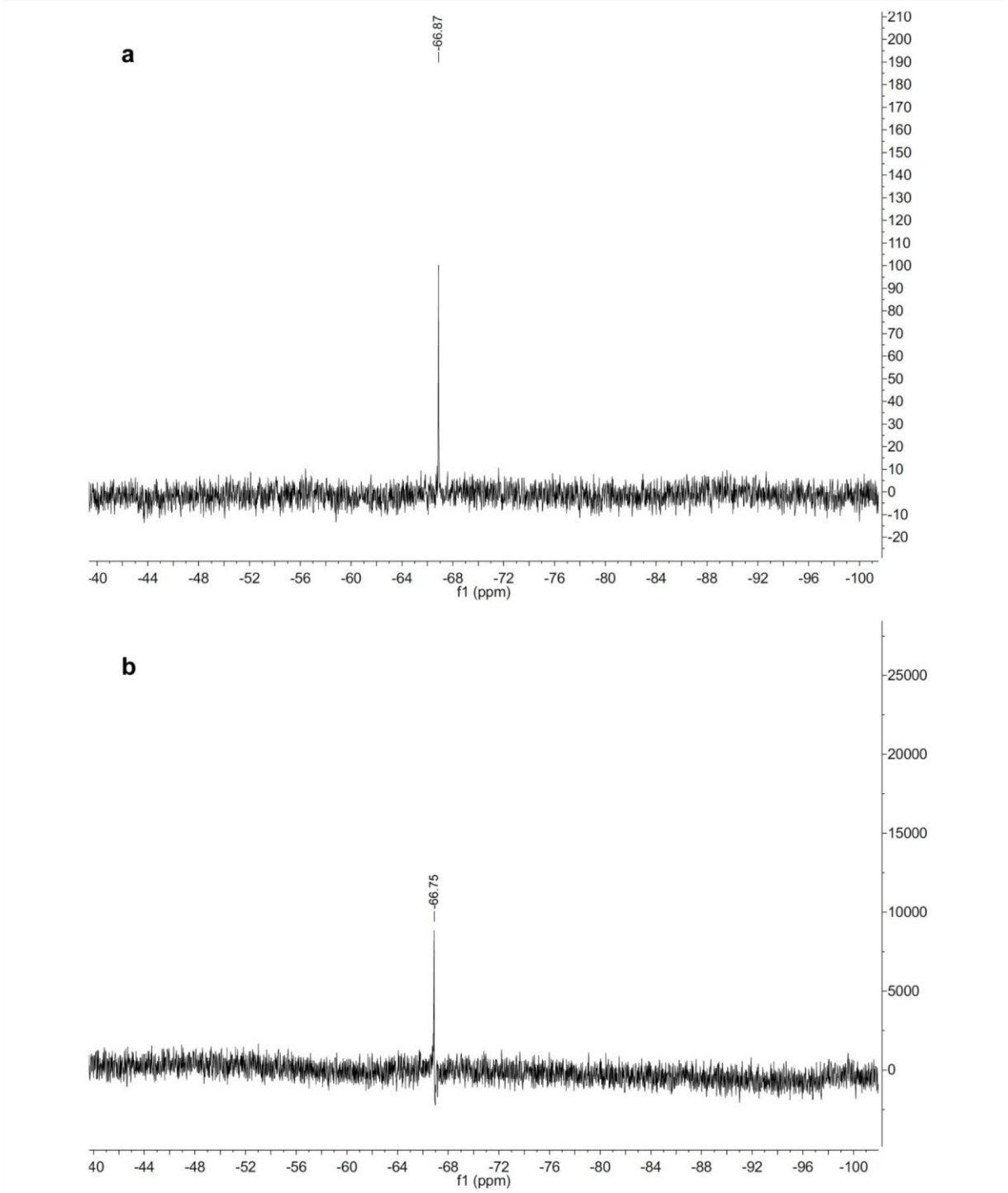

Fig. S6: (a) ^{29}Si-NMR of **2**, (b) ^{29}Si-NMR of **3**, the NMR spectra were base-line corrected using MestReNova.

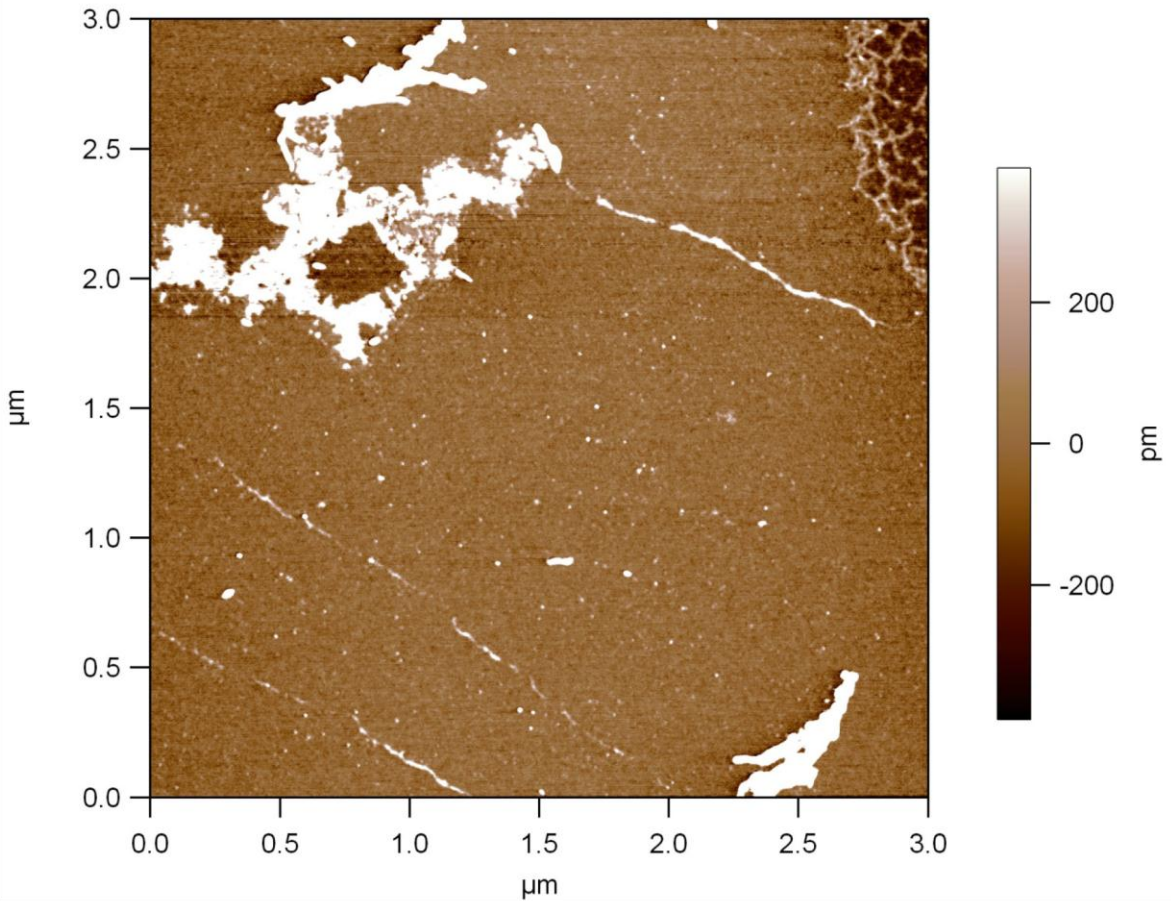

Fig. S7: AFM image of aggregated and randomly distributed COSS particles **1**.

a

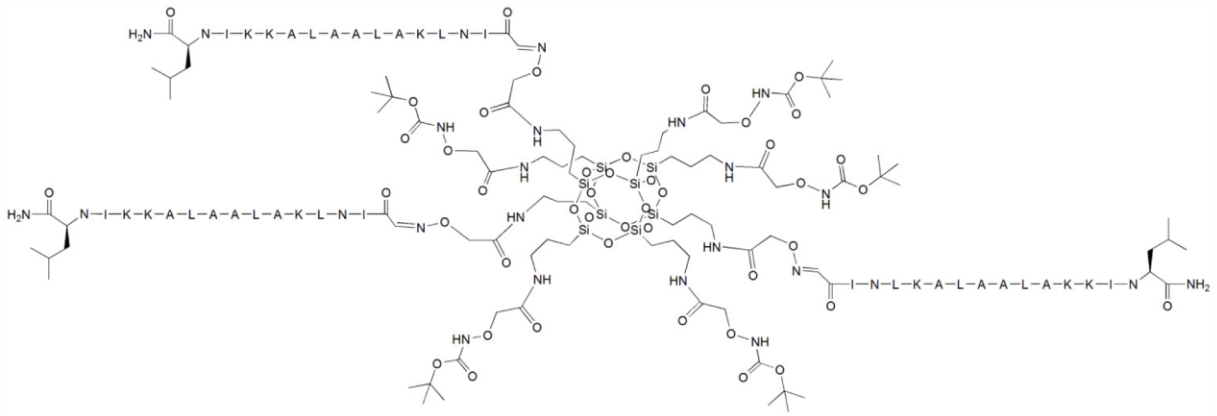

b

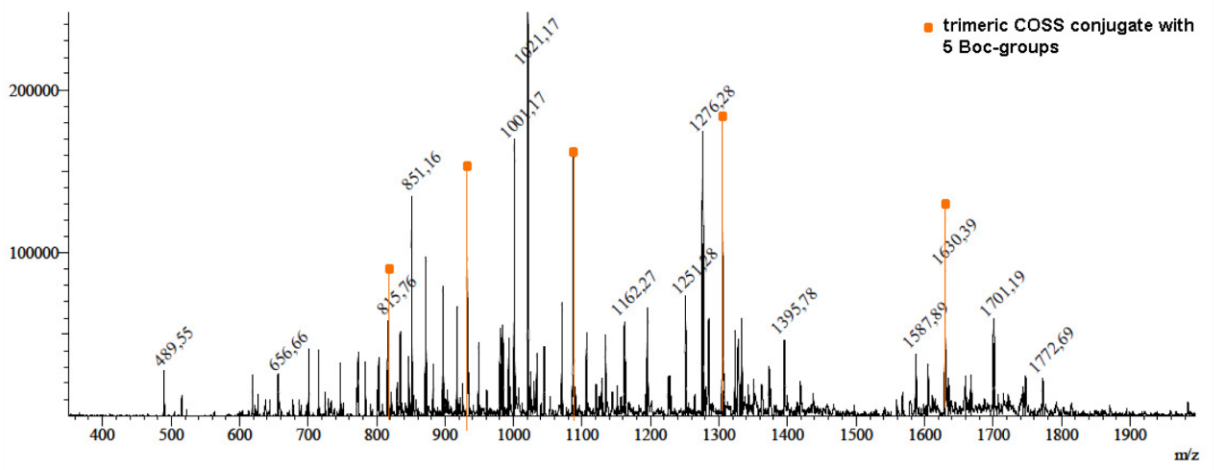

Fig. S8: (a) proposed structure of reaction intermediates in the synthesis of **6**. (b) ESI-MS spectrum of the reaction mixture after 30 min.

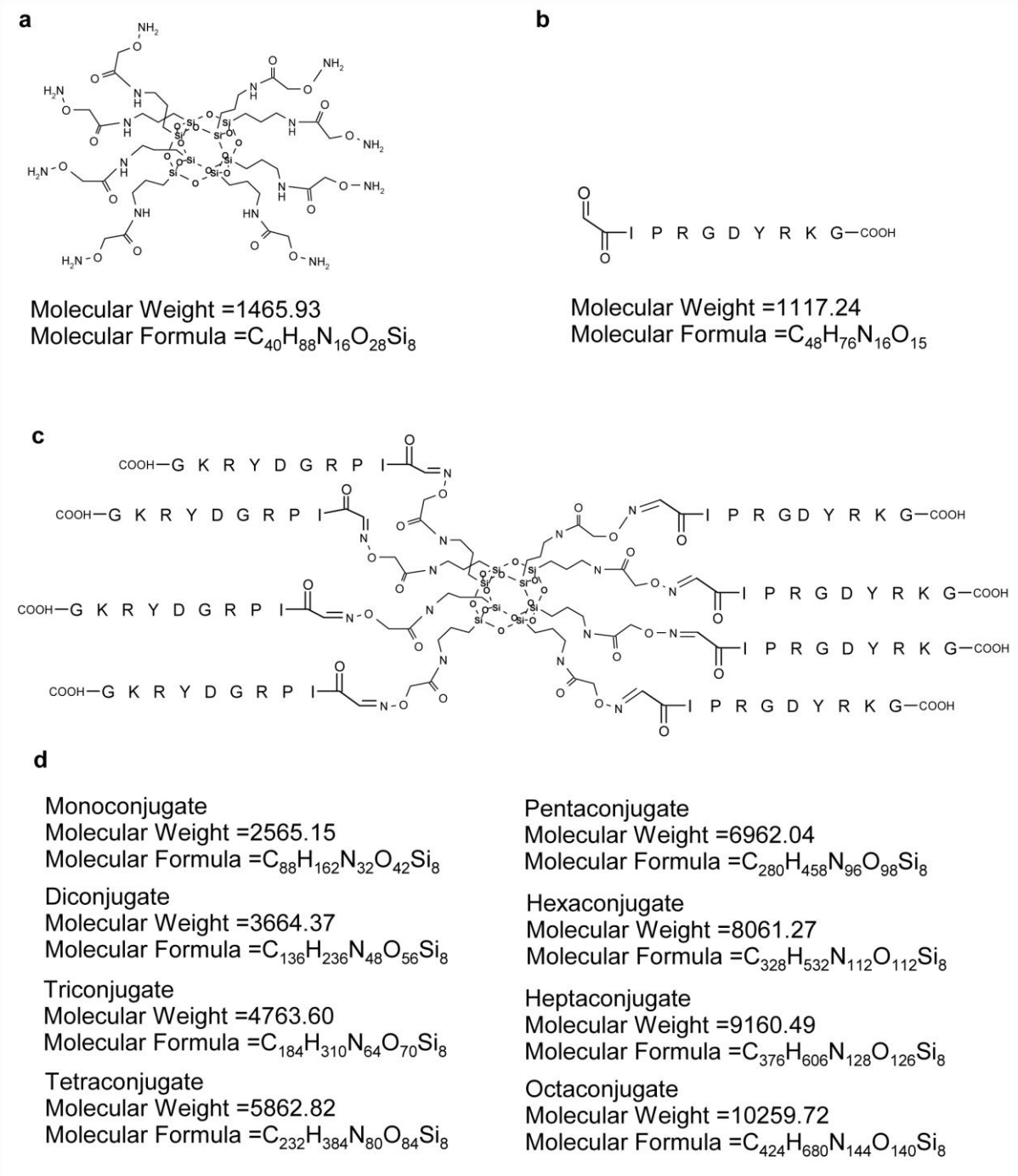

Fig. S9: (a) unprotected aminooxy COSS particle, (b) periodate oxidized **p4**, (c) possible conjugation products **4**.

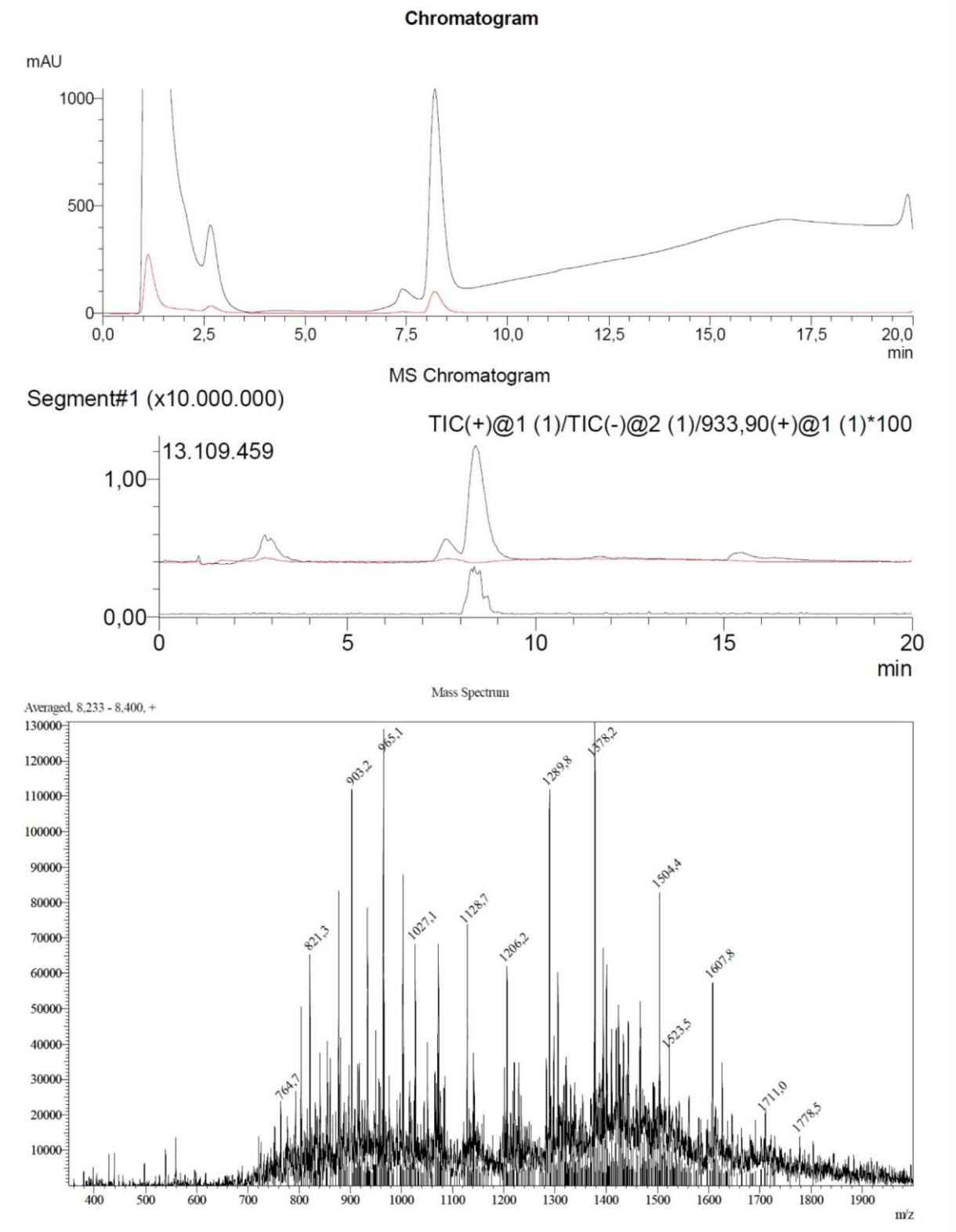

Fig. S10: LC-MS monitoring of the synthesis of **4**: analysis after overnight reaction.

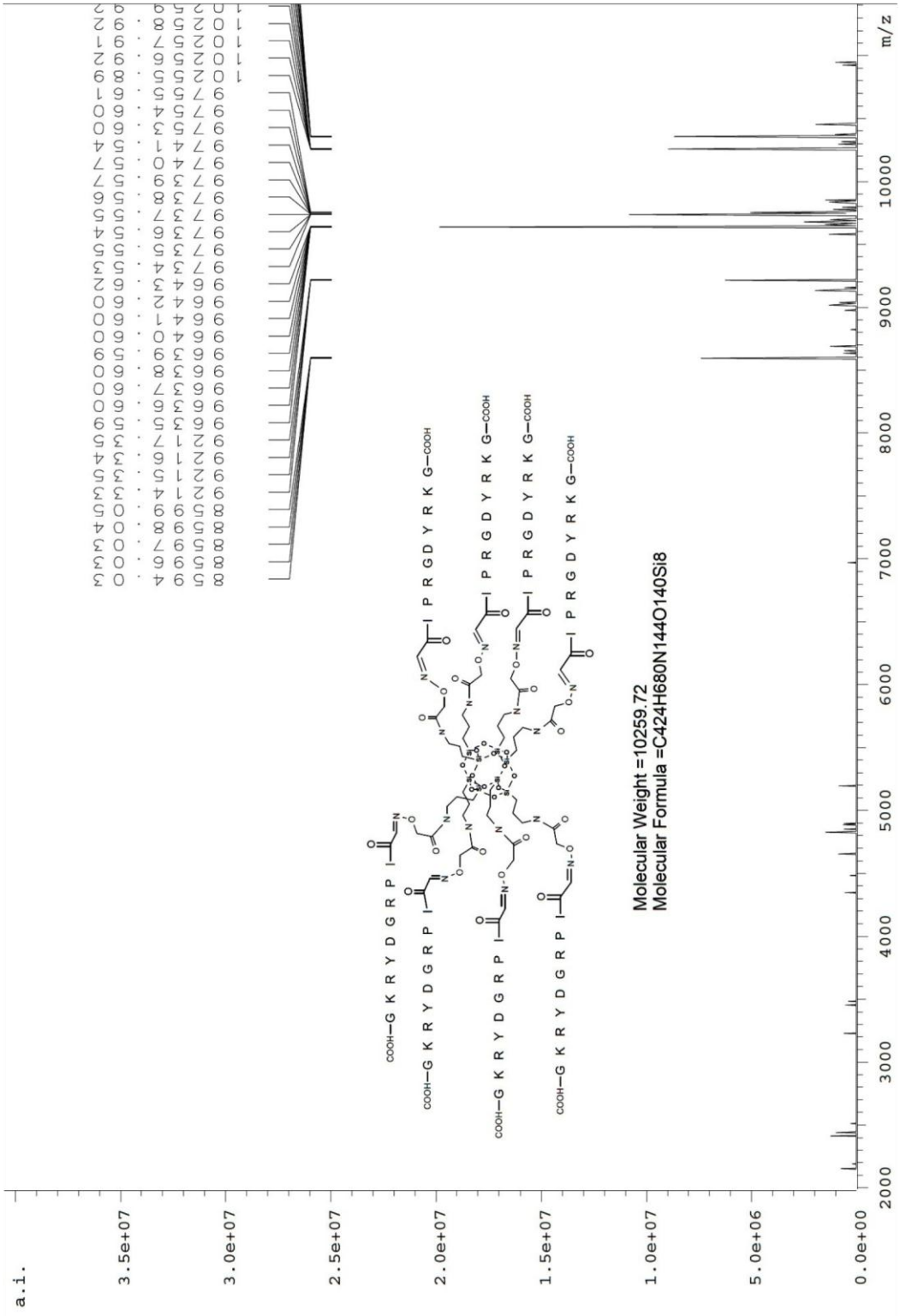

Fig. S11: Synthesis of **4**: deconvoluted ESI MS spectrum of the reaction mixture.

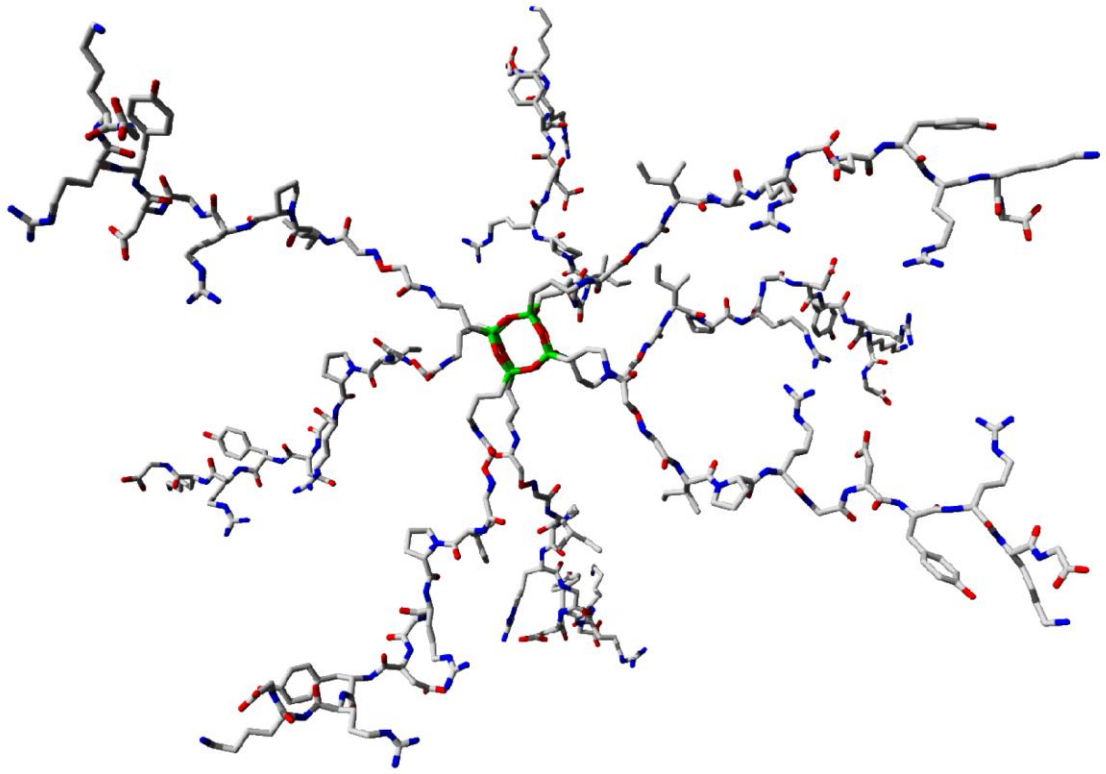

Fig. S12: 3D representation (sticks) of compound **4**. The model was generated using the YASARA structure package. After modelling of the COSS core atoms and connectivities an energy minimization procedure was applied. The respective peptide structures (compare **p4**) were attached, and the core coordinates were fixed. The resulting conjugate **4** was simulated in 0.9 % (m/v) NaCl aq. at pH 7 and 298 K for 0.1 ns using the AMBER03 force field. Blue: nitrogen, green: silicon, red: oxygen, grey: carbon, hydrogen was left out for clarity. Representative diameters were measured as distances of *C*-terminal carboxylic carbons of peptide ligands attached to opposing corners of the COSS cage. The measured values were: 7.21 nm, 6.69 nm, 6.16 nm, and 5.61 nm. The resulting average diameter was 6.42 ± 0.69 nm.

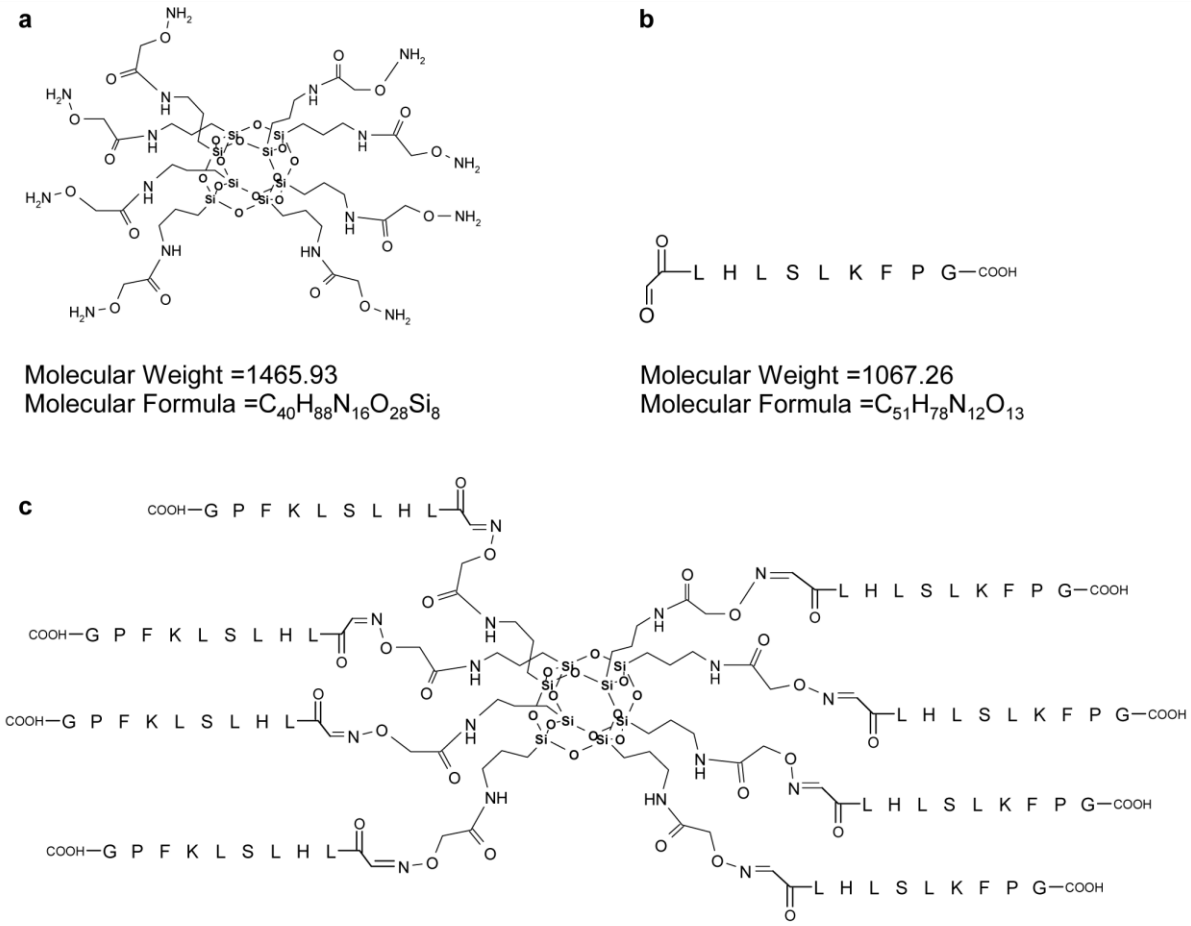

Fig. S13: (a) unprotected aminooxy COSS particle, (b) periodate oxidized **p5**, (c) possible conjugation products **5**.

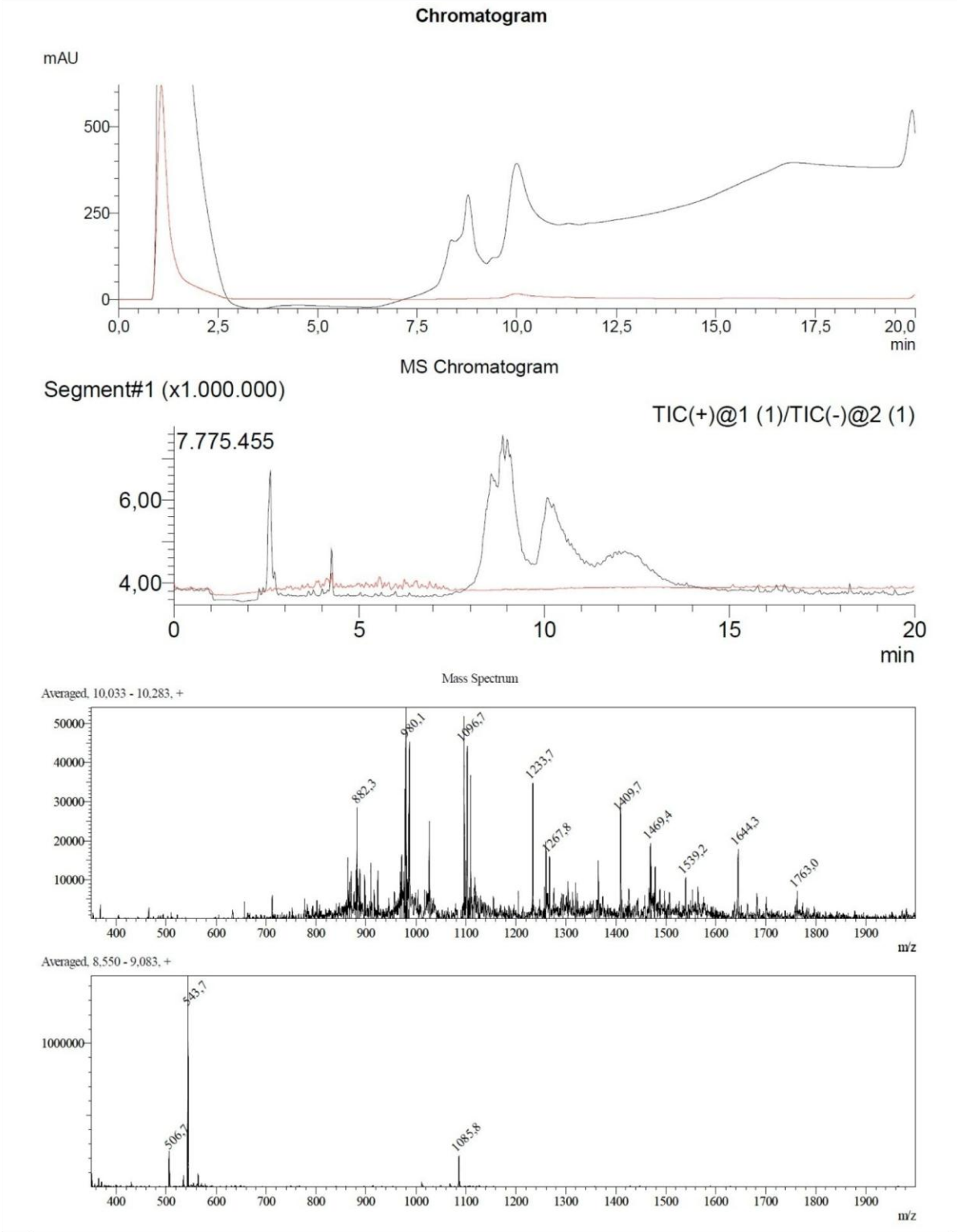

Fig. S14: LC-MS monitoring of the synthesis of **5**: analysis after overnight reaction.

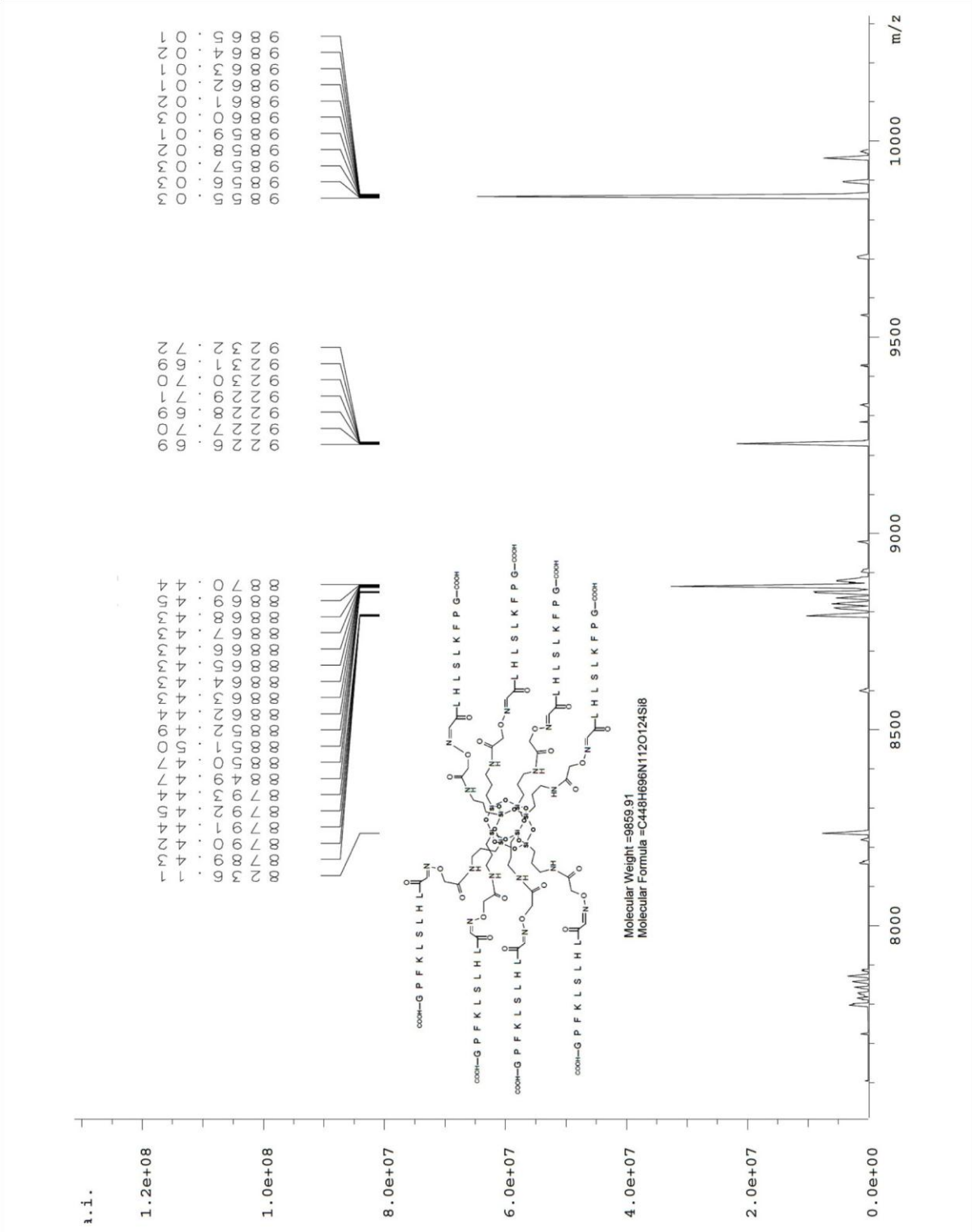

Fig. S15: Synthesis of **5**: deconvoluted ESI MS spectrum of the reaction mixture.

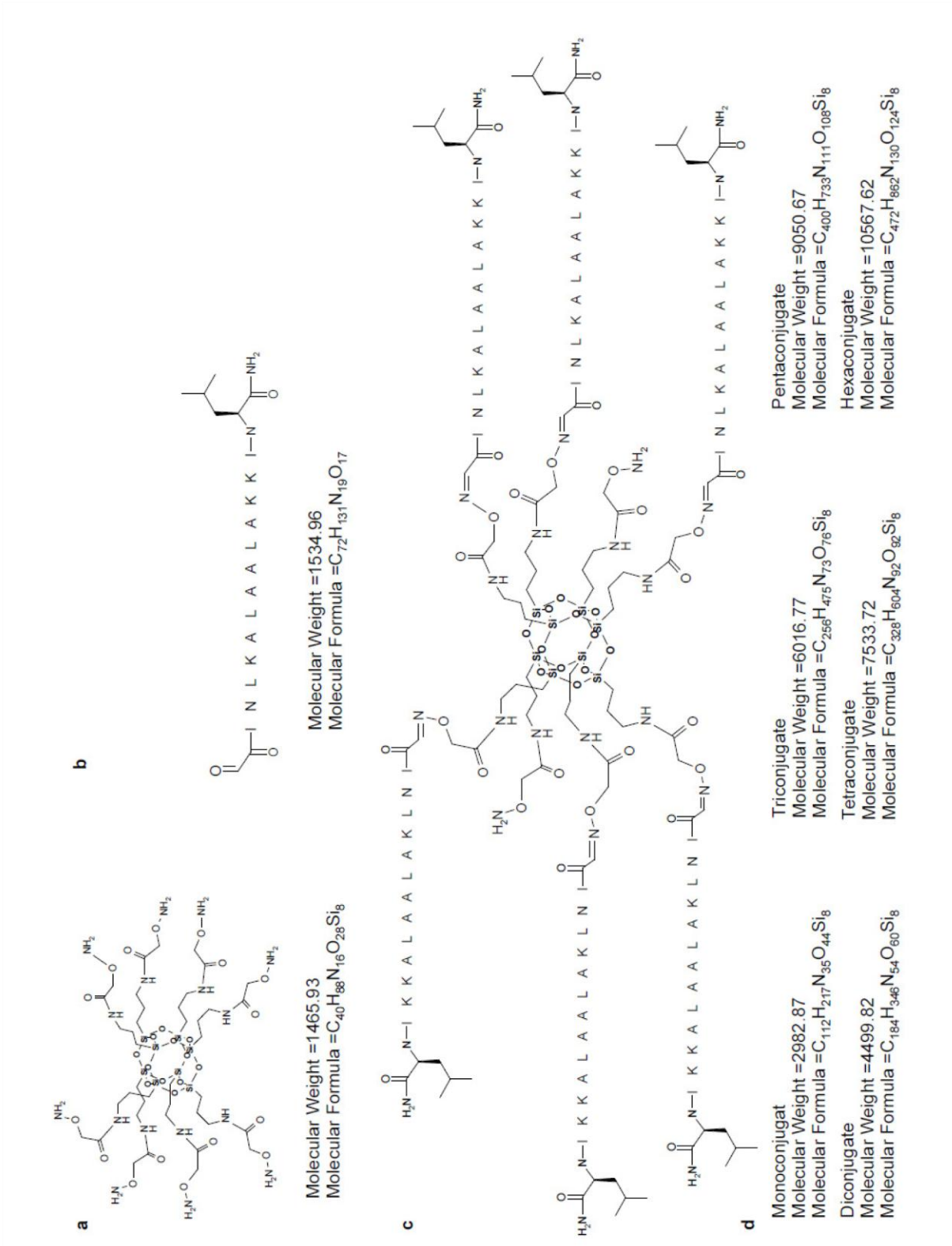

Fig. S16: (a) unprotected aminooxy COSS particle, (b) periodate oxidized **p6**, (c) possible conjugation products **6**.

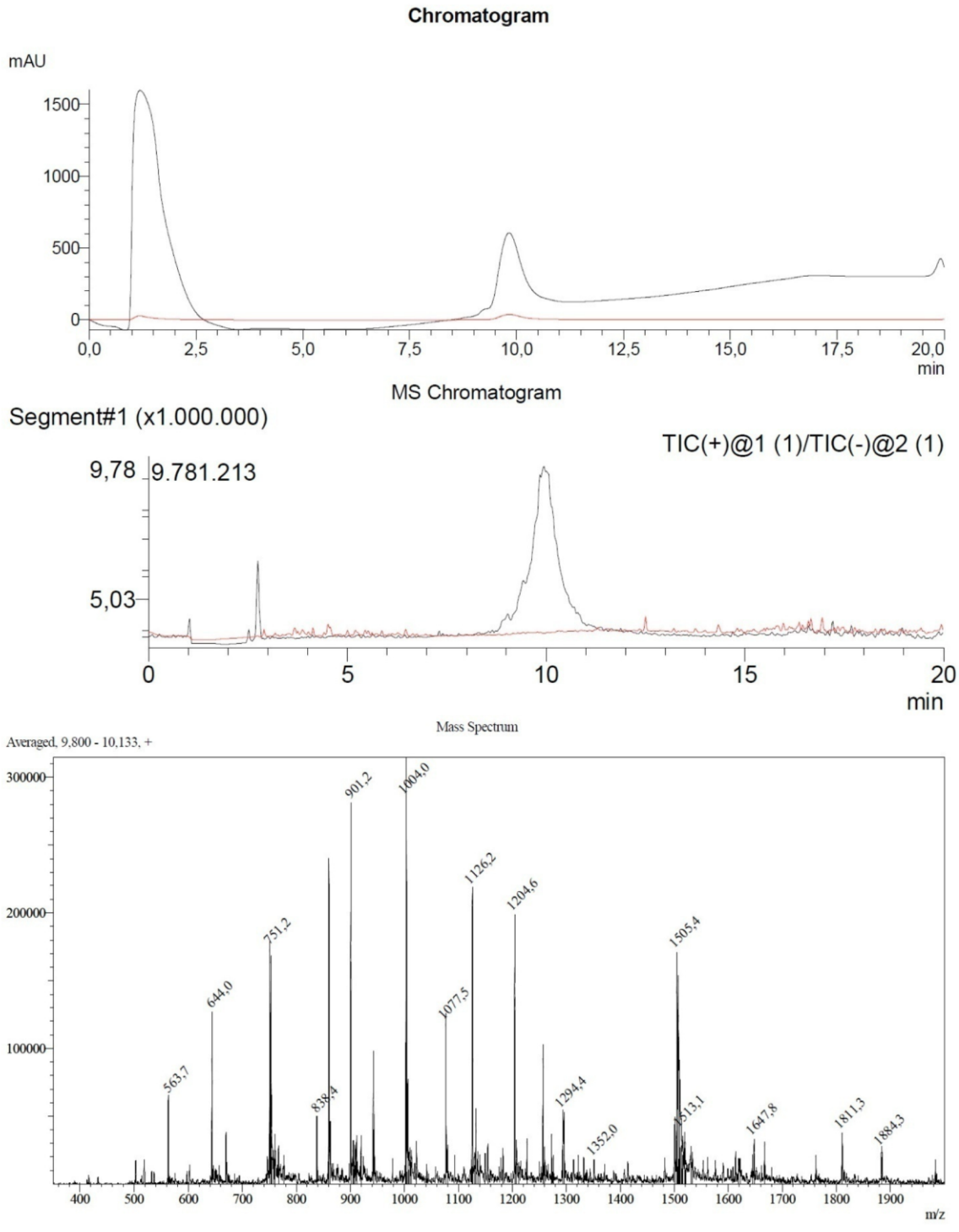

Fig. S17: LC-MS monitoring of the synthesis of **6**: analysis after overnight reaction.

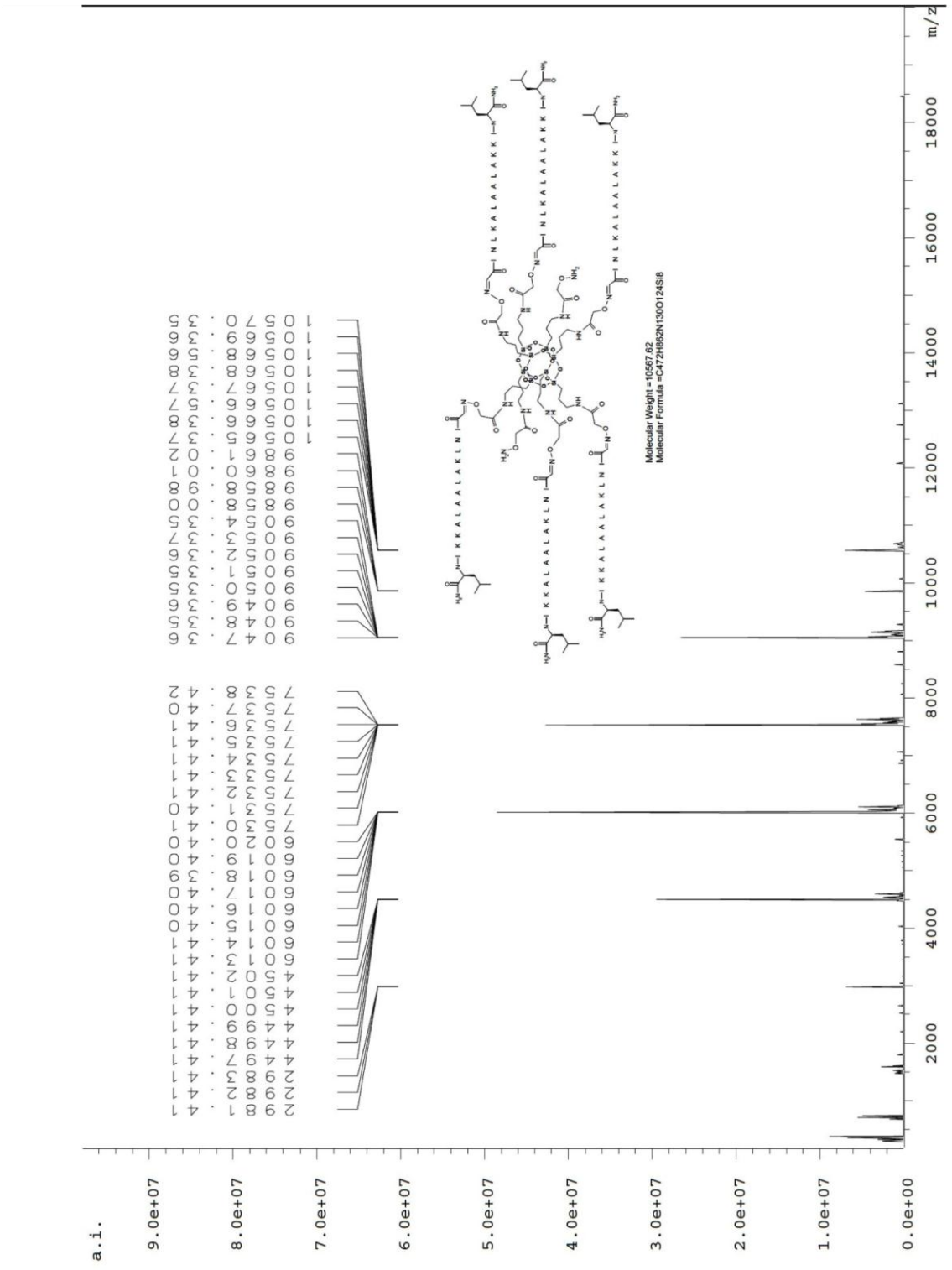

Fig. S18: Synthesis of **6**: deconvoluted ESI MS spectrum of the reaction mixture.

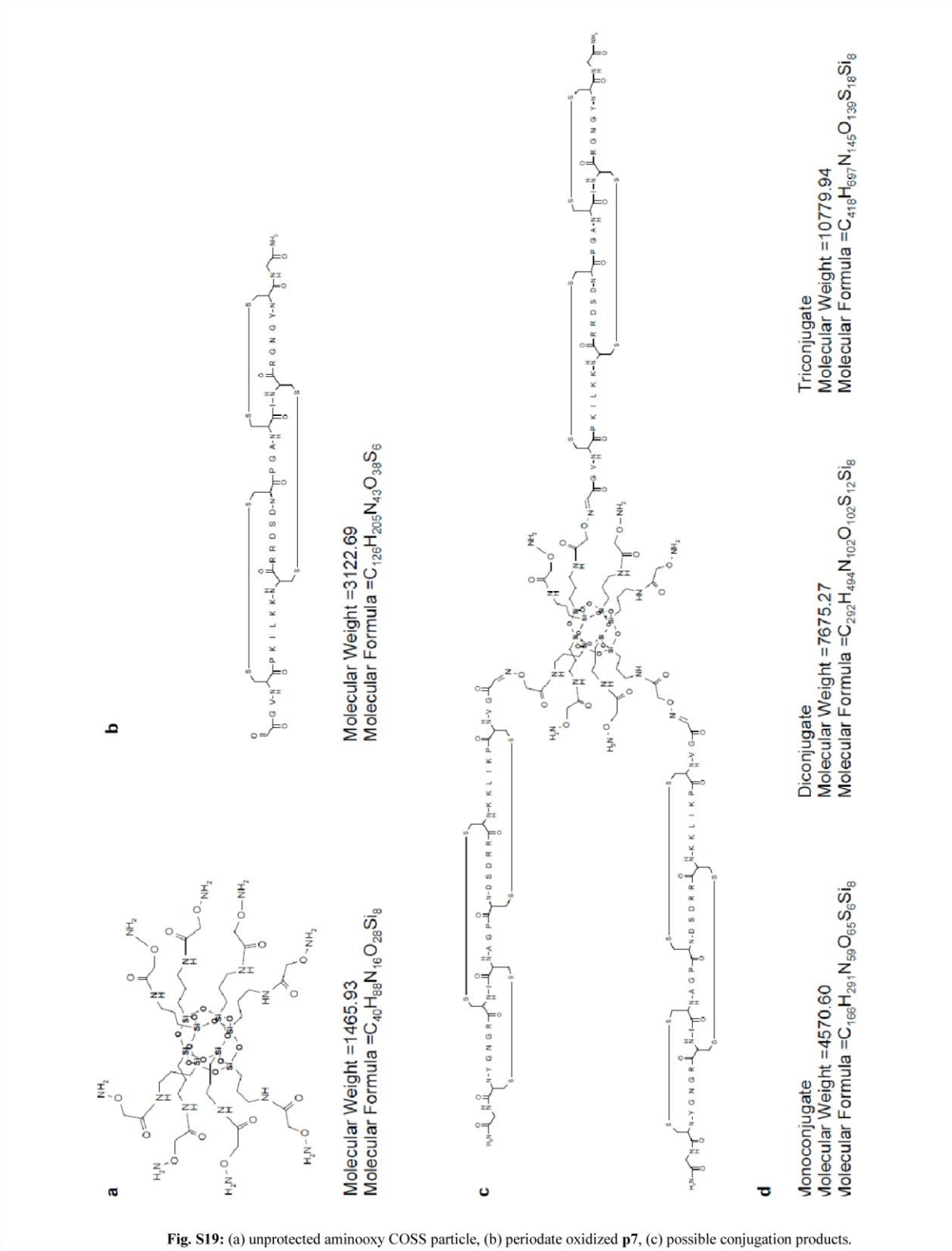

Fig. S19: (a) unprotected aminooxy COSS particle, (b) periodate oxidized **p7**, (c) possible conjugation products.

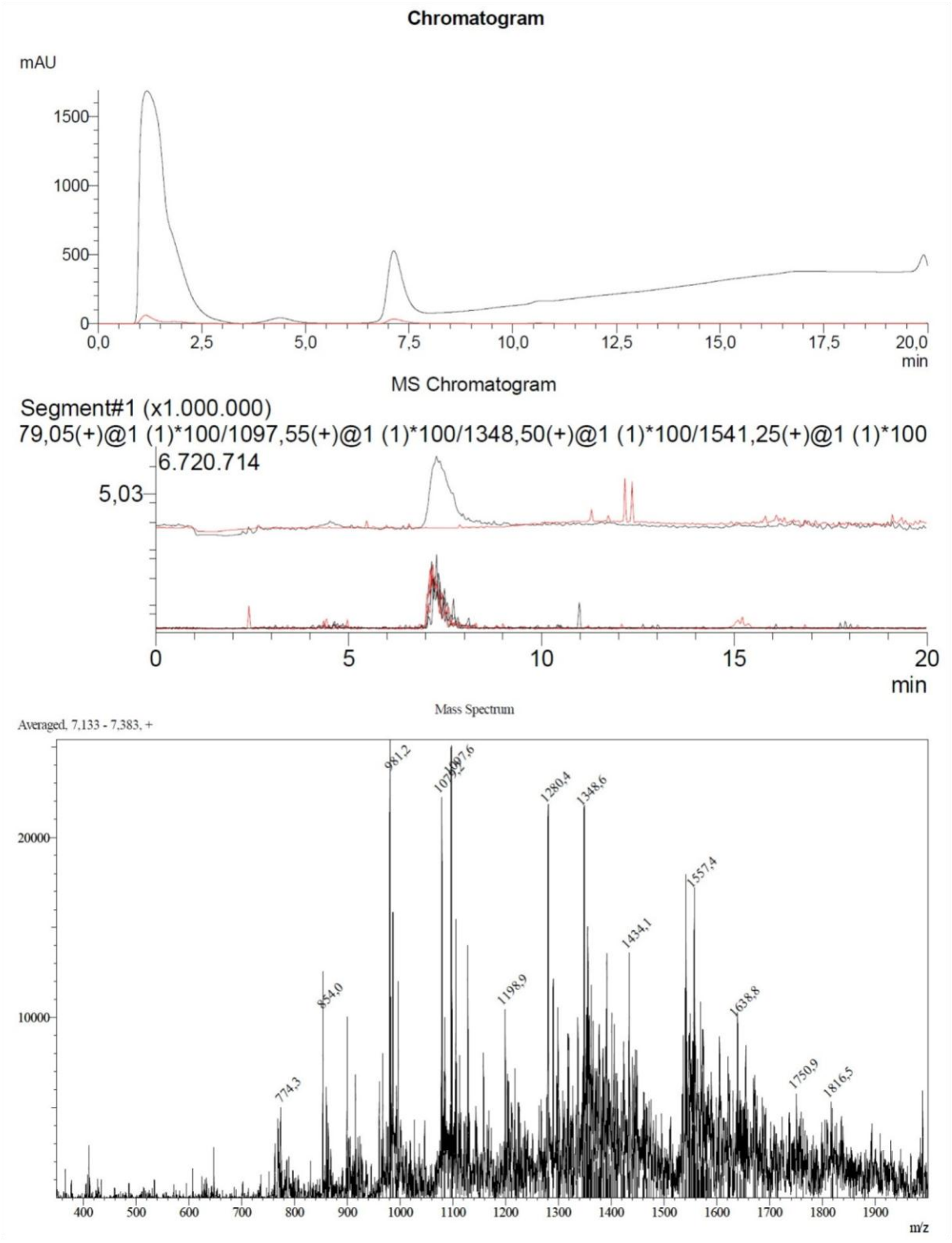

Fig. S20: LC-MS monitoring of the synthesis of **7**: analysis after overnight reaction.

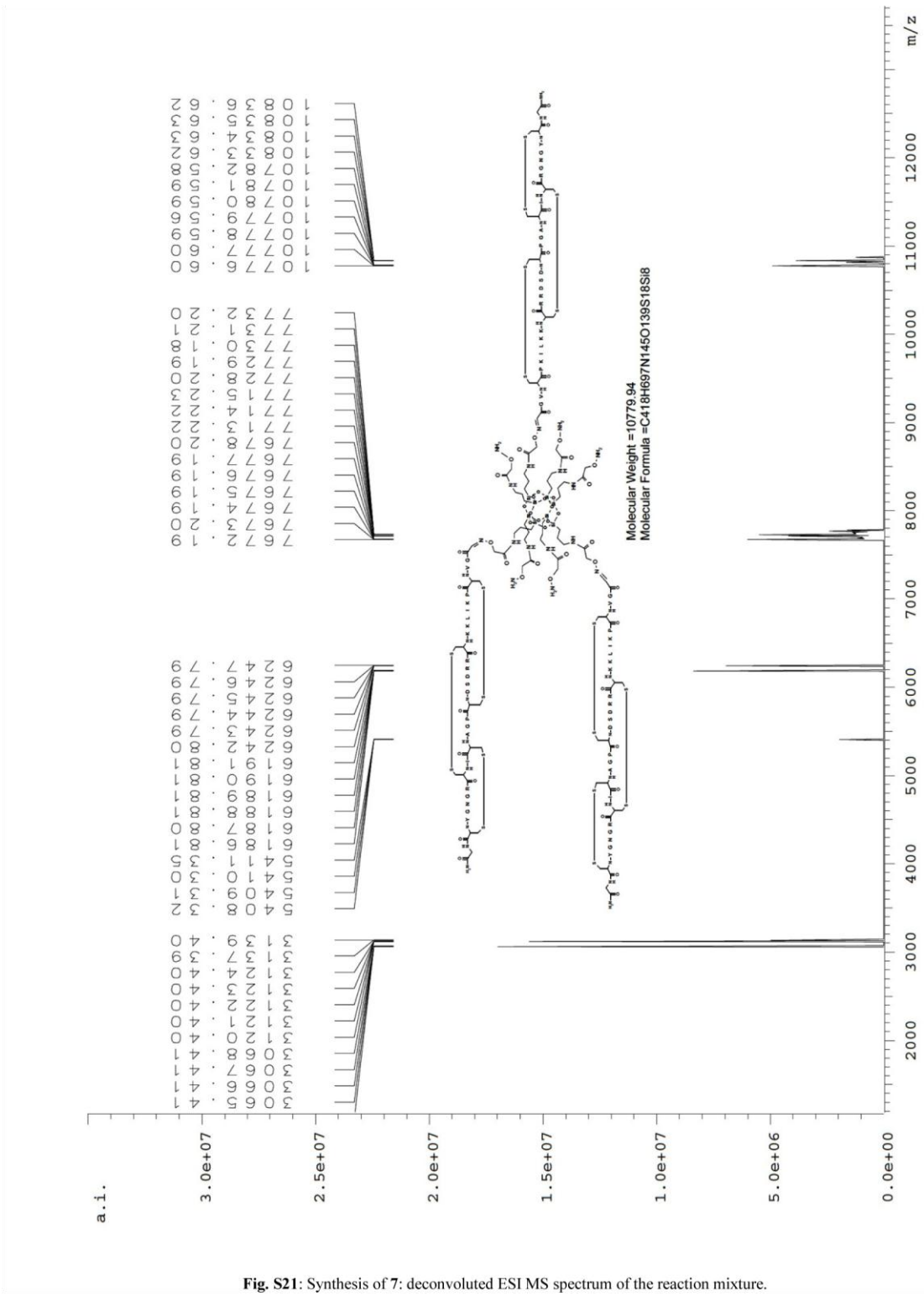

Fig. S21: Synthesis of **7**: deconvoluted ESI MS spectrum of the reaction mixture.

a

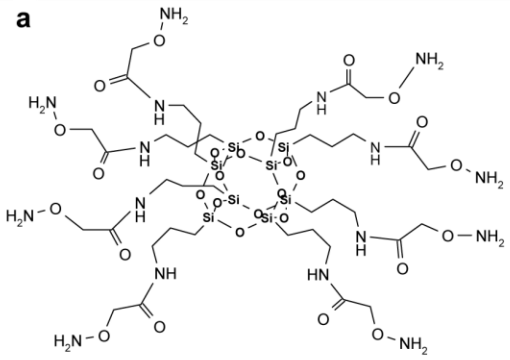

Molecular Weight =1465.93
Molecular Formula =$C_{40}H_{88}N_{16}O_{28}Si_8$

b

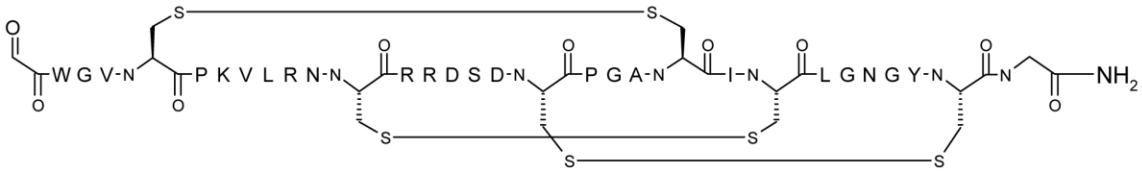

Molecular Weight =3265.79
Molecular Formula =$C_{134}H_{206}N_{44}O_{40}S_6$

c

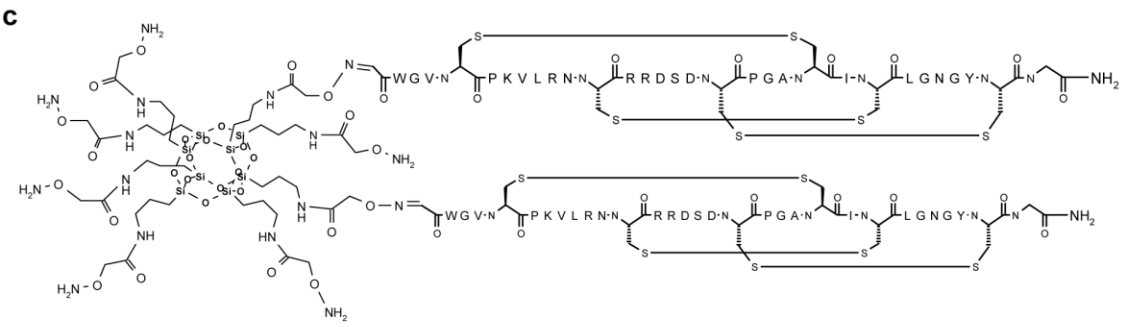

d

Monoconjugate
Molecular Weight =4713.70
Molecular Formula =$C_{174}H_{292}N_{60}O_{67}S_6Si_8$

Diconjugate
Molecular Weight =7961.48
Molecular Formula =$C_{308}H_{496}N_{104}O_{106}S_{12}Si_8$

Fig. S22: (a) unprotected aminooxy COSS particle, (b) periodate oxidized **p8**, (c) possible conjugation products **8**.

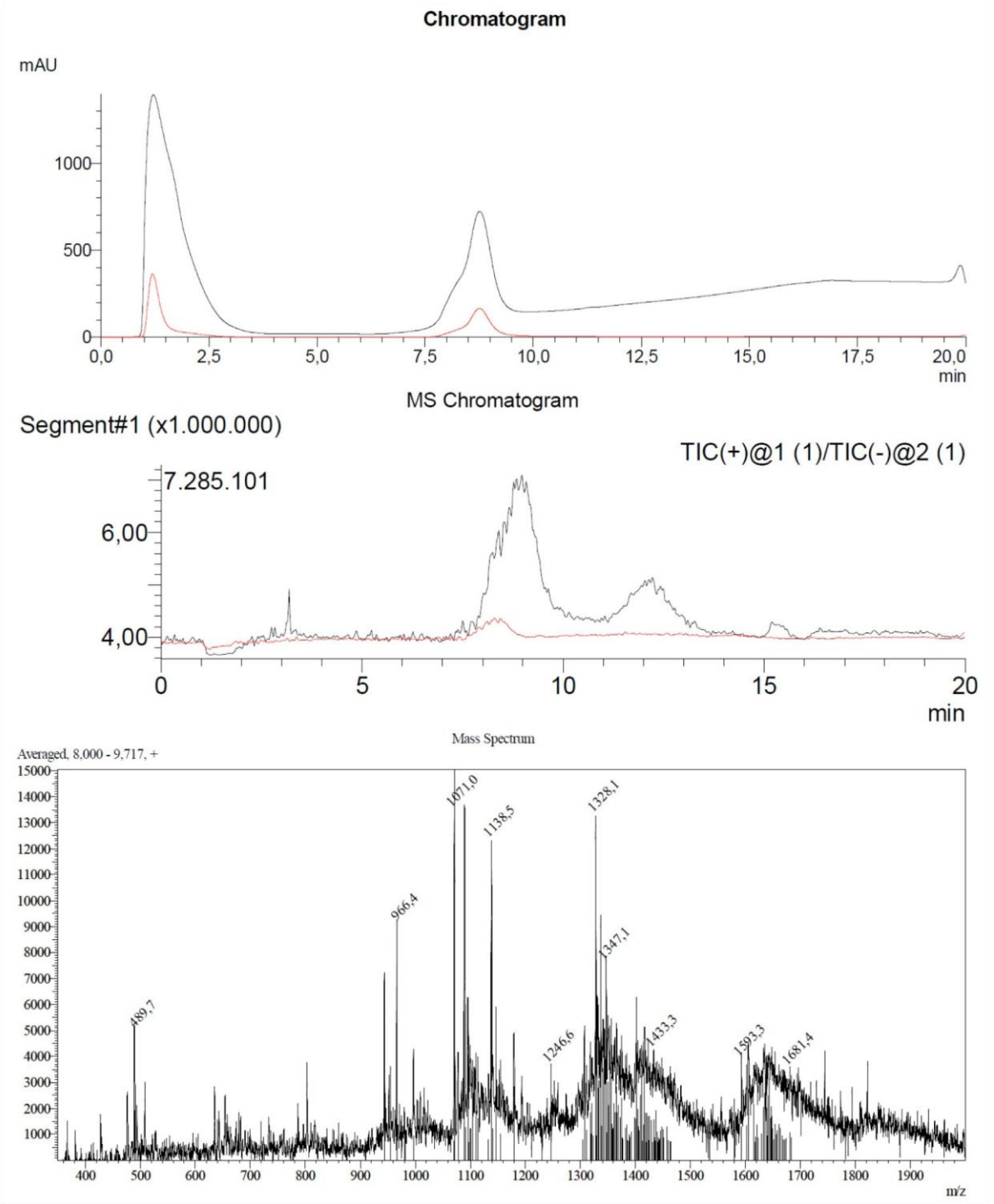

Fig. S23: LC-MS monitoring of the synthesis of **8**: analysis after overnight reaction.

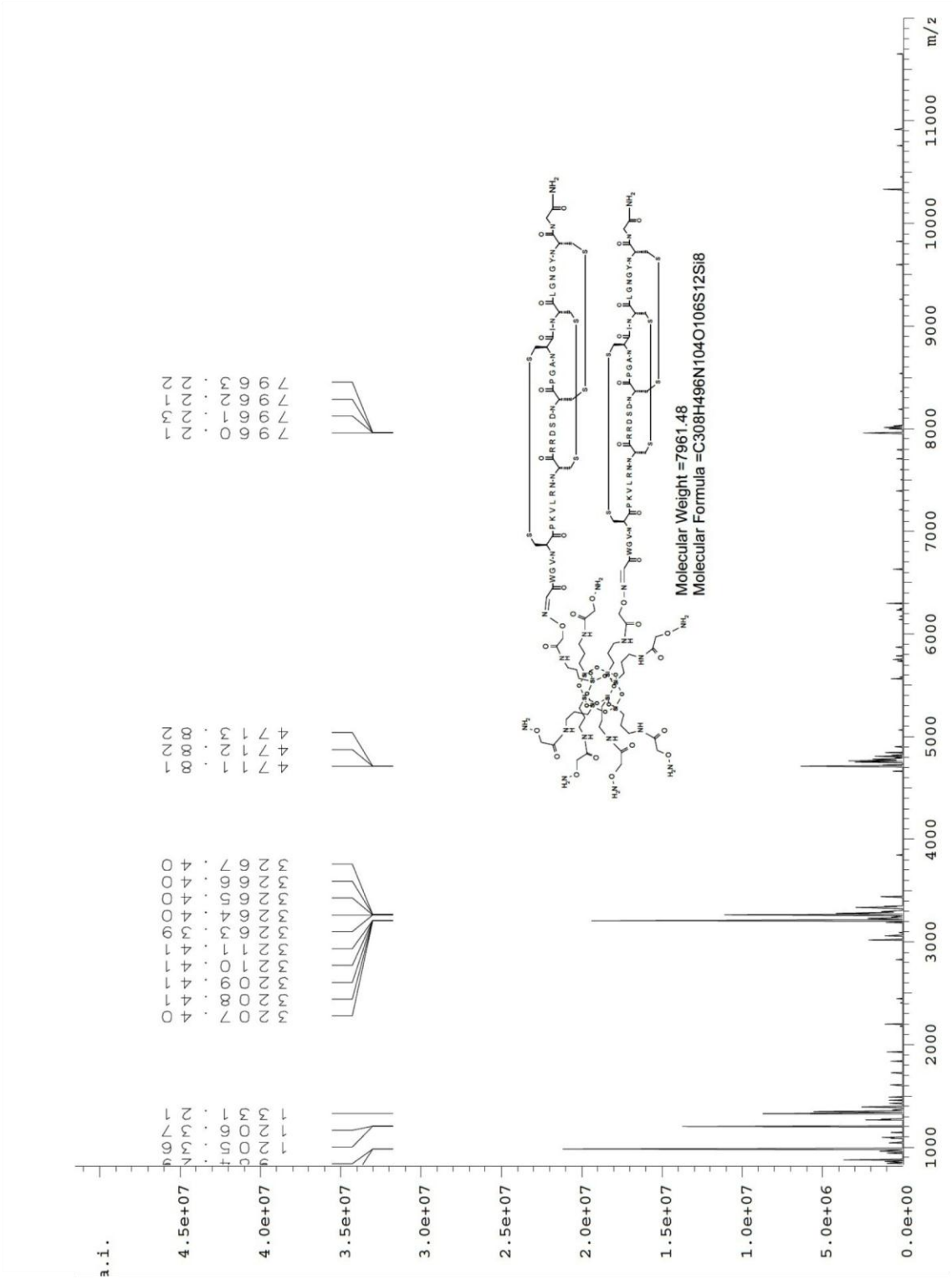

Fig. S24: Synthesis of **8**: deconvoluted ESI MS spectrum of the reaction mixture.

a

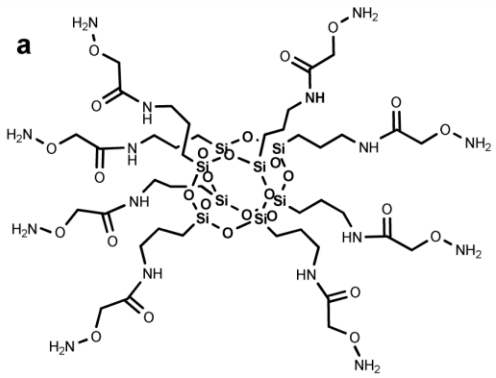

Chemical Formula: C40H88N16O28Si8 $C_{40}H_{88}N_{16}O_{28}Si_8$
Molecular Weight: 1465.901465.9011

b

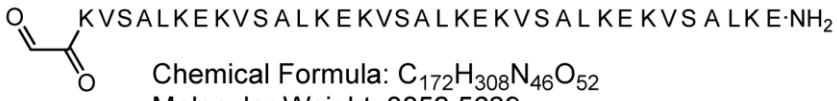

Chemical Formula: $C_{172}H_{308}N_{46}O_{52}$
Molecular Weight: 3852.5629

c

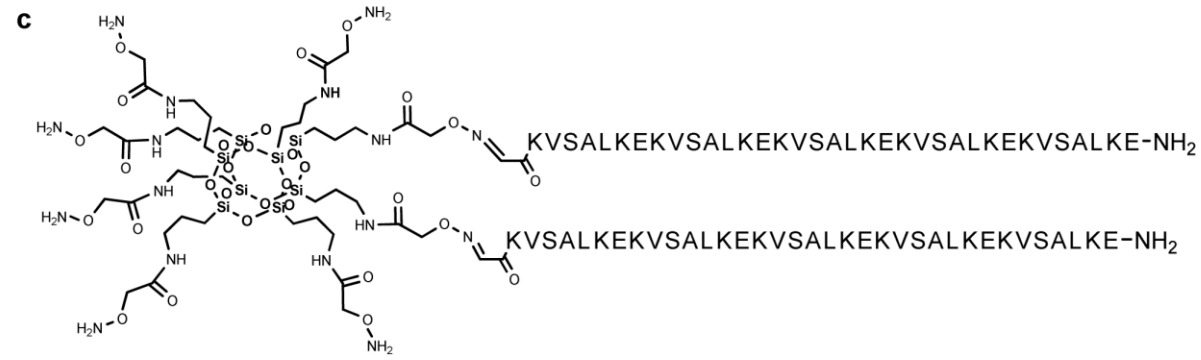

d

Monoconjugate
Chemical Formula: $C_{212}H_{394}N_{62}O_{79}Si_8$
Molecular Weight: 5300.44

Diconjugate
Chemical Formula: $C_{384}H_{700}N_{108}O_{130}Si_8$
Molecular Weight: 9134.99

Fig. S25: (a) unprotected aminooxy COSS particle, (b) periodate oxidized **p9**, (c) possible conjugation products **9**.

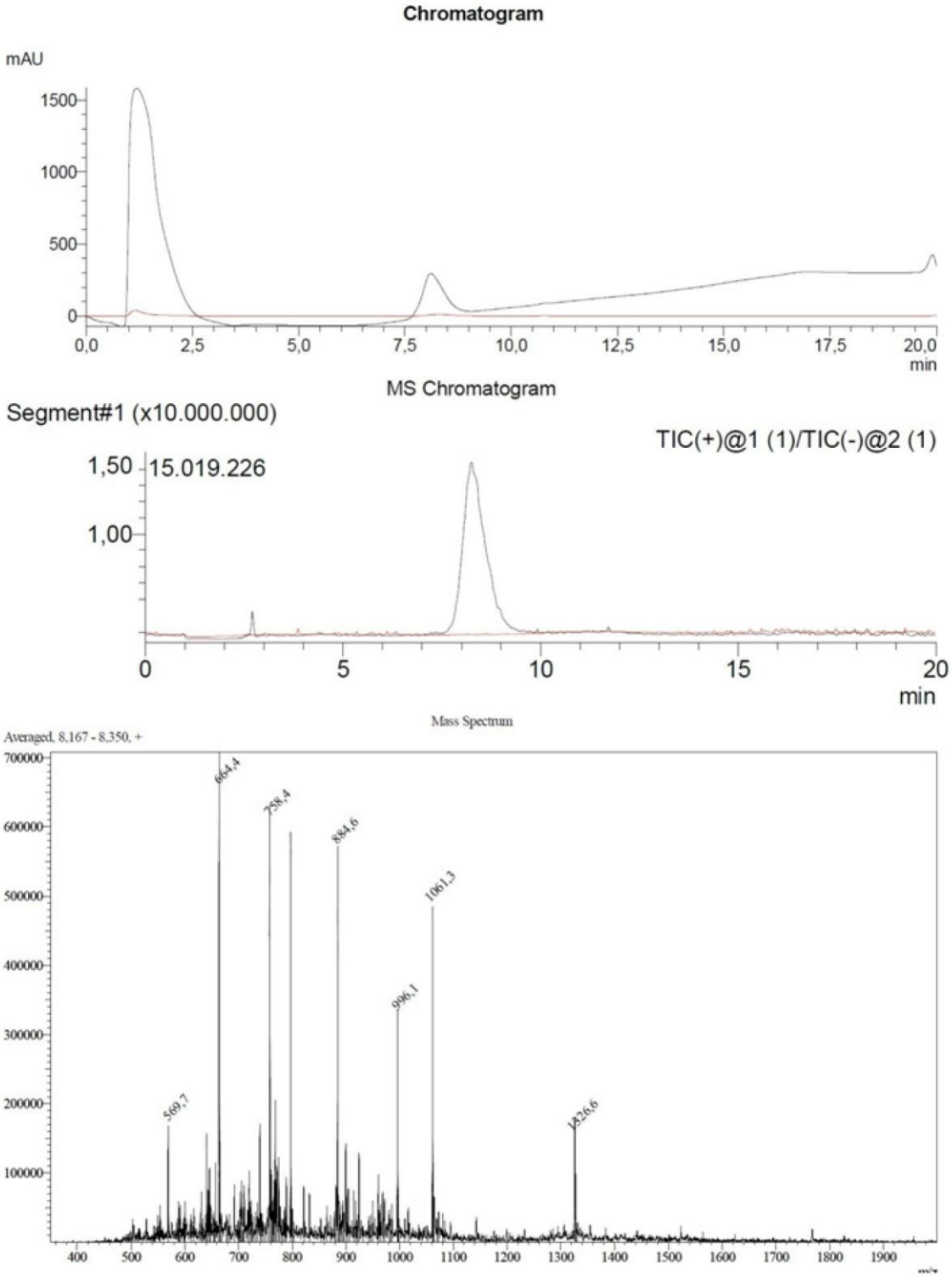

Fig. S26: LC-MS monitoring of the synthesis of **9**: analysis after overnight reaction.

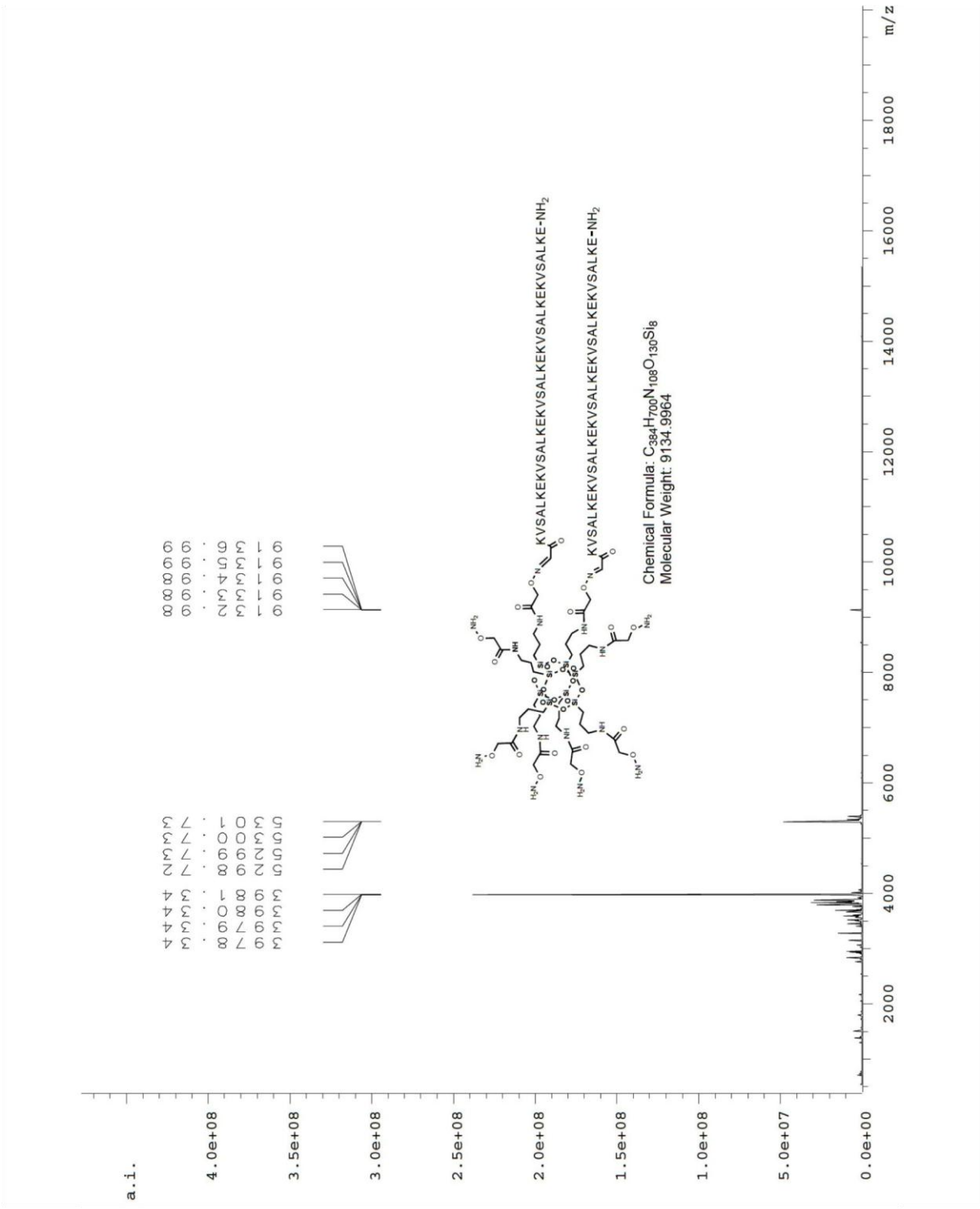

Fig. S27: Synthesis of **9**: deconvoluted ESI MS spectrum of the reaction mixture.

4.3. Analytische der Verbindungen aus Teil 3.3.

Die Nummerierung der Verbindungen entspricht: Hörner et al., Org. Biomol. Chem., 2013, **11**, 2258-2265.

Compound 2 (Fmoc-L-cysteine heptaamino-COSS) and 2a (Fmoc-S-trityl-L-cysteine heptaamino-COSS)

Fig. S1: Chemical structure of trityl protected (**2a**) and unprotected Fmoc-L-cysteine heptaamino-COSS **2**
Fig. S2: Analytical RP-HPLC traces of trityl protected (**2a**) and deprotected Fmoc-L-cysteine heptaamino-COSS **2**
Fig. S3: HR-MS measurement of Fmoc-S-Trt-L-cysteine heptaamino-COSS **2a**
Fig. S4: LC-MS (ESI) measurement of compound **2**

Compound 3 (FITC-labeled PCNA binding peptide)

Fig. S5: Amino acid sequence and chemical structure of FITC-labeled PCNA binding peptide **3**
Fig. S6: Analytical HPLC traces of FITC-labeled PCNA binding peptide **3**
Fig. S7: LC-MS (ESI) measurements of the purified and FITC-labeled PCNA binding peptide **3**

Compound 4 (PCNA binding peptide coupled to Fmoc-L-cysteine heptaamino-COSS)

Fig. S8: Chemical structure of compound **4**
Fig. S9: Analytical RP-HPLC traces of compound **4**
Fig. S10: HR-MS measurement of a compound **4**
Fig. S11: FT-IR spectrum of compound **4**

Compound 5 (Cys-β-Ala-FITC hepataamino-COSS), 5a (Cys-(S-trt)-beta-Ala-FITC), and 5b (Cys-(S-trt)-β-Ala-FITC hepataamino-COSS)

Fig. S12: Chemical structure of compound **5a**
Fig. S13: Analytical RP-HPLC traces of compound **5a**
Fig. S14: LC-MS (ESI) measurement of compound **5a**
Fig. S15: Chemical structure of trityl-protected (**5b**) and unprotected fluoresceine-labeled COSS particle **5**
Fig. S16: LC-MS (ESI) measurement of a trityl-protected fluoresceine-labeled COSS particle **5b**
Fig. S17: Analytical RP-HPLC traces and MS analysis of fluoresceine-labeled COSS particle **5**

Microirradiation experiment and subsequent co-localization of PCNA-binding peptide and RFP-labeled PCNA

Fig. S18: Fluorescence microscopic analysis of irradiated HeLa cells

Compound 2 (Fmoc-L-cysteine heptaamino-COSS) and 2a (Fmoc-S-trityl-L-cysteine heptaamino-COSS)

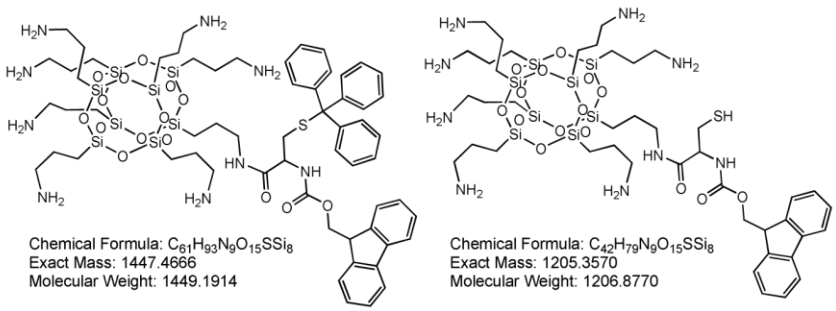

Fig. S1: Chemical structure of trityl-protected compound **2a** (left) and unprotected Fmoc-L-cysteine heptaamino-COSS **2** (right).

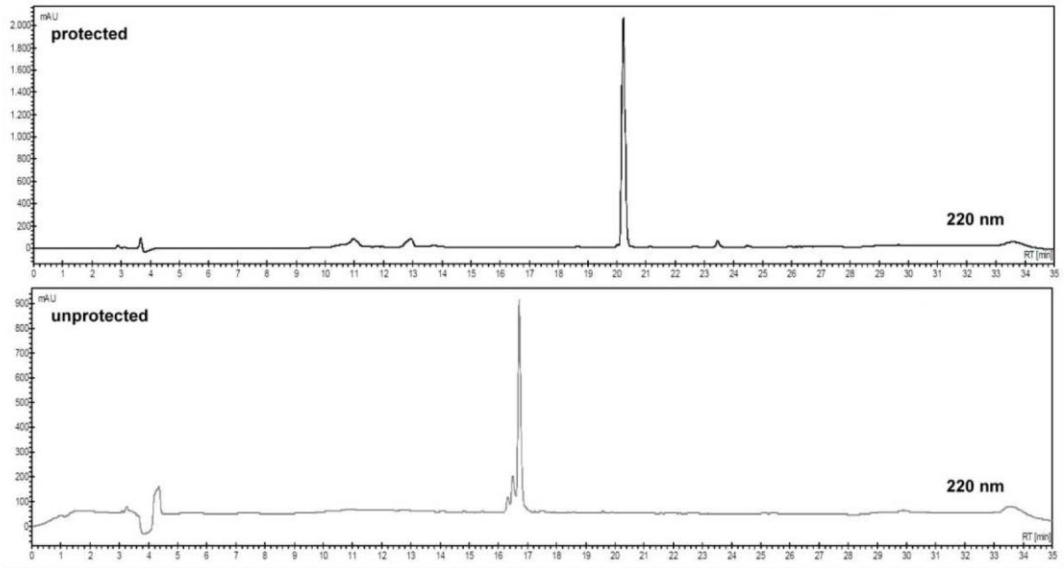

Fig. S2: Analytical RP-HPLC traces of trityl-protected (**2a**) and deprotected Fmoc-L-cysteine heptaamino-COSS **2**. (*Varian* 940-LC equipped with a *Phenomenex* Luna C_{18} column (5u, 100 A, 250×4.60 mm, 5 µm). Eluent A: 0.1% aq. trifluoroacetic acid (TFA), eluent B: 90 % aq. acetonitrile in 0.1% aq. TFA; 10 → 80% B in 20 min preceded by 5 min isocratic 10 % B at a flow rate of 1 mL min^{-1}).

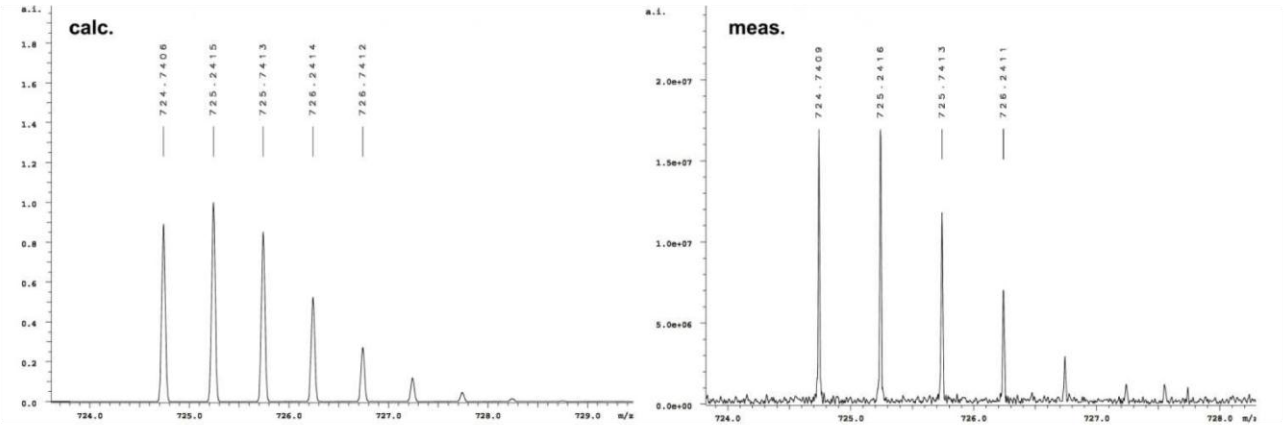

Fig. S3: HR-MS measurement of Fmoc-S-Trt-L-cysteine heptaamino-COSS **2a**; left: calculated isotopic pattern $[M+2H]^{2+}$= 724.7406; right: measured isotopic pattern $[M+2H]^{2+}$= 724.7409.

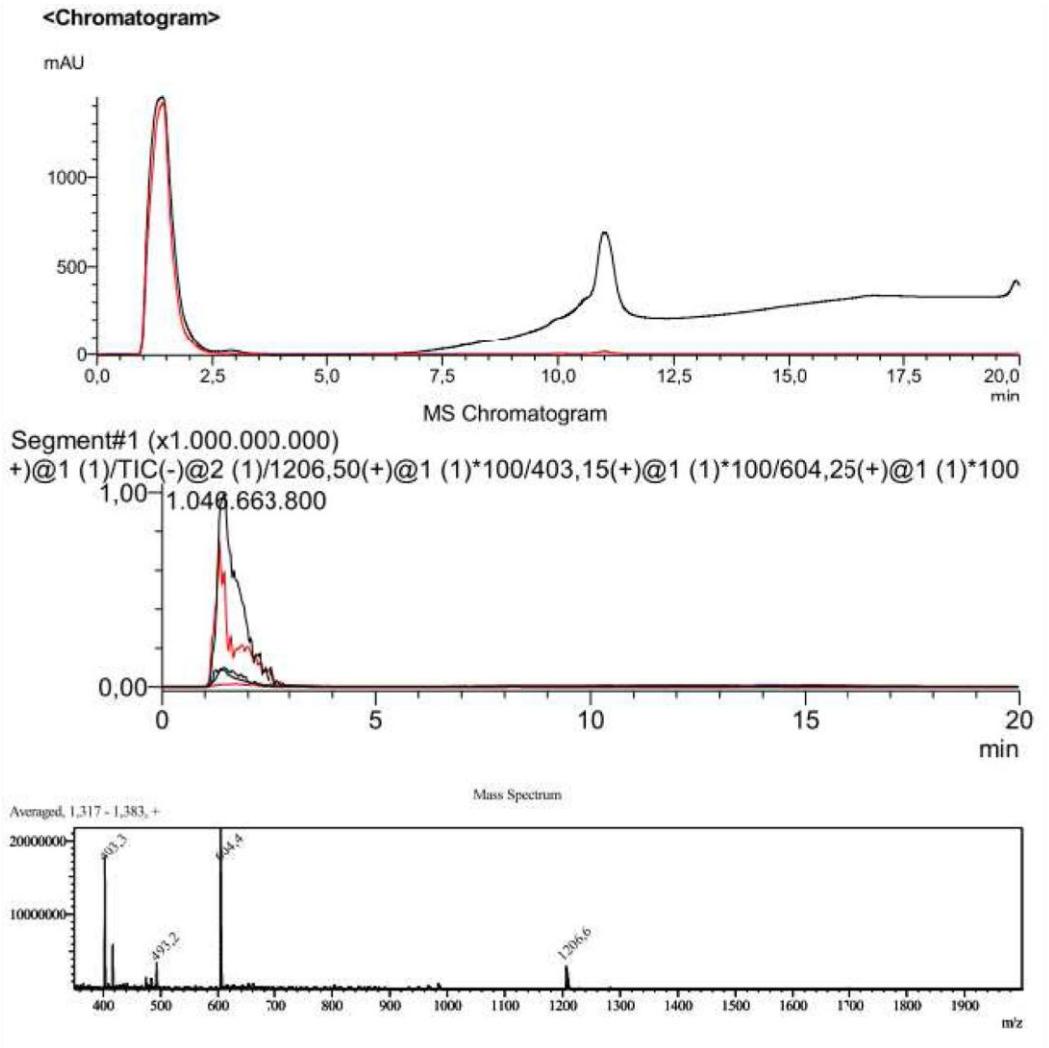

Fig. S4 LC-MS (ESI) measurement of compound **2**.

Compound 3 (FITC-labeled PCNA binding peptide)

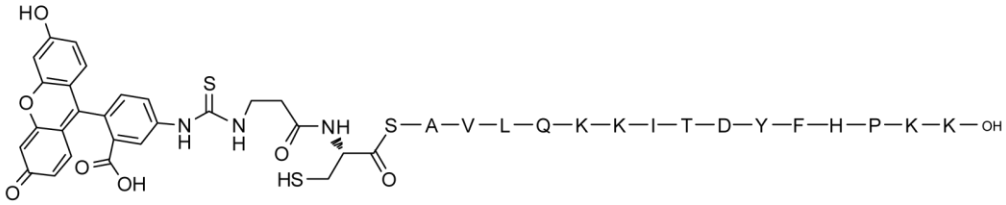

Chemical Formula: $C_{116}H_{164}N_{26}O_{30}S_2$
Exact Mass: 2465,15
Molecular Weight: 2466,83

Fig. S5: Amino acid sequence and chemical structure of FITC-labeled PCNA binding peptide **3**.

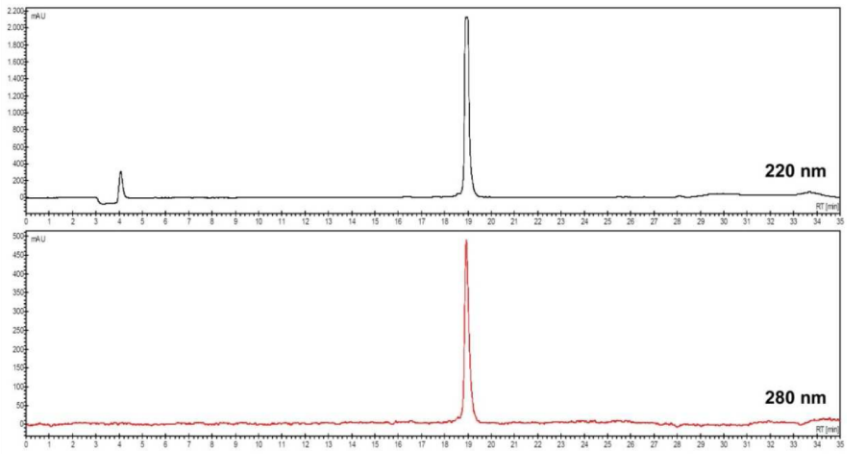

Fig. S6: Analytical RP-HPLC traces of FITC-labeled PCNA binding peptide **3** (*Varian* 940-LC equipped with a *Phenomenex* Luna C_{18} column (5u, 100 A, 250×4.60 mm, 5 µm). Eluent A: 0.1% aq. trifluoroacetic acid (TFA), eluent B: 90 % aq. acetonitrile in 0.1% aq. TFA; 25 → 50% B in 20 min preceded by 5 min isocratic 25 % B at a flow rate of 1 mL min^{-1}).

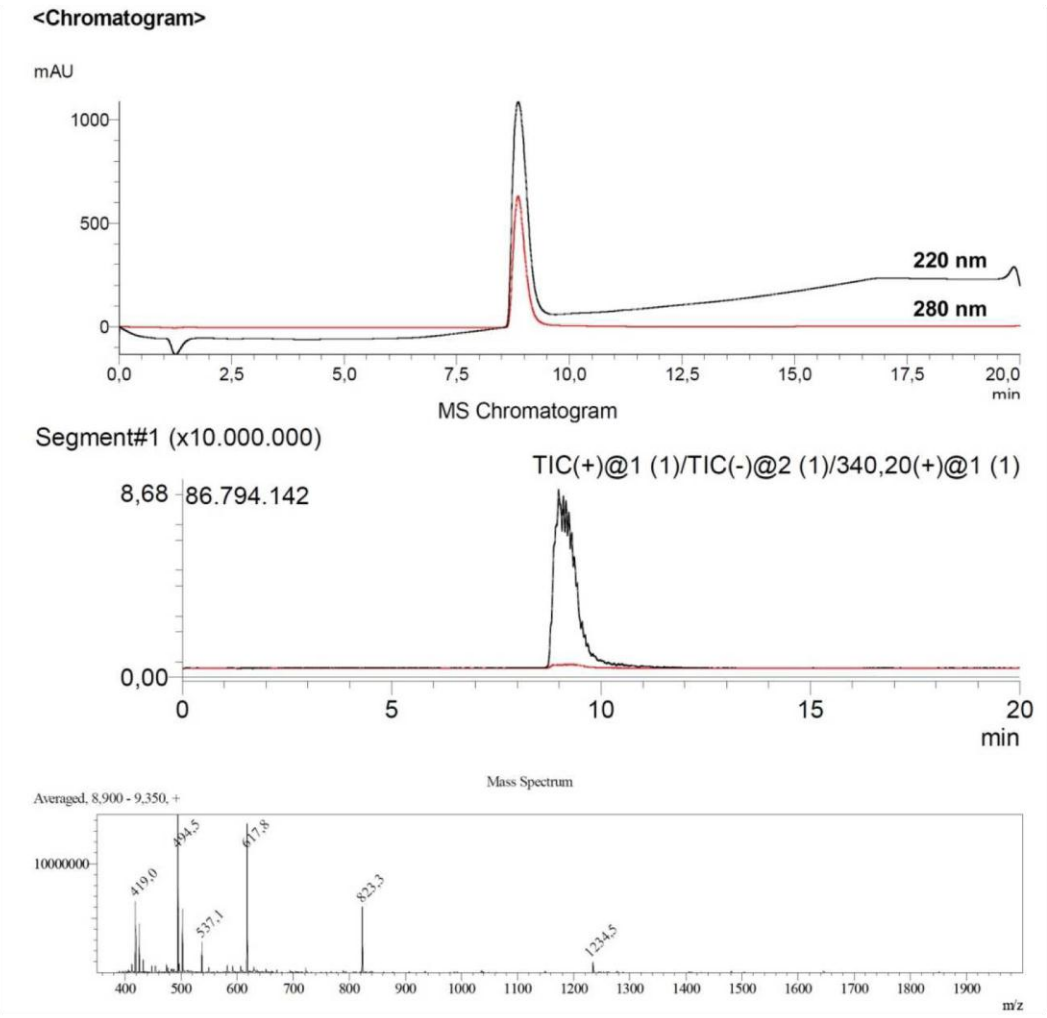

Fig. S7: LC-MS (ESI) measurement of the purified FITC-labeled PCNA binding peptide **3**.

Compound 4 (PCNA binding peptide coupled to Fmoc-L-cysteine heptaamino-COSS)

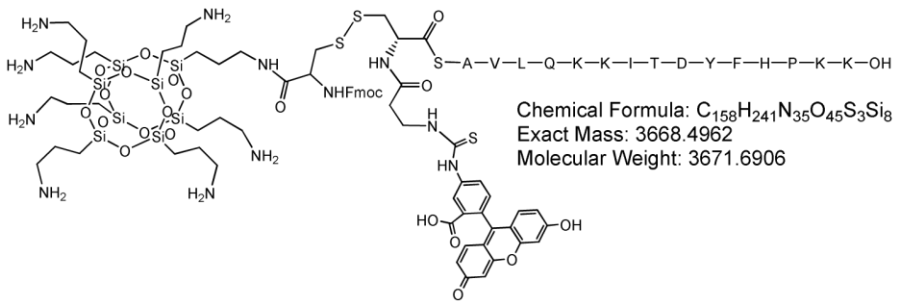

Fig. S8: Chemical structure compound **4**.

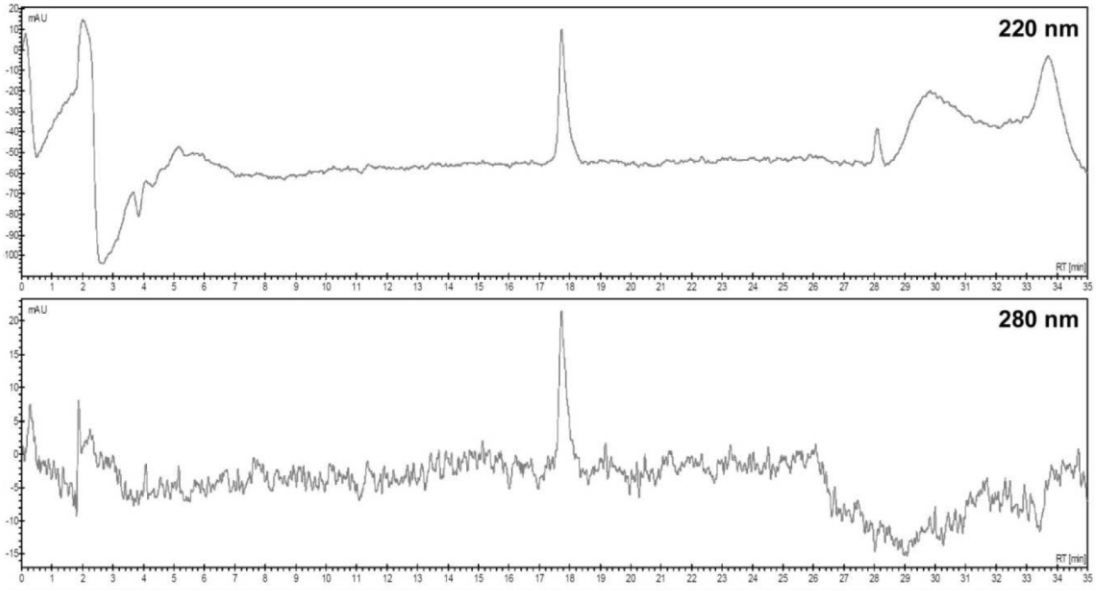

Fig. S9: Analytical RP-HPLC traces of compound **4** (*Varian* 940-LC equipped with a *Phenomenex* Luna C_{18} column (5u, 100 A, 250×4.60 mm, 5 µm). Eluent A: 0.1% aq. trifluoroacetic acid (TFA), eluent B: 90 % aq. acetonitrile in 0.1% aq. TFA; 25 → 50% B in 20 min preceded by 5 min isocratic 10 % B at a flow rate of 1 mL min^{-1}).

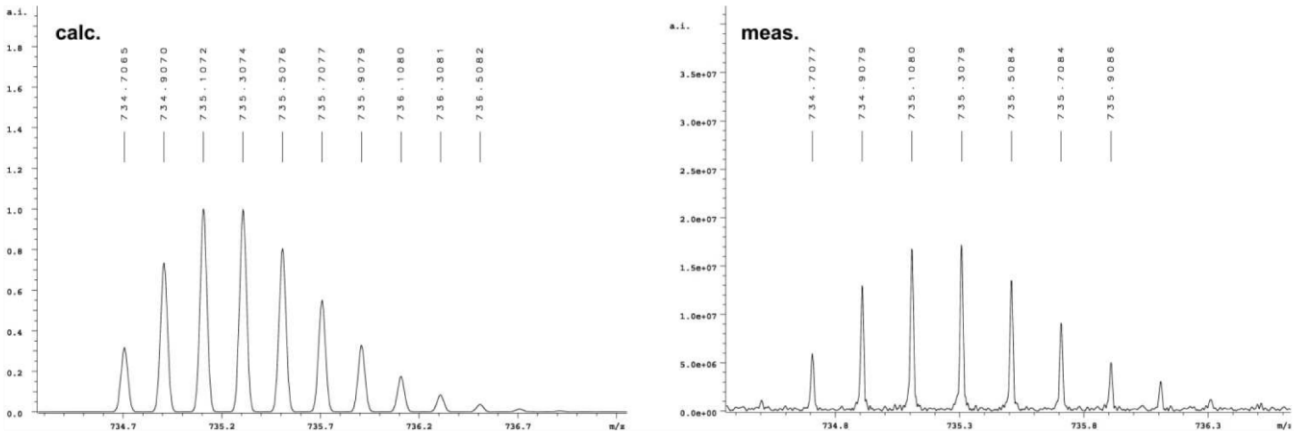

Fig. S10: HR-MS measurement of compound **4**; left: calculated isotopic pattern $[M+5H]^{5+}$= 734.7065; right: measured isotopic pattern $[M+5H]^{5+}$= 734.7077.

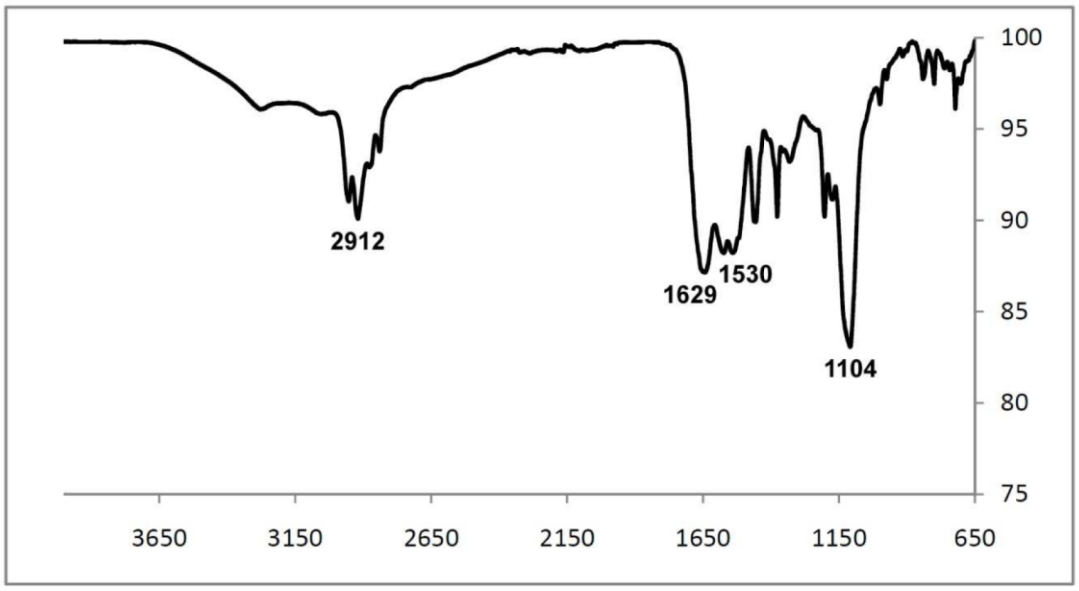

Fig. S11: FT-IR spectrum of compound **4**.

Compound 5 (Cys-β-Ala-FITC hepataamino-COSS), 5a (Cys-(S-trt)-beta-Ala-FITC), and 5b (Cys-(S-trt)-β-Ala-FITC hepataamino-COSS)

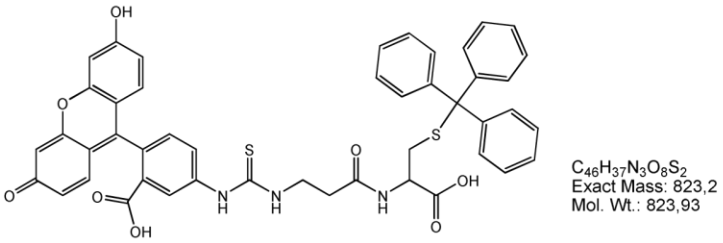

Fig. S12: Chemical structure of compound **5a**.

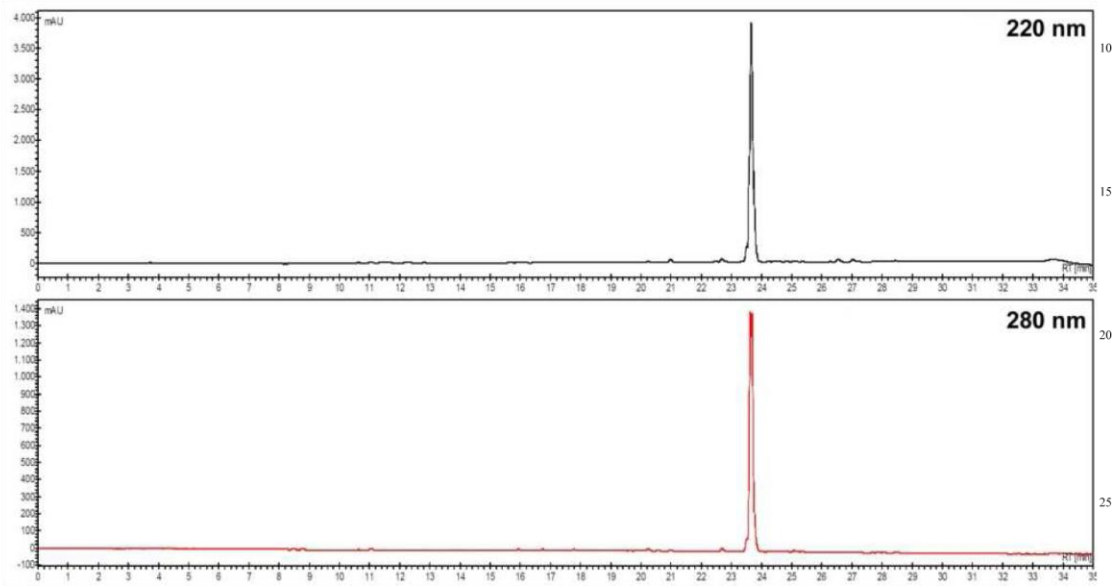

Fig. S13: Analytical RP-HPLC traces of compound **5a**. (*Varian* 940-LC equipped with a *Phenomenex* Luna C_{18} column (5u, 100 A, 250×4.60 mm, 5 µm). Eluent A: 0.1% aq. trifluoroacetic acid (TFA), eluent B: 90 % aq. acetonitrile in 0.1% aq. TFA; 10 → 100% B in 20 min preceded by 5 min isocratic 10 % B at a flow rate of 1 mL min^{-1}).

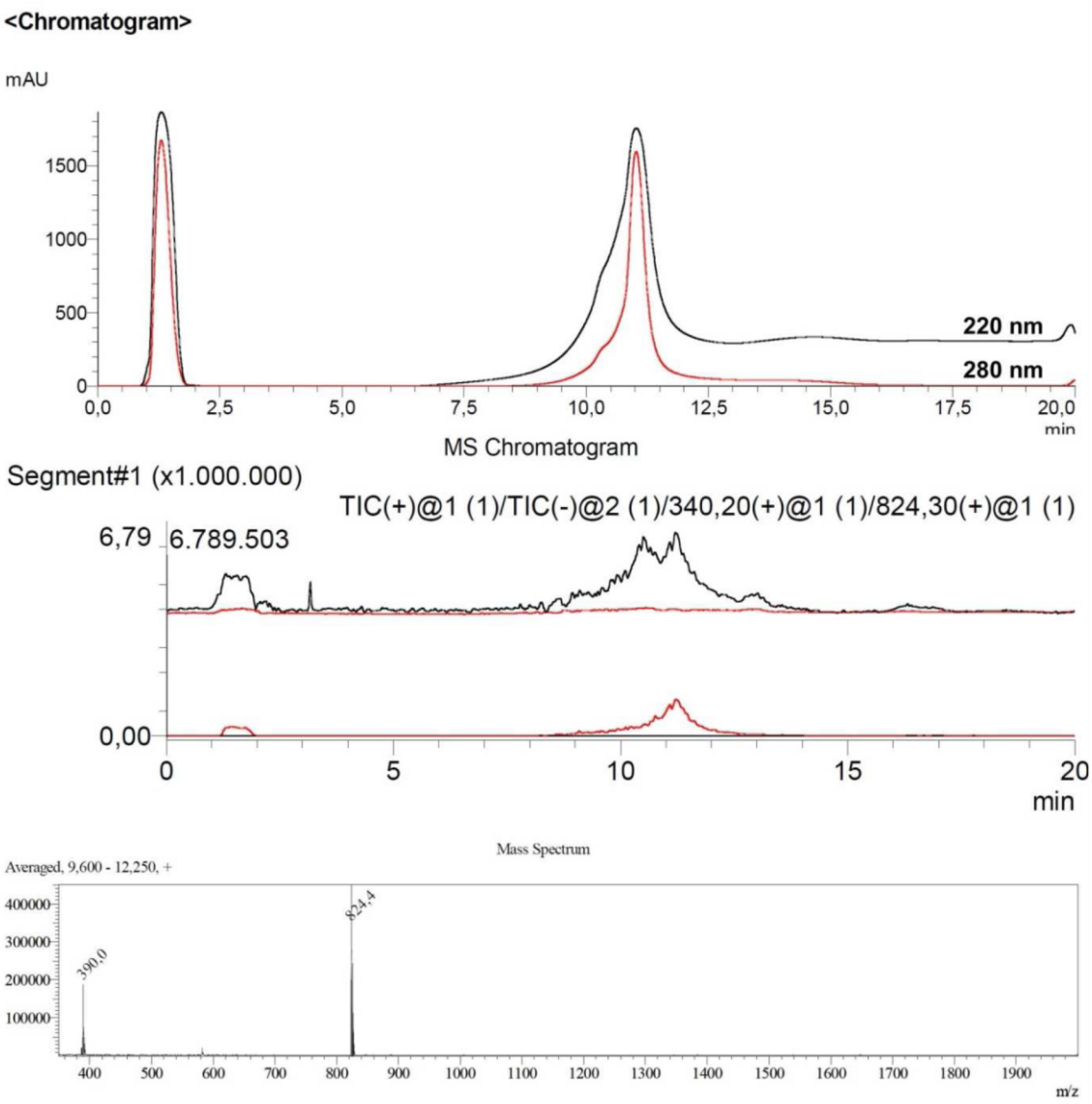

Fig. S14: LC-MS (ESI) measurement of compound **5a**.

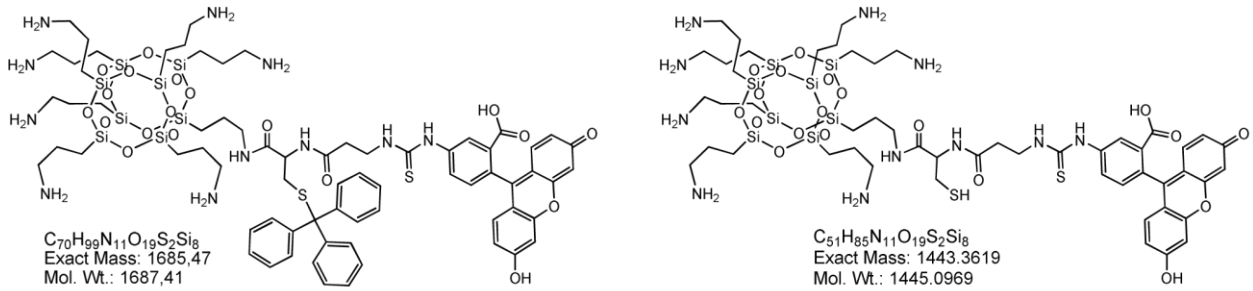

Fig. S15: Chemical structures of trityl protected **5b** (left) and unprotected fluorescein-labeled COSS particle **5** (right).

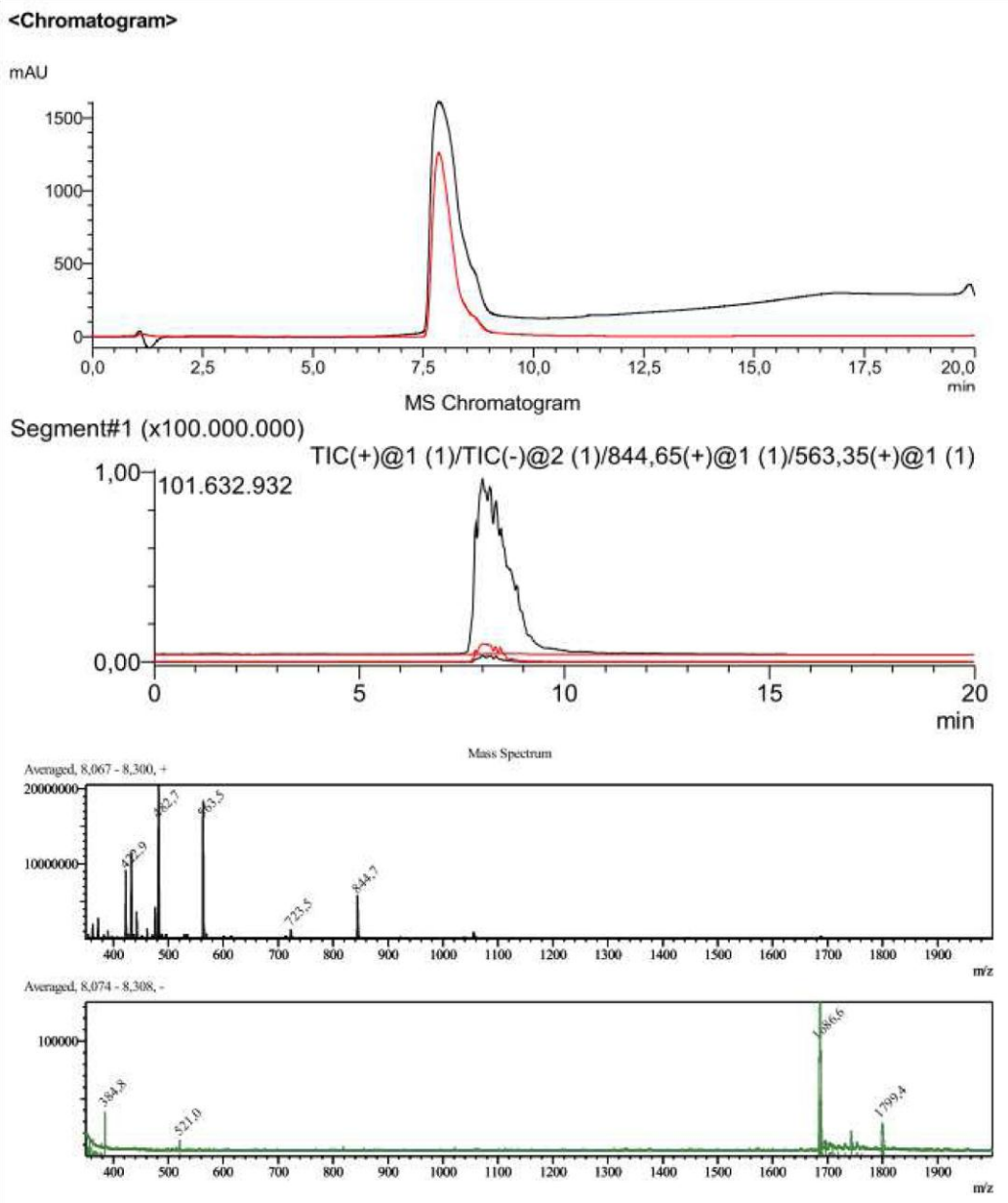

Fig. S16: LC-MS (ESI) measurement of trityl protected fluoresceine labeled COSS particle **5b**.

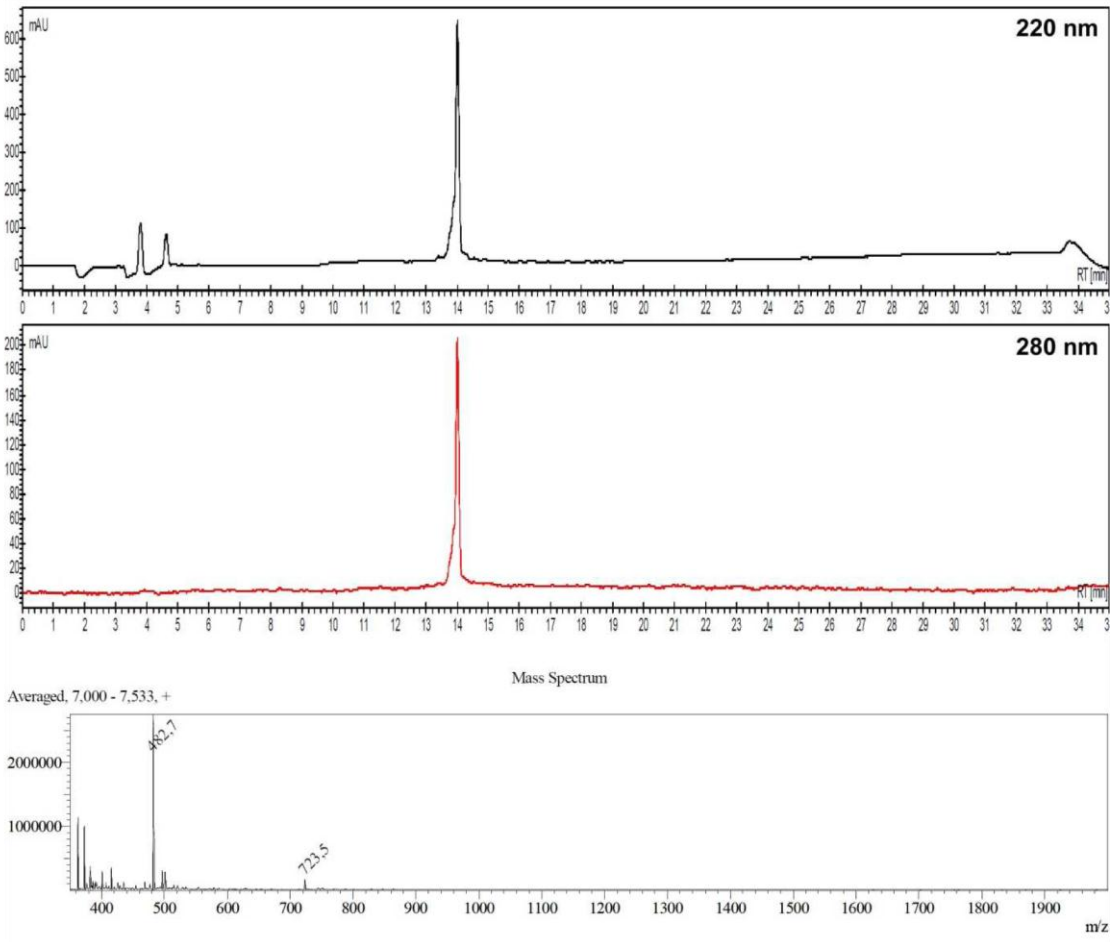

Fig. S17: Analytical RP-HPLC traces (*Varian* 940-LC equipped with a *Phenomenex* Luna C_{18} column (5u, 100 A, 250×4.60 mm, 5 µm). Eluent A: 0.1% aq. trifluoroacetic acid (TFA), eluent B: 90 % aq. acetonitrile in 0.1% aq. TFA; 10 → 100% B in 20 min preceded by 5 min isocratic 10 % B at a flow rate of 1 mL min^{-1}) and MS analysis of fluoresceine-labeled COSS particle **5**.

Microirradiation experiment and subsequent co-localization of PCNA binding peptide and RFP labeled PCNA

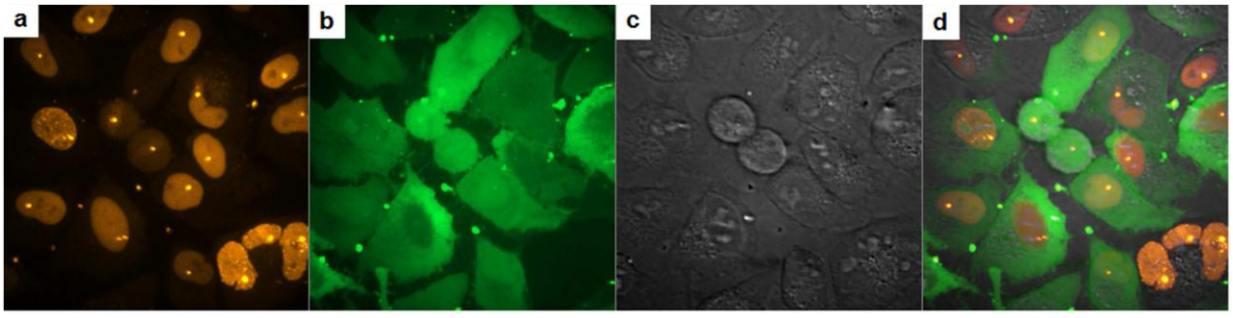

Fig. S18: Fluorescence microscopic analysis of irradiated HeLa cells. (a) PCNA (red) (b) fluorescein labeled peptide (green); (c) contrast image ; (d) overlay.

Sebastian Fabritz
Heidenreichstr. 29
64287 Darmstadt

22.10.2012

Eidesstattliche Erklärung

Ich erkläre hiermit an Eides Statt, dass ich meine Dissertation selbstständig und nur mit den angegebenen Hilfsmitteln angefertigt habe.

Sebastian Fabritz

Sebastian Fabritz
Heidenreichstr. 29
64287 Darmstadt

22.10.2012

Erklärung

Ich erkläre hiermit, noch keinen Promotionsversuch unternommen zu haben.

Sebastian Fabritz

Curriculum vitae

Sebastian Fabritz
Heidenreichstr. 29
64287 Darmstadt
SebastianFabritz@gmx.de
Geburtsdatum: 17.07.1982
Geburtsort: Worms
Nationalität: Deutsch

Akademische Ausbildung

bis **Oktober 2012**
Doktorarbeit: "Bioconjugation of Peptides on Cube-octameric Silsesquioxanes"
Prof. Dr. Harald Kolmar, Institut für Organische Chemie & Biochemie
Technische Universität Darmstadt

Tätigkeitsschwerpunkte:

Peptidchemie:	*Flüssig- und Festphasen basierte Synthesen, manuelle und automatisierte Synthesen, mikrowellenunterstützte Synthesen, Fmoc Strategie, Synthesen von langen Peptiden und Miniproteinen, „Faltungen" von Peptiden, Makrozyklisierung von Peptiden, orthogonale Schutzgruppenstrategien, Seitenketten-modifikationen, Fluoreszenzlabeling, Oligomerisierung*
Organische Chemie:	*Klassische organische Synthesen, Biokonjugationen/ligationen, Synthesen von peptidbasierten Buildingblocks*
Bioinspirierte anorganische Chemie:	*Sehr umfangreiche Erfahrung mit der Synthese und Analytik von polyhedralen Silsesquioxan-Nanopartikeln, Synthesen von anorganischen Chimären, Biokonjugationen an anorganischen Nanopartikeln*
Analytik:	*MS, IR, NMR, AFM, Mikrotiterplatten-Analytik, Entwicklung und Auswertung von Enzymassays, Chromatographie*
RP-HPLC:	*Methodenentwicklung, Wartung, Analytik und semipreparative Aufreinigungen*
LC-MS:	*Beratung, Methodenentwicklung, Auswertung und Wartung/ Instandhaltung*
Führung:	*Anleitung von Diplom- und Bachelorstudenten, Leiten von Grund- und Vertiefungspraktikanten, Gruppenleiter bei vorlesungs-begleitenden Übungen/Seminaren*

Publikationen:

[1] Olga Avrutina, Martin Empting, Sebastian Fabritz, Matin Daneschdar, Holm Frauendorf, Ulf Diederichsen and Harald Kolmar, *Application of copper(I) catalyzed azide–alkyne [3+2] cycloaddition to the synthesis of template-assembled multivalent peptide conjugates, Org. Biomol. Chem.*, 2009, **7**, 4177-4185.
[2] Sebastian Fabritz, Dirk Heyl, Viktor Bagutski, Martin Empting, Eckhard Rikowski, Holm Frauendorf, Ildiko Balog, Wolf-Dieter Fessner, Jörg. J. Schneider, Olga Avrutina and Harald Kolmar, *Towards click bioconjugations on cube-octameric silsesquioxane scaffolds*, *Org. Biomol. Chem.*, 2010, **8**, 2212-2218.

[3] Martin Empting, Olga Avrutina, Reinhard Meusinger, Sebastian Fabritz, Michael Reinwarth, Markus Biesalski, Stephan Voigt, Gerd Buntkowsky, Harald Kolmar, *"Triazole Bridge": Disulfide-Bond Replacement by Ruthenium-Catalyzed Formation of 1,5-Disubstituted 1,2,3-Triazoles*, *Angew. Chem. Int. Ed.*, 2011, **50**, 5207–5211.
[4] Sebastian Fabritz, Sebastian Hörner, Martin Empting, Doreen Könning, Michael Reinwarth, Christian Dietz, Bernhard Glotzbach, Holm Frauendorf, Harald Kolmar and Olga Avrutina, *From Pico to Nano: Biofunctionalization of Cube-octameric Silsesquioxanes by Peptides and Miniproteins, Org. Biomol. Chem.*, 2012, **10**, 6287-6293.
[5] Sebastian Fabritz,‡ Franziska Maaß,‡ Olga Avrutina, Tim Heiseler, Björn Steinmann and Harald Kolmar, *A sensitive method for rapid detection of alkyl halides and dehalogenase activity using a multistep enzyme assay*, *AMB Express*, 2012, **2**:51.
[6] Michael Reinwarth, Bernhard Glotzbach, Michael Tomaszowski, Martin Empting, Sebastian Fabritz Olga Avrutina, Harald Kolmar, *Oxidative folding of peptides with cystine-knot architecture: kinetic studies and optimization of folding conditions*, *ChemBioChem*, 2013, **14**, 137-146.
[7] Sebastian Fabritz,‡* Sebastian Hörner,‡ Olga Avrutina and Harald Kolmar, *Bioconjugation on Cube-Octameric Silsesquioxanes*, *Org. Biomol. Chem.*, 2013, **11**, 2224-2236.
[8] Sebastian Hörner,‡ Sebastian Fabritz,‡ Henry D. Herce, Olga Avrutina, Christian Dietz, Robert W. Stark, M. Cristina Cardoso and Harald Kolmar, *Cube-octameric silsesquioxane-mediated cargo peptide delivery into living cancer cells*, *Org. Biomol. Chem.,* 2013, **11**, 2258-2265.

März – September 2008
Diplomarbeit "The 'on water' click reaction - a new method for the preparation of bioactive peptide oligomers."
Preisträger der Dr. Anton-Keller-Stiftung für sehr gute Leistungen in der Diplomchemiker-Hauptprüfung (Gesamturteil: sehr gut).
Prof. Dr. Harald Kolmar, Institut für Organische Chemie & Biochemie
Technische Universität Darmstadt

2004 – 2008
Hauptstudium an der Technischen Universität Darmstadt
Schwerpunkte: Biochemie, organische und makromolekulare Chemie
Biochemisches Forschungsprojekt: "Imino–Cyclotides: Total Chemical Synthesis by Fmoc–SPPS"

2004 – 2005
Auslandsstudium an der University of Bristol, UK
Forschungsprojekt: "Asymmetric Allylic Alkylation (AAA) of an *exo*-Tricyclic Cyclopentenyl Acetate"

2002 – 2004
Grundstudium an der Technischen Universität Darmstadt

Schulausbildung

2002
Abitur am Lessing–Gymnasium Lampertheim (Gesamtnote: 1,7)

Zusätzliche Qualifikationen

April 2011
Seminar: Projektmanagement in der Wissenschaft -Führungskompetenz und Erfolgsstrategie-

Januar 2011
Seminar: Führungskompetenz für Wissenschaftler

November 2010
Seminar: Konstruktiver Umgang mit Konflikten am Arbeitsplatz

November 2010
Sachkundekurs für Laserschutzbeauftragte

Sprachen

Deutsch, Muttersprache
Englisch, verhandlungssicher
Französisch, gute Kenntnisse

Darmstadt, 22. Oktober 2012

Sebastian Fabritz